

REPUBLIC OF CAMEROON
Peace-Work-Fatherland

THE UNIVERSITY OF YAOUNDE I

POST GRADUATE SCHOOL OF SCIENCE,
TECHNOLOGY AND GEOSCIENCES

RESEARCH AND POSGRADUATE TRAINING UNIT
IN CHEMISTRY AND APPLICATIONS



REPUBLIQUE DU CAMEROUN
Paix-Travail-Patrie

UNIVERSITE DE YAOUNDE I

CENTRE DE RECHERCHE ET DE FORMATION
DOCTORALE EN SCIENCES TECHNOLOGIQUES ET
GEOSCIENCES

UNITE DE RECHERCHE ET DE FORMATION
DOCTORALE EN CHIMIE ET APPLICATIONS

DEPARTMENT OF ORGANIC CHEMISTRY
DEPARTEMENT DE CHIMIE ORGANIQUE

LABORATORY OF FUNGI AND PLANT NATURAL PRODUCTS
LABORATOIRE DES SUBSTANCES NATURELLES DES PLANTES ET DES CHAMPIGNONS
MICROSCOPIQUES

“Chemical study of *Duguetia staudtii* Engl. & Diels Chatrou (Annonaceae) and
Psorospermum tenuifolium Hook.f. (Hypericaceae): Microfilaricidal activities
and LC-ESI-MS applications”

THESIS

Defended Publicly in Partial Fulfilment of the Requirements for the Award of a
Doctorate/Ph.D Degree in Organic Chemistry

By:

MBOBDA WAFO Alexis Sylvain
Registration n°: 97T476
MSc in Organic Chemistry



Under the co-supervision of:

KOUAM FOGUE Siméon
Professor

TCHOUANKEU Jean Claude
Professor

Academic year : 2022/2023



DEPARTEMENT DE CHIMIE ORGANIQUE
DEPARTMENT OF ORGANIQUE CHEMISTRY

ATTESTATION DE CORRECTION DE THESE DE DOCTORAT/Ph.D

Je soussigné, **Augustin Ephrem NKENGFACK**, *Professeur*, Université de Yaoundé I et Président du Jury de soutenance de thèse de Doctorat / Ph.D de Monsieur. **MBOBDA WAFO Alexis Sylvain**, Matricule **97T476**, atteste que le candidat a effectivement corrigé sa thèse soutenue le 22 Septembre 2022 dans la Salle S01/02 du Nouveau bloc pédagogique et intitulée : **"Chemical study of *Duguetia staudtii* Engl. & Diels Chatrou (Annonaceae) and *Psorospermum tenuifolium* Hook.f. (Hypericaceae): Microfilaricidal activities and LC-ESI-MS applications"**, conformément aux observations et recommandations du Jury.

En foi de quoi la présente attestation lui est établie et délivrée pour servir et valoir ce que de droit.

Le Président du Jury

A. NKENGFACK

Le Rapporteur

Les Membres du Jury

F. ATCHADI
Alexis WAFO

LIST OF PERMANENT TEACHING STAFF

UNIVERSITÉ DE YAOUNDÉ I Faculté des Sciences Division de la Programmation et du Suivi des Activités Académiques		THE UNIVERSITY OF YAOUNDE I Faculty of Science Division of Programming and Follow-up of Academic Affairs
LISTE DES ENSEIGNANTS PERMANENTS		LIST OF PERMANENT TEACHING STAFF

ANNÉE ACADEMIQUE 2023/2024

(Par Département et par Grade)

DATE D'ACTUALISATION 04 Juin 2024

ADMINISTRATION

DOYEN : TCHOUANKEU Jean- Claude, *Professeur*

VICE-DOYEN / DPSAA: ATCHADE Alex de Théodore, *Professeur*

VICE-DOYEN / DSSE : NYEGUE Maximilienne Ascension, *Professeur*

VICE-DOYEN / DRC : NOUNDJEU Pierre, *Maître de Conférences*

Chef Division Administrative et Financière : NDOYE FOE Florentine Marie Chantal, *Maître de Conférences*

Chef Division des Affaires Académiques, de la Recherche et de la Scolarité DAARS : AJEAGAH Gideon AGHAINDUM, *Professeur*

1- DÉPARTEMENT DE BIOCHIMIE (BC) (43)
--

N°	NOMS ET PRÉNOMS	GRADE	OBSERVATIONS
1.	BIGOGA DAIGA Jude	Professeur	En poste
2.	FEKAM BOYOM Fabrice	Professeur	En poste
3.	KANSCI Germain	Professeur	En poste
4.	MBACHAM FON Wilfred	Professeur	En poste
5.	MOUNDIPA FEWOU Paul	Professeur	<i>Chef de Département</i>
6.	NGUEFACK Julienne	Professeur	En poste
7.	NJAYOU Frédéric Nico	Professeur	En poste
8.	OBEN Julius ENYONG	Professeur	En poste
9.	ACHU Merci BIH	Maître de Conférences	En poste
10.	AKINDEH MBUH NJI	Maître de Conférences	En poste
11.	ATOGHO Barbara MMA	Maître de Conférences	En poste
12.	AZANTSA KINGUE GABIN BORIS	Maître de Conférences	En poste
13.	BELINGA née NDOYE FOE F. M. C.	Maître de Conférences	<i>Chef DAF / FS</i>
14.	DAKOLE DABOY Charles	Maître de Conférences	En poste

LIST OF PERMANENT TEACHING STAFF

15.	DONGMO LEKAGNE Joseph Blaise	Maître de Conférences	En poste
16.	DJUIDJE NGOUNOUE Marceline	Maître de Conférences	En poste
17.	DJUIKWO NKONGA Ruth Viviane	Maître de Conférences	En poste
18.	EFFA ONOMO Pierre	Maître de Conférences	<i>VD/FS/Univ Ebwa</i>
19.	EWANE Cécile Annie	Maître de Conférences	En poste
20.	KOTUE TAPTUE Charles	Maître de Conférences	En poste
21.	LUNGA Paul KEILAH	Maître de Conférences	En poste
22.	MANANGA Marlyse Joséphine	Maître de Conférences	En poste
23.	MBONG ANGIE M. Mary Anne	Maître de Conférences	En poste
24.	MOFOR née TEUGWA Clotilde	Maître de Conférences	<i>Doyen FS / UD</i> s
25.	NANA Louise épouse WAKAM	Maître de Conférences	En poste
26.	NGONDI Judith Laure	Maître de Conférences	En poste
27.	Palmer MASUMBE NETONGO	Maître de Conférences	En poste
28.	PECHANGO NSANGO Sylvain	Maître de Conférences	En poste
29.	TCHANA KOUATCHOUA Angèle	Maître de Conférences	En poste
30.	BEBEE Fadimatou	Chargée de Cours	En poste
31.	BEBOY EDJENGUELE Sara N.	Chargé de Cours	En poste
32.	FONKOUA Martin	Chargé de Cours	En poste
33.	FOUPOUAPOUOGNIGNI Yacouba	Chargé de Cours	En poste
34.	KOUOH ELOMBO Ferdinand	Chargé de Cours	En poste
35.	MBOUCHE FANMOE Marceline J.	Chargé de Cours	En poste
36.	OWONA AYISSI Vincent Brice	Chargé de Cours	En poste
37.	WILFRED ANGIE ABIA	Chargé de Cours	En poste
38.	BAKWO BASSOGOG Christian Bernard	Assistant	En Poste
39.	ELLA Fils Armand	Assistant	En Poste
40.	EYENGA Eliane Flore	Assistant	En Poste
41.	MADIESSE KEMGNE Eugenie Aimée	Assistant	En Poste
42.	MANJIA NJIKAM Jacqueline	Assistant	En Poste
43.	WOGUIA Alice Louise	Assistant	En Poste

2- DÉPARTEMENT DE BIOLOGIE ET PHYSIOLOGIE ANIMALES (BPA) (49)

N°	NOMS ET PRÉNOMS	GRADE	OBSERVATIONS
1.	AJEAGAH Gideon AGHAINDUM	Professeur	<i>DAARS/FS</i>
2.	DIMO Théophile	Professeur	En Poste
3.	DJIETO LORDON Champlain	Professeur	En Poste
4.	DZEUFJET DJOMENI Paul Désiré	Professeur	En Poste
5.	ESSOMBA née NTSAMA MBALA	Professeur	<i>CD et Vice Doyen/FMSB/Uyi</i>

LIST OF PERMANENT TEACHING STAFF

6.	KEKEUNOU Sévilor	Professeur	<i>Chef de Département (a.i)</i>
7.	NJAMEN Dieudonné	Professeur	En poste
8.	NOLA Moïse	Professeur	En poste
9.	TAN Paul VERNYUY	Professeur	En poste
10.	TCHUEM TCHUENTE Louis Albert	Professeur	<i>Inspecteur de service / Coord.Progr./MINSANTE</i>
11.	ZEBAZE TOGOUET Serge Hubert	Professeur	En poste
12.	ALENE Désirée Chantal	Maître de Conférences	<i>Vice Doyen/ Uté Ebwa</i>
13.	ATSAMO Albert Donatien	Maître de Conférences	En poste
14.	BILANDA Danielle Claude	Maître de Conférences	En poste
15.	DJIOGUE Séfirin	Maître de Conférences	En poste
16.	GOUNOUE KAMKUMO Raceline épse FOTSING	Maître de Conférences	En poste
17.	JATSA BOUKENG Hermine épse MEGAPTCHÉ	Maître de Conférences	En Poste
18.	KANDEDA KAVAYE Antoine	Maître de Conférences	En poste
19.	LEKEUFACK FOLEFACK Guy B.	Maître de Conférences	En poste
20.	MAHOB Raymond Joseph	Maître de Conférences	En poste
21.	MBENOUN MASSE Paul Serge	Maître de Conférences	En poste
22.	MEGNEKOU Rosette	Maître de Conférences	En poste
23.	MOUNGANG Luciane Marlyse	Maître de Conférences	En poste
24.	NOAH EWOTI Olive Vivien	Maître de Conférences	En poste
25.	MONY Ruth épse NTONE	Maître de Conférences	En Poste
26.	MVEYO NDANKEU Yves Patrick	Maître de Conférences	En poste
27.	NGUEGUIM TSOFAK Florence	Maître de Conférences	En poste
28.	NGUEMBOCK	Maître de Conférences	En poste
29.	TAMSA ARFAO Antoine	Maître de Conférences	En poste
30.	TOMBI Jeannette	Maître de Conférences	En poste
31.	AMBADA NDZENGUE GEORGIA ELNA	Chargé de Cours	En poste
32.	BASSOCK BAYIHA Etienne Didier	Chargé de Cours	En poste
33.	ETEME ENAMA Serge	Chargé de Cours	En poste
34.	FEUGANG YOUNSSI François	Chargé de Cours	En poste
35.	FOKAM Alvine Christelle Epse KENGNE	Chargé de Cours	En poste
36.	GONWOUO NONO Legrand	Chargé de Cours	En poste
37.	KOGA MANG DOBARA	Chargé de Cours	En poste
38.	LEME BANOCK Lucie	Chargé de Cours	En poste
39.	MAPON NSANGO Indou	Chargé de Cours	En poste
40.	METCHI DONFACK MIREILLE FLAURE EPSE GHOUMO	Chargé de Cours	En poste
41.	NGOULATEU KENFACK Omer Bébé	Chargé de Cours	En poste

LIST OF PERMANENT TEACHING STAFF

42.	NJUA Clarisse YAFI	Chargée de Cours	<i>Chef Div. Uté Bamenda</i>
43.	NWANE Philippe Bienvenu	Chargé de Cours	En poste
44.	TADU Zephyrin	Chargé de Cours	En poste
45.	YEDE	Chargé de Cours	En poste
46.	YOUNOUSSA LAME	Chargé de Cours	En poste
47.	KODJOM WANCHE Jacguy Joyce	Assistante	En poste
48.	NDENGUE Jean De Matha	Assistant	En poste
49.	ZEMO GAMO Franklin	Assistant	En poste

3- DÉPARTEMENT DE BIOLOGIE ET PHYSIOLOGIE VÉGÉTALES (BPV) (32)

N°	NOMS ET PRÉNOMS	GRADE	OBSERVATIONS
1.	AMBANG Zachée	Professeur	<i>Chef de Département</i>
2.	DJOCGOUE Pierre François	Professeur	En poste
3.	MBOLO Marie	Professeur	En poste
4.	MOSSEBO Dominique Claude	Professeur	En poste
5.	NDONGO BEKOLO	Professeur	En poste
6.	ZAPFACK Louis	Professeur	En poste
7.	ANGONI Hyacinthe	Maître de Conférences	En poste
8.	BIYE Elvire Hortense	Maître de Conférences	En poste
9.	MAHBOU SOMO TOUKAM. Gabriel	Maître de Conférences	En poste
10.	MALA Armand William	Maître de Conférences	En poste
11.	MBARGA BINDZI Marie Alain	Maître de Conférences	<i>DAAC /UD/a</i>
12.	NGALLE Hermine BILLE	Maître de Conférences	En poste
13.	NGONKEU MAGAPTCHE Eddy L.	Maître de Conférences	<i>CT / MINRESI</i>
14.	TONFACK Libert Brice	Maître de Conférences	En poste
15.	TSOATA Esaïe	Maître de Conférences	En poste
16.	ONANA JEAN MICHEL	Maître de Conférences	En poste
17.	DJEUANI Astride Carole	Chargé de Cours	En poste
18.	GONMADGE CHRISTELLE	Chargé de Cours	En poste
19.	MAFFO MAFFO Nicole Liliane	Chargé de Cours	En poste
20.	MANGA NDJAGA JUDE	Chargé de Cours	En poste
21.	NNANGA MEBENGA Ruth Laure	Chargé de Cours	En poste
22.	NOUKEU KOUAKAM Armelle	Chargé de Cours	En poste
23.	NSOM ZAMBO EPSE PIAL ANNIE CLAUDE	Chargé de Cours	<i>En détachement/UNESCO MALI</i>
24.	GODSWILL NTSOMBOH NTSEFONG	Chargé de Cours	En poste
25.	KABELONG BANAHOU Louis-Paul-Roger	Chargé de Cours	En poste
26.	KONO Léon Dieudonné	Chargé de Cours	En poste
27.	LIBALAH Moses BAKONCK	Chargé de Cours	En poste

LIST OF PERMANENT TEACHING STAFF

28.	LIKENG-LI-NGUE Benoit C	Chargé de Cours	En poste
29.	TAEDOUNG Evariste Hermann	Chargé de Cours	En poste
30.	TEMEGNE NONO Carine	Chargé de Cours	En poste
31.	DIDA LONTSI Sylvere Landry	Assistant	En poste
32.	METSEBING Blondo-Pascal	Assistant	En poste

4- DÉPARTEMENT DE CHIMIE INORGANIQUE (CI) (27)

N°	NOMS ET PRÉNOMS	GRADE	OBSERVATIONS
1.	GHOGOMU Paul MINGO	Professeur	<i>Ministre Chargé de Mission PR</i>
2.	NANSEU NJIKI Charles Péguy	Professeur	En poste
3.	NDIFON Peter TEKE	Professeur	<i>CT MINRESI</i>
4.	NENWA Justin	Professeur	En poste
5.	NGOMO Horace MANGA	Professeur	<i>Vice Chancellor/UB</i>
6.	NJIOMOU C. épse DJANGANG	Professeur	En poste
7.	NJOYA Dayirou	Professeur	En poste
8.	ACAYANKA Elie	Maître de Conférences	En poste
9.	EMADAK Alphonse	Maître de Conférences	En poste
10.	KAMGANG YOUNBI Georges	Maître de Conférences	En poste
11.	KEMMEGNE MBOUGUEM Jean C.	Maître de Conférences	En poste
12.	KENNE DEDZO GUSTAVE	Maître de Conférences	En poste
13.	MBEY Jean Aime	Maître de Conférences	En poste
14.	NDI NSAMI Julius	Maître de Conférences	<i>Chef de Département</i>
15.	NEBAH Née NDOIRI Bridget NDOYE	Maître de Conférences	<i>Sénatrice/SENAT</i>
16.	NYAMEN Linda Dyorisse	Maître de Conférences	En poste
17.	PABOUDAM GBAMBIE AWAWOU	Maître de Conférences	En poste
18.	TCHAKOUTE KOUAMO Hervé	Maître de Conférences	En poste
19.	BELIBI BELIBI Placide Désiré	Maître de Conférences	<i>Chef Service/ ENS Bertoua</i>
20.	CHEUMANI YONA Arnaud M.	Maître de Conférences	En poste
21.	KOUOTOU DAOUDA	Maître de Conférences	En poste
22.	MAKON Thomas Beauregard	Chargé de Cours	En poste
23.	NCHIMI NONO KATIA	Chargée de Cours	En poste
24.	NJANKWA NJABONG N. Eric	Chargé de Cours	En poste
25.	PATOUOSSA ISSOFA	Chargé de Cours	En poste
26.	SIEWE Jean Mermoz	Chargé de Cours	En Poste
27.	BOYOM TATCHEMO Franck W.	Assistant	En Poste

LIST OF PERMANENT TEACHING STAFF

5- DÉPARTEMENT DE CHIMIE ORGANIQUE (CO) (35)

N°	NOMS ET PRÉNOMS	GRADE	OBSERVATIONS
1.	Alex de Théodore ATCHADE	Professeur	<i>Vice-Doyen / DPSAA</i>
2.	DONGO Etienne	Professeur	<i>Vice-Doyen/FSE/UYI</i>
3.	NGOUELA Silvère Augustin	Professeur	<i>Chef de Département UDS</i>
4.	PEGNYEMB Dieudonné Emmanuel	Professeur	<i>Recteur U.Bertoua/ Chef de Département</i>
5.	MBAZOA née DJAMA Céline	Professeur	En poste
6.	MKOUNGA Pierre	Professeur	En poste
7.	TCHOUANKEU Jean-Claude	Professeur	<i>Doyen /FS/ UYI</i>
8.	AMBASSA Pantaléon	Maître de Conférences	En poste
9.	EYONG Kenneth OBEN	Maître de Conférences	En poste
10.	FOTSO WABO Ghislain	Maître de Conférences	En poste
11.	KAMTO Eutrophe Le Doux	Maître de Conférences	En poste
12.	KENMOGNE Marguerite	Maître de Conférences	En poste
13.	KOUAM Jacques	Maître de Conférences	En poste
14.	MVOT AKAK CARINE	Maître de Conférences	En poste
15.	NGO MBING Joséphine	Maître de Conférences	<i>Chef de Cellule MINRESI</i>
16.	NGONO BIKOBO Dominique Serge	Maître de Conférences	<i>C.E.A/ MINESUP</i>
17.	NOTE LOUGBOT Olivier Placide	Maître de Conférences	<i>Dir ENS/Uté Bertoua</i>
18.	NOUNGOUE TCHAMO Diderot	Maître de Conférences	En poste
19.	TABOPDA KUATE Turibio	Maître de Conférences	En poste
20.	TAGATSING FOTSING Maurice	Maître de Conférences	En poste
21.	OUAHOUE WACHE Blandine M.	Maître de Conférences	En poste
22.	ZONDEGOUNBA Ernestine	Maître de Conférences	En poste
23.	MESSI Angélique Nicolas	Chargé de Cours	En poste
24.	MUNVERA MFIFEN Aristide	Chargé de Cours	En poste
25.	NGNINTEDO Dominique	Chargé de Cours	En poste
26.	NGOMO Orléans	Chargée de Cours	En poste
27.	NONO NONO Éric Carly	Chargé de Cours	En poste
28.	OUETE NANTCHOUANG Judith Laure	Chargée de Cours	En poste
29.	SIELINOUE TEDJON Valérie	Chargé de Cours	En poste
30.	TCHAMGOUE Joseph	Chargé de Cours	En poste
31.	TSAFFACK Maurice	Chargé de Cours	En poste
32.	TSAMO TONTSA Armelle	Chargé de Cours	En poste
33.	TSEMEUGNE Joseph	Chargé de Cours	En poste
34.	NDOGO ETEME Olivier	Assistant	En poste
35.	NGUEMDJO CHIMEZE Valery Wilfried	Assistant	En poste

LIST OF PERMANENT TEACHING STAFF

6- DEPARTEMENT DES ENERGIES RENOUVELABLES (ER) (1)			
N°	NOMS ET PRÉNOMS	GRADE	OBSERVATIONS
1.	BODO Bertrand	Professeur	<i>Chef de Département</i>

7- DÉPARTEMENT D'INFORMATIQUE (IN) (22)
--

N°	NOMS ET PRÉNOMS	GRADE	OBSERVATIONS
1.	ATSA ETOUNDI Roger	Professeur	<i>Chef de Division des SI/ MINESUP</i>
2.	FOUDA NDJODO Marcel Laurent	Professeur	<i>Inspecteur Général Académique/ MINESUP</i>
3.			
4.	NDOUNDAM René	Maître de Conférences	En poste
5.	ABESSOLO ALO'O Gislain	Chargé de Cours	<i>Chef de Cellule MINFOPRA</i>
6.	AMINOU HALIDOU	Chargé de Cours	<i>Chef de Département</i>
7.	DJAM Xaviera YOUH - KIMBI	Chargé de Cours	En Poste
8.	DOMGA KOMGUEM Rodrigue	Chargé de Cours	En poste
9.	EBELE Serge Alain	Chargé de Cours	En poste
10.	HAMZA Adamou	Chargé de Cours	En poste
11.	JIOMEKONG AZANZI Fidel	Chargé de Cours	En poste
12.	KOUOKAM KOUOKAM E. A.	Chargé de Cours	En poste
13.	MELATAGIA YONTA Paulin	Chargé de Cours	En poste
14.	MESSI NGUELE Thomas	Chargé de Cours	En poste
15.	MONTHÉ DJIADEU Valéry M.	Chargé de Cours	En poste
16.	NZEKON NZEKO'O ARMEL JACQUES	Chargé de Cours	En poste
17.	OLLE OLLE Daniel Claude Georges Delort	Chargé de Cours	<i>Directeur Adjoint ENSET Ebolowa</i>
18.	TAPAMO Hyppolite	Chargé de Cours	En poste
19.	BAYEM Jacques Narcisse	Assistant	En poste
20.	EKODECK Stéphane Gaël Raymond	Assistant	En poste
21.	MAKEMBE. S. Oswald	Assistant	<i>Directeur CUTI</i>
22.	NKONDOCK. MI. BAHANACK.N.	Assistant	En poste

8- DÉPARTEMENT DE MATHÉMATIQUES (MA) (33)
--

N°	NOMS ET PRÉNOMS	GRADE	OBSERVATIONS
1.	AYISSI Raoult Domingo	Professeur	<i>Chef de Département</i>
2.	KIANPI Maurice	Maître de Conférences	En poste
3.	MBANG Joseph	Maître de Conférences	En poste
4.	MBEHOU Mohamed	Maître de Conférences	<i>Chef de Division/ENSPY</i>

LIST OF PERMANENT TEACHING STAFF

5.	MBELE BIDIMA Martin Ledoux	Maître de Conférences	<i>Chef de Département de modélisation et applications industrielles/ENSPY</i>
6.	NOUNDJEU Pierre	Maître de Conférences	<i>VDRC/FS/UYI</i>
7.	TAKAM SOH Patrice	Maître de Conférences	En poste
8.	TCHAPNDA NJABO Sophonie B.	Maître de Conférences	<i>Directeur/AIMS Rwanda</i>
9.	TCHOUNDJA Edgar Landry	Maître de Conférences	En poste
10.	AGHOUKENG JIOFACK Jean Gérard	Chargé de Cours	<i>Chef Cellule MINEPAT</i>
11.	BOGSO ANTOINE Marie	Chargé de Cours	En poste
12.	BITYE MVONDO Esther Claudine	Chargé de Cours	En poste
13.	CHENDJOU Gilbert	Chargé de Cours	En poste
14.	DJIADU NGAHA Michel	Chargé de Cours	En poste
15.	DOUANLA YONTA Herman	Chargé de Cours	En poste
16.	KIKI Maxime Armand	Chargé de Cours	En poste
17.	LOUMNGAM KAMGA Victor	Chargé de Cours	En poste
18.	MBAKOP Guy Merlin	Chargé de Cours	En poste
19.	MBATAKOU Salomon Joseph	Chargé de Cours	En poste
20.	MENGUE MENGUE David Joël	Chargé de Cours	<i>Chef Dpt /ENS Université d'Ebolowa</i>
21.	MBIAKOP Hilaire George	Chargé de Cours	En poste
22.	NGUEFACK Bernard	Chargé de Cours	En poste
23.	NIMPA PEFOUKEU Romain	Chargée de Cours	En poste
24.	OGADOA AMASSAYOGA	Chargée de Cours	En poste
25.	POLA DOUNDOU Emmanuel	Chargé de Cours	<i>En stage</i>
26.	TENKEU JEUFACK Yannick Léa	Chargé de Cours	En poste
27.	TCHEUTIA Daniel Duviol	Chargé de Cours	En poste
28.	TETSADJIO TCHILEPECK M. Eric.	Chargé de Cours	En poste
29.	FOKAM Jean Marcel	Assistant	En poste
30.	GUIDZAVAI KOUCHERE Albert	Assistant	En poste
31.	MANN MANYOMBE Martin Luther	Assistant	En poste
32.	MEFENZA NOUNTU Thiery	Assistant	En poste
33.	NYOUMBI DLEUNA Christelle	Assistant	En poste

9- DÉPARTEMENT DE MICROBIOLOGIE (MIB) (24)

N°	NOMS ET PRÉNOMS	GRADE	OBSERVATIONS
1.	ESSIA NGANG Jean Justin	Professeur	<i>Chef de Département</i>
2.	NYEGUE Maximilienne Ascension	Professeur	<i>VICE-DOYEN / DSSE</i>
3.	SADO KAMDEM Sylvain Leroy	Professeur	En poste

LIST OF PERMANENT TEACHING STAFF

4.	ASSAM ASSAM Jean Paul	Maître de Conférences	En poste
5.	BOUGNOM Blaise Pascal	Maître de Conférences	En poste
6.	BOYOMO ONANA	Maître de Conférences	En poste
7.	KOUITCHEU MABEKU Epse KOUAM Laure Brigitte	Maître de Conférences	En poste
8.	RIWOM Sara Honorine	Maître de Conférences	En poste
9.	NJIKI BIKOÏ Jacky	Maître de Conférences	En poste
10.	TCHIKOUA Roger	Maître de Conférences	<i>Chef de Service de la Scolarité</i>
11.	ESSONO Damien Marie	Chargé de Cours	En poste
12.	LAMYE Glory MOH	Chargé de Cours	En poste
13.	MEYIN A EBONG Solange	Chargé de Cours	En poste
14.	MONI NDEDI Esther Del Florence	Chargé de Cours	En poste
15.	NKOUDOU ZE Nardis	Chargé de Cours	En poste
16.	NKOUÉ TONG Abraham	Chargé de Cours	En poste
17.	TAMATCHO KWEYANG Blandine Pulchérie	Chargé de Cours	En poste
18.	SAKE NGANE Carole Stéphanie	Chargé de Cours	En poste
19.	TOBOLBAÏ Richard	Chargé de Cours	En poste
20.	EZO'O MENGO Fabrice Télésfor	Assistant	En poste
21.	EHETH Jean Samuel	Assistant	En poste
22.	MAYI Marie Paule Audrey	Assistant	En poste
23.	NGOUE NAM Romial Joël	Assistant	En poste
24.	NJAPNDOUNKE Bilkissou	Assistant	En poste

10. DEPARTEMENT DE PHYSIQUE (PHY) (42)

N°	NOMS ET PRÉNOMS	GRADE	OBSERVATIONS
1.	BEN- BOLIE Germain Hubert	Professeur	En poste
2.	BIYA MOTTO Frédéric	Professeur	<i>DG/HYDRO Mekin</i>
3.	DJUIDJE KENMOE épouse ALOYEM	Professeur	En poste
4.	EKOBENA FOU DA Henri Paul	Professeur	<i>Vice-Recteur. Uté Ngaoundéré</i>
5.	ESSIMBI ZOBO Bernard	Professeur	En poste
6.	EYEBE FOU DA Jean sire	Professeur	En poste
7.	HONA Jacques	Professeur	En poste
8.	NANA ENGO Serge Guy	Professeur	En poste
9.	NANA NBENDJO Blaise	Professeur	En poste
10.	NDJAKA Jean Marie Bienvenu	Professeur	<i>Chef de Département</i>
11.	NJANDJOCK NOUCK Philippe	Professeur	En poste
12.	NOUAYOU Robert	Professeur	En poste

LIST OF PERMANENT TEACHING STAFF

13.	SAIDOU	Professeur	<i>Chef de centre/IRGM/MINRESI</i>
14.	SIMO Elie	Professeur	En poste
15.	TABOD Charles TABOD	Professeur	<i>Doyen FSUniv/Bda</i>
16.	TCHAWOUA Clément	Professeur	En poste
17.	WOAFO Paul	Professeur	En poste
18.	ZEKENG Serge Sylvain	Professeur	En poste
19.	ENYEGUE A NYAM épouse BELINGA	Maître de Conférences	<i>Chef de Division de la formation continue et à distance/ENSPY</i>
20.	FEWO Serge Ibraïd	Maître de Conférences	En poste
21.	FOUEJIO David	Maître de Conférences	<i>Chef Cell/ MINADER</i>
22.	MBINACK Clément	Maître de Conférences	En poste
23.	MBONO SAMBA Yves Christian U.	Maître de Conférences	En poste
24.	MELI'I Joelle Larissa	Maître de Conférences	En poste
25.	MVOGO ALAIN	Maître de Conférences	En poste
26.	NDOP Joseph	Maître de Conférences	En poste
27.	SIEWE SIEWE Martin	Maître de Conférences	En poste
28.	VONDOU Derbetini Appolinaire	Maître de Conférences	En poste
29.	WAKATA née BEYA Annie Sylvie	Maître de Conférences	<i>Directeur/ENS/UYI</i>
30.	WOULACHE Rosalie Laure	Maître de Conférences	<i>En stage depuis février 2023</i>
31.	ABDOURAHIMI	Chargé de Cours	En poste
32.	AYISSI EYEBE Guy François Valérie	Chargé de Cours	En poste
33.	CHAMANI Roméo	Chargé de Cours	En poste
34.	DJIOTANG TCHOTCHOU Lucie Angennes	Chargée de Cours	En poste
35.	EDONGUE HERVAIS	Chargé de Cours	En poste
36.	KAMENI NEMATCHOUA Modeste	Chargé de Cours	En poste
37.	LAMARA Maurice	Chargé de Cours	En poste
38.	NGA ONGODO Dieudonné	Chargé de Cours	En poste
39.	OTTOU ABE Martin Thierry	Chargé de Cours	<i>Directeur Unité de production des réactifs/IMPM</i>
40.	TEYOU NGOUPO Ariel	Chargé de Cours	En poste
41.	WANDJI NYAMSI William	Chargé de Cours	En poste
42.	SOUFFO TAGUEU Merimé	Assistant	En poste

LIST OF PERMANENT TEACHING STAFF

11- DÉPARTEMENT DE SCIENCES DE LA TERRE (ST) (39)

N°	NOMS ET PRÉNOMS	GRADE	OBSERVATIONS
1.	BITOM Dieudonné-Lucien	Professeur	<i>Doyen / FASA /Uds</i>
2.	EKOMANE Emile	Professeur	<i>Chef Div./Uté Ebolowa</i>
3.	GANNO Sylvestre	Professeur	En poste
4.	NDAM NGOUPAYOU Jules-Remy	Professeur	En poste
5.	NDJIGUI Paul-Désiré	Professeur	<i>Chef de Département</i>
6.	NGOS III Simon	Professeur	En poste
7.	NKOUMBOU Charles	Professeur	En poste
8.	ONANA Vincent Laurent	Professeur	<i>Chef de Département/Uté. Eb.</i>
9.	YENE ATANGANA Joseph Q.	Professeur	<i>Chef Div. /MINTP</i>
10	BISSO Dieudonné	Maître de Conférences	En poste
11.	Elisé SABABA	Maitre de Conférences	En poste
12.	EYONG John TAKEM	Maître de Conférences	En poste
13.	FUH Calistus Gentry	Maître de Conférences	<i>Sec. D'Etat/MINMIDT(ai)</i>
14.	GHOGOMU Richard TANWI	Maître de Conférences	<i>Chef de Div. /Uté Bertoua</i>
15.	MBIDA YEM	Maitre de Conférences	En poste
16.	MBESSE Cécile Olive	Maitre de Conférences	En poste
17.	METANG Victor	Maître de Conférences	En poste
18.	NGO BIDJECK Louise Marie	Maître de Conférences	En poste
19.	NGUEUTCHOUA Gabriel	Maître de Conférences	<i>CEA/MINRESI</i>
20.	NJILAH Isaac KONFOR	Maître de Conférences	En poste
21.	NYECK Bruno	Maître de Conférences	En poste
22.	TCHAKOUNTE J. épouse NUMBEM	Maître de Conférences	<i>Chef. Cell /MINRESI</i>
23.	TCHOUANKOUE Jean-Pierre	Maître de Conférences	En poste
24.	TEMGA Jean Pierre	Maître de Conférences	En poste
25.	ZO'O ZAME Philémon	Maître de Conférences	<i>DG/ART</i>
26.	ANABA ONANA Achille Basile	Chargé de Cours	En poste
27.	BEKOA Etienne	Chargé de Cours	En poste
28.	ESSONO Jean	Chargé de Cours	En poste
29.	MAMDEM TAMTO L. E. épouse BITOM	Chargée de Cours	En poste
30.	NGO BELNOUN Rose Noël	Chargée de Cours	En poste
31.	NGO'O ZE ARNAUD	Chargé de Cours	En poste
32.	NOMO NEGUE Emmanuel	Chargé de Cours	En poste
33.	NTSAMA ATANGANA Jacqueline	Chargée de Cours	En poste
34.	TCHAPTCHET TCHATO De P.	Chargé de Cours	En poste
35.	TEHNA Nathanaël	Chargé de Cours	En poste

LIST OF PERMANENT TEACHING STAFF

36.	FEUMBA Roger	Chargé de Cours	En poste
37.	MBANGA NYOBE Jules	Chargé de Cours	En poste
38.	KOAH NA LEBOGO Serge P.	Assistant	En poste
39.	TENE DJOUKAM J. F., épse KOUANKAP N.	Assistante	En poste

Répartition chiffrée des Enseignants de la Faculté des Sciences de l'Université de Yaoundé I

NOMBRE D'ENSEIGNANTS

DÉPARTEMENT	Professeurs	Maîtres de Conférences	Chargés de Cours	Assistants	Total
BCH	8 (01)	21 (12)	8 (04)	6 (04)	43 (21)
BPA	11 (01)	19 (09)	16 (05)	3 (02)	49 (17)
BPV	6 (01)	10 (02)	14 (08)	2 (00)	32 (11)
CI	7 (01)	14 (04)	5 (01)	1 (00)	27 (06)
CO	7 (01)	15 (05)	11 (05)	2 (00)	35 (11)
ER	1 (00)		/	/	1 (0)
IN	2 (00)	2 (00)	14 (01)	4 (00)	22 (01)
MAT	1 (00)	8 (00)	19 (02)	5 (01)	33 (03)
MIB	3 (01)	7 (03)	9 (05)	5 (02)	24 (11)
PHY	18 (01)	12 (04)	11 (01)	1 (00)	42 (06)
ST	09 (00)	16 (03)	12 (03)	2 (01)	39 (07)
Total	73 (07)	124 (42)	120 (35)	31 (10)	347 (94)

Soit un total de

347 (94) dont :

- Professeurs **73 (07)**
- Maîtres de Conférences **124 (42)**
- Chargés de Cours **120 (35)**
- Assistants **31 (11)**

() = Nombre de Femmes

94

TABLE OF CONTENTS

THESIS	I
TABLE OF CONTENTS	XIII
DECLARATION OF HONOR	XVIII
DEDICACE	XIX
ACKNOWLEDGEMENTS	XX
GLOSSARY	XXII
LIST OF FIGURES	XXV
LIST OF SCHEMES	XXIX
LIST OF TABLES	XXXI
ABSTRACT	XXXIV
RESUME	XXXVI
GENERAL INTRODUCTION	1
CHAPTER 1: LITERATURE REVIEW	5
I.1. GENERALITIES ON ONCHOCERCIASIS	6
I.1.1 Definition	6
I.1.2. Epidemiology	6
I.1.3. Transmission and development in human being	8
I.1.4. Treatment	9
I.2. GENERAL INFORMATION ON THE ANNONACEAE FAMILY	10
I.2.1. The genus <i>Duguetia</i> former <i>Pachypodanthium</i>	11
I.2.2. Botanical review on <i>D. staudtii</i>	11
I.2.3. Ethnomedicinal uses	13
I.2.4. Previous chemical studies on the genus <i>Duguetia</i>	14
I.2.5. Pharmacological activities of some isolated compounds from the genus <i>Duguetia</i>	16
I.2.6. Generalities on flavonoids	16
I.2.7. Generalities on Lignans	24
I.3. GENERAL INFORMATION ON THE HYPERICACEAE FAMILY AND ON THE GENUS <i>PSOROSPERMUM</i>	27
I.3.1. Hypericaceae family	27
I.3.2. The genus <i>Psorospermum</i>	27
I.3.2.1. BOTANICAL REVIEW ON <i>P. TENUIFOLIUM</i>	27
I.3.3. Biological review of the genus <i>Psorospermum</i>	33
I.3.4. Generalities on dihydroanthracénones	34
I.3.5. Review of Phenylpropanoids from medicinal plants	37
I.3.6. Review on the Liquid Chromatography-Mass Spectrometry (LC-MS)	41
CHAPTER 2: RESULTS AND DISCUSSION	63
CHAPTER 2: RESULTS AND DISCUSSION	64
II.1. PLANT MATERIAL, EXTRACTION, ISOLATION, LC-MS DETECTION AND STRUCTURAL IDENTIFICATION OF COMPOUNDS OF <i>DUGUETIA STAUDTII</i>	64
II.1.1. PLANT MATERIAL, EXTRACTION AND ISOLATION OF COMPOUNDS OF <i>DUGUETIA STAUDTII</i>	64
II.1.2. LC/MS DETECTION OF COMPOUNDS OF <i>DUGUETIA Staudtii</i>	67
II.1.3. CHARACTERISATION AND IDENTIFICATION OF ISOLATED COMPOUNDS OF <i>DUGUETIA STAUDTII</i>	71

II.2. PLANT MATERIAL, EXTRACTION, ISOLATION, LC-MS DETECTION AND STRUCTURAL IDENTIFICATION OF COMPOUNDS OF <i>PSOROSPERMUM TENUIFOLIUM</i> _____	113
II.2.1. PLANT MATERIAL, EXTRACTION AND ISOLATION OF COMPOUNDS OF <i>PSOROSPERMUM Tenuifolium</i> _____	113
II.2.2. LC-MS DETECTION OF COMPOUNDS OF <i>PSOROSPERMUM TENUIFOLIUM</i> _____	115
II.2.3. CHARACTERIZATION AND STRUCTURAL IDENTIFICATION OF COMPOUNDS OF <i>PSOROSPERMUM TENUIFOLIUM</i> _____	119
II.2.4. BIOGENETIC RELATIONSHIP OF ISOLATED COMPOUNDS _____	156
II.3. BIOLOGICAL ACTIVITIES _____	158
II.3.1. Main target: Microfilaricidal activity _____	158
II.3.2. Others activities _____	160
II.4. CHEMOTAXONOMIC AND CHEMOPHENETIC SIGNIFICANCE OF SOME COMPOUNDS ISOLATED RESPECTIVELY FROM <i>D. STAUDTII</i> AND <i>P. TENUIFOLIUM</i> _____	163
II.4.1. CHEMOTAXONOMIC SIGNIFICANCE OF SOME COMPOUNDS ISOLATED FROM <i>D. STAUDTII</i> _____	163
II.4.2. CHEMOPHENETIC SIGNIFICANCE OF SOME COMPOUNDS ISOLATED <i>P. TENUIFOLIUM</i> _____	163
GENERAL CONCLUSION AND PERSPECTIVES _____	165
CHAPTER 3: EXPERIMENTAL PART _____	168
CHAPTER 3: EXPERIMENTAL PART _____	169
III.1. MICROFILARICIDAL SCREENING OF CRUDE EXTRACTS _____	169
III.1.1. Preparation of stock solutions _____	169
III.1.2. Preparation of mammalian cells _____	169
III.1.3. Isolation of <i>Onchocerca ochengi microfilariae (mf)</i> and screening _____	169
III.1.4. Isolation of <i>O. ochengi</i> adult worms and screening _____	170
III.1.5. Isolation and screens on <i>Loa loa microfilariae</i> _____	171
III.2. UREASE ASSAY _____	172
III.3. X-RAY CRISTALLOGRAPHY OF SOME COMPOUNDS ISOLATED _____	172
III.3.1. X-ray analysis of costunolide _____	172
III.3.2. X-ray analysis of pachypodostyflavone _____	174
III.4. PRE-FORMULATION OF A PHYTODRUG FROM ACTIVE FRACTION DS 11 _____	176
III.4.1. Acute oral toxicity _____	176
III.4.2. Principle of the test _____	176
III.4.3. Procedure _____	177
III.4.4. Observation of animals and recording of the body weight. _____	177
III.5. GENERAL INSTRUMENTAL PROCEDURES _____	177
III.5.1. Plant material _____	178
III.5.2. Extraction of <i>D. staudtii</i> and <i>P. tenuifolium</i> _____	178
III. 6. CHARACTERISTIC TESTS OF CLASSES OF ISOLATED COMPOUNDS _____	184
III.6.1. Feric chloride ($FeCl_3$) test: characteristic for phenols _____	184
III.6.2. Shinoda test: characteristic for flavonoids _____	184
III.6.3. Liebermann-Burchard test: characteristic for triterpenoids and steroids _____	184
III.7. PHYSICAL AND SPECTROSCOPIC CHARACTERISTICS OF COMPOUNDS ISOLATED FROM BOTH PLANTS _____	185
REFERENCES _____	191

DECLARATION OF HONOR

I hereby declare that this thesis entitled “*Chemical study of Duguetia staudtii* Engl. & Diels Chatrou (Annonaceae) and *Psorospermum tenuifolium* Hook.f. (Hypericaceae): Microfilaricidal activities and LC-ESI-MS applications” was thought and written by myself under the Co-direction of Professor Simeon Fogue Kouam, Higher Teachers’ Training College, and Professor Jean Claude Tchouankeu, Faculty of Science, University of Yaounde I, within the framework of the Yaoundé-Bielefeld Graduate School for Natural Products with Antiparasite and Antibacterial Activity (YaBiNaPA).

I confirm that this work is original and therefore hasn’t yet been presented elsewhere.

Date: June 25, 2024

Venue: Yaounde, Cameroon

MBOBDA Wafo Alexis Sylvain, *MSc in Organic Chemistry*

In our capacity of Supervisors of the candidate’s thesis, we hereby certify that the above statements are true to the best our knowledge.

Date: June 25, 2024

Venue: Yaounde, Cameroon

KOUAM Fogue Simeon, *Professor* TCHOUANKEU Jean Claude, *Professor*

DEDICACE

This thesis is dedicated to the living souls of my family, the household of the saints and in loving recognition to my beloved mother Nana Marguerite, emeritus household coordinator now awaiting the return of Christ.

ACKNOWLEDGEMENTS

The present Ph.D research work was carried out at the Higher Teachers' Training College of the University of Yaoundé I and fully supported by the German Academic Exchanges Services (DAAD) through the Yaoundé-Bielefeld Bilateral Graduate School Natural Products with Antiparasite and Antibacterial Activity (YaBiNaPA);

I thank my supervisors: Professors Kouam Fogue Simeon and Tchouankeu Jean Claude for having accepted to supervise my works;

I am indebted to the head of the Department of Organic Chemistry of the Faculty of Science of University of Yaounde I, Professor Nkengfack Augustin Ephrem for his loving care;

I am also grateful to the Coordinators of the YaBiNaPA graduate School, Professors Sewald Norbert and Lenta Ndjakou Bruno for their leadership through the collaborative project between Bielefeld University (Germany) and the University of Yaoundé I (Cameroon);

I also wish to thank other members of the YaBiNaPA Graduate School namely Professor Ngadjui Tchaleu Bonaventure and Professor Kapche Wabo Gilbert Deccaux for their advices;

I would like to thank the lecturers of the Department of Organic Chemistry of the Faculty of Science and the Department of Chemistry of the Higher Teachers' Training College of the University of Yaoundé I for the training received;

My gratitude and sincere recognition to Dr. Mountessou, B.Y.G. and Dr. Ngouonpe, W.A along with to the members of my laboratory at the Higher Teachers' Training College of the University of Yaoundé I;

My special thanks and heartfelt blessings to my brothers and sisters, sons and daughters, grandsons and grand-daughters in and out the motherland as well as the household of the saints for their constant love, prayers and care;

Finally, special recognition to my fellow Ph.D students of the YaBiNaPA Graduate School namely Mbekou Kanko Ines Michelle, Tegasne Catherine, Wouamba Njonte Steven Collins, Pagna Mawouma Issah Julio, and to those who directly or indirectly shared the burden of this challenge in or out season.

To you all, Thanks and God bless you in the compassionate and prevailing name of our Lord Jesus-Christ.

Amen!

GLOSSARY

EtOAc	Ethyl acetate
<i>brd</i>	Broad doublet
<i>brs</i>	Broad singlet
ca.	Circa (used to indicate approximate and estimated data)
CC	Column Chromatography
CoA	Coenzyme A
DEPT	Distortionless Enhancement by Polarization Transfer
COSY	Correlated Spectroscopy
HMBC	Heteronuclear Multiple Bond Connectivity
HMQC	¹ H-detected Heteronuclear Multiple Quantum Coherence
HRESIMS	High Resolution Electrospray Ionization Mass Spectrum
NMR	Nuclear Magnetic Resonance
<i>s</i>	Singlet
<i>d</i>	Doublet
<i>t</i>	Triplet
<i>dd</i>	Doublet of doublet
<i>dt</i>	Doublet of triplet
<i>ddd</i>	Doublet of doublet of doublet
DMSO	Dimethylsulfoxide
PE	Petroleum Ether
DCM	Dichloromethane
MeOH	Methanol
XRD	X-ray Diffraction
IR	Infra-red
UV	Ultraviolet
UV-vis	Ultraviolet visible
FT-IR	Fourier Transform – Infrared Spectroscopy
TLC	Thin Layer Chromatography
VLC	Vacuum Liquid Chromatography
SLC	Solid Liquid Chromatography
<i>J</i>	Coupling constant

<i>m</i>	Multiplet
mp	Melting point
mult.	Multiplicity
[M+H] ⁺	Pseudomolecular ion
ppm	Part <i>per</i> million (chemical shift unit)
FDA	Food and Drug Administration
WHO	World Health Organization
NTD	Neglected Tropical Disease
DEC	Diethylcarbamazine
DAAD	German Academic Exchange Service
LC-MS	Liquid Chromatography Mass Spectrometry
YaBiNaPA	Yaounde-Bilefeld Graduate School Natural Products with Antiparasite and Antibacterial Activity
PhD	Doctor of Philosophy
APOC	African Programme for Onchocerciasis Control
RP-HPLC	Reverse phase High Pressure Liquid Chromatography
HPLC	High Pressure Liquid Chromatography
DCCC	Droplet Counter-Current Chromatography
¹³ C	Carbon-13
¹ H	Proton
GPS	Global Positioning System
HNC	Herbier National du Cameroun
MTT	Tetrazolium salts
APCI	Atmospheric Pressure Chemical Ionization
MALDI	Matrix-Assisted Laser Desorption/Ionization
MS	Mass Spectrometry
EI	Electron Impact
CI	Chemical Ionization
FAB	Fast Atom Bombardment
ESI	Electrospray Ionization
WGS	Wideband Global Satcom
BPC	Base Peak Chromatogram

MSE	Molecular Size Exclusion
LIT	Linear Ion Trap
EM	Electron Multipliers
FC	Faraday Cup
mf	microfilariae
PSI	Pounds / Square Inch
CFM	Cubic Feet / Minute
SFC	Supercritical Fluid Chromatography
POC	Point of Care

LIST OF FIGURES

FIGURE 1. ESTIMATED PREVALENCE OF EYE WORM HISTORY IN AFRICA (A) AND CAMEROON (B).....	6
FIGURE 2. GEOGRAPHIC DISTRIBUTION OF ONCHOCERCIASIS WORLDWIDE.....	7
FIGURE 3. LIFE CYCLE OF <i>O. VOLVULUS</i>	9
FIGURE 4. (A) TRUNK (MBOBDA, 2017), (B) LEAVES, AND (C) FRUITS OF <i>DUGUETIA STAUDTII</i>	12
FIGURE 5. VIEW OF GEOGRAPHIC DISTRIBUTION IN THE TROPICS AND IN CAMEROON OF <i>DUGUETIA STAUDTII</i>	12
FIGURE 6. TRUNC - SHRUBS, FLOWERS AND FRUIT OF <i>P. TENUIFOLIUM</i>	28
FIGURE 7. GEOGRAPHIC DISTRIBUTION OF THE SPECIES OF THE GENUS <i>PSOROSPERMUM</i> (REPRESENTED IN GREEN COLOR)	29
FIGURE 8. BASIC COMPONENTS OF A LC/MS SYSTEM.....	41
FIGURE 9. SCHEMATIC DIAGRAM ILLUSTRATING TOF IN MASS SPECTROMETRY.....	43
FIGURE 10. SCHEMATIC DIAGRAM OF A QUADRUPOLE CONSISTING OF FOUR PARALLEL METAL RODS AND EACH OPPOSING ROD PAIR IS CONNECTED TOGETHER ELECTRICALLY.....	43
FIGURE 11. SCHEMATIC DIAGRAM OF A LIT AND ORBITRAP OF ION TRAP.....	44
FIGURE 12. SCHEMATIC DIAGRAM OF A FOURIER TRANSFORM ION CYCLOTRON RESONANCE MASS SPECTROMETER.....	44
FIGURE 13. SCHEMATIC DIAGRAM ILLUSTRATING POPULAR ELECTRON IONIZATION METHODS FOR MS.....	46
FIGURE 14. SCHEMATIC DIAGRAM ILLUSTRATING CHEMICAL IONIZATION FOR MS.....	47
FIGURE 15. SCHEMATIC DIAGRAM ILLUSTRATING ATMOSPHERIC PRESSURE CHEMICAL IONIZATION (APCI) FOR MS.....	48
FIGURE 16. SCHEMATIC DIAGRAM ILLUSTRATING MALDI FOR MS (MUNSON, 2006).....	48
FIGURE 17. SCHEMATIC DIAGRAM ILLUSTRATING ELECTROSPRAY IONIZATION (ESI) FOR MS (MUNSON, 2006).....	49
FIGURE 18. SCHEMATIC DIAGRAM ILLUSTRATING HOW A DETECTED INCOMING ION IS CONVERTED INTO A MEASURABLE SIGNAL USING AN EM DETECTOR.....	50
FIGURE 19. SCHEMATIC DIAGRAM OF A FARADAY CUP ION DETECTOR.....	51
FIGURE 20. SCHEMATIC DIAGRAM OF A PHOTOMULTIPLIER CONVERSION DYNODE DETECTOR.....	51
FIGURE 21. SCHEMATIC DIAGRAM OF NANOSCALE SECONDARY ION MASS SPECTROMETER WITH A DOUBLE FOCUSING MAGNETIC SECTION MASS SPECTROMETER INCORPORATING A MULTICollectOR SYSTEM AND STATIC MAGNETIC FIELD....	52
FIGURE 22. NEW GENERATION OF PUMPS IN HPLC.....	53
FIGURE 23 : MACROSEP BIO AND BIO-GOLD WIDE PORE COLUMNS.....	54
FIGURE 24. CHROMEGAPORE MOLECULAR SIZE EXCLUSION (MSE) COLUMNS.....	55
FIGURE 25. GREENSEP SUPERCRITICAL FLUID CHROMATOGRAPHY (SFC) COLUMNS.....	56
FIGURE 26. THE INFLUENCE OF TURNAROUND TIME.....	59
FIGURE 27. LC-MS CHROMATOGRAM OF THE ACTIVE (DCM/MeOH (1:1, v/v - 250 µg/mL) EXTRACT OF <i>D. STAUDTII</i> (A).....	68
FIGURE 28. LC-MS CHROMATOGRAM OF THE ACTIVE DS11 (30 µg/mL) FRACTION OF <i>D. STAUDTII</i> (B).....	68
FIGURE 29. BPC OF TWO UNKNOWN COMPOUNDS (RT: 3.3 AND 3.4 MIN) AND TWO KNOWN (RT: 3.7 AND 3.9 MIN) DETECTED FROM THE SUB-FRACTION C.....	68
FIGURE 30. BPC OF ONE UNKNOWN COMPOUND DETECTED FROM THE SUB-FRACTION D OF <i>D. STAUDTII</i> RESPECTIVELY AT RT: 4.1 MIN (E).....	68
FIGURE 31. BPC OF ONE UNKNOWN COMPOUND DETECTED FROM THE SUB-FRACTION E OF <i>D. STAUDTII</i> RESPECTIVELY AT RT: 5.2 (F) MIN.....	69
FIGURE 32. HR-ESI-MS SPECTRUM OF DSB 1.....	71
FIGURE 33. EXPERIMENTAL FT-IR SPECTRUM OF DSB 1 IN METHANOL.....	72
FIGURE 34. EXPERIMENTAL UV-VIS SPECTRA OF DSB 1 IN METHANOL.....	72

FIGURE 35. ^{13}C NMR (125 MHz, CDCl_3) SPECTRUM OF DSB 1	73
FIGURE 36. ^1H NMR (500, CDCl_3) SPECTRUM OF DSB 1	73
FIGURE 37. DEPT 135 SPECTRUM OF DSB 1	74
FIGURE 38. HMQC SPECTRUM OF DSB 1	74
FIGURE 39. HMBC SPECTRUM OF DSB 1	76
FIGURE 40. COSY SPECTRUM OF DSB 1	76
FIGURE 41. HR-ESI-MS SPECTRUM OF DSB 2	79
FIGURE 42. ^1H NMR SPECTRUM OF DSB 2 (500 MHz, CDCl_3)	80
FIGURE 43. HMQC SPECTRUM OF DSB 2	80
FIGURE 44. HR-ESI-MS SPECTRUM OF DSB 3	82
FIGURE 45. ^1H NMR SPECTRUM (500 MHz, CDCl_3) OF DSB 3	83
FIGURE 46. ^{13}C NMR SPECTRUM (100 MHz, PYRIDINE- D_5) OF DSB 3	83
FIGURE 47. HR-ESI-MS SPECTRUM OF DSB 4	85
FIGURE 48. ^1H NMR SPECTRUM (500 MHz, MeOH) OF DSB 4	86
FIGURE 49. ^{13}C NMR SPECTRUM OF DSB 5 (100 MHz, CD_3OD)	89
FIGURE 50. ^1H NMR SPECTRUM OF DSB 5 (400 MHz, CD_3OD)	89
FIGURE 51. HMBC SPECTRUM OF DSB 5	90
FIGURE 52. NOESY SPECTRUM OF DSB 5	91
FIGURE 53. DEPT - HSQC SPECTRUM OF DSB 5	91
FIGURE 54. COSY SPECTRUM OF DSB 5	92
FIGURE 55. HR-ESI -MASS SPECTRUM OF DSB 6	94
FIGURE 56. ^{13}C - NMR SPECTRUM (125 MHz, CDCl_3) OF DSB 6	95
FIGURE 57. ^1H - NMR SPECTRUM (500 MHz, CDCl_3) OF DSB 6	96
FIGURE 58. NOESY SPECTRUM OF DSB 6	96
FIGURE 59. HR-ESI-MS SPECTRUM OF DSB 7	98
FIGURE 60. ^1H - NMR SPECTRUM (500 MHz, CDCl_3) OF DSB 7	98
FIGURE 61. DEPT SPECTRUM OF DSB 7	100
FIGURE 62. HR-ESI-MS SPECTRUM OF DSB 8	101
FIGURE 63. ^{13}C -NMR SPECTRUM (125 MHz, ACETONE- D_6) OF DSB 8	102
FIGURE 64. ^1H - NMR SPECTRUM (500 MHz, ACETONE- D_6) OF DSB 8	102
FIGURE 65. COSY SPECTRUM OF DSB 8	103
FIGURE 66. DEPT 135 SPECTRUM OF DSB 8	103
FIGURE 67. HMBC SPECTRUM OF DSB 8	104
FIGURE 68. HR-ESI-MS SPECTRUM OF DSB 9	106
FIGURE 69. ^{13}C - NMR SPECTRUM (125 MHz, PYRIDINE- D_5) OF DSB 9	107
FIGURE 70. ^1H - NMR SPECTRUM (500 MHz, PYRIDINE- D_5) OF DSB 9	107
FIGURE 71. HR-ESI-MASS SPECTRUM OF DSB 10	109
FIGURE 72. ^{13}C -NMR (125 MHz, CDCl_3 AND CD_3OD) OF DSB 10	110
FIGURE 73. ^1H -NMR (500 MHz, CD_3OD) OF DSB 10	110
FIGURE 74. BPC OF TWO UNKNOWN COMPOUNDS (R_T : 4.2 AND 6.0 MIN) AND VISMIONE D (R_T : 4.8 MIN) DETECTED FROM THE CRUDE EXTRACT OF <i>P. tenuifolium</i> – BELOW 74A. CHROMATOGRAM OF THE CRUDE EXTRACT OF <i>P. tenuifolium</i> FOR THE DETECTION OF EMODIN AND 74B. BPC OF THE PUR COMPOUND EMODIN (R_T : 3.8 MIN) DETECTED THROUGH THE LC-MS GUIDED ISOLATION FROM THE CRUDE EXTRACT OF <i>P. tenuifolium</i>	115
FIGURE 75. CHROMATOGRAM OF THE SUB-FRACTION B' OF THE CRUDE EXTRACT OF <i>P. tenuifolium</i>	117

FIGURE 76. BPC OF THE PUR COMPOUND (+)-CATECHIN (R_T : 1.5 MIN) DETECTED THROUGH THE LC-MS GUIDED ISOLATION FROM THE SUB-FRACTION B' OF THE CRUDE EXTRACT OF <i>P. TENUIFOLIUM</i>	117
FIGURE 77. HR-ESI-MASS SPECTRUM OF PTB 1	119
FIGURE 78. IR SPECTRUM OF PTB 1 IN KBR.....	120
FIGURE 79. ^{13}C NMR SPECTRUM (125 MHz, PYRIDINE- D_5) OF PTB 1	120
FIGURE 80. ^1H NMR SPECTRUM (500 MHz, PYRIDINE- D_5) OF PTB 1.....	121
FIGURE 81. COSY SPECTRUM OF THE GLYCOSE MOIETY OF PTB 1	122
FIGURE 82. COSY SPECTRUM OF THE AA'BB' AND AA' MOIETIES OF PTB 1	122
FIGURE 83. KEY CROSS PEAKS ON HMBC SPECTRUM OF PTB 1	123
FIGURE 84. HMQC SPECTRUM OF PTB 1	124
FIGURE 85. HR-ESI-MASS SPECTRUM OF PTB 2	126
FIGURE 86. ^{13}C NMR SPECTRUM (125 MHz, ACETONE- D_6) OF PTB 2.....	127
FIGURE 87. ^1H NMR SPECTRUM (500 MHz, ACETONE- D_6) OF PTB 2	127
FIGURE 88. HR-ESI-MASS SPECTRUM OF PTB 3	129
FIGURE 89. ^1H NMR SPECTRUM (500 MHz, CDCl_3) OF PTB 3.....	130
FIGURE 90. HR-ESI-MS OF PTB 4.....	132
FIGURE 91. ^1H NMR SPECTRUM (500 MHz, ACETONE- D_6) OF PTB 4	133
FIGURE 92. HR-ESI-MS OF PTB 5	136
FIGURE 93. ^{13}C - NMR SPECTRUM OF PTB 5 (125 MHz, ACETONE - D_6).....	136
FIGURE 94. ^1H NMR SPECTRUM OF PTB 5 (500 MHz, ACETONE - D_6)	136
FIGURE 95. DEPT 135 SPECTRUM OF PTB 5	137
FIGURE 96. ^{13}C - NMR SPECTRUM (125 MHz, CDCl_3) OF PTB 6	139
FIGURE 97. ^1H - NMR SPECTRUM (500 MHz, CDCl_3) OF PTB 6	139
FIGURE 98. DEPT 135 SPECTRUM OF PTB 6	140
FIGURE 99. ^{13}C NMR SPECTRUM (125 MHz, CDCl_3) OF PTB 7	142
FIGURE 100. ^1H - NMR SPECTRUM (500 MHz, CDCl_3) OF PTB 7.....	142
FIGURE 101. DEPT 135 SPECTRUM OF PTB 7	143
FIGURE 102. HR-ESI-MS SPECTRUM OF PTB 8.....	145
FIGURE 103. ^1H NMR SPECTRUM OF PTB 8	146
FIGURE 104. COSY SPECTRUM OF PTB 8	146
FIGURE 105. ^{13}C NMR SPECTRUM OF PTB 9.....	148
FIGURE 106. ^1H -NMR SPECTRUM OF PTB 9	149
FIGURE 107. DEPT 135 NMR SPECTRUM OF PTB 9.....	149
FIGURE 108. ^1H -NMR SPECTRUM OF PTB 10.....	150
FIGURE 109. DEPT 135 SPECTRUM OF PTB 10.....	151

LIST OF SCHEMES

SCHEME 1. STRUCTURES OF SOME IMPORTANT CLASSES OF FLAVONOIDS.....	17
SCHEME 2. BASIC FLAVONES SKELETON	18
SCHEME 3. THE SHIKIMIC ACID AS PRECURSOR FOR THE SYNTHESIS OF L-PHE AND PHENOLIC COMPOUNDS.....	18
SCHEME 4. GENERAL PHENYLPROPANOID AND FLAVONOID BIOSYNTHETIC PATHWAYS	19
SCHEME 5. ABSORPTION BANDS OF THE BENZOYL AND CYNAMOYL SYSTEMS	21
SCHEME 6. DIAGNOSTIC MASS SPECTRAL FRAGMENTATION PATHWAYS FOR FLAVONES	24
SCHEME 7. BASIC STRUCTURE OF DIHYDROANTHRACENONES.....	34
SCHEME 8. DEGRADATION OF DIHYDROANTHRACENONES (VISMIONE) IN SOLUTION	35
SCHEME 9. COMMON ATROCHRYSONE SKELETON FOR DIHYDROANTHRACENONES	35
SCHEME 10. BASIC STRUCTURE 9,10-ANTHRACENEDIONE	36
SCHEME 11. (A) POLYKETIDE PATHWAY FOR ANTHRAQUINONE BIOSYNTHESIS. (B) SHIKIMATE PATHWAY FOR ANTHRAQUINONE BIOSYNTHESIS	36
SCHEME 12. DIVERSIFICATION OF PHENYLPROPANOIDS BASED ON THE GENERAL PHENYLPROPANOID PATHWAY	38
SCHEME 13. EXTRACTION AND ISOLATION FLOWCHART OF COMPOUNDS FROM THE BARK OF <i>D. STAUDTII</i>	65
SCHEME 14. EXTRACTION AND ISOLATION FLOWCHART OF COMPOUNDS FROM THE BARK OF <i>D. STAUDTII</i>	67
SCHEME 15. KEYS HMBC CORRELATIONS (A) AND A VIEW OF THE XRD (B) OF DSB 1	77
SCHEME 16. KEY NOESY AND HMBC CORRELATIONS OF COMPOUND DSB 5	92
SCHEME 17. EXTRACTION AND ISOLATION FLOWCHART OF COMPOUNDS FROM THE STEM BARK OF <i>P. TENNUIFOLIUM</i> .	114
SCHEME 18. HYDROLYSIS REACTION (A) AND KEY COSY (BLUE) AND SELECTED HMBC (RED) CORRELATIONS (B) OF PTB 1	124
SCHEME 19. SELECTED HMBC CORRELATIONS OF PTB 2	128
SCHEME 20. KEY HMBC (BLUE) CORRELATIONS OF PTB 5	138
SCHEME 21. HYPOTHETICAL BIOSYNTHETIC PATHWAY LEADING TO MAIN ISOLATED COMPOUNDS FROM <i>D. STAUDTII</i>	156
SCHEME 22. HYPOTHETICAL BIOSYNTHETIC PATHWAY LEADING TO ISOLATED COMPOUNDS FROM <i>P. TENNUIFOLIUM</i>	157
SCHEME 23. HYPOTHETICAL STRUCTURE–ACTIVITY RELATIONSHIPS OF THREE ISOLATED FLAVONOIDS	162
SCHEME 24. (A) ORTEP REPRESENTATION AS DETERMINED BY X-RAY, AND (B) THEORETICALLY OPTIMISED STRUCTURE OF COSTUNOLIDE 110 THROUGH RIGAKU SUPERNOVA DIFFRACTOMETER	173
SCHEME 25. 3D STRUCTURE OF PACHYPODOSTYFLAVONE 105 THROUGH RIGAKU SUPERNOVA DIFFRACTOMETER	175
SCHEME 26. HPLC COLUMNS.....	180

LIST OF TABLES

TABLE 1. PHYLOGENIC CLASSIFICATION OF <i>ONCHOCERCA VOLVULUS</i>	8
TABLE 2. TAXONOMIC CLASSIFICATION OF THE GENUS <i>DUGUETIA</i>	11
TABLE 3. COMMON NAMES OF <i>DUGUETIA STAUDTII</i> LOCALLY USED IN AFRICA.....	13
TABLE 4. TETRAHYDROJATRORRHIZINE AND TETRAHYDROPROTOBERBERINE ALKALOIDS FROM CHEMICALLY INVESTIGATED <i>DUGUETIA</i> SPECIES.....	14
TABLE 5. PHARMACOLOGY ACTIVITIES OF SOME COMPOUNDS AND CHEMOTAXONOMIC MARKERS FROM <i>DUGUETIA</i> GENUS	16
TABLE 6. UV ABSORPTION RANGES FOR FLAVONOIDS (MARKAHM, 1982; AGRAWAL 1989).....	22
TABLE 7. ¹ H-NMR CHEMICAL SHIFTS FOR FLAVONOIDS (MABRY AND MARKHAM, 1975).....	22
TABLE 8. NOMENCLATURE OF LIGNANS.....	26
TABLE 9. TAXONOMIC CLASSIFICATION OF THE GENUS <i>PSOROSPERMUM</i>	28
TABLE 10. SOME LOCAL NAMES USED IN AFRICA IN THE GENUS <i>PSOROSPERMUM</i>	29
TABLE 11. TRITERPENES ISOLATED FROM <i>PSOROSPERMUM</i> SPECIES.	31
TABLE 12. FLAVONOIDS ISOLATED FROM <i>PSOROSPERMUM</i> SPECIES.....	31
TABLE 13. SOME XANTHONES ISOLATED FROM <i>PSOROSPERMUM</i> SPECIES.....	31
TABLE 14. VISMIONES ISOLATED FROM <i>PSOROSPERMUM</i> SPECIES.....	32
TABLE 15. SOME ANTHRONES ISOLATED FROM <i>PSOROSPERMUM</i> SPECIES.....	32
TABLE 16. ANTHRANOL AND LACTONE ISOLATED FROM <i>PSOROSPERMUM</i> SPECIES	32
TABLE 17. SOME BIANTRONES ISOLATED FROM <i>PSOROSPERMUM</i> SPECIES.....	33
TABLE 18. SOME ANTHRAQUINONES ISOLATED FROM <i>PSOROSPERMUM</i> SPECIES	33
TABLE 19. LIST OF BIOLOGICAL ACTIVITIES REPORTED FROM CERTAIN SPECIES OF THE GENUS <i>PSOROSPERMUM</i>	34
TABLE 20. SOME PHENYLPROPANOIDS FROM THE HYPERICACEAE FAMILY	40
TABLE 21. SOME CHARACTERISTICS OF NEW GENERATION OF PUMPS IN HPLC	53
TABLE 22. SOME CHARACTERISTICS OF WIDE PORE COLUMNS	54
TABLE 23. SOME CHARACTERISTICS OF MSE COLUMNS	55
TABLE 24. SOME CHARACTERISTICS OF SFC COLUMNS.....	56
TABLE 25. PEAK LIST WITH MASS-TO-CHARGE RATIO (M/Z) VALUES, RETENTION TIMES OF SOME DETECTED COMPOUNDS (1-30) FROM (DCM/MEOH (1:1, v/v) EXTRACT AND DS11 (30 µG/ML) FRACTION OF <i>D. STAUDTII</i>	69
TABLE 26. PEAK LIST WITH LISTED M/Z VALUES AND RETENTION TIMES OF SOME COMPOUNDS DETECTED FROM A SUB-FRACTION A34 OF <i>D. STAUDTII</i>	70
TABLE 27. ISOLATED COMPOUNDS FROM <i>D. STAUDTII</i> SORTED BY CLASS AND RETENTION TIME	70
TABLE 28. ¹ H- AND ¹³ C-NMR DATA OF COMPOUND DSB 1 IN CDCl ₃	78
TABLE 29. COMPARATIVE ¹ H-NMR DATA OF DSB 2 (500, CDCl ₃) WITH PACHYPODOL 16 (500, CDCl ₃)	81
TABLE 30. COMPARATIVE ¹ H-, ¹³ C-NMR DATA OF DSB 3 WITH KUMATAKENIN 106.....	84
TABLE 31. COMPARATIVE ¹ H-NMR DATA OF DSB 4 WITH MYRICETIN 3, 7, 3', 5'-TETRAMETHYL ETHER.....	87
TABLE 32. NMR SPECTRAL DATA (400 MHz, CDCl ₃) OF DSB 5	93
TABLE 33. COMPARATIVE ¹³ C-NMR SPECTRAL DATA OF DSB 6 (CDCl ₃) WITH PACHYPOSTAUDIN B.....	97
TABLE 34. COMPARATIVE ¹ H-, ¹³ C-NMR SPECTRAL DATA OF DSB 7 (125 MHz, CDCl ₃) WITH PACHYPOPHYLLIN 13 (75 MHz, CDCl ₃).....	100
TABLE 35. COMPARATIVE ¹³ C (125 MHz, CDCl ₃) NMR SPECTRAL DATA OF DSB 8 WITH COSTUNOLIDE 110 ¹³ C (100 MHz, CDCl ₃) NMR	105
TABLE 36. COMPARATIVE ¹ H-NMR SPECTRAL DATA OF DSB 9 IN PYRIDINE-D ₅ WITH CORYPALMINE 5.....	108

TABLE 37. COMPARATIVE ¹³ C-NMR SPECTRAL DATA OF DSB 10 WITH POLYCARPOL AND ANOMANOL A.	112
TABLE 38. NON EXHAUSTIVE PEAK LIST FOR DETECTED COMPOUNDS WITH LISTED M/Z VALUE AND RETENTION TIME FROM <i>PSOROSPERMUM SP.</i>	118
TABLE 39. COMPOUNDS ISOLATED PER CLASS FROM THE STEM BARK OF <i>P. TENUIFOLIUM</i>	118
TABLE 40. ¹ H (500 MHz) AND ¹³ C (125 MHz) NMR ASSIGNMENTS OF PTB 1 IN PYRIDINE- <i>D</i> ₅	125
TABLE 41. ¹³ C-NMR DATA OF PTB 2 AND EMODIN 77	128
TABLE 42. ¹ H-NMR DATA OF PTB 3 AND OF PHYSCION 79 IN CDCl ₃	131
TABLE 43. COMPARISON OF ¹ H- (500 MHz) NMR DATA OF PTB 4 IN ACETONE- <i>D</i> ₆ AND OF 2-PRENYLEMODIN IN DMSO- <i>D</i> ₆	134
TABLE 44. COMPARISON OF ¹ H- (500 MHz) NMR DATA OF PTB 5 IN ACETONE- <i>D</i> ₆ AND ¹ H- (60 MHz) NMR DATA OF 2-GERANYLEMODIN IN DMSO- <i>D</i> ₆	137
TABLE 45. COMPARISON OF ¹ H- (500 MHz) NMR DATA OF PTB 6 AND ¹ H- (60 MHz) NMR DATA OF 3-GERANYLOXYEMODIN IN CDCl ₃	140
TABLE 46. COMPARISON OF ¹ H- (500 MHz) NMR DATA OF PTB 7 AND ¹ H- (400 MHz) NMR DATA BIANTHRONE A3A/3B IN CDCl ₃	144
TABLE 47. COMPARATIVE ¹ H (500 MHz, ACETONE - <i>D</i> ₆) NMR DATA OF PTB 8 WITH THOSE OF (+)-CATECHIN 64 ...	147
TABLE 48. COMPARATIVE ¹³ C-NMR DATA OF PTB 9 (DMSO- <i>D</i> ₆) WITH BETULINIC ACID (BA); PTB 10 (CDCl ₃) WITH LUPEOL AND PTB 11 (CDCl ₃) WITH LUPEOL ACETATE (LA).....	153
TABLE 49 : COMPARATIVE ¹ H-NMR DATA OF PTB 12 WITH DAUCOSTEROL 118	155
TABLE 50. <i>ONCHOCERCA OCHENGI</i> MICROFILARIAE (MF) PRIMARY SCREEN	158
TABLE 51. SCREENING OF FRACTIONS ON <i>O. OCHENGI</i> ADULT WORMS AND (MF) OF <i>D. STAUDTII</i>	159
TABLE 52. CYTOTOXIC POTENCIES OF SOME COMPOUNDS ON KB3-1 CELL LINES.....	161
TABLE 53. IC ₅₀ FOR SOME COMPOUNDS ISOLATED FROM <i>D. STAUDTII</i>	161
TABLE 54. CRYSTAL DATA AND STRUCTURE REFINEMENT FOR COSTUNOLIDE 110.....	174
TABLE 55. CRYSTAL DATA AND STRUCTURE REFINEMENT FOR DSB 1.....	176
TABLE 56. CHROMATOGRAM OF THE FRACTIONATION OF 114.0 G AFTER THE PARTITION OF 150.0 G OF THE C.E. OF <i>D. STAUDTII</i>	179
TABLE 57. VLC OF THE BIOACTIVE EXTRACT OF THE STEM BARK OF <i>D.</i>	180
TABLE 58. CHROMATOGRAM OF THE DCM SOLUBLE AND BIOACTIVE FRACTION A OF <i>D. STAUDTII</i>	181
TABLE 59. CHROMATOGRAM OF THE SUB-FRACTION A34 FROM THE DCM SOLUBLE FRACTION OF <i>D. STAUDTII</i>	181
TABLE 60. CHROMATOGRAM OF THE MEOH SOLUBLE FRACTION B OF THE STEM BARK OF <i>D. STAUDTII</i>	182
TABLE 61. SLP OF THE BIOACTIVE EXTRACT OF THE STEM BARK OF <i>P. TENUIFOLIUM</i>	182
TABLE 62. CHROMATOGRAM OF THE SUB-FRACTION B' FROM THE EtOAc SOLUBLE FRACTION OF <i>P. TENUIFOLIUM</i>	183
TABLE 63. CHROMATOGRAM OF THE SUB-FRACTION F9 FROM THE EtOAc SOLUBLE FRACTION OF <i>P. TENUIFOLIUM</i>	183
TABLE 64. CHROMATOGRAM OF THE SUB-FRACTIONS F11 AND F12 FROM THE EtOAc COMBINED TO FRACTION C' FROM BUOH SOLUBLE FRACTION OF <i>P. TENUIFOLIUM</i>	184

ABSTRACT

This thesis presents the “Chemical study of *Duguetia staudtii* Engl. & Diels Chatrou (Annonaceae) and *Psorospermum tenuifolium* Hook.f. (Hypericaceae): Microfilaricidal activities and LC-ESI-MS applications”. The chemical study carried out on extracts from the bark of the two plants yielded four active fractions. Following the method described by Cho-Ngwa et al. (2010), *D. staudtii* extract was 100% active on microfilariae and scrutinized at 250 mg/ml, followed by DS11 fraction which was tested at 30 mg/ml. By means of Liquid Chromatography Mass Spectrometry (LC-MS), sixteen (16) compounds were detected from both plants among which three (03) new (DSB 1, DSB 5 and PTB 1) along with thirteen (13) already known. Among the latter compounds, twelve (12) and the non detected ones (06) were isolated later on from the dichloromethane/methanol (1:1, v/v) extracts and all their structures were completely elucidated through chromatographic methods such as Column Chromatography (CC), Thin Layer Chromatography (TLC) and on the basis of their spectroscopic data such as basic one- and two-dimensional Nuclear Magnetic Resonance spectroscopy (1D, and 2D-NMR), Infrared spectroscopy (IR spectroscopy) and Ultra-Violet spectroscopy (UV spectroscopy). In addition, the Melting Point (MP) and the Optical Rotation (OR) of some compounds have been provided. Moreover, some structures were determined by comparison with their NMR data obtained from the literature.

Overall, among the compounds obtained, three (03) were found to be new derivatives and nineteen (19) were already reported in the literature. The isolated compounds are sorted into nine (09) classes of secondary metabolites as follows:

- **05 flavonoids:** Pachypodostyflavone 105 which is a novel derivative isolated from *Duguetia staudtii* along with pachypodol 16, kumatakenin 106, 5,4'-dihydroxy-3,7,3',5'-tetramethoxy flavone 107 and (+)-catechin 64;
- **03 bisnorlignans:** Pachypolignan 109, a new derivative in addition to pachypophillin 13 and pachypostaudin-B 11;
- **01 alkaloid:** Corypalmine 5;
- **01 sesquiterpene:** Costunolide 110, a newly isolated derivative from the genus *Duguetia* also;
- **01 new phenylpropanoid glycoside derivative :** Psorospermoside 113, isolated from *Psorospermum tenuifolium*;

- **04 triterpenoides:** Lupeol [116](#), lupeol acetate [117](#), betulinic acid [60](#), polycarpol [111](#);
- **01 steroid:** Daucosterol [118](#);
- **01 bianthrone:** Bianthrone A3a/A3b [115](#);
- **05 anthraquinones:** 3-geranyloxyemodin [55](#), 2-geranylemodin [114](#), 2-prenyl emodin [78](#), emodin [77](#) and physcion [79](#);

Furthermore, the new derivative pachypodostyflavone [105](#), isolated as crystal, was obtained from the XRD experiment using a Rigaku supernova diffractometer that permitted to deduce the absolute configuration of the chiral centre assigned as (S). In addition, costunolide was also obtained as a crystal and its X-ray crystallography also carried out and its two chiral centre were found to be assigned as (6R, 7S).

The detection of constituents from the two plants done by LC-MS and the Scifinder database, along with the literature review were useful to differentiate between novel and known secondary metabolites.

In addition, several compounds were submitted to antiinflammatory tests. Thus 5,4'-dihydroxy-3,7,3'5'-tetramethoxyflavone [107](#), pachypodol [16](#) and kumakatemin [106](#), showed a good activity with IC₅₀ ranging from 3.89 to 14.13 µg/mL on luminol/zymosan and lucigenin, compared to the reference drug ibuprofen (14.30 µg/mL). The new compound pachypolignan [109](#) showed a notable urease inhibition with an IC₅₀ of 20.2 µg/mL compared to 21.6 µg/mL for the potent inhibitor Thiourea.

The extract and compounds of *Psorospermum tenuifolium* were evaluated for their cytotoxic activities on human squamous cell carcinoma KB-3-1. Although this extract was not active, it contained the most active compounds **emodin** [77](#) and **2-geranylemodin** [114](#) with potencies (IC_{50s}: **11.4 µM**; **19.0 µM**) respectively close to the standard drug **griseofulvin** (17-21 µM).

Keywords: *Duguetia staudtii*, *Psorospermum tenuifolium*, lignan, flavone, antifilaricidal, LC/MS.

RESUME

Cette thèse présente « l'étude chimique de *Duguetia staudtii* Engl. & Diels Chatrou (Annonaceae) et *Psorospermum tenuifolium* Hook.f. (Hypericaceae) : Activités microfilaires et Applications à la CL-SM ». En effet, l'étude chimique menée sur les extraits des deux plantes a conduit à 4 fractions actives. Par la méthode décrite par Cho-Ngwa et al. (2010), l'extrait de *D. staudtii* avec 100% d'inhibition sur les microfilaires a été testé à 250 mg/ml, suivi de sa fraction active DS11 testée à 30 mg/ml. A la faveur de la Chromatographie Liquide couplée à la Spectrométrie de Masse (CLSM), seize (16) composés ont été détectés parmi lesquels trois (03) nouveaux (DSB 1, DSB 5 et PTB 1) ainsi que treize (13) autres déjà connus de la littérature. Douze (12) de ces derniers et ceux non-détectés (06) furent isolés à partir des extraits au dichlorométhane/méthanol (1:1 ; v/v) et toutes leurs structures ont été complètement élucidées par des méthodes chromatographiques telles que la Chromatographie sur Colonne (CC), la Chromatographie sur Couche Mince (CCM) et sur la base de leur données spectroscopiques telles que la Résonance Magnétique Nucléaire à une et deux dimensions (1D, 2D-RMN), la spectroscopie Infra rouge (IR) et la spectroscopie Ultra-violet (UV). De plus, les points de fusion et le pouvoir rotatoire de certains composés ont été donnés. Certains composés ont été déterminés en comparaison à ceux déjà décrits dans la littérature.

En général, parmi les composés isolés, trois (03) sont des dérivés nouveaux et dix-neuf (19) ont déjà été décrits dans la littérature. Les composés isolés sont regroupés en neuf (09) classes de métabolites secondaires ainsi qu'il suit :

- **05 flavonoïdes** : pachypodostyflavone 105 qui est un dérivé nouveau isolé de *Duguetia staudtii*, pachypodol 16, kumatakenine 106, 5,4'-dihydroxy-3,7,3',5'-tétraméthoxyflavone 107 et (+)-catechine 64;
- **03 bisnorlignanes** : pachypolignan 109 qui est un dérivé nouveau y compris le pachypophilin 13 et la pachypostaudin- B 11 ;
- **01 alcaloïde** : corypalmine 5;
- **01 sesquiterpène** : costunolide 110, un dérivé nouvellement isolé du genre *Duguetia* ;
- **01 glycoside de phenylpropanoïde**: psorospermoside 113 qui est un dérivé nouveau isolé de *Psorospermum tenuifolium* ;
- **04 triterpénoïdes** : lupéol 116, acétate de lupéol 117, acide bétulinique 60 et polycarpol 111;

- **01 stéroïde** : Daucosterol 118;
- **01 bianthrone** : bianthrone A3a/A3b 115;
- **05 anthraquinones** : 3-geranyloxyemodin 55, 2-géranylemodin 114, 2-prenyl emodin 78, émodine 77 et le physcion 79 ;

De plus, le dérivé nouveau pachypodostyflavone 105, obtenu sous forme cristalline a été entièrement caractérisé par un diffractomètre de type Rigaku supernova et la configuration absolue du centre chiral a été trouvé comme égal à (S). Par ailleurs, le composé connu costunolide a été aussi obtenu sous forme cristalline et son analyse cristallographique a permis d'attribuer aux deux carbones chiraux la configuration absolue (6R, 7S).

Pour différencier les métabolites secondaires nouveaux de ceux déjà connus, les constituants du mélange de chaque plante ont été soumis à l'analyse LC-MS afin de les détecter au moyen de la base de données Scifinder et au regard de la revue de la littérature existante.

Plusieurs composés ont été soumis aux tests d'activités antiinflammatoires. Ainsi, les composés : 5,4'-dihydroxy-3,7,3'5'-tetramethoxyflavone 107, pachypodol 16 et kumakatenine 106, ont montré une meilleure activité avec des Cl_{50} de l'ordre de 3,89 à 14,13 μ M sur les luminol/zymosan et lucigenin, comparé au médicament de référence l'ibuprofène ($Cl_{50} = 14.30 \mu$ M). Le composé nouveau pachypolignan a montré une inhibition à l'uréase avec une IC_{50} importante de l'ordre de 20,2 μ M contre 21,6 μ M pour l'inhibiteur de référence, la Thiourea.

L'évaluation de la cytotoxicité de l'extrait et des composés isolés de *P. tenuifolium* a été réalisée sur la lignée cellulaire KB-3-1 avec la **griséofulvine** comme référence ($Cl_{50} = 17-21 \mu$ M). Les résultats obtenus ont montré que l'extrait n'était pas actif mais contenait des composés plus actifs tels que l'**émodine** ($Cl_{50} = 11,4 \mu$ M) 77 et la **2-géranylemodine** ($Cl_{50} = 19 \mu$ M) 114 qui par contre ont présenté une activité proche de la référence.

Mots clés : *Duguetia staudtii*, *Psorospermum tenuifolium*, lignane, flavone, antifilaricidal, CL/MS



GENERAL INTRODUCTION

Throughout the history of civilization, humans have relied on natural products (NP) as a primary source of medicines. According to the World Health Organization (WHO), the significance of NP in health care is supported by a report that 80% of people worldwide still rely on traditional medicines for healthcare in general (WHO, 2019; Farnsworth et al. 1985) and in certain African countries, up to 90% of the population still relies exclusively on plants as a source of medicines specifically in Ethiopia where herbal remedies are used for their primary healthcare (Chintamunnee, 2012). However, following the fourth WHO (2017) report on neglected tropical diseases (NTDs), 17 diseases caused by bacteria and parasites, are classified as NTDs. Endemic in 149 tropical and subtropical countries, NTDs affect more than 1 billion people annually, including 875 million children in developing economies. These diseases are also responsible for over 500,000 deaths per year and are characterized by long-term disability and severe pain. Current clinically used drugs against NTDs are far from ideal. Some of the limitations associated with current chemotherapeutic agents include widespread drug resistance, severe adverse effects, lengthy treatment duration, unfavourable toxicity profiles, and complicated drug administration procedures. The use of some drug regimens is also jeopardized by their limited availability to overcome the effect of these NTDs worldwide. Among the NTDs listed in the WHO (2017) report, an estimated 37 million people almost exclusively in Africa, are currently infected by Onchocerciasis. This NTD caused by the filarial worm *Onchocerca volvulus* and transmitted from individual to individual by *Simulium* black flies that breed in fast flowing rivers, hit hardest those living in rural agricultural areas.

With respect to the NTDs, international control programmes for Onchocerciasis have been implemented since the 1970s. In fact, insecticide spraying to eliminate the vector was supplemented by, and ultimately replaced from the 1990s by, mass administration of ivermectin 1, the actual drug and the macrocyclic lactone currently recommended to kill microfilariae and prevent their release by the adult worms for several months. In 2015, 119 million people received ivermectin 1 treatment, representing 64.1% coverage of those requiring it. Unfortunately, ivermectin is not macrofilaricidal nor effective to tackle the adults' worms of this parasitic skin and eye disease. In addition, ivermectin 1 which is only a control measure has to be taken twice a year till the death of adult's worms which could occur 14 years later (Ndjonka et al 2018). Such a prolonged time of treatment raises the risk of resistance to the



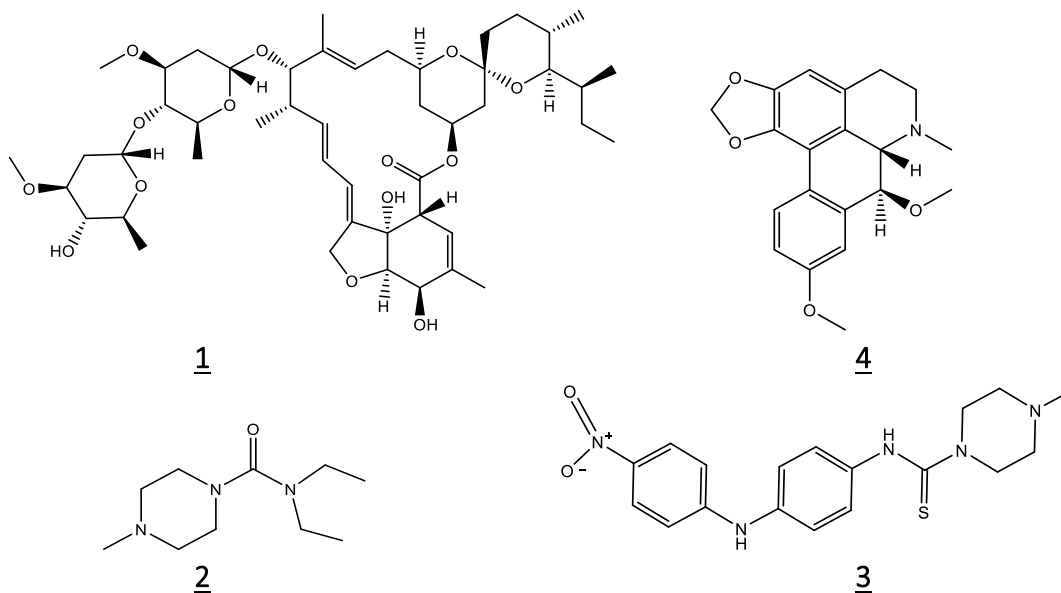
parasite. Moreover, the use of this drug is hampered in areas where Loiasis, a blood and tissue filariid parasite, and Onchocerciasis are co-endemic. As the result, the most important risk encountered in distributing Ivermectin 1 to patients in those areas is the development of an encephalopathic syndrome in people with very high levels of *Loa loa* and the presence of severe adverse events (Cho-Ngwa et al. 2016). Other available drugs such as diethylcarbamazine 2, amocazine 3, and many others are not always active at all stages of development of the parasite and also have serious and sometimes fatal side effects (Nyasse et al. 2006).

Due to the permanent problem faced by Ivermetin 1 through growing resistance induced by the human parasite *Onchocerca volvulus*, there is a constant need for the search of new drugs to improve the known ones in the treatment of diseases in the researchers' perspective. Therefore in the case of Onchocerciasis, many authors/investigators list the development of a macrofilaricide as the most needed item to guarantee elimination success. We agree but are aware of the technical difficulties and challenges associated with such an effort as well as the tedious and lengthy process of certifying the safety of such a drug, especially for mass distribution. If a candidate macrofilaricide were available and extremely safe, a rapid diagnostic test for live fertile adult worms would also be needed that would show to whom the drug should be given. Making this approach operational on a large scale is therefore crucial and, if successful, could be used as part of an integrated control program after transmission has been interrupted (Cupp et al. 2011).

According to the literature, several plants were assessed as potential sources of drug to give alternatives to the limitations observed on the previous and still current drugs used to date. In this regard, why do not try to solve this burden of the adult's worms with families of plants known to be effective? For instance, the barks of *Cassia fikifiki* and *Cassia aubrevilleri* are used in Liberian folk medicine against Onchocerciasis (Nyasse et al. 2006). In addition, few studies against parasite were conducted with *D. staudtii* (Ndjonka et al. 2018). Also, Titanji et al. (1990) evaluated the anti-Onchocerca ochengi activity in *vitro* on microfilariae, with Oliverine 4 from *D. staudtii* (Annonaceae). Despite the efforts employed for the control of onchocerciasis, to the best of our knowledge, the latter has remained a significant public health problem, due mainly to the lack of safe and effective adult worm drugs and/or microfilaricides that do not kill *Loa loa* microfilariae (mf) (Ngwewondo et al. 2019). Furthermore, apart from the claimed efficacy of *Psorospermum febrifugum*, another specie of the genus, in support of its use in the



traditional treatment of onchocerciasis, no scientific evidence for this claim has been documented (Abongwa et al. 2021). So, the emergency of alternative drugs need orientated research to medicinal plants as an effective option for better solutions against Onchocerciasis.



Therefore, the German Academic Exchange Service, DAAD, through the collaborative project between Bielefeld University, Germany, and the University of Yaoundé 1, Cameroon, gathered in the Yaoundé-Bielefeld Graduate School for Natural Products with Antiparasite and Antibacterial Activity, YaBiNaPA, has provided fundings and tools for educating PhD students in an interdisciplinary and translational way and also to create a scientific communication platform between biologists, chemists, pharmacologists, the public, and traditional healers. The aim being also as part of our thesis, to contribute to the ongoing fight against the adult worms by searching a safe and active fraction to formulate an anti-*onchocerca* lead compound that could help to tackle the parasite *onchocerca volvulus* of Onchocerciasis. To achieve this objective, and on the basis of ethnopharmacological information, we have focused our attention on “**Chemical study of *Duguetia staudtii* Engl. & Diels Chatrou (Annonaceae) and *Psorospermum tenuifolium* Hook.f. (Hypericaceae): Microfilaricidal activities and LC-ESI-MS Applications**”, two Cameroonian medicinal plants that are used by traditional healers against lots of targets such as cutaneous infections and subcutaneous wounds. More specifically, we tried:

- to harvest and extract the stem bark from both plants *D. staudtii* and *P. tenuifolium*;
- to first of all evaluate the biological activities and LC-ESI-MS analysis of the extracts;



- and to carry out phytochemical studies of the two plants studied.

This work is divided into three chapters: firstly the literature review on Onchocerciasis, Annonaceae and Hypericaceae families in chapter one, followed by Chapter two with the results and discussion while in the third chapter, we will focus on the experimental part, the “how to” of our thesis.



CHAPTER 1: LITERATURE REVIEW



I.1. GENERALITIES ON ONCHOCERCIASIS

I.1.1 Definition

Onchocerca is one of the largest genus within the Onchocercidae family with 34 described species which display a worldwide distribution (Lefoulon et al. 2017). Onchocerciasis is an eye and skin disease caused by a worm (filaria) known scientifically as *Onchocerca volvulus*. This genus is transmitted to humans through the bite of a blackfly (*simulium* species) and characterized by nodular swellings on the skin and eye lesions that can result in blindness (Djafsia et al. 2015). Its life cycle begins with copulation and fertilization of the female by the male worm. (Hendy, 2018) reported that Blacklock through his work in Sierra Leone in 1926, firstly discovered that Onchocerciasis was a vector-borne disease and demonstrated that *O. volvulus* larvae (microfilariae) develop to transmissible (infective) stages in human biting blackflies (Cupp et al. 2011).

I.1.2. Epidemiology

Onchocerca volvulus is thought to have originated from an ancestral bovine parasite that was probably introduced to humans during the domestication of cattle in Africa (WHO, 2015). *Onchocerca* infections are found in tropical climates. The main burden is in 31 countries in sub-Saharan Africa including Cameroon (Figure 1).

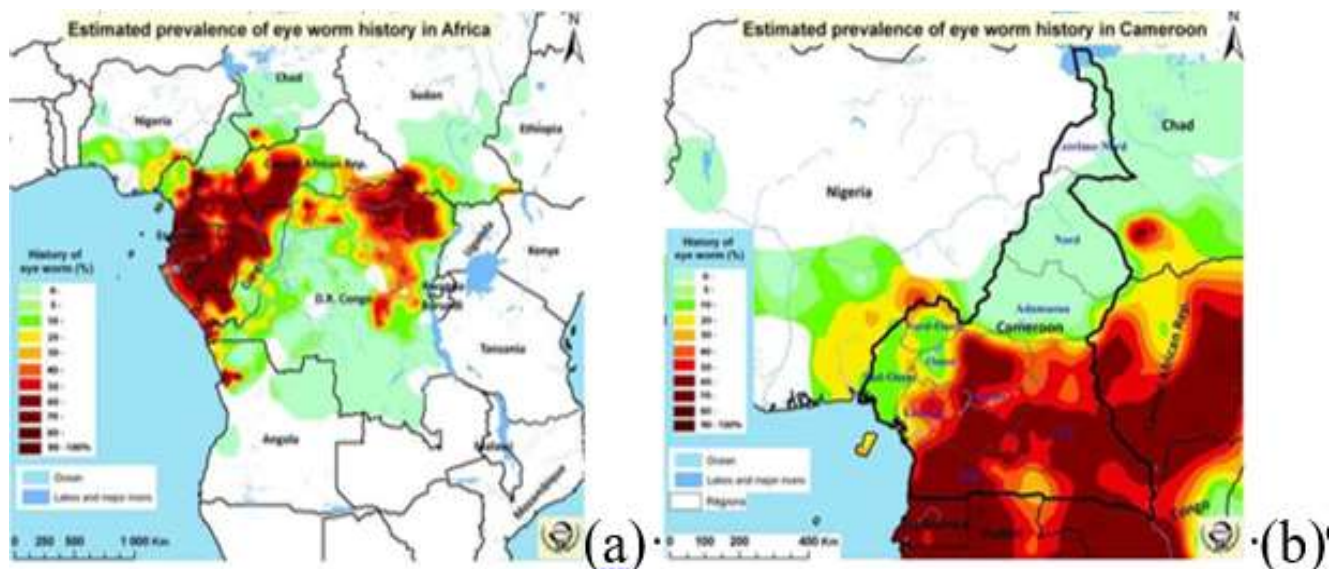


Figure 1. Estimated prevalence of eye worm history in Africa (a) and Cameroon (b)

This parasite which is endemic in 19 African countries (Dikti et al. 2017), is distributed worldwide and is classified following the WHO (2017) report as one of the NTDs (Figure 2).

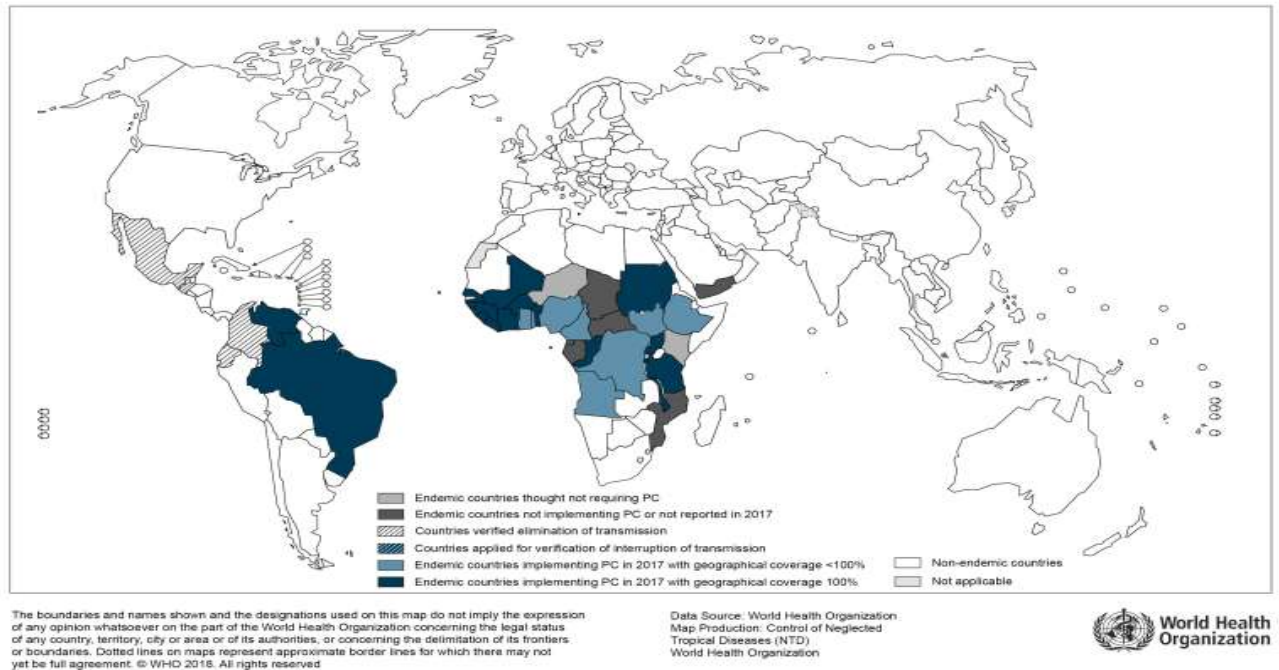


Figure 2. Geographic distribution of Onchocerciasis worldwide

It is the second leading infectious cause of blindness worldwide transmitted by black flies of the genus *Simulium* (Cho-Ngwa et al. 2016). According to some figures of the WHO, this disease afflicts nearly 37 million people globally, with 99 % of all the cases living in sub-Saharan Africa (WHO, 2007). Also, the Cameroonian public health ministry in 2004, estimated about 28% of the population is affected by the disease and more than 1 million suffering from skin alteration due to Onchocerciasis (Ndjonka et al. 2010). Furthermore, about 110,000 km² of land in Cameroon has been left uncultivated owing to the disease, with economic consequences. In Ngaoundere and in the Adamawa region, the prevalence of *O. volvulus* and *Onchocerca ochengi* are estimated to be around 30% and 65%, respectively (Ndjonka et al. 2010). The bovine parasite *Onchocerca ochengi* in cattle is considered to be the closest relative in phylogeny to *O. volvulus* and is also transmitted by *Simulium damnosum*. It is currently the best model available for performing research in chemotherapy and immunology of onchocerciasis, and it is demonstrated that drugs used against the bovine parasite also affect the human parasite (Dikti et al. 2017). Both parasites are transmitted to humans and cattle by the same vector (*Simulium*). The Global Burden of Disease Study estimated that in 2017 there were at least 20.9 million people infected worldwide, of which 14.6 million had skin disease and 1.15 million had vision loss. In addition, 86 million people live in high risk areas of the African Programme for Onchocerciasis Control (APOC) countries. Onchocerciasis



is responsible for about 270,000 cases of blindness and 500,000 cases of visual impairment (Dikti et al. 2017). The phylogenic classification of *Onchocerca volvulus* is given in Table 1 below (<https://animaldiversity.org>).

Table 1. Phylogenic classification of *Onchocerca volvulus*

Domain	Eukarya
Kingdom:	Animalia
Phylum	Nematoda
Order	Spirurida
Family	Onchocercidae
Genus	<i>Onchocerca</i>
Specie	<i>Onchocerca volvulus</i>

I.1.3. Transmission and development in human being

Transmission occurs when blackfly ingests skin-circulating microfilariae while taking a blood meal from an infected person (Hendy, 2018). Then an infected blackfly (genus *Simulium*) introduces third-stage filarial larvae onto the skin of the human host, where they penetrate into the bite wound (1). Like all filarial worms, the first larval stage (L1) is preceded by the microfilaria, which is the stage ingested by *Simulium*; and the (L3) is the stage which is infective to man. In subcutaneous tissues the larvae (2) develop into adult filariae, which commonly reside in nodules in subcutaneous connective tissues (3). Adults can live in the nodules for approximately 10–15 years (Cho-Ngwa et al. 2016). Some nodules may contain numerous male and female worms. Females measure 33 to 50 cm in length and 270 to 400 μm in diameter, while males measure 19 to 42 mm by 130 to 210 μm . In the subcutaneous nodules, the female worms are capable of producing microfilariae for approximately 10–15 years. The microfilariae, measuring 220 to 360 μm by 5 to 9 μm and unsheathed, have a life span of approximately 12–15 months. They are occasionally found in peripheral blood, urine, and sputum but are typically found in the skin and in the lymphatics of connective tissues (4). A blackfly ingests the microfilariae during a blood meal (5). After ingestion, the microfilariae migrate from the blackfly's midgut through the hemocoel into the thoracic muscles (6). There the microfilariae develop into first-stage larvae (7) and subsequently into third-stage infective larvae (8). The third-stage infective larvae migrate to the blackfly's



proboscis (9) and can infect another human when the fly takes a blood meal (1) (Figure 3) (Global Health, Division of Parasitic Diseases, 2019).

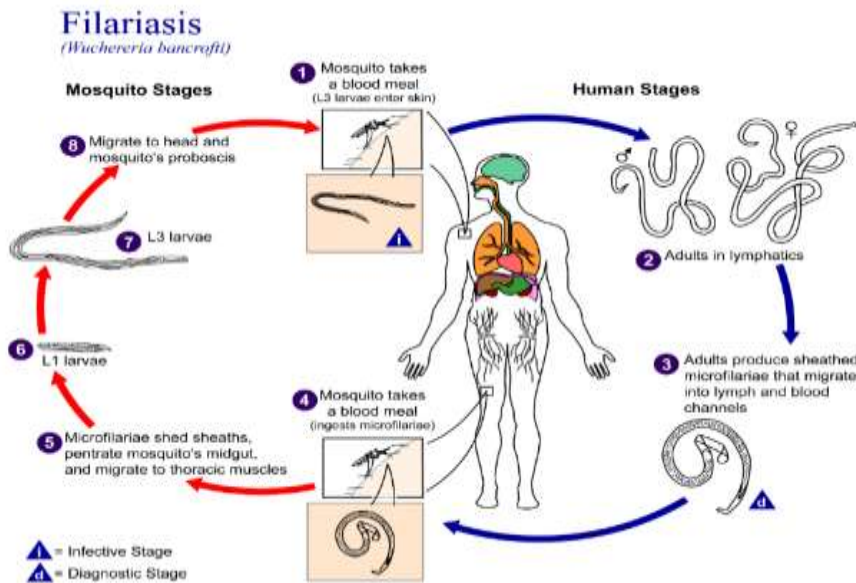


Figure 3. Life cycle of *O. volvulus*

I.1.4. Treatment

The treatment relies largely on the only recommended drug ivermectin, as the current control measures for Onchocerciasis. In Africa, several field of studies have achieved significant reductions in the transmission of infection by repeated annual mass treatments with ivermectin (Cho-**Ngwa et al. 2010**). However, the use of this drug is limited in areas of *Loa loa* co-endemicity due to severe adverse events observed in people with high *L. loa* microfilaraemia because of the good activity of the drug on the *L. loa* mf in blood. Moreover, ivermectin which is recommended for chemotherapy and MDA (Hendy, 2018; Cho-**Ngwa et al. 2016**), is only microfilaricidal and requires continuous delivery for at least 14 years (which corresponds to the life span of the adult worm) to interrupt transmission and clear Onchocerciasis from a human population (Cho-**Ngwa et al. 2016**; Ngwewondo, 2018). Lastly, parasites isolated from communities with sub-optimal responses to annual treatment in Ghana showed genetic changes observed with resistance to ivermectin in other nematodes. Therefore, there is the need for a safe and effective microfilaricidal drug against Onchocerciasis that will be able to cure the infection and break transmission cycles, or at least, an alternative microfilaricide that does not kill *L. loa* mf.

Several species of the Annonaceae family have showed anti-Onchocerca activity



Cho-Ngwa et al. (2016) and Ndjonka et al. (2018). They include: *Annona senegalensis*, *Polyalthia suaveolens* and *Pachypodanthium staudtii* known to date as *Duguetia staudtii*.

I.2. GENERAL INFORMATION ON THE ANNONACEAE FAMILY

The Annonaceae family is a pantropical flowering plant and the most species-rich of Magnoliales. This family contributes significantly to the diversity of trees and lianas in Neotropical and rain forests of the Old World with nearly 2400 species in 108 genera currently recognized in the Annonaceae family. These species have been an easily identifiable entity ever since the standardization of the use of plant family names (Chatrou et al. (2012)). The plants of the Annonaceae have traditionally been considered as part of the order Magnoliales as illustrated in the taxonomic classification (Table 2) (Cronquist, 1981). In the most recent consensus, the Magnoliales and Laurales constitute one of the two sister clades in the Magnoliidae, which are commonly regarded as the most “primitive” angiosperms in older classifications. The botanical features of the Annonaceae family can vary from species to species depending upon its origin, climate, and topography. Its botanical diversity can range from trees to shrubs, evergreen climbers, with elongated cylindrical-shaped intracellular resin channels. The aromatic flowers bloom before they are completely developed. Furthermore, they are axillary, singular or grouped, hermaphrodite, and regular in shape. The stamens are typically considerable in numbers, hypogenous, and spirally arranged. Fruits are made up of clusters of berries and that are widely consumed in tropical regions due to their high nutritional value. Seeds are usually enlarged and have irregular surfaced endosperm with a small embryo. Given the large number of species in Annonaceae, a useful and stable infra-familial classification is necessary to ease communication and retrieve also information (Chatrou et al. 2012). Annonaceae exhibit important biological activity in general with several species that showed anti-Onchocerca activity (Ndjonka et al. 2018). Many different secondary metabolites have been reported in this family including alkaloids, saponins, tannins and cardiac glycosides (Ajaiyeoba et al. 2006). The Annonaceae family contents several genera such as *Duguetia*, former *Pachypodanthium*.

**Table 2.** Taxonomic classification of the genus *Duguetia*

Taxonomy of the Plant	
Kingdom	Plantae
Phylum	Tracheophyta
Class	Magnoliopsida
Order	Magnoliales
Family	Annonaceae
Genus	<i>Duguetia</i>
Specie	<i>staudtii</i>

1.2.1. The genus *Duguetia* former *Pachypodanthium*

Support for the past distinction of *Pachypodanthium* from *Duguetia* appears to be absent. Several novel characters, or characters so far not incorporated into phylogenetic analyses, are used. It is demonstrated that the critical reassessment of classical morphological characters, and the search for new ones, may well advance phylogenetic resolution within Annonaceae (Chatrou et al. 2000). *Duguetia* (accepted name), now including *Pachypodanthium*, is a genus with 93 species, 89 of which occur in the Neotropics, and the remaining four in Africa. *Duguetia* is the third largest genus of Annonaceae in the Neotropics. (Maas et al. 2003). The genus *Duguetia* belongs to the family of Annonaceae that comprises about 120-130 genera and 2500 species. 43 additional species representing 23 genera of Annonaceae have been reported in the literature for the treatment of fevers, malaria and headache. *Duguetia* comprises several species with the majority in tropical America and 4 species in West and Central Africa such as *Duguetia barteri* (Benth.) Chatrou, *Duguetia confinis* (Engl. & Diels) Chatrou, *Duguetia dilabens* Chatrou & Repetur and *Duguetia staudtii* (Engl. & Diels) Chatrou.

1.2.2. Botanical review on *D. staudtii*

Also called 'Ntom' by the Ewondo in the Centre region of Cameroon, *D. staudtii* Engl & Diels Chatrou is a large-bole forest tree up to 40 m in height with more or less flat crown, horizontal branches and long narrow leaves. *D. staudtii* is easy to recognize by the presence of minute stellate hair on the undersurface of the leaves and by the fruits whose surface is similar to that of a pineapple. The stem is straight, cylindrical up to 70 cm in diameter with rough brownish-grey bark deeply fissured lengthways which has a pungent taste when fresh. The yellow color of the slash quickly turns brown on exposure, twigs yellowish- brown, hairy, longitudinally wrinkled, branches shortly tomatoes, wood similar to walnuts but yellowish-



white to greenish-brown. The fruits are globe-ellipsoid 4-6 cm in diameter with many sessile monocarps very close together and loosely united at base, ribbed, reddish and flesh when mature (Figure 4).



Figure 4. (A) Trunk (MBOBDA, 2017), (B) leaves, and (C) fruits of *Duguetia staudtii*.

The flowers pale yellow, solitary or up to three on very short stalks, buds globose and completely surrounded by two bracts, three sepals very concave with dense yellowish hair, six petals in two series, globose, largely ovate, very numerous anthers with red heads. The leaves alternate, long and very narrow 4-5 times as long as broad, elongated, tapered shortly at each end, acuminate at apex, margins wavy, leathery, smooth sparsely covered with scattered stellate hairs on lower surface, pairs of upcurving lateral nerves, hairy mid rib, longitudinally ridged underneath, petiole very short with reddish hairs. This plant is widely distributed throughout the West and Central African region around Sierra Leone to Zaire in dense evergreen forest. (Figure 5) (Dieter, 1996; Cronquist, 1981).



Figure 5. View of geographic distribution in the tropics and in Cameroon of *Duguetia staudtii*.



1.2.3. Ethnomedicinal uses

Also known as Molombo in the East region of Cameroon, Ntuen in the federal state of Nigeria, this plant used locally in Africa is differently named from Sierra Leone to Cameroon as illustrated in **Table 3**.

Table 3. Common names of *Duguetia staudtii* locally used in Africa

Cameroon	Ntom, Molombo
Nigeria	Ntokon, Ntuen
Sierra leone	Mononui, Malenguli
Liberia	Gpaladio, Gpaladuo, Djirrowa-tu, Zree-chu
Ivory coast	Aniukéti, Anokuiti, Niangro Miedzo, Diu-diu, Yorohutu
Ghana	Okyiraa, Dankwakyire, Dua-wisa, Okyeraa, Pae-aduasã, Dua-wusa, Awasa-makyina, Duawisa, Kumdwe

(<https://plants.jstor.org/compilation/pachypodanthium.staudtii>)

In fact, the bark decoctions commonly used in traditional medicine in Africa continent are taken to treat cough and cold and even more as other complaint of respiratory tracts also as purgative anthelmintics and aphrodisiac. From the Western to the Central African traditional medicine healers, the plant is used as antimalarial phytomedicine. The bark has a pungent taste when fresh and it is put to a number of medicinal uses. In Ghana, it is boiled and used as chest medicine. They are used in mouth wash against toothache and to wash hair to treat lice. A paste of pounded bark is applied externally to treat small pox and measles. The bark is also used to treat tumor, edema, leprosy and gonorrhoea. In addition, pulped bark with kola nut is taken against gastrointestinal problems (**Dieter, 1996**). The bark decoction is used to kill body vermin. In Ivory Coast, it is used for bronchitis. Furthermore, the bark pulped in a mortar with kola nut is eaten to treat gastrointestinal pains. It is used along with other ingredient for tumor. In Congo, the bark decoction of *D. staudtii* is used for cough medicine, it has analgesic properties and so, is good for tooth ache and it is utilized in the treatment and prevention of dropsy, swelling, oedema, gout, pulmonary troubles, tumors, cancer and vermifuges (**Burkill, 1985**). Furthermore, a decoction of the stem bark of *D. staudtii* obtained by scraping the bark with a large knife, or leaves (100 g) soaked in water for 20 min are used in the preparation of a drink which is taken to get rid with headaches. Similarly, a decoction of leaves is used for bathing the head



<https://plants.jstor.org/compilation/pachypodanthium.staudtii>).

An attempt has been made to investigate the genus *Duguetia* and some secondary metabolites are reported in the literature (Carollo et al. 2006).

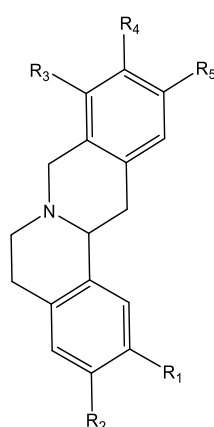
I.2.4. Previous chemical studies on the genus *Duguetia*

Many studies have been conducted on the secondary metabolites present in different parts of *Duguetia* plants, from which essential oils, aromatic compounds, monoterpenes, diterpenes, triterpenes, flavonoids (Carollo et al. 2006), and most typically alkaloids have been isolated and characterized (Pérez et Cassels, 2010; Rodrigues et al. 2016). The stem bark of *D. staudtii* yielded tertiary isoquinoline, tetrahydroprotoberberine alkaloids such as corypalmine and discretine; some aporphines, N-methylpachypodanthin, pachypodanthin, pachystaudine and nor-pachystaudine as well as staudine (Dieter, 1996). In addition, three bisnorlignans, pachypophyllin, pachypostaudin-A and pachypostaudin-B were reported from the stem bark of *Pachypodanthium staudtii* known today as *Duguetia staudtii* (Ngadjui et al. 1989).

Alkaloids isolated from *Duguetia* species constitute the largest group of secondary metabolites. Corypalmine **5**, Isocorypalmine **6**, Govanine **7**, and Discretamine **8** as mentioned in Table 4 are tetrahydrojatrorrhizine alkaloids and the most common among these reported Alkaloids, (Pérez et Cassels, 2010).

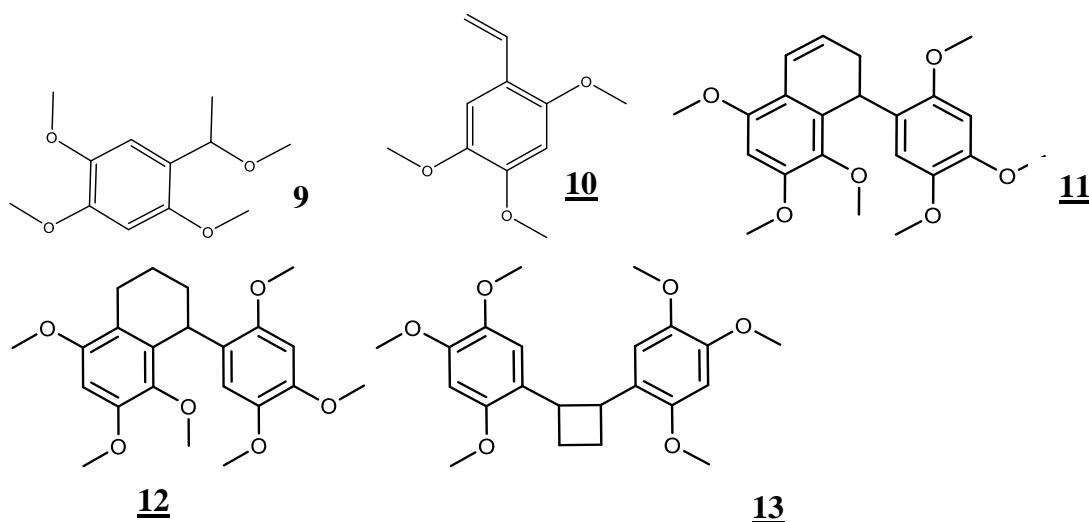
Table 4. Tetrahydrojatrorrhizine and tetrahydroprotoberberine alkaloids from chemically investigated *Duguetia* species

Compound name and Structure	Species	Reference
(-)- Corypalmine 5 R ₁ = OMe – R ₂ = OH R ₃ = OMe – R ₄ =OMe R ₅ =H	<i>D. trunciflora</i> <i>D. confinis</i> <i>D. staudtii</i>	(Pérez et Cassels, 2010)
(-)- Isocorypalmine 6 R ₁ = OH – R ₂ = OMe R ₃ = OMe – R ₄ =OMe; R ₅ =H	<i>D. confinis</i> <i>D. staudtii</i>	
(-)- Govanine 7 R ₁ = OH – R ₂ = OMe R ₃ = H – R ₄ =OMe - R ₅ = OMe	<i>D. confinis</i>	
(-)- Discretamine 8 R ₁ = OMe – R ₂ = OMe R ₃ = OMe – R ₄ =OH - R ₅ = H	<i>D. furfuraceae</i> <i>D. trunciflora</i>	

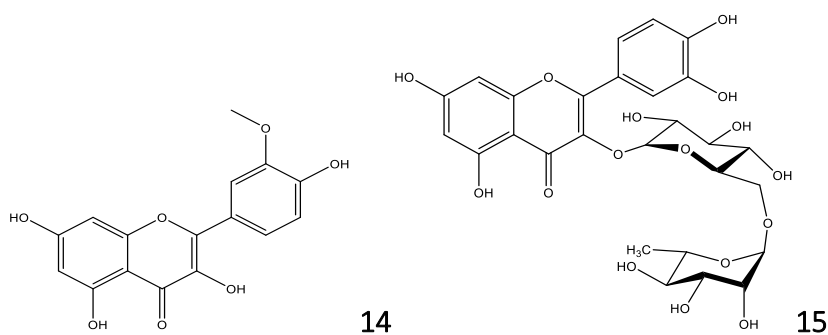




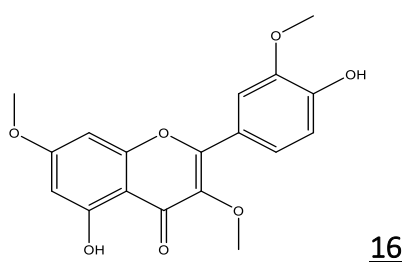
In addition, **Mathouet et al. (2007)** reported the isolation of the phenylpropanoid 1,2,4-trimethoxy-5-(1-methoxy-ethyl)-benzene **9** from the dried and powdered barks of *P. confine*. From the bark of *Pachypodanthium (Duguetia today) staudtii*, **Ngadjui et al (1989)** reported the isolation of 2,4,5-trimethoxystyrene **10**, and some bisnorlignans such as Pachypostaudin-B **11** Pachypostaudin-A, **12** and Pachypophyllin **13**



Carollo et al. (2006) reported the isolation of isorhamnetin **14** isolated from the twigs and leaves of *D. furfuracea*. Whereas **Soares de Araujo Pinho et al. (2016)** reported the isolation of rutin **15** from the leaves of *D. furfuracea*.



Mathouet et al. (2007) reported the isolation of pachypodol **16** from the dried and powdered barks of *P. confine* using cyclohexane and dichloromethane as solvents.





I.2.5. Pharmacological activities of some isolated compounds from the genus *Duguetia*

In Table 5 below, is summarized the activities reported in the literature about the genus *Duguetia*.

Table 5. Pharmacology activities of some compounds and chemotaxonomic markers from *Duguetia* genus

Classes	Compounds	Activities	References
Alkaloids	Corypalmine <u>5</u>	Antimicrobial	Pérez et Cassels, 2010
	Discretamine <u>8</u>	Hypotensive	Pérez et Cassels, 2010
	Oliverine <u>4</u>	Antifilaricidal	Titanji et al. 1990
Flavonoids*	Isorhamnetin <u>14</u>	Anti-trypanocidal	Carollo et al. 2006
	Rutin <u>15</u>	Antifungal	Soares de Araujo et al. 2016
Styrene	2,4,5-trimethoxystyrene <u>10</u>	Insecticidal	Koona et Bouda, 2004
Lignans*	Pachypophyllin <u>13</u>	-	Ngadjui et al. 1989; Ngouonpe et al. 2019

*: Chemotaxonomic markers

- : Not tested

I.2.6. Generalities on flavonoids

Considering that part of this study carried out led to the isolation of a new methoxylated flavone, we will give a brief background of this class of secondary metabolites.

I.2.6.1. Distribution and importance of Flavonoids in the nature

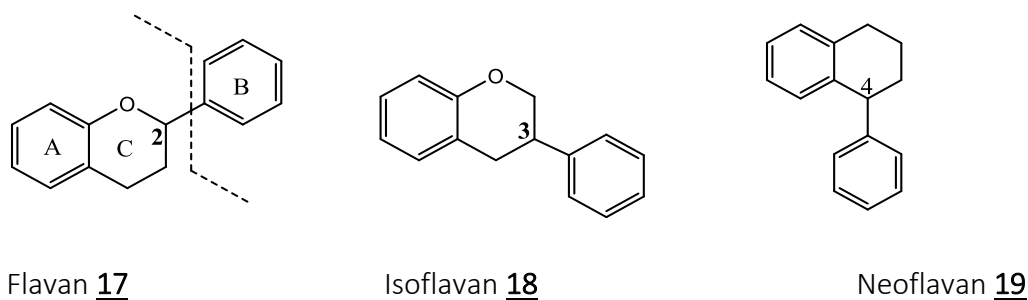
Flavonoids are one of the most diverse and widespread groups of natural products with a prominent place among the natural phenols. They are usually found in different parts (roots, stem, bark, leaves, fruits, etc.) of terrestrial plants. The importance of flavonoids in foods (fruits, vegetables, and grains) means that it is indispensable to have suitable means of determining their content. Flavonoids have been shown in recent years to be of vital significance to mankind as well as to plants. They have been strongly implicated as active contributors to the health benefits of beverages such as tea and wine, foods such as fruit and vegetables, chocolate and others (Oyvind et Markham, 2006).

I.2.6.2. Types of Flavonoids

Flavonoids are a large and diverse group of specialized metabolites comprising over 9000 distinct chemical units. The basic skeleton of a flavonoid is a structure constituted of 15 carbon atoms arranged in three rings C₆-C₃-C₆ structure formed by the stepwise condensation of a phenylpropanoyl-CoA starter molecule, mostly p-coumaroyl-CoA, with three malonyl-CoA units, each of which undergoes decarboxylation, and by the subsequent cyclization of the polyketide chain to form a phloroglucinol ring. They can be divided into a variety of classes such



as flavones (e.g., apigenin, and luteolin), flavonols (e.g., quercetin, kaempferol and myricetin), flavanones (e.g., flavanone, hesperetin, and naringenin), and others (Oyvind et Markham, 2006). Depending on the position of the linkage of the aromatic ring to the benzopyrano (chromano) moiety; this group of natural products may be divided into three classes: flavan 17, isoflavan 18 and neoflavan 19 (Scheme 1) (Bankeu, 2011).



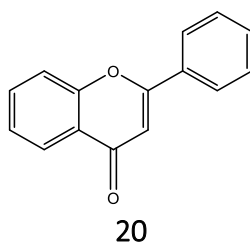
Scheme 1. Structures of some important classes of flavonoids

I.2.6.2.1. Flavans (C₆-C₃-C₆ Backbone)

The basic flavan skeleton that forms all flavonoids is a 15-carbon phenylpropanoid core (C₆-C₃-C₆ system), which is arranged into two aromatic rings (A and B) linked by a heterocyclic pyran ring (C) (Scheme 1) (Nan Jiang et al. 2016). The various classes of flavonoids differ in the level of oxidation and pattern of substitution of the C-ring, while individual compounds within a class differ in the pattern of substitution of the A -and B-rings (Oyvind et Markham, 2006).

I.2.6.2.2. Flavones

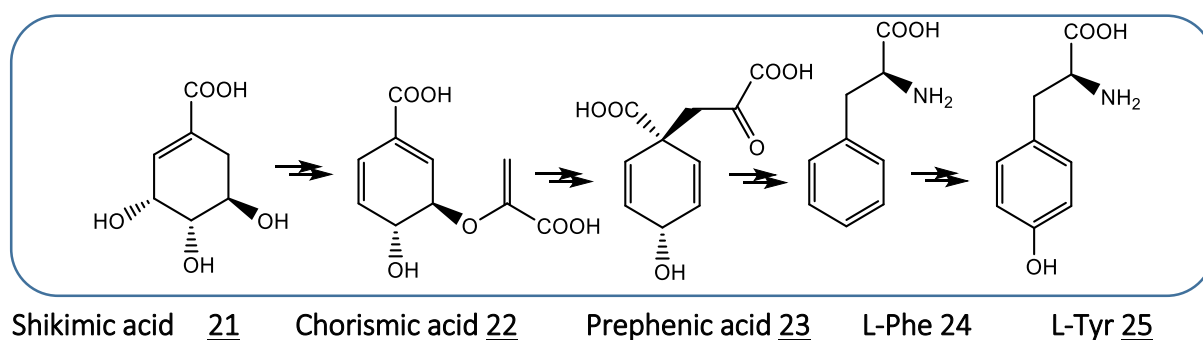
Flavones are one of the largest groups of some basic flavane skeleton. They are characterized in their basic skeleton (Scheme 2), by the presence of a double bond between C-2 and C-3 and the attachment of the B ring to C-2 (Nan Jiang et al. 2016). They are one of the most frequently occurring subclasses of flavonoids and differ from the flavonols by the lack of a hydroxyl residue at position 3 of the C-ring. Flavones are more than 500 distinct compounds reported with their numbers steadily increasing. About 60 new flavones were reported between 2007 and 2009 (Veitch and Grayer 2011). Like in all natural product groups, their chemical diversity is achieved by manifold modifications of the flavone backbone substituents. These modifications lead to differing chemical properties of the individual flavone entities. In addition to their diversity of functions to plants, viz., physiological, biochemical, and ecological, flavones also exert biological activities on animals, providing important nutritional value (Nan Jiang et al. 2016).



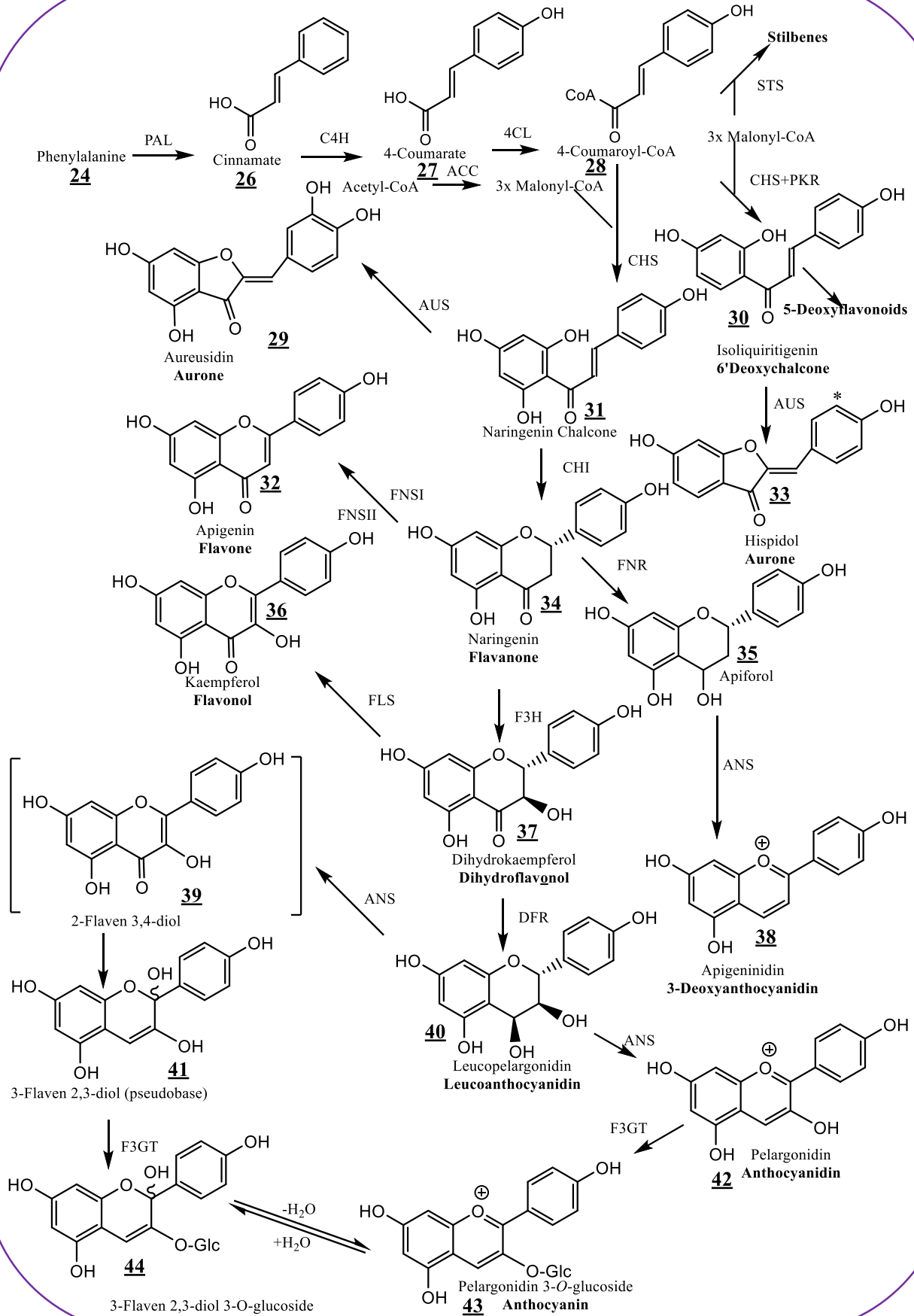
Scheme 2. Basic flavones skeleton

I.2.6.3. Biosynthesis of Flavonoids

Phenolic compounds are the product of the plant aromatic pathway, which consists of three main sections, the shikimate, phenylpropanoid, and the flavonoid routes. The flavonoid pathway is part of the larger phenylpropanoid pathway, which produces a range of other secondary metabolites, such as phenolic acids, lignins, lignans, and stilbenes. The key flavonoid precursors are phenylalanine, obtained via the shikimate pathway (shikimic acid 21, → Chorismic acid 22 → Prephenic acid 23 → L-Phe 24 → L-Tyr 25) (Scheme 3) and malonyl-CoA to get to phenylpropanoid and flavonoid biosynthetic pathways. (PAs : Proanthocyanidins; ANR : Anthocyanidin Reductase; ANS : Anthocyanidin Synthase; C4H: Cinnamate-4-hydroxylase; CHI : Chalcone Isomerase; CHR : Chalcone Reductase; CHS : Chalcone Synthase; 4CL : 4-Coumaroyl; CoA-ligase : CoEnzyme ligase; DFR : Dihydroflavonol-4-reductase; F3H : Flavanone 3-hydroxylase; FNSI : Flavone Synthase I; FNSII : Flavone Synthase II; F3H : Flavonoid 3-hydroxylase; IFR : Isoflavone Reductase; IFS : Isoflavone Synthase Glossary PAL : Phenyl alanine Ammonia-lyase) (Scheme 4) (Oyvind et Markham, 2006).



Scheme 3. The shikimic acid as precursor for the synthesis of L-Phe and phenolic compounds



Scheme 4. General Phenylpropanoid and flavonoid biosynthetic pathways



The principal aromatic phenolic compounds synthesized from L-Phe **24** and L-Tyr **25** are cinnamic acids and esters, coumarins, phenylpropenes, chromones (C_6-C_3), stilbenes, anthraquinones ($C_6-C_2-C_6$), chalcones, flavonoids, isoflavonoids, neoflavonoids ($C_6-C_3-C_6$), and their dimers and trimers, respectively ($C_6-C_3-C_6$)_{2,3}, lignans, neolignans (C_6-C_3)₂, lignans (C_6-C_3)_n, aromatic polyketides, or diphenylheptanoids ($C_6-C_7-C_6$) (Cheynier et al. 2013).

I.2.6.4. Extraction of Flavonoids

Dry plant material used is generally ground into a powder. For extraction, it is advisable when the collected plant material is fresh to dry and the appropriate solvent is chosen as a function of the type of flavonoid required. (Oyvind et Markham, 2006). Polarity is an important consideration here. Less polar flavonoids (e.g., isoflavones, flavanones, methylated flavones, and flavonols) are extracted with chloroform, dichloromethane, diethyl ether, or ethyl acetate, while flavonoid glycosides which can be degraded by enzyme action, are extracted with alcohols or alcohol–water mixtures (Sharma et Janmeda, 2014).

I.2.6.5. Purification of Flavonoids

Many different solvent systems have been employed for the separation of flavonoids using TLC (Oyvind et Markham, 2006). Column chromatography using normal phase silica, reverse phase silica, and/or sephadex along with thin layer chromatography are classical techniques that are still very useful for purification of flavonoids (Agrawal, 1989). Although these techniques do not reduce the separation time, they only simplify the isolation of complex constituents from crude plant extracts and can use several systems of solvent mixtures depending on the nature of the stationary phase including chloroform-methanol, acetone-methanol-water, acetone-water, methanol-water, methanol-water-formic acid *etc* (Bankeu, 2011). If HPLC has been extensively used for analytical purposes, Droplet Counter-Current Chromatography (DCCC) is still an ideal method for the isolation of flavonoids on preparative scale. In addition, centrifugal thin layer chromatography and rotation locular counter-current chromatography are other new promising techniques, with no application in the field of flavonoids to this date (Agrawal, 1989).

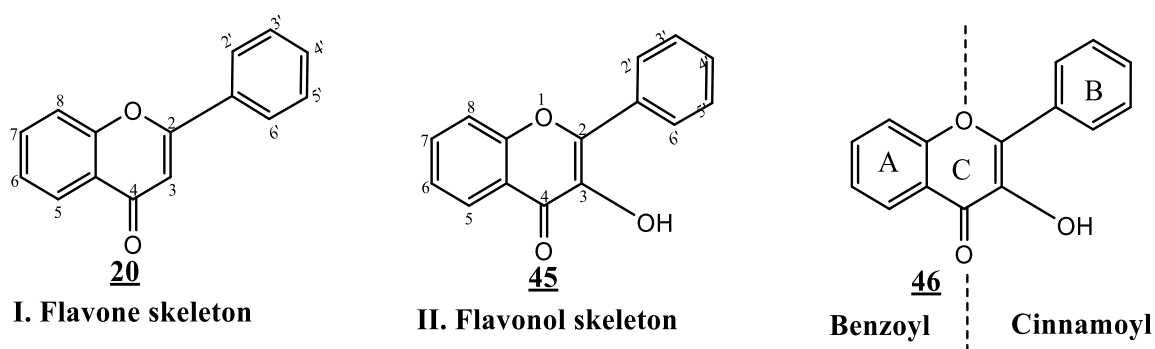


I.2.6.6. General methods for flavonoid structure elucidation

The study of flavonoids is essential in having the means available for their separation (analytical and preparative) and isolation. Within the last four decades, classical methods of structure determination of flavonoids have been replaced by more convenient spectroscopic techniques such as Ultra-Violet (UV), Infra-red (IR), Mass spectrometry (MS) and Nuclear Magnetic Resonance (NMR) spectroscopy (Oyvind et Markham, 2006). To date since NMR spectroscopy is still used to establish the environment and the nature of carbon and hydrogen atoms, the detection of functional groups and electronic conjugation in a molecule rely on spectroscopic measurements in the IR, UV and visible regions (Agrawal, 1989).

I.2.6.6.1. Ultra-Violet (UV)

The UV spectrum of a flavonoid is usually determined in ethanol or methanol (Agrawal, 1989). It is used to help the identification of flavonoid types and the definition of oxygenation patterns (Mabry et Markham, 1975). In the case of flavones, the methanol spectra reveal two characteristic UV absorption bands with two major absorption peaks in the region 240 - 400 nm. These two peaks are commonly referred to as Band I (usually 300 - 380 nm) and Band II (usually 240 - 280 nm). Band I is associated with absorption due to the B-ring cinnamoyl system, and Band II with absorption involving the A-ring benzoyl system (Scheme 5) (Mabry et al. 1970). In Table 6 below, is given the ranges of the principal maxima for each flavonoid types cited.



Scheme 5. Absorption bands of the benzoyl and cinnamoyl systems

**Table 6.** UV absorption ranges for flavonoids (Markahm, 1982; Agrawal 1989)

Band I (nm)	Band II (nm)	Flavonoid type
304–350	250–280	Flavones
<i>ca</i> 310-330 (weak)	<i>ca</i> 270	Isoflavanones
328–360	250–280	Flavonols (3-OH substituted)
350–385	250–280	Flavonols (3-OH free)
	<i>ca</i> 281-300	Isoflavans
310–330 shoulder	245–275	Isoflavones
<i>ca</i> 315 (sh)	280-300	Retenoids
300–330 shoulder	275–295	Flavanones
340-350 (intense)		Coumestans
340–390	230–270 (less intense)	Chalcones
380–430	230–270 (less intense)	Aurones
465–560	230–280	Anthocyanidins and anthocyanins
300–310 (less intense)		Phenyl coumarin

Although IR, UV, MS and ^1H NMR spectroscopic studies are often sufficient to unequivocally establish structures, there are occasion when isomeric structures are not distinguished. These are often polyoxygenated flavonoids or flavonoids with 6- and 8-substituents. In **table 7** below, are listed some positions of ^1H NMR chemical shifts for flavones.

Table 7. ^1H -NMR chemical shifts for flavonoids (Mabry and Markham, 1975)

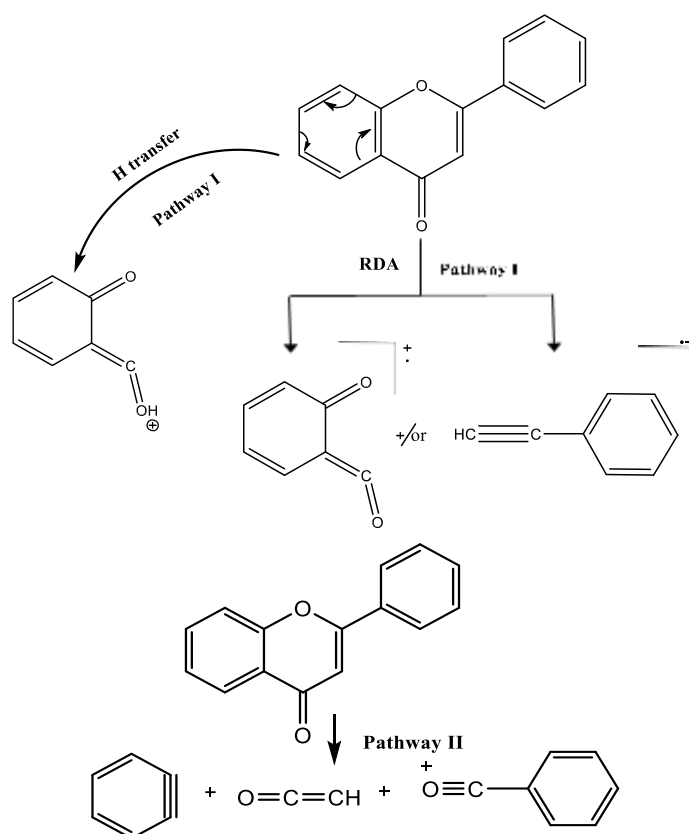
Positions	Range of δ values
H-3	6.0–8.0 (Flavone)
H-5	7.7–8.2
H-6	5.7–6.4
H-8	5.9–6.5

I.2.6.6.2. Mass Spectrometry (MS)

A prerequisite for successful MS is that the flavonoid should be sufficiently volatile and stable in high vacuum within the mass spectrometer. Most flavonoids are sufficiently volatile between 100–230 °C. This analytical technique is very useful in the determination of the molecular weight. MS has been used successfully for the structure determination of flavonoids (Agrawal, 1989). The ionization methods used for flavonoid analysis can be classified as gas-



phase methods including EI and CI, desorption methods including FAB and MALDI, and spray methods including ESI and APCI. The amount of structural information obtained for flavonoids from a mass spectrum depends on the ionization method used. When soft ionization methods like ESI and APCI are applied on flavonoids in LC–MS system, fragmentation of the flavonoids is not commonly seen in the spectra (**Agrawal, 1989**). The mass spectrum consists of a series of signals each of which represents a charged fragment of the parent flavonoid produced by electron impact within the spectrometer. The exact molecular weight for each fragment to the nearest 0.001 mass unit, may be measured if the mass spectrometer is capable of high resolution MS. This information enables calculation of the precise molecular formula for the molecular ion and for all fragment ions (**Agrawal, 1989**). Concerning the fragmentation of flavonoids on electron impact, it occurs in a limited number of predictable ways. These are detailed in a number of reviews. The first objective in interpreting a flavonoid MS is to identify the unfragmented molecular ion $[M]^+$ and then to relate other major fragments to it by rationalizing the loss in molecular weight using recognized fragmentation pathways (**Agrawal, 1989**). The molecular ion which must represent a reasonable molecular weight normally appears as a major peak in the MS of aglycones and must be an even mass number due to the presence of only oxygen, carbon and hydrogen atoms. Characteristic fragments in the MS originate by fission of the molecular ion into ring A and B derived fragments. These fragmentations usually involve one of the two competing pathways, I in retro-Diels Alder (RDA) and II (**Scheme 6**) (**Agrawal, 1989**).



Scheme 6. Diagnostic mass spectral fragmentation pathways for flavones

1.2.7. Generalities on Lignans

Lignans can be found in more than 60 families of vascular plants and have been isolated from different plant parts: roots and rhizomes, woody parts, stems, leaves, fruits and seeds. They are found in most fiber-rich plants, including grains such as wheat, barley, and oats; legumes such as beans, lentils, and soybeans; and vegetables such as garlic, asparagus, broccoli, and carrots (Calvo-Flores et al. 2015).

1.2.7.1. Methods of isolation of Lignans from plants

Mass spectrometers coupled or not with a chromatographic separation have become the technique of choice to analyze lignans. Reverse phase high-performance liquid chromatography (RP-HPLC) is the most commonly used analytical technique for detection and quantification of lignans (Calvo-Flores et al. 2015). The choice of method for the extraction of lignans varies widely depending on the sample and the molecular structure of the products. A wide range of methods is available as isolation procedures for lignans. For extracting lignans, there are two main steps: first, the application of polar solvents to different parts of the plants



containing the lignans; and second, the dissolution of the resulting extracts in water and reextraction with nonpolar solvents. However, new and appropriate methods for the analysis of lignans from plant sources and body fluids have also been applied during the last decade. In this regard, conventional chromatographic methods, including RP-HPLC, remain the most useful and commonly applied techniques. Lipid substances are present in all plants and since they are soluble in organic solvents, it is advisable to separate them at an early stage by extraction with hexane or petroleum ether. Phenolic natural products have only limited solubility in hexane, especially when a free hydroxyl group is present. Nevertheless, in a search for lignans, it is necessary to monitor a concentrated extract by thin layer chromatography (TLC) and/or, if possible, by HPLC. The tendency to extract lignan, including free phenols, is accentuated if a mixture of hexane and diethyl ether is used to remove lipids (**Calvo-Flores et al. 2015**).

1.2.7.2. Solvent extraction

Several lignans were obtained by an initial extraction with EtOH and fractionally extracting the residue successively with hexane, chloroform, *n*-butanol, and water. It is to be expected that hot alcoholic solvents will remove all lignans and their glycosides from plant material. Glycosides may be concentrated by partitioning them into the aqueous phase of a two-phase system (**Calvo-Flores et al. 2015**).

1.2.7.3. Structure determination of Lignans

The structures of extracted and synthesized lignans have been confirmed using NMR techniques, together with the classical melting point determination, IR and UV spectroscopy, for more than 60 years. Single-crystal X-ray analysis remains the most reliable method for determining the absolute configurations of lignans. Nevertheless, many other techniques are involved in the structural elucidation of lignans. Among them, 1D and 2D NMR analyses as well as high-resolution mass spectrometry (HRMS), UV and infrared (IR) spectra, are the most important. In addition, the analysis of their circular dichroism (CD) and nuclear Overhauser effect spectroscopy (NOESY) is useful when more than one chiral center is present, and the lignans have optical properties. Chemical methods, such as Mosher's ester modification, may also help (**Calvo-Flores et al. 2015**).

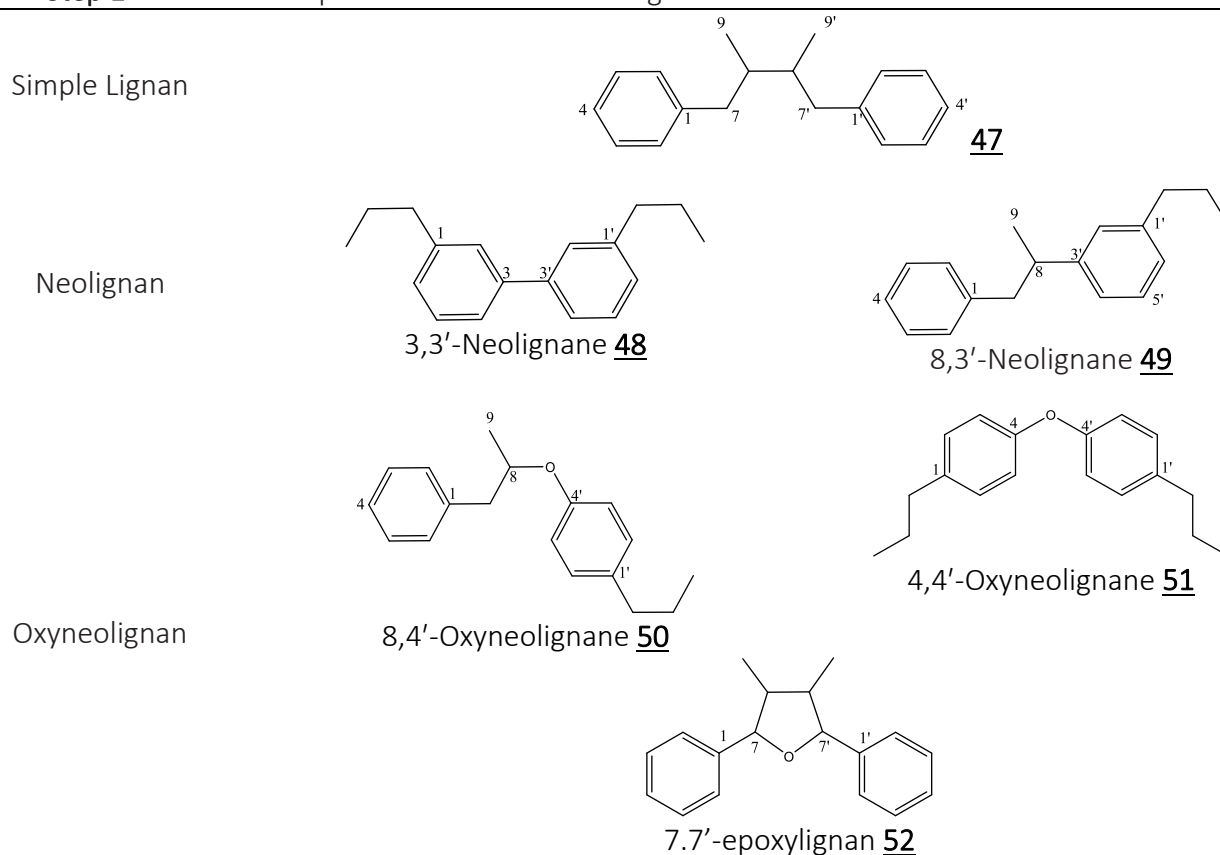


I.2.7.4. Nomenclature of Lignans

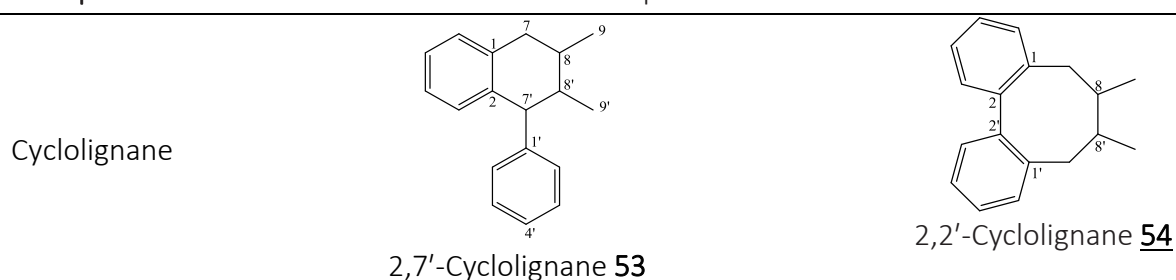
The nomenclature of the diverse range of structures classified as lignans depends largely on trivial names and, if necessary, on the appropriate numbering derived from the systematic name. The structural diversification of such biogenetically related group of compounds limits the utility of a systematic nomenclature, since it disguises structural similarities. The system followed for naming the structures is based on the original system introduced by Freudenberg and Weinges, later extended by Moss, and now accepted by IUPAC. It follows the trivial or semi-systematic names, which are commonly given as synonyms within the entries to provide the chemical abstract service (CAS) name. Some examples of these trivial names are collected in Table 8 (Calvo-Flores et al. 2015).

Table 8. Nomenclature of Lignans

Step 1: Fundamental parent structure according to Moss



Step 2: After modifications of the fundamental parent structures





I.3. GENERAL INFORMATION ON THE HYPERICACEAE FAMILY AND ON THE GENUS *PSOROSPERMUM*

I.3.1. Hypericaceae family

Species in the family of Hypericaceae are annual or perennial herbs or shrubs with simple and untoothed leaves that grow opposite each other along the stem. The leaves may be dotted with tiny black or translucent spots (Gallé, 2015). The flowers are arranged in branched inflorescences and are radially symmetrical. There are 4 or 5 sepals and 4 or 5 petals; these attach below the ovary (i.e., the ovary is superior), and the sepals tend to stay on the plant after the other flower parts have fallen. The flowers have both pollen-bearing and ovule-bearing parts, often with many stamens. The stamens have long filaments and may sometimes be fused together. There are 3-5 styles, which are sometimes fused together at their bases. The fruit is a dry capsule that opens to release its many seeds. Species in the Hypericaceae were formerly considered to be part of the Clusiaceae (Gallé, 2015).

I.3.2. The genus *Psorospermum*

The genus *Psorospermum* Baker (tribe Vismieae, family Guttiferae, subfamily Hypericoideae) comprises 55 species mostly trees, shrubs growing in tropical regions of South America, Africa and Madagascar (Gallé, 2015). This genus is very similar in morphology to *Vismia* and, differing mainly in fruits (Gallé, 2015).

I.3.2.1. Botanical review on *P. tenuifolium*

P. tenuifolium as many species belonging to the genus is made up of hermaphrodite flowers which are composed of five vile sepals provided with linear longitudinal glands and five vile petals inside and provided with longitudinal glands and swollen nectariferous tissues at the base. In addition, pentaloculated ovaries containing one or sometimes two ova per cell have a basal placenration. They are topped with five free styles. The seeds are large and surmounted by a fleshy testa with punctate glands. The fruit is a berry as shown in **Figure 6** below (Gallé, 2015).



Figure 6. Trunc - Shrubs, flowers and fruit of *P. tenuifolium*
(https://www.wildflowers-and-weeds.com/Plant_Families/Hypericaceae.htm accessed April 8, 2020)

I.3.2.2. Taxonomy

The classification of **Cronquist (1981)** (**Table 9**) included the current genera of Hypericaceae in the Clusiaceae or Guttifereae in the order of Theales. The genus *Psorospermum* from Hypericaceae family is proposed by certain authors to join the other African and Madagascan species of Vismieae. They would need to be subjected to taxonomic revision in order to correctly redefine the three genera *Harungana*, *Psorospermum* and *Vismia* belonging to the tribe. The genera *Vismia* and *Psorospermum* are not monophyletic. According to **Gallé (2015)**, further molecular and morphological studies would be necessary before any taxonomic changes.

Table 9. Taxonomic classification of the genus *Psorospermum*

Kingdom	<i>Plantae</i>
Phylum	Tracheophyta
Class	Magnoliopsida
Oracle	Malpighiales
Juss. Family	Hypericaceae
Genus	<i>Psorospermum</i> Spach
Species	<i>Tenuifolium</i> Hook. F.



I.3.2.3. Some local names in the genus

In Table 10 below are reported the local names of *Psorospermum* used in Africa (Gallé, 2015).

Table 10. Some local names used in Africa in the genus *Psorospermum*

<i>Psorospermum</i> species	Names uses in Africa
<i>Psorospermum febrifugum</i> Spach	<i>Bakanbo, gorinyika</i> in Bariba (Benin); <i>votolo, votila, nsoko-nsoko</i> in Kikongo; <i>muti-a-mper</i> in Yanzi (DRC); <i>umukubagwa</i> in Kirundi (Burundi); <i>topota-vaso</i> in Umubundu (Angola); <i>kitunu</i> in Zaramo (Tanzania); <i>wanzokoroma</i> in Agni (Ivory Coast).
<i>Psorospermum senegalensis</i> Spach	<i>Kotidakuma</i> in Firdou (Senagal); <i>kashekaji</i> (Nigeria); <i>kéti diankouma</i> in Malinké (Guinea)
<i>Psorospermum corymbiferum</i> Hochr.	<i>Soungalani</i> in Malinké (Ivory Coast); <i>karijakuma</i> in Bambara and Malinké (Mali); <i>etki diankouma</i> in Fulbe (East Africa)
<i>Psorospermum androsaemifolium</i> Baker	<i>Tsifady, harongampanihy, fanerana and hazomafaika</i> (Madagascar)

I.3.2.4. Geographic distribution

The geographical distribution established mainly from herbarium samples and descriptions from various flora shows the presence of the genus *Psorospermum* throughout tropical and equatorial Africa as well as in Madagascar (Figure. 7) (Gallé, 2015).

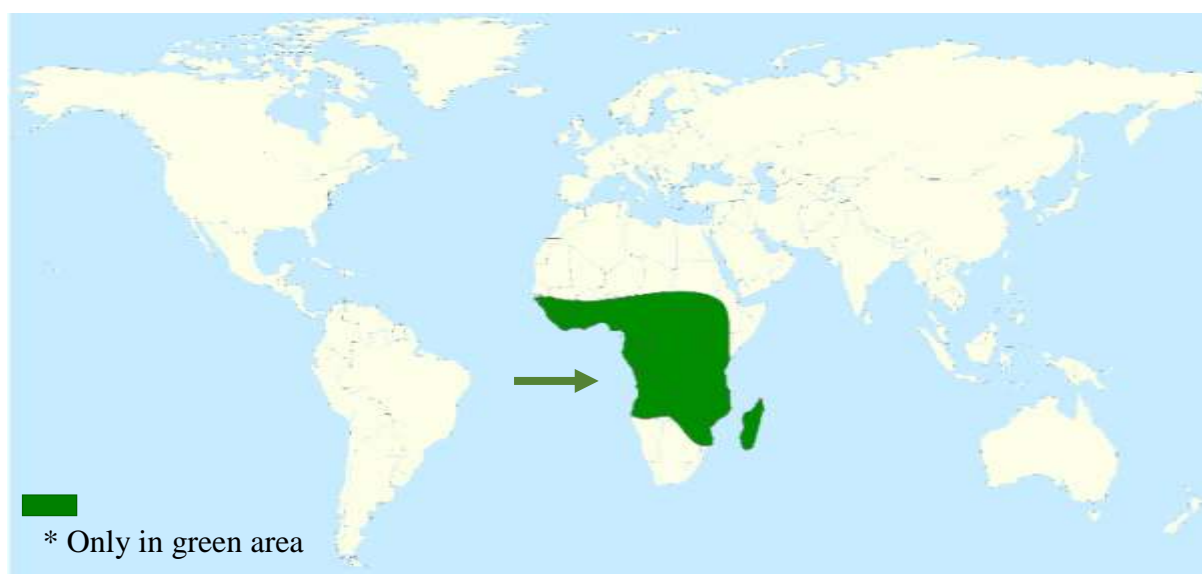


Figure 7. Geographic distribution of the species of the genus *Psorospermum* (represented in green color)



I.3.2.5. Ethnomedicinal uses

Most of the species of the genus have been used for centuries in the ethnomedicinal traditions of indigenous African populations as febrifugal, antidote against poisons, purgative, stomachic and as a remedy for the treatment of leprosy, skin diseases (like dermatitis, scabies and eczemas) and subcutaneous wounds (Gallé, 2015). The bark and leafy stems generally are used in decoction and orally for the care of fevers. The leaves and roots are mainly used for the treatment of diarrhea and other gastrointestinal disorders. Some species are also used in psychiatric, rheumatic, gynecological and infectious problems (Gallé, 2015). Decoction of the barks of *P. febrifugum* is recommended orally in Central and East Africa to treat cases of haemorrhagic dysentery and prevent miscarriages in cattle (Gallé, 2015). The widespread bioactivities of *Psorospermum* genus prompted many teams of researchers around the world to investigate the phytochemical aspect of its species.

I.3.2.6. Previous chemical studies on the genus *Psorospermum*

The secondary metabolites isolated from *Psorospermum* genus include simple and *O*- and *C*-prenylated anthraquinones, anthrones and bianthrone, vismione, flavonoids, long chain alcohols, steroids, tannins, terpenes, simple and *O*- and *C*-prenylated xanthenes and alkaloids, (Epifano et al. 2013). Tsaffack et al. (2009) investigated the chemical composition of the bark extract of *Psorospermum adamauense* obtained 3- geranyloxyemodin 55. In addition, Vismiaquinone 56, α - and β -amyrin 57 were isolated from the methanol extract of the leaves of *Psorospermum androsaemifolium* (Poumale et al. 2011). Kouam et al. (2010) reported the isolation and characterization of friedelan-3-one 58, friedelan-3-ol 59 and finally betulinic acid 60 have been reported from *Psorospermum aurantiacum* (Gallé, 2015). Secondary metabolites isolated from some *Psorospermum* species are here reported as shown in Tables 11-18.

**Table 11.** Triterpenes isolated from *Psorospermum* species.

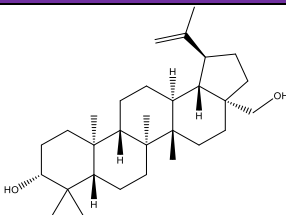
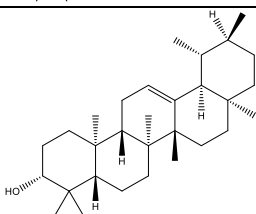
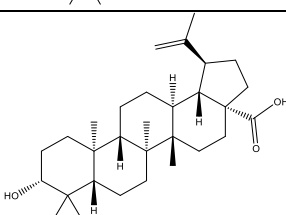
Compounds	Structures	Species	References
Betulin <u>61</u>		<i>P. tenuifolium</i>	
α -amyrin <u>62</u>		<i>P. androsaemifolium</i>	(Gallé, 2015)
Betulinic acid <u>60</u>		<i>P. glaberrimum</i>	

Table 12. Flavonoids isolated from *Psorospermum* species

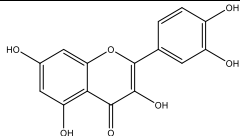
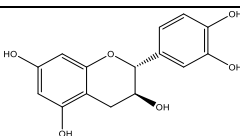
Compounds	Structures	Species	References
Quercetin <u>63</u>		<i>P. androsaemifolium</i>	(Poumale et al. 2011; Gallé, 2015)
Catechin <u>64</u>		<i>P. adamauense</i>	(Gallé, 2015)

Table 13. Some xanthenes isolated from *Psorospermum* species

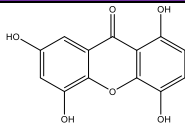
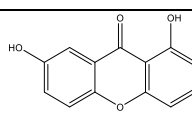
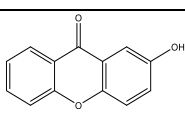
Compounds	Structures	Species	References
1,4,5,7-tetrahydroxyxanthone <u>65</u>		<i>P. adamauense</i>	(Tsaffack et al. 2013)
1,7-dihydroxyxanthone <u>66</u>		<i>P. aurantiacum</i>	(Gallé, 2015)
2-hydroxyxanthone <u>67</u>		<i>P. molluscum</i>	



Table 14. Vismiones isolated from *Psorospermum* species

Compounds	Structures	Species	References
Vismione A <u>68</u>		<i>P. febrifugum</i>	(Gallé, 2015)
Vismione D <u>69</u>		<i>P. aurantiacum</i> <i>P. tenuifolium</i>	(Delle Monache et al. 1987b) ; (Gallé, 2015)
Vismione H <u>70</u>		<i>P. tenuifolium</i>	

Table 15. Some anthrones isolated from *Psorospermum* species

Compounds	Structures	Species	References
3-geranyloxy emodianthranone <u>71</u>		<i>P. adamauense</i>	(Tsaffack et al. 2009; Gallé, 2015)
2-geranylemodine anthrone <u>72</u>		<i>P. corymbiferum</i>	

Table 16. Anthranol and lactone isolated from *Psorospermum* species

Compounds	Structures	Species	References
Kenganthranol E <u>73</u>		<i>P. aurantiacum</i>	(Kouam et al. 2010)
Psorolactone A <u>74</u>		<i>P. glaberrimum</i>	(Botta et al. 1987; Gallé, 2015)

**Table 17.** Some bianthrone isolated from *Psorospermum* species

Compounds	Structures	Species	References
Bianthrone A1 <u>75</u>		<i>P. aurantiacum</i> <i>P. tenuifolium</i>	(Gallé, 2015); (Delle Monache et al. 1987b)
Febrifuquinone <u>76</u>		<i>P. febrifugum</i>	(Gallé, 2015)

Table 18. Some Anthraquinones isolated from *Psorospermum* species

Compounds	Structures	Species	References
3-geranyloxyemodine <u>55</u>			
Emodin <u>77</u>		<i>P. adamauense</i>	(Tsaffack et al. 2013; Gallé, 2015)
2-prenylemodine <u>78</u>			
Physcion <u>79</u>		<i>P. androsaemifolium</i>	(Poumale et al. 2011)

1.3.3. Biological review of the genus *Psorospermum*

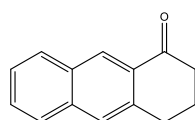
The reported pharmacological activities of its natural compounds refer to antifilarial (Abongwa et al. 2021), antibacterial, anti-protozoal, anti-fungal, anti-viral, anticancer, anti-oxidant, and neuroprotective effects (Epifano et al. 2013; Gallé, 2015). The reported biological activities of some species of *Psorospermum* are encountered in Table 19.

**Table 19.** List of biological activities reported from certain species of the genus *Psorospermum*

Nº.	Activities	Plants Source	References
1	Antifilarial	<i>P. febrifugum</i>	(Abongwa et al. 2021)
2	Anti-bacterial	<i>P. aurantiacum</i>	(Epifano et al. 2013; Gallé, 2015)
3	Anti-fungal	<i>P. corymbiferum</i>	(Epifano et al. 2013)
4	Anti-cancer	<i>P. febrifugum</i>	(Epifano et al. 2013)
6	Anti-protozoal	<i>P. guineense</i>	(Gallé, 2015)
7	Anti-oxidant	<i>P. aurantiacum</i>	(Epifano et al. 2013)
8	Neuroprotective	<i>P. febrifugum</i>	(Epifano et al. 2013)
9	Antimicrobial	<i>P. adamauense</i>	(Gallé, 2015)
10	Antimicrobial	<i>P. adrosaemifolium</i>	(Poumale, 2008)
11	Cytotoxic	<i>P. molluscum</i>	(Epifano et al. 2013)
12	Anti-viral and Cytotoxic	<i>P. febrifugum</i>	
13	Antileishmanial	<i>P. guineense</i>	(Gallé, 2015)
14	Antiplasmodial	<i>P. glaberrimum</i>	
15	Anti-inflammatory	<i>P. tenuifolium</i>	(Zubair et al. 2009)

I.3.4. Generalities on dihydroanthracénones

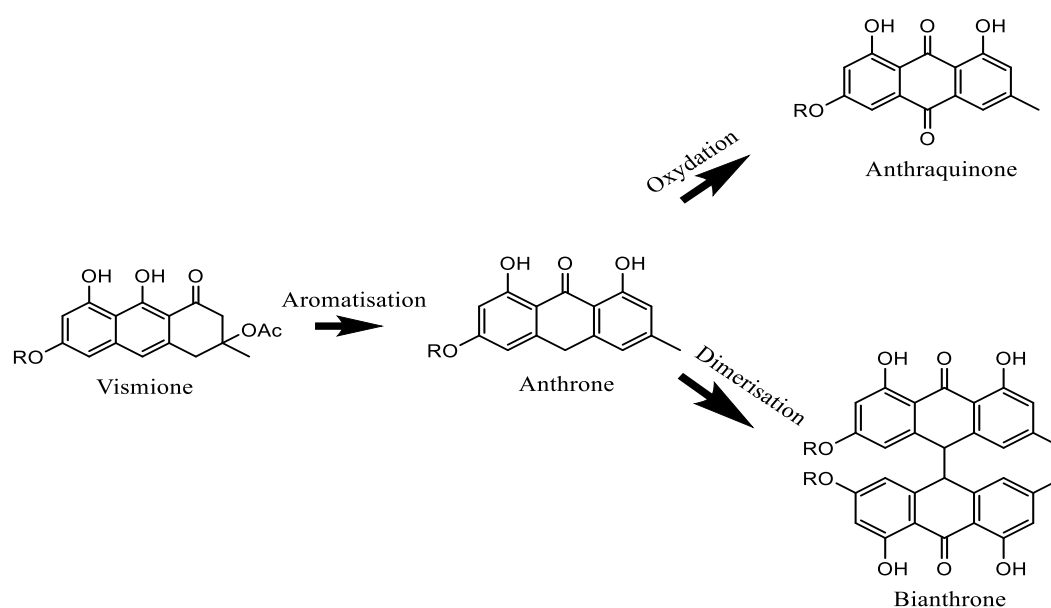
The dihydroanthracenones also called pre-anthraquinones are precursors of anthrones and anthraquinones (Tables 15 and 18) which are found in certain macro and micromycetes and higher plants. They are characterized by a basic tricyclic structure of 3,4-dihydroanthracene-1(2H)-one **80** (Scheme 7) on which various substituents are present (Gallé, 2015).

**80**

Scheme 7. Basic structure of dihydroanthracenones

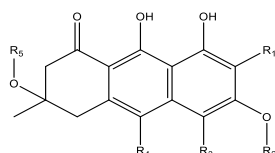
I.3.4.1. Stability of dihydroanthracenones in solution

Gallé (2015) reported a preliminary study on the stability of vismiones (dihydroanthracenone) and found that they are very reactive in solution in the DMSO and quick to degradation into their corresponding anthrone and anthraquinone forms as shown in Scheme 8 below.



Scheme 8. Degradation of dihydroanthracenones (vismione) in solution

Dihydroanthracenones Monomeric types have been identified in several botanical families. Less recent phytochemical studies have led to the isolation of multiple structures within Xanthorrhoeaceae, Fabaceae and Hypericaceae. The dihydroanthracenones isolated from the Hypericaceae family, mainly *C*- or *O*-prenylated or geranylated, have been grouped within the vismiones subfamily which contains a common atrochryson skeleton (**Scheme 9**) (Gallé, 2015).



81

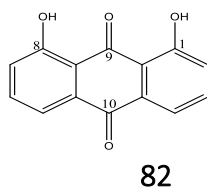
Scheme 9. Common atrochryson skeleton for dihydroanthracenones

I.3.4.2. Generalities on Anthraquinones

Anthraquinones are a group of compounds abundant in the universe of natural substances. They are classified as quinones, and their derivatives are the largest group of natural quinones. Benzoquinones and naphthoquinones are also part of this group. Anthraquinones constitute the largest group of natural pigments, with approximately 700 compounds described. About 200 of these compounds were isolated from plants, while the rest were isolated from lichens and fungi (Duval et al. 2016). They are found in all plant parts: roots, rhizomes, fruits, and flowers. Most of these compounds are derived from the basic structure 9,10-anthracenedione **82**, a tricyclic aromatic organic compound (**Scheme 10**). These



compounds can also be found in various foods consumed by humans, being present in peas, cabbage, and lettuce (Dave and Ledwani 2012; Gaspar Diaz-Mun ~oz et al. 2018).

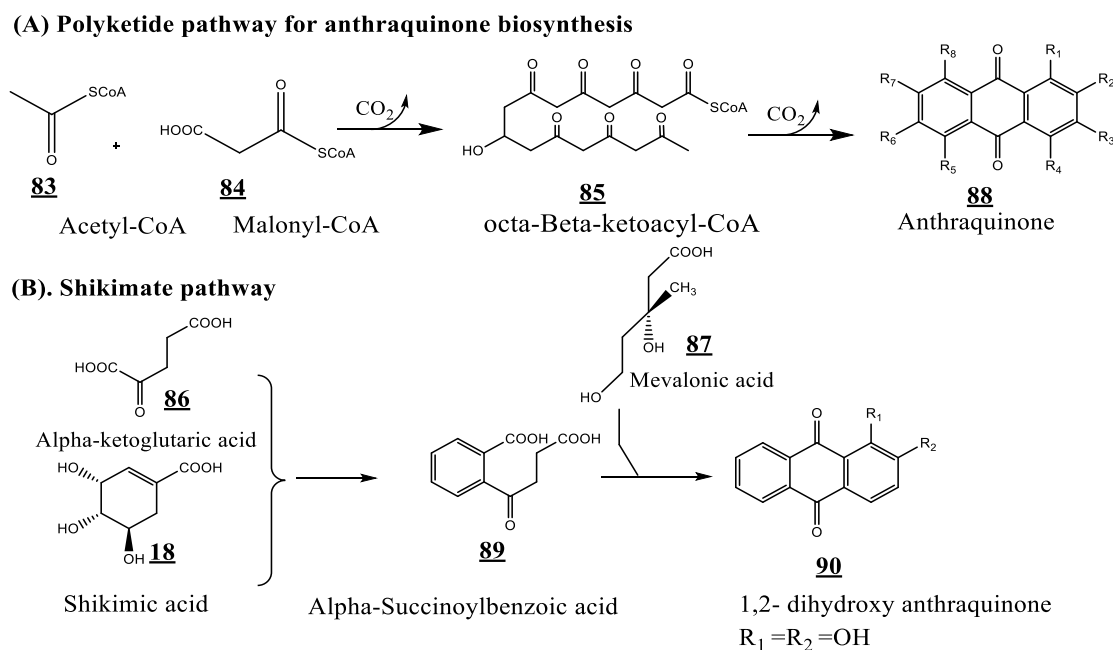


Scheme 10. Basic structure 9,10-anthracenedione

Anthraquinones and their precursors, the anthrones, are substances common in many different organisms, ranging from bacteria and fungi to plants and some animals. In animals, anthraquinones are present in few species that include very different animals from different habitats. Some marine invertebrates, such as the starfish and the sea lilies, contain anthraquinones. In addition, some species of insects produce anthraquinones as defensive compounds (Gaspar Diaz-Mun ~oz et al. 2018).

I.3.4.2.1. Biosynthesis of Anthraquinones

Anthraquinone biosynthesis lead to two main routes : (A) the polyketide pathway, from acetyl-CoA **83** to anthraquinones and (B) the shikimate route, which occurs by the addition of succinoylbenzoic acid **89** and shikimic acid **18** leading to 1,2-dihydroxyanthraquinones **90** (Scheme 11) (Gaspar Diaz-Mun ~oz et al. 2018).



Scheme 11. (A) Polyketide pathway for anthraquinone biosynthesis. (B) Shikimate pathway for anthraquinone biosynthesis



I.3.4.2.2. Biological activities on Anthraquinones

Several biological activities have been described in the literature for anthraquinones among which antitumor activity, antiinflammatory, diuretic, antiarthritic, antifungal (Gaspar Diaz-Mun˜oz et al. 2018; Wuthi-udomlert et al. 2010), antibacterial (Fosso et al. 2012), antimalarial and antioxidant activities (Dave and Ledwani 2012). In addition, anthraquinones have laxative activity, which is found mainly in physcion 79, chrysophanol 91, aloe-emodin 92, and rhein. Physcion 79 is one of the most important representatives with laxative activity.

I.3.5. Review of Phenylpropanoids from medicinal plants

Phenylpropanoids, which contain one or several C₆-C₃ fragments, are widely distributed in nature but have only recently attracted the attention of researchers searching for promising biologically active compounds (BAC) and synthesizing effective medicines based on them.

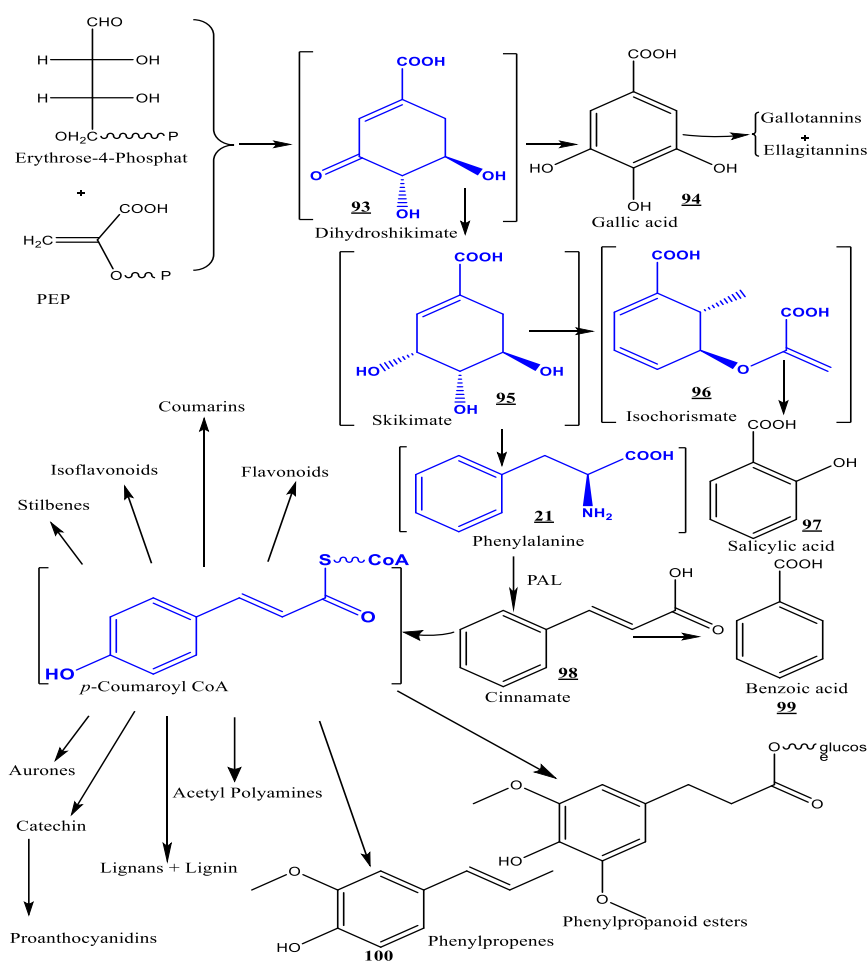
I.3.5.1. Distribution and classification of Phenylpropanoids

The literature on the distribution in plants of the most important phenylpropanoids indicates that plants of the families composites or asters (Asteraceae), orpines (Crassulaceae), aralias (Araliaceae), figworts (Scrophulariaceae), willows (Salicaceae), plantains (Plantaginaceae), mezereums (Thymelaeaceae), mints (Lamiaceae), and olives (Oleaceae) are rich sources of BAC (Kurkin, 2003).

With respect to the classification of phenylpropanoids, it is based on current impressions of the biosynthesis of phenolic compounds, in which cinnamyl alcohols and cinnamic acids play key roles. Though a large number of new phenylpropanoids has been found, there is still no generally accepted classification of this group of compounds. The nomenclature used by various investigators in discussing the structures of phenylpropanoids is unwieldy. Phenylpropanoids can conveniently be treated as a large class of natural compounds consisting of simple and complex phenylpropanoids (Kurkin, 2003).

I.3.5.2. Biosynthesis of Phenylpropanoids

The plant shikimate pathway is the entry to the biosynthesis of phenylpropanoids. The metabolites of the shikimate pathway and the central metabolite, 4-coumaroyl CoA, are shaded in blue as shown in **Scheme 12** below.



Scheme 12. Diversification of Phenylpropanoids based on the general phenylpropanoid pathway

I.3.5.3. Isolation and purification of Phenylpropanoids

Isolation and purification of phenylpropanoids require a separate examination because many phenylpropanoids, especially lignan glycosides and conjugates of phenylethanoids, are noncrystalline compounds. Also refined preparative methods of isolation, including high-pressure liquid chromatography (HPLC), made success in this area possible. Furthermore it should be emphasized that many phenylpropanoid glycosides were isolated using preparative HPLC. In addition, favorable extraction conditions, evaporation methods, and other technical operations are advisable for isolating phenylpropanoids. Fractionation by various organic solvents followed by the use of column chromatography with thin (3-5 cm) sorbent layers is also effective for separating phenylpropanoids (Kurkin, 2003).

I.3.5.4. Spectral and chemical properties on Phenylpropanoid structure

Structural analysis of phenylpropanoid glycosides is rapidly developing. However, this area has not yet been reviewed. In fact, all chemical and spectral methods that are used to establish structures of natural compounds are also used in structural investigations of



phenylpropanoids. Nuclear magnetic resonance (NMR) is the most informative method. For example, Proton magnetic resonance (PMR) spectra of glycosides containing cinnamic acid derivatives exhibit characteristic doublets for protons of the side chain ($-\text{CH}=\text{CH}-$) with a spin-spin coupling constant (SSCC) of 16 Hz (the chemical shift of H-7 is 7.5-8.0 ppm; of H-8, 6.2-6.5 ppm). Moreover, the comparison of PMR spectra of starting glycosides and their acetates can reveal aromatic and aliphatic OH groups (singlets of aromatic acetoxy groups resonate at weaker field) and the structure of the carbohydrate moiety. A 3H singlet at 3.8-4.0 ppm is observed in the PMR if the glycoside contains an aromatic methoxyl. Also, signals of the 2H- α_1 (on C-8) and 2H- β_1 (on C-7) protons are diagnostic for the phenylethanol fragment. These appear in the PMR as two 2H triplets with SSCC 7 Hz (2.83 and 3.95 ppm, respectively). The signals of the cinnamyl and phenylethyl aromatic protons are affected by the substituents. In particular, the aromatic protons in *p*-substituted structures resonate as two 2H doublets with SSCC 9 Hz (H-2,6; H-3,5) (Kurkin, 2003).

I.3.5.5. ^{13}C NMR and Mass spectrometry of Phenylpropanoids

^{13}C NMR has been used successfully for structural analysis of phenylpropanoids, especially for establishing the structure of the carbohydrate and when determining the site of attachment of the cinnamic acid (Kurkin, 2003). Mass spectrometry is also useful in structural studies of phenylpropanoids (Kurkin, 1991). It should be noted that the molecular ion $[\text{M}]^+$ of phenylpropanoid glycosides can appear only if field-desorption mass spectrometry (FD-MS) or fast-atom-bombardment mass spectrometry (FAB-MS) is used. Also, the Electron-impact mass spectrometry (EI-MS) is used to study phenylpropanoid glycosides and could detect characteristic fragments. EI-MS was also used to study compounds containing cinnamyl alcohols.

I.3.5.6. Ultra-violet and Infrared spectroscopies of Phenylpropanoids

With respect to UV and IR spectroscopies, these techniques are also used for structural investigations of phenylpropanoids. In fact, IR spectra of phenylpropanoids containing an ester, have a characteristic absorption band at $\sim 1700\text{ cm}^{-1}$ (C=O). In addition concerning cinnamoylamides, their IR spectra contain absorption bands near 1750 cm^{-1} (amide C=O) (Kurkin, 1991). UV spectra of phenylpropanoids are also rather characteristic and enable the nature of the compounds to be determined. Thus, UV spectra of Chlorogenic acid **101** which contain hydroxycinnamic acids, have practically the same absorption maxima as the free

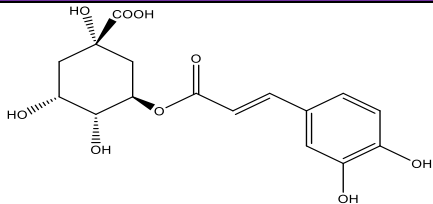
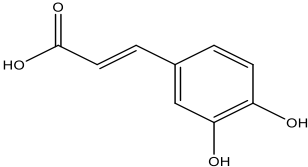


hydroxycinnamic acids. Furthermore, strong absorption maxima at 250-280 nm are characteristic of the UV spectra of cinnamyl alcohols (Kurkin, 2003).

I.3.5.7. Previous chemical and biological studies on Phenylpropanoids of Hypericaceae family

To the best of our knowledge, phenylpropanoid and its glycoside derivatives have not yet been isolated from the genus *Psorospermum* but Shakya et al. (2019) reported these secondary metabolites from the genus *Hypericum* in the Hypericaceae family as shown in Table 20.

Table 20. Some phenylpropanoids from the Hypericaceae family

Compounds	Biological activities	Specie	References
 Chlorogenic acid <u>101</u>	Antimicrobial	<i>Hypericum perforatum</i>	(Shakya et al. 2019)
 Caffeic acid <u>102</u>	Antibacterial		(Kurkin et al. 2003)

I.3.5.8. Pharmacologic properties of Phenylpropanoids

Kurkin et al. (2003) reported the antimicrobial activity of phenylpropanoids. They showed that caffeic acid 102 and several of its derivatives have the highest antibacterial activity toward *Staphylococcus aureus*. Moreover, antimicrobial, analgetic, anti-inflammatory, and expectorant properties of phenylpropanoids have also been reported along with anticancer properties as other pharmacological activities found in phenylpropanoids.

Thus, phenylpropanoids, which occur in many medicinal plants, are very interesting for fabricating effective tonic immunostimulating, anticancer, hepatoprotective, antimicrobial, and anti-inflammatory phytopreparations. This provided a basis to recognize phenylpropanoids as an independent group of BAC and was reflected in the chemical classification of medicinal plants (Kurkin, 2002).



I.3.6. Review on the Liquid Chromatography-Mass Spectrometry (LC-MS)

Liquid chromatography mass spectrometry (LC-MS) is the main method for detecting drugs (Tarui et al. 2014) and their major metabolites in vivo, and can provide high enough sensitivity, specificity, and molecular structural information for the qualitative assay of drugs and their metabolites.

I.3.6.1. Principle of LC/MS

Typical LC/MS system is combination of HPLC with mass spectrometer (MS) using interface (ionization source). Coupled HPLC-MS is one of the most important techniques of the last decade of the 20th century. The combination offers the possibility of taking advantage of chromatography as a separation method and MS as an identification tool. The mass spectrometer is one of the most sensitive methods of molecular analysis (Li et al. 2000). MS consists of three main components: the ion source, the mass analyzer, and the detector (Figure 8). In ion source, a sample is ionized, usually to cations by loss of an electron. Then in the mass analyzer, the ions are sorted and separated according to their mass to charge ratio. Finally in the detector, the separated ions are detected and relative abundance is recorded. In addition, the sample introduction system is essential to admin the samples into the ion source. Whereas a computer and software are needed to control the instrument, obtain data and compare spectra according to the database. As a result, mass spectrum, a plot of the ion signal as a function of the mass-to-charge ratio, is created, which is used to determine the elemental or isotopic nature of a sample, the masses of particles and of molecules, and to elucidate the chemical structures of molecules. (Korfmacher et al. 2005, Lim et Lord, 2002).

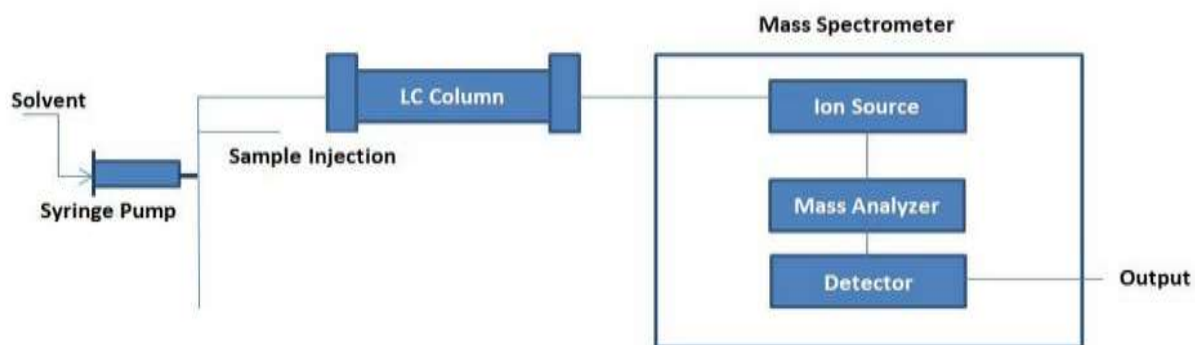


Figure 8. Basic components of a LC/MS system



Furthermore, combining the two analytical methods as mentioned above reduces experimental error and improves accuracy. LC-MS provides superior specificity and sensitivity compared to direct injection methods. When combined with stable isotope dilution, LC/MS can be used to develop highly accurate and reproducible assays (James, 2009).

The mass analyzer is the heart of the mass spectrometer, which takes ionized masses and separates them based on mass to charge ratios.

1.3.6.2. Main components of the mass spectrometer

1.3.6.2.1. Mass analysers

There are several general types of mass analyzers, including magnetic sector, time of flight, quadrupole and ion trap.

↓ Magnetic sector mass analyzer

In Magnetic Sector Mass analyzer, ions are accelerated so that they have the same kinetic energy. All the ions are accelerated into a focused beam. And then the ions are deflected by the magnetic field according to masses of ions. The lighter ions have more deflection than the heavier ones. The amount of deflection depends on the number of the positive charges. When similar ions pass through the magnetic field, they all will be deflected to the same degree and will all follow the same trajectory path. Those ions which are not selected will collide with either side of the flight tube wall or will not pass through the slit to the detector (Schwartz, 2002); (Scigelova et al. 2006).

↓ Time of flight (TOF)

A time of flight analyzer consists of a pulsed ion source, an accelerating grid, a field-free flight tube, and a detector (Figure 9). The flight time needed by the ions with a particular mass to charge, accelerated by a potential voltage, to reach the detector placed at a distance, can be calculated from a formula. Pulsing of the ion source is required to avoid the simultaneous arrival of ions of different m/z at the detector. At high masses, not all the ions of the same m/z values reach their ideal velocities. To fix this problem, often a reflection which consists of a series of ring electrodes with high voltage is added to the end of the flight tube. Because of the high voltage, an ion is reflected in the opposite direction, when it is into the reflection. For the ions of same m/z value, faster ions travel further than the slower ones into the reflections. In this way, both the slow and fast ions of the same m/z value reach the detector at the same time. The



reflection increases resolution by narrowing the broadband range of flight times for a single m/z value (Schwartz, 2002); (Scigelova et al. 2006).

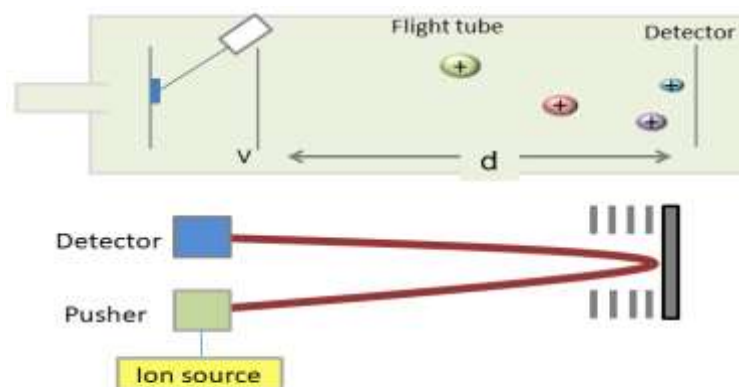


Figure 9. Schematic diagram illustrating TOF in mass spectrometry

↓ Quadrupole

The quadrupole consists of four parallel metal rods and each opposing rod pair is connected together electrically (Figure 10). One pair of rods is applied with a radio frequency (RF) voltage while another one is applied with a direct current (DC) voltage. At a given DC and RF combination, only the ions of a particular m/z show a stable trajectory and can be transmitted to the detector, while other ions with unstable trajectories don't pass the road, because the amplitude of their oscillation becomes infinite. By changing DC and RF in time, usually at a fixed ratio, ions with different m/z values can be transmitted to the detector one after another (Schwartz, 2002); (Scigelova et al. 2006).

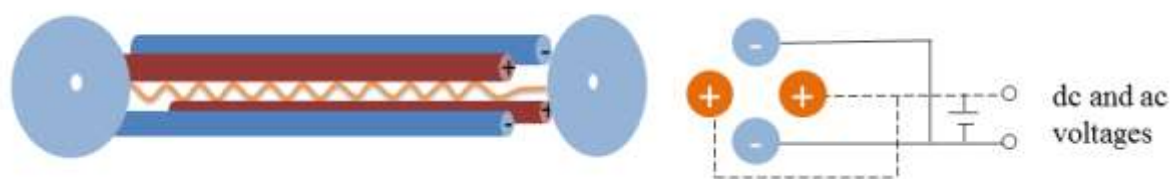


Figure 10. Schematic diagram of a quadrupole consisting of four parallel metal rods and each opposing rod pair is connected together electrically



↓ Ion trap

An ion trap is a device that uses an oscillating electric field to store ions. There are several common types of ion trap: 3D ion trap, linear ion trap, orbitrap and Fourier transform ion cyclotron resonance (Munson, 2006).

- **Quadrupole ion trap (QIT)**

Quadrupole ion trap is also called 3 dimension ion trap. The QIT mass spectrometer uses three electrodes to trap ions in a small volume. It consists of a cylindrical ring electrode and two end-cap electrodes. A mass spectrum is obtained by changing the electrode voltages to eject the ions from the trap. The end-cap electrodes contain holes for the introduction of ions from an external ion source and for the ejection of ions toward an external detector.

- **Linear Ion Trap (LIT) and Orbitrap**

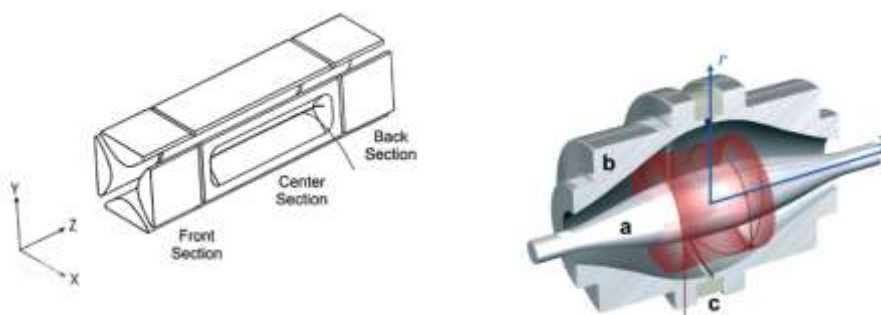


Figure 11. Schematic diagram of a LIT and Orbitrap of ion trap

- **The Fourier Transform Ion Cyclotron Resonance (FT-ICR)**

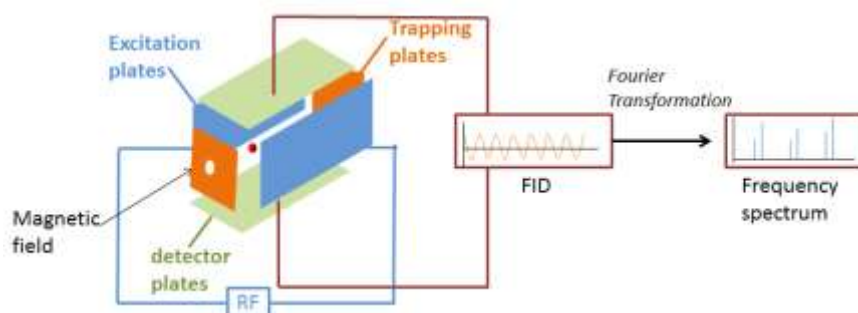


Figure 12. Schematic diagram of a Fourier Transform Ion Cyclotron Resonance mass spectrometer



By creating a potential well for the ions, the linear ion trap can be used as a mass filter or as a trap. The linear ion trap uses a set of quadrupole rods to confine ions radially by a two-dimensional radio frequency (RF) field. A static electrical potential can confine the ions axially. They are confined by application of appropriate RF and DC voltages with their final position maintained within the center section of the ion trap. The RF voltage is adjusted and multi-frequency resonance ejection waveforms are applied to the trap to eliminate all but the desired ions in preparation for subsequent fragmentation and mass analysis (Munson, 2006).

Orbitrap is the newest addition to the family of high-resolution mass analyzer. In orbitrap, moving ions are trapped in an electrostatic field. The electrostatic attraction towards the central electrode is compensated by a centrifugal force that arises from the initial tangential velocity of ions. The electrostatic field which ions experience inside the orbitrap forces them to move in complex spiral patterns. The axial component of these oscillations is independent of initial energy, angles and positions, and can be detected as an image current on the two halves of an electrode encapsulating the orbitrap. A Fourier transform is employed to obtain oscillation frequencies for ions with different masses, resulting in an accurate reading of their m/z (Munson, 2006).

The Fourier Transform Ion Cyclotron Resonance mass spectrometer (**Figure 12**) consists of three main sections: excitation plates, trapping plates, detector plates, and they consist a cell. Ions which are affected by a magnetic field move at a cyclotron frequency. After a radio frequency voltage at the same frequency of cyclotron frequency is applied, the ions absorb energy and accelerate to a larger orbit radius than their original path. After excitation, the cyclotron radius of ions still remains the larger state. And as the ions around approach to the top and bottom plate, the electrons travel from top to bottom. The motion of electrons between these two plates produces a detectable current. The decay over time of the image current resulting after applying a short radio-frequency sweep is transformed from the time domain into a frequency domain signal by a Fourier transform (Munson, 2006).

1.3.6.2.2. Ionization source

Most common ionization sources are Electrospray ionization (ESI), Atmospheric pressure chemical ionization (APCI) and Matrix-assisted laser desorption/ionization (MALDI). Apart from this Electron impact (EI) and Chemical ionization (CI) or negative chemical ionization are also used as ionization source in MS (Sparkman et al. 2006). There are several types of ion source which are usually used in a mass spectrometer.



↓ **Electron Ionization (EI)**

Known as one of the first and popular ionization methods for mass spectrometry. EI is appropriate for organic molecules whose relatively molecule weight is below 600. In this technique, a current passes a wire filament and produces electrons for ionization. Then an electric field accelerates these electrons to produce a beam of high energy electrons. When a molecule passes this high energy electrons beam, an electron can be expelled from the molecule to produce an ion. EI (**Figure 13**) works well for many gas phase molecules, so it always works with gas chromatography (GC), which can be incorporated for the separation of mixtures of thermally stable and volatile gases. Although EI works well for many gas phase molecules, it does have some disadvantages. EI causes extensive fragmentation, therefore the molecular ion is not observed for many compounds (**Munson, 2006**).

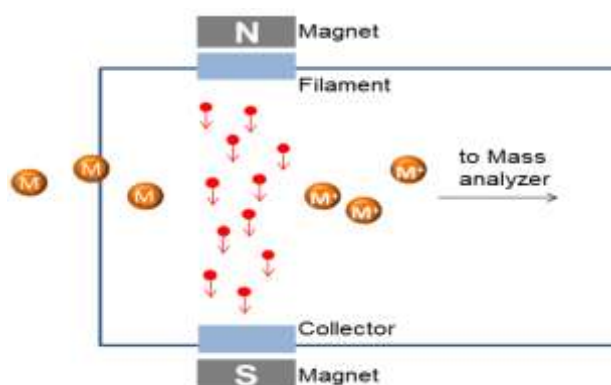
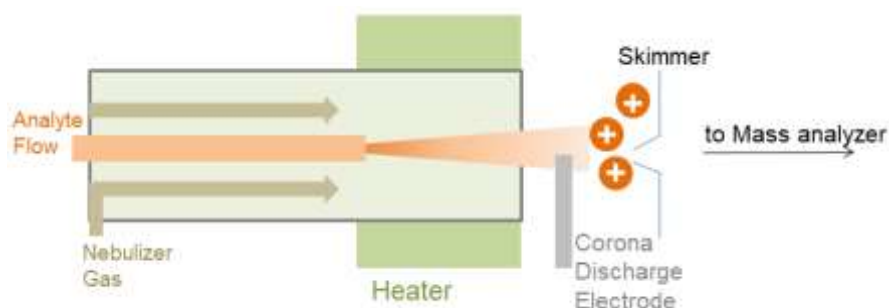


Figure 13. Schematic diagram illustrating popular Electron ionization methods for MS

↓ **Chemical Ionization (CI)**

Chemical ionization is a lower energy process than EI. In CI, ions are produced by the collision of the samples with ions of a reagent gas that are present in the ion source. Inside the ion source, the reagent gas is extremely more than samples. Reagent gas is first subjected to electron impact to produce reagent gas ions by the fast electrons from the filament. Sample ions are produced by the ion-molecule reactions of reagent gas ions and sample molecules. In general, reagent gas molecules are present in the ratio of about 100:1 with respect to sample molecules. Some common reagent gases include methane, ammonia, and isobutene. Positive and negative ions of the sample are formed by reactions with this plasma as shown in **Figure 14** below. Like EI, CI usually works with gas chromatography. CI has the same general limitations



→ Figure 15. Schematic diagram illustrating Atmospheric Pressure Chemical Ionization (APCI) for MS

↓ Matrix-Assisted Laser Desorption/Ionization (MALDI)

Matrix-assisted laser desorption/ionization (MALDI) is a technique to allow the high molecular weight compounds into the gas phase as intact ions. The mechanism of MALDI consists of three processes. Firstly, the sample is mixed with a suitable matrix material in excess and applied them to a plate. Secondly, a pulsed laser irradiates the sample, the matrix material cause rapid vibrational excitation by absorbing the laser irradiation, which leads to the localized disintegration of the solid solution. Finally, the analyte molecules are ionized by being protonated or deprotonated, and can then be accelerated into a mass analyzer. The time-of-flight (TOF) analyzers are always used with the MALDI ionization source (Figure 16).

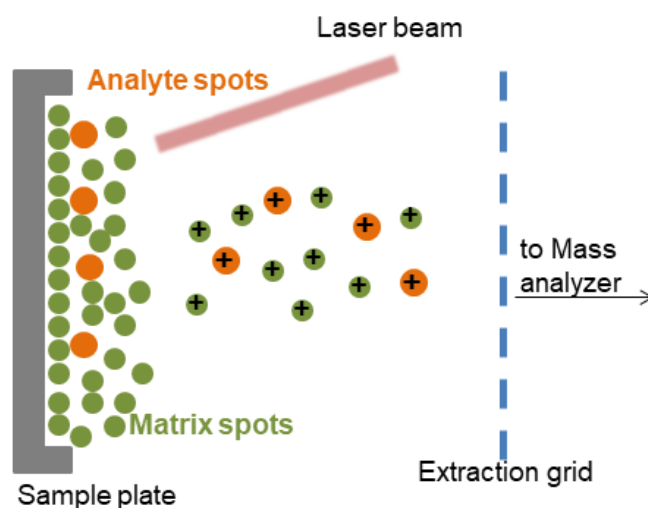


Figure 16. Schematic diagram illustrating MALDI for MS (Munson, 2006)



↓ **Electrospray ionization (ESI)**

ESI is a soft ionization technique (**Figure 17**), which is useful for biological molecules of large molecular mass, because this process turns the macromolecule ionized into small droplets instead of fragmenting the macromolecules into smaller charged particles. ESI uses an electrical stress between the ESI probe exit and the counter electrode, which is located few millimeters from the probe. The process results in the generation of highly charged droplets directly from the infused solution. With the help of another stream of heat or dry gas, which are often called desolvation gas, the charged droplets are continuously reduced in size by evaporation of the solvent, leading to an increase of surface charge density and a decrease of the droplet radius. This leads to the Columbic repulsion between the charges present in the droplet and then forms individual gas phase analyte ions, that critical point known as the Rayleigh limit. Finally, the ions are guided into a mass analyser.

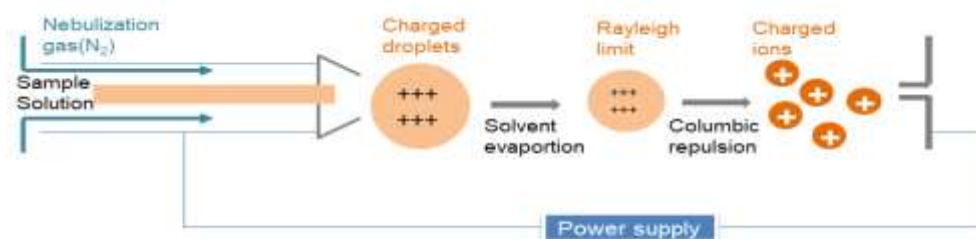


Figure 17. Schematic diagram illustrating Electro spray ionization (ESI) for MS (Munson, 2006)

1.3.6.2.3. Common types of ion detector for mass spectrometry

A key element to all mass spectrometry (MS) systems is the type of detector (**Koppenaar et al. 2005**) used to convert a current of mass separated ions into measurable signal. Different types of detectors are used depending upon factors including dynamic range, spatial information retention, noise and suitability to the mass analyzer. Some of the commonly used types include electron multipliers (EM), Faraday cups (FC), photomultiplier conversion dynodes and array detectors.



- **Electron multipliers (EM)**

The essence of an EM (**Figure 18**) is a serial connection of discrete metal plates called dynodes that amplifies a current of ions by a factor of $\sim 10^8$ into a measurable current of electrons. An immense advantage of EM detectors is that, when calibrated properly, they are noiseless and single ion counting is possible. When a single secondary ion enters the EM, it is stopped by the first conversion dynode. The energy of impact is dissipated in part by ejection of electrons from the dynode material, creating an electrical charge. Additional electrons are ejected by a cascade process through subsequent dynodes. At the final dynode the accumulated charge is measured as a voltage pulse (**Allen, 1947**).

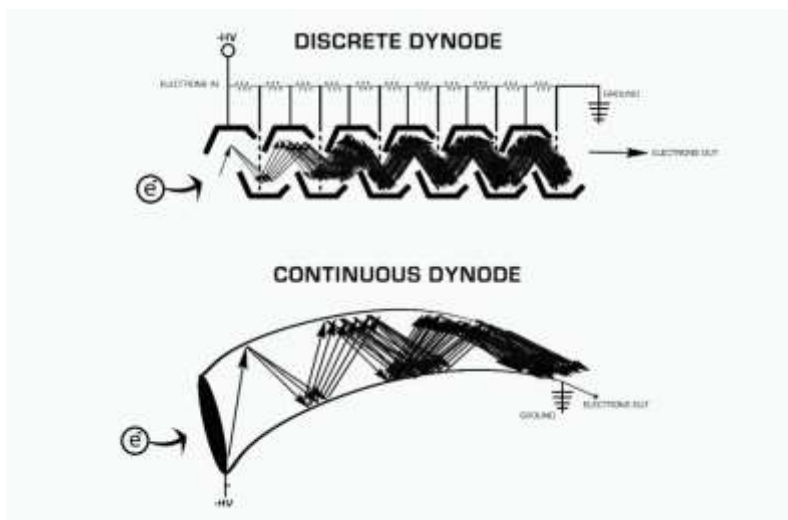


Figure 18. Schematic diagram illustrating how a detected incoming ion is converted into a measurable signal using an EM detector

- **Faraday cups (FC)**

FC detectors (**Figure 19**) are relatively simple and cheap devices. Their main strength is the ability to measure higher ion currents where the EM struggles. It consists of a hollow conducting electrode connected to ground through a high resistance. The ions hitting the collector cause a flow of electrons from ground through the resistor and the resulting potential drop across the resistor is amplified. The elementary charge on a single ion is 1.6×10^{-19} C. Therefore, a count rate of 1×10^6 c/s (about the upper realistic limit for EM detector usage) would produce a current of 1.6×10^{-13} A. Even with a resistance as high as 10^{11} W connected to ground, the amplifier must be able to detect a potential drop of 16 mV. Thus, measuring lower currents will become more difficult as the thermal and electronic noise in the resistor and



amplifier circuitry will have a large effect on precision. Often these components will be enclosed within an evacuated, thermally controlled chamber (Brown et al. 1956).

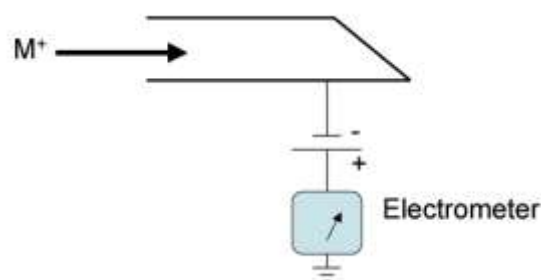


Figure 19. Schematic diagram of a Faraday cup ion detector

- Photomultiplier conversion dynode detector

In a photomultiplier conversion dynode detector (Figure 20) the ions initially strike a dynode which results in electron emission. The electrons produced then strike a phosphor screen which in turn releases photons. The photons then pass into the multiplier where amplification occurs in a cascade fashion – much like with the electron multiplier. The main advantage of using photons is that the multiplier portion of the detector can be kept sealed in a vacuum, preventing contamination and greatly extending the lifetime of the detector.

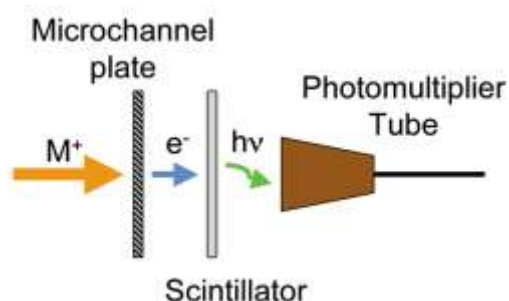


Figure 20. Schematic diagram of a photomultiplier conversion dynode detector

- Array detectors

The first detector on a MS was an array detector, a photographic film. Since that time, array detectors have evolved into a variety of types using different principles. They can cover a broad range of detector types and systems (Barnes et al. 2004) but can be generally broken down into two types. Firstly, the detectors that can measure many ions of differing mass-to-charge ratio (m/z) values simultaneously. Perhaps the simplest “array” detector can be found on those MS systems that combine both EM and FC detectors. For isotope ratio measurements,



the most abundant isotope can be measured using the FC, while the weaker abundant isotope, yielding a much smaller ion current, is more suited for measurement on an EM. Secondly, the detectors that are position sensitive. In fact, array detectors for position sensitive measurements have used microchannel plates for many years. The array consists of upwards of 106 microscopic glass channels, each 5–50 μm in diameter, bound together in a honeycomb-type array and electrically connected. Each channel operates as a continuous-dynode EM with a gain in the order of 10^4 . Though very useful for position sensing of the ions, it provides more qualitative than quantitative information unless extremely well and frequently calibrated as aging effects are an issue. The main limitations of such devices are their inability to measure simultaneous ion arrivals and thus their dynamic range is limited to about 10^4 - 10^5 Hz. **Figure 21** below showed a nanoscale secondary ion mass spectrometer which has 6 movable and 1 fixed EM detectors, permitting simultaneous analysis of 7 different masses (Nuñez et al. 2018). These are associated with mass spectrometers that disperse ions according to their m/z value, such as in magnetic sector instruments.

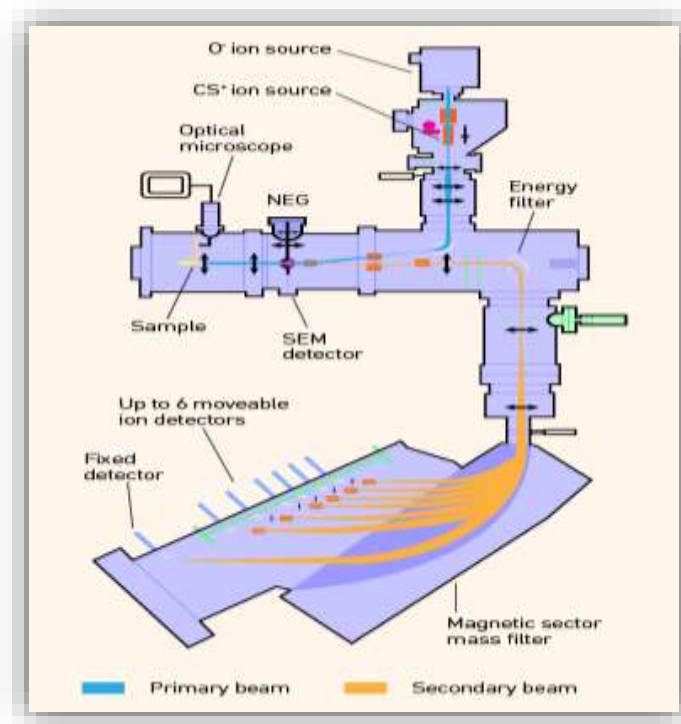


Figure 21. Schematic diagram of nanoscale secondary ion mass spectrometer with a double focusing magnetic section mass spectrometer incorporating a multicollector system and static magnetic field



I.3.6.2.4. Some new generation HPLC pumps

Liquid chromatography is a vitally important technology utilized across a number of industries, including food safety, pharmaceutical development, environmental monitoring and various industrial and consumer product applications. Although these industries may vary greatly, the LC applications they utilize all demand precision, accuracy and flexibility to meet their unique analytical goals. **Figure 22** below exhibited an important component of the HPLC. <https://www.perkinelmer.com/fr/category/lc-instruments>

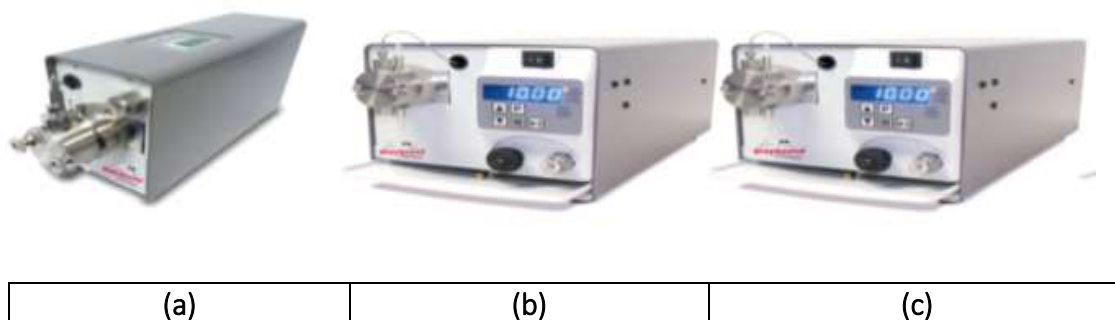


Figure 22. New generation of pumps in HPLC

Table 21. Some characteristics of new generation of pumps in HPLC

	Pump model		
	(a) (M1 Class)	(b) (ML, MX & MXT CLASS)	(c) (LS & LST Class)
	Low Profile Single Piston Isocratic Pumps	Single Piston Isocratic Pumps	Single Piston High Performance Isocratic Pumps
Max flow rate*/pressure	10 mL/2,000 PSI 40mL/500 PSI	10 mL/5,000 PSI 40 mL/900 PSI	5 mL/6,000 PSI ; 10 mL /6,000 PSI ; 40 mL/1,600 PSI
Flow accuracy	Within 2% of set flow rate 10mL- 0.20 mL/min and above; Within 5% of set flow rate 40mL- 0.80 mL/min and above	Within 2% of set flow rate 10mL- 0.20 mL/min and above	Within 2% of set flow rate 10mL- 0.20 mL/min and above
Dimensions (h x w x d)	14 x 8 x 27 cm	17 x 18 x 41 cm	16.5 x 18 x 41 cm

*Flow rate is dependent on solvent selection and operating pressure - 1 PSI = 0,069 bar = 6897.8 Pa.

<https://www.greyhoundchrom.com/Content/Images/uploaded/files>.



I.3.6.2.5. Some LC columns

1. MacroSep BIO and BIO-Gold Wide Pore Columns

We have developed a line of wide pore columns (**Figure 23**) to provide the bio analytical chromatographer with a highly efficient state-of-the-art base deactivated wide pore HPLC column. This column is based upon ultra-high purity metal free silica containing highly controlled pores of 300 Å diameter. This column technology is a superior tool for the analysis of proteins, peptides, and other biomolecules.



Figure 23 : MacroSep BIO and BIO-Gold Wide Pore Columns

Table 22. Some characteristics of Wide Pore Columns

Wide Pore Columns			
Material Characteristics			
Phase	Particle Size (µm)	Pore Size (Å)	pH Range
C18	3, 5, 10	300	2-8
Biphenyl	1.9, 3, 5, 10	400, 1200	2-9
Diphenyl	1.9, 3, 5, 10	400, 1200	2-9
Naphthyl	1.9, 3, 5, 10	400, 1200	2-9
Features and Benefits	<ul style="list-style-type: none">Wide pore surface for the analysis of proteins and peptides;Ultra-high purity metal free silica for improved peak shape, especially for basic compounds;State-of-the-art base deactivation to ensure superior recoveries of proteins and peptides.		

Chromegapore Molecular Size Exclusion (MSE) Columns

Size Exclusion chromatography separates molecules based on their size. The MSE (**Figure 24**) columns are available in a wide variety of particle and pore sizes: in Silica, TMS bonded to silica, and Diol bonded to silica. Silica and TMS columns are recommended for the analysis of polymers that are organic soluble. Diol columns are recommended for samples that are water soluble, such as proteins, peptides, and water-soluble synthetic polymers. They can



be packed into columns of various dimensions and are available in a variety of pore sizes (60 - 1000 Å).



Figure 24. Chromegapore Molecular Size Exclusion (MSE) Columns

Table 23. Some characteristics of MSE columns

	MSE columns			
	Material Characteristics			
	Phase	Particle Size (µm)	Pore Size (Å)	pH Range
	Diol	5	60, 100, 300, 500, 1000	2-8
	Silica	5	60, 100, 300, 500, 1000	2-8
	TMS (C1)	5	60, 100, 300, 500, 1000	2-8
Features and Benefits	<ul style="list-style-type: none"> Five pore sizes (60, 100, 300, 500, and 1000 Å) to allow separation of molecules of different size; Three phases (Diol, Silica, and TMS) to accommodate both aqueous and organic soluble samples. 			

GreenSep Supercritical Fluid Chromatography (SFC) Columns

They are specifically engineered for SFC separations, paying close attention to bonding coverage, density and all factors leading to high capacity phases which exhibit excellent selectivity and peak shape. Many of the GreenSep SFC columns designed for basic and acidic compounds do not require mobile phase additives that are commonly required with other brands of phases. The SFC (Figure 25) range features a variety of selectivities offering orthogonality. All of these materials are available in analytical and also semi-preparative (10 mm), and preparative (20 mm, 30 mm and 50 mm) dimensions.



Figure 25. GreenSep Supercritical Fluid Chromatography (SFC) Columns

Table 24. Some characteristics of SFC columns

Columns	
Material Characteristics	
Phase	Particle Size (µm) Pore Size (Å) pH Range
Amine	1.8, 3, 5, 10 120 2-10
Basic	1.8, 3, 5, 10 120 2-10
Silica	1.8, 3, 5, 10 120 2-10
Features and Benefits	<ul style="list-style-type: none"> GreenSep are specifically designed for superior separation, selectivity, peak shape, and loading capacity compared to conventional normal-phase HPLC materials adapted for SFC; Highly efficient columns with superior reproducibility produced from our rigorous bonding procedures; Directly scalable from analytical to preparative on the same media to streamline purification and maximise operational efficiency; Many phases have been specifically engineered using functional group chemistry that don't require mobile phase additives such as triethyl amine.

<https://resources.perkinelmer.com/lab-solutions/resources/docs/CAT-ES-Industries-LC-Columns-Catalog-204316.pdf>

1.3.6.3. Requirements of LC-MS instrumentation

The use of LC-MS in many application areas within analytical science continues to grow almost exponentially. Listed below are some pointers as to the applicability of both HPLC as a separative technique and MS as a means of detecting analyte species. So, for HPLC analysis, the following are required:

- the analyte must be soluble in the mobile phase;



- samples over a wide polarity range including ionic samples can be analysed;
- there is no real upper molecular weight limit and large proteins of many thousands of Daltons may be analysed;
- samples are prepared in a solvent system that has the same or less organic solvent than the mobile phase;
- the effluent mobile phase with separated compound from the liquid chromatography is interfaced with the ionization source of the Mass spectrometer;
- Usually LC used in LC-MS is HPLC. The principle of separation in HPLC, is normal phase mode or reverse phase mode of adsorption. Normal phase constricts with polar stationary phase with non-polar solvent/mobile phase and reverse phase constricts with non-polar stationary phase with polar solvent/mobile phase. Normal phase mode not widely used in biomedical research and not advisable for pharmaceutical applications since most of the drug are polar in nature and takes longer time to be elute and detected. Reverse phase mode have wide range of pharmaceutical application.

I.3.6.4. Applications of LC/MS

LC-MS/LC-MS/MS are most widely used in food industries, pharmaceutical and chemical industries for quantitative and qualitative analysis (**Kaufmann et al. 2002**). Applications of LC-MS/MS are as follows:

- Isolation and analysis of natural products. In fact, crude natural product extracts, which represent extremely complex mixtures of numerous compounds, can be analyzed successfully by using appropriate hyphenated techniques such as LC-MS;
- Chemical fingerprinting and quality control of herbal medicine. Several analytical protocols based on LC-MS fingerprinting have been developed and integrated into a high-throughput analytical program incorporating standard methods, template structure determination, and structural libraries (**Patel et al. 2010**).
- Dereplication strategies employ a combination of separation science, spectroscopic detection technologies, and on-line database searching. Thus, the combination of HPLC with structurally informative spectroscopic detection techniques, e.g., MS, and NMR, could allow crude extracts or fractions to be screened not just for biological activity but also for structural classes;



- Metabolomics - The aim of metabolomics, for example, plant metabolomics, is to provide a better understanding of metabolic or other physiological phenotypes through global genome-related technology;
- Chemotaxonomy or Chemical taxonomy - LC-MS was also found to be useful in chemotaxonomic studies based on flavonoid profiles in legumes. (Patel et al. 2010).
- Molecular weight determination - Able to determine the molecule weight of chemical substance, pharmaceutical substances, proteins, etc;
- Structural determination/elucidation: Tandem mass spectrometry used to determine structural information using mass spectral fragmentations;
- Pharmaceutical applications: It's used to determine the pharmacokinetic profile of the pharmaceuticals like drug, drug metabolites/degradation product, impurities and chiral impurities. The separation and detection of chiral impurities in pharmaceuticals are of great importance because the D-isomer of a drug can have different pharmacological, metabolic and toxicological activities from the L-isomer;
- Food and Environmental applications: use to identify aflatoxins (toxic metabolic product in certain fungi), determine the vitamin D3 in poultry fed supplements, etc.

I.3.6.4.1. Application of Mass Spectrometry in the Synthesis and Characterization of Metal Nanoclusters

In recent years, MS has been widely used in the characterization of metal nanoclusters (Lu et al. 2015). MS has now become an indispensable tool in metal nanocluster research. Also, during the past decade, various MS techniques have been used in the studies of gold, silver, copper, noble metals, and their doped or alloyed nanoclusters. However, high-quality MS spectra of cluster samples need optimized MS experimental conditions. For different cluster systems, how to get the optimal conditions, such as the type of MS, selection of matrix, etc., is the critical step to easily obtain the correct composition information on metal nanoclusters. We believe that MS will have more wide applications in the field of metal nanoclusters in the future (Lu et al. 2015).



I.3.6.4.2. Applications of Mass Spectrometry for Clinical Diagnostics: The Influence of Turnaround Time

The need for reduced clinical turnaround times has influenced chemical instrumentation. The focus on the development of modern mass spectrometry (MS) and its application in clinical diagnosis is point out. With increased functionality that takes advantage of novel front-end modifications and computational capabilities, MS can now be used for non-traditional clinical analyses, including applications in clinical microbiology for bacteria differentiation and in surgical operation rooms. **Figure 26** below summarizes here the recent developments in the field that have enabled such capabilities, which include miniaturization for point-of-care (POC) testing, direct complex mixture analysis via ambient ionization, chemical imaging and profiling, and systems integration (**Swiner et al. 2020**).

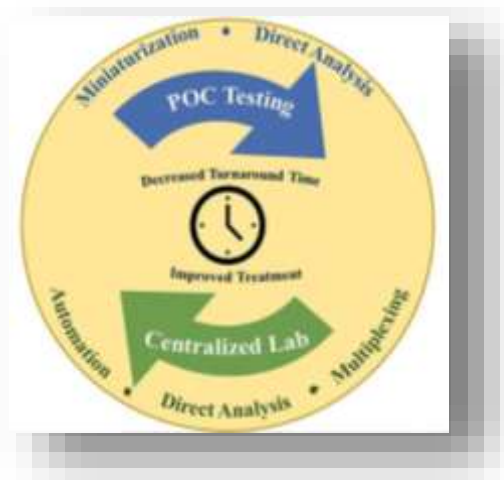


Figure 26. The Influence of Turnaround Time

I.3.6.5. Applications of LC/MS in the detection

Detection sensitivity in this technique is limited to 10⁻⁸ μl, and needs large volume to increase the sensitivity of the detection. By using ESI high mass sample, non-volatile molecules, liquids can be ionized and disadvantage of this source of ionization with poor sensitivity, low fragmentation and source is instable.

The application of LC/MS is very useful in situations that involve a huge number of compounds, such as environmental effluents. LC-MS provides a tool for differentiating this huge plant multifariousness because of this technique's capability of analyzing a broad variety of metabolites together with secondary metabolites (e.g., alkaloids, glycosides, phenyl



propanoids, flavonoids, isoprenes, glucosinolates, terpenes, benzoids) and extremely polar and/or higher mass molecules (oligosaccharides and lipids). LC-MS is found to be an efficient method in flavonoid analysis, particularly for their glycosidic derivatives and acylated conjugates (De Rijke et al. 2006).

With the advent of new ionization approaches, especially atmospheric pressure, the technique has established itself firmly in many areas of research. Therefore, in drug detection (Van Bocxlaer et al. 2000) and flavonoid analysis (De Villiers et al. 2016), ESI and APCI are the ideal ionization sources used.

I.3.6.5.1. Detection of drugs

The advent of robust, bioanalytically compatible combinations of liquid chromatographic separation with mass spectrometric detection really opens new perspectives in terms of mass spectrometric identification of difficult molecules (e.g., polar metabolites) or biopolymers with toxicological relevance, high throughput, and versatility (Van Bocxlaer et al. 2000). Therefore, LC-MS was proven to be an effective method to detect drugs for overdose patients, especially for drugs that were not detected by other screening methods or when there was no information about overdosed drugs. For treating critical patients with a suspicion of drug overdose under such conditions, clinicians should utilize LC-MS if available, or decide to transfer the patients to higher-level facilities where LC-MS is available (Yagihashi et al. 2020).

I.3.6.5.2. Detection of Flavonoids

Detection of flavonoids depends on their chemical properties and sensitivity of the analytes. Some compounds are identified based on the retention time of reference standards and UV absorption spectrum. Two compounds may be closely related and elute at the same time but are separated based on their differences in absorption spectra through multiple wavelength detection systems. Acetonitrile and methanol do not interfere during the detection of UV-Vis absorption bands at 240–285 nm and 300–560 nm of A and B rings of the flavonoid aglycones because of their low UV cut-off λ_{max} values at 190 nm and 205 nm. In the case of flavones, the substitution patterns of hydroxy and methoxy groups and the types of glycosides (C or O-glycosides) result in small variation of the wavelength range of both the bands (Annie Bligh et al. 2013). Protonated $[M+H]^+$ and deprotonated $[M-H]^-$ ions are observed with low cone voltages during flavonoid analysis with small fragmentation patterns. Adducts such as $[M-H+AcONa]^-$, $[M+HSO_4]^-$, and $[M-H+AcONa+MeOH]^-$ are commonly detected based on the



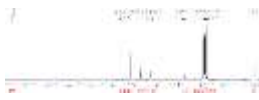
composition of the mobile phase used (De Villiers et al. 2016). Sodium and potassium adducts are often seen during flavonoids analysis in ESI (+ve mode). These are formed during storage of the sample in glass solution and are detected during the analysis of flavanol-3-O-glycosides and isoflavones (Cuyckens et Claeys 2004). Loss of water (18 Da), CO (28 Da) and C₂H₂O (42 Da) and combined loss of H₂O and CO (46 Da) are commonly observed in less characterized flavonoids with little fragmentation patterns. O-methylated isoflavones, flavones, and flavonols show the loss of methyl radical with product ion [M+H-15]⁺. Further, the combined loss of methyl group and water [M+H-33]⁺ is also observed during analysis of flavonoids (De Rijke et al. 2006).

I.3.6.6. Some limitations of LC/MS

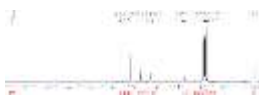
- The major disadvantage of LC/MS is that it only works with volatile buffers that are required to avoid fouling of the API interface;
- LC-MS has another disadvantage is that the residual impurities being analyzed should be ionized;
- Phosphate buffer is not compatible with the LC/MS analysis, which is the most commonly used buffer in HPLC method development;
- LC-MS is an expensive technique both in terms of capital and analysis costs;
- This is not a portable instrument; it requires special and more space;
- To operate and data analysis of the liquid chromatography and mass spectrometry (LC-MS) requires a skilled and trained person;
- The LC-MS has a high maintenance cost as compared with other analytical instruments.
- Besides limitations in selectivity due to the occurrence of "isobaric" interferences, unpredictable ion yield attenuations, known as "ion suppression effect," have to be considered. In addition, most LC-MS/MS methods used in clinical laboratories are still laboratory-developed tests ("in-house assays") operating on very heterogeneous instrument configurations. Consequently, assay heterogeneity and lack of traceability to reference procedures or materials may lead to an increased imprecision in proficiency testing as well as inaccurate result reporting if basic rules of assay validation and "post marketing" surveillance are violated. (Seger, 2012)



In partial conclusion, we noticed that the two key elements in natural product research are the isolation and purification of compounds present in crude extracts or fractions obtained from various natural sources, and the unambiguous identification of the isolated compounds (**Patel et al. 2010**). The characterization of secondary metabolites in crude natural product extracts or fractions demands high degree of sophistication, and richness of structural information, sensitivity, and selectivity. Thus, the development of various hyphenated techniques has provided the natural product researchers with extremely powerful new tools that can provide excellent separation efficiency as well as acquisition of on-line complementary spectroscopic data on an LC peak of interest within a complex mixture.



CHAPTER 2: RESULTS AND DISCUSSION



CHAPTER 2: RESULTS AND DISCUSSION

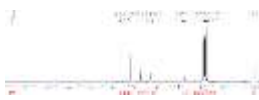
II.1. PLANT MATERIAL, EXTRACTION, ISOLATION, LC-MS DETECTION AND STRUCTURAL IDENTIFICATION OF COMPOUNDS OF *DUGUETIA STAUDTII*II.1.1. PLANT MATERIAL, EXTRACTION AND ISOLATION OF COMPOUNDS OF *DUGUETIA STAUDTII*

The barks of *D. staudtii* were successively collected in June 2016 and in July 2017 in the Dja forest at Lomié-Bertoua [GPS coordinates provided by system WGS8: Altitude 665 m; Latitude N 4°34'38''; Longitude E 13°41'04''], in the East Region of Cameroon. The botanical identification was done by Mr. Victor Nana, a botanist at the National Herbarium of Cameroon where the samples were registered under the voucher specimen 52711HNC.

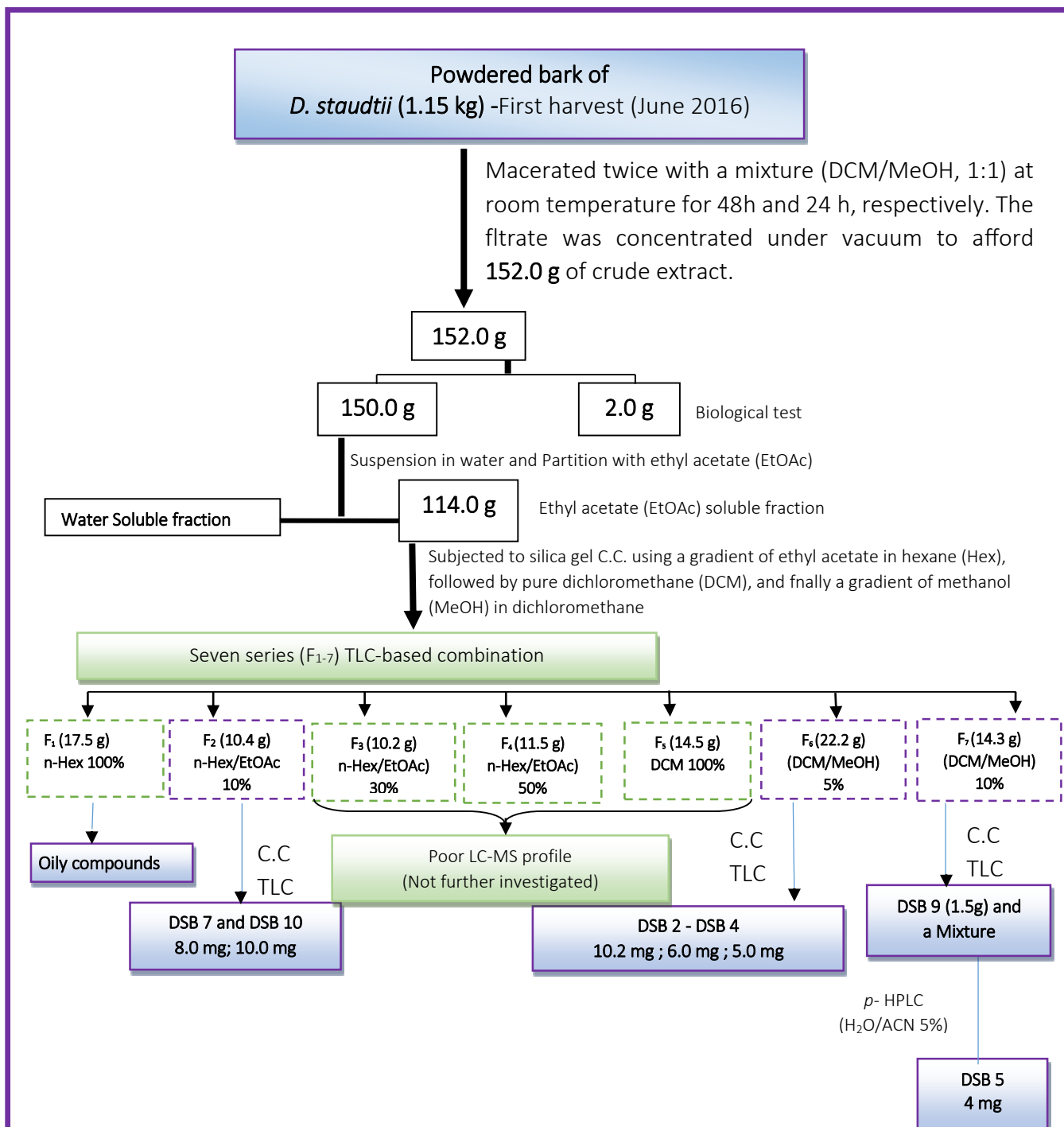
The air-dried and powdered stem barks (1.15 kg) and (~5.9 kg) obtained respectively for the first and second harvest of *D. staudtii* were macerated and extracted two times with a mixture of dichloromethane/methanol (1:1, v/v) at room temperature during 48h (first extraction) - 24 h (second extraction) for the first harvest and 72h (first extraction) - 24 h (second extraction) for the second one. Each mixture was filtered and the evaporation of the solvent under vacuum afforded respectively (152 g) and (382 g) of a brown crude residue. The second extract (**Scheme 14**) showed 100% activity on microfilariae (mf) and on *O. ochengi* adult female worms both at 250 µg/mL, indicating the inhibition of mfs motility, through the reduction of MTT to formazan.

In addition, the crude extract of the second harvest was analysed by High Performance Liquid Chromatography (HPLC) coupled to both diode array and Mass Spectrometry (MS) detectors. The latter was used with an Electrospray Ionization (ESI) source in positive ion mode. Due to its LC-MS' profile (**Figures 27-31**), part of the first extract (150 g) was suspended in water and partitioned with ethyl acetate (EtOAc) to yield 114 g of extract which was then subjected to silica gel column chromatography using a gradient of ethyl acetate in hexane (Hex), followed by pure dichloromethane (DCM), and finally a gradient of methanol (MeOH) in dichloromethane.

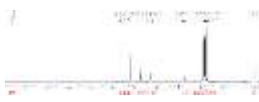
The active (DCM/MeOH (1:1) crude extract of the barks of *D. staudtii* was successively subjected to Liquid Chromatography coupled to Mass Spectrometry (LC-MS) analysis (**Tables 25-27**) and Vacuum Liquid Chromatography (VLC) as well as Column Chromatography (CC) techniques (**Tables 57-67**).



Seven compounds (DSB 2-4, 5, 7, 9-10) isolated from three of the seven main sub-fractions obtained. These sub-fractions were named F₁ (pure Hex), F₂ (Hex/ EtOAc, 10%), F₃ (Hex/ EtOAc, 30%), F₄ (Hex/ EtOAc, 50%), F₅ (pure DCM), F₆ (DCM/MeOH, 5%), F₇ (DCM/MeOH, 10%) as shown in **Scheme 13** below.



Scheme 13. Extraction and isolation flowchart of compounds from the bark of *D.staudtii*



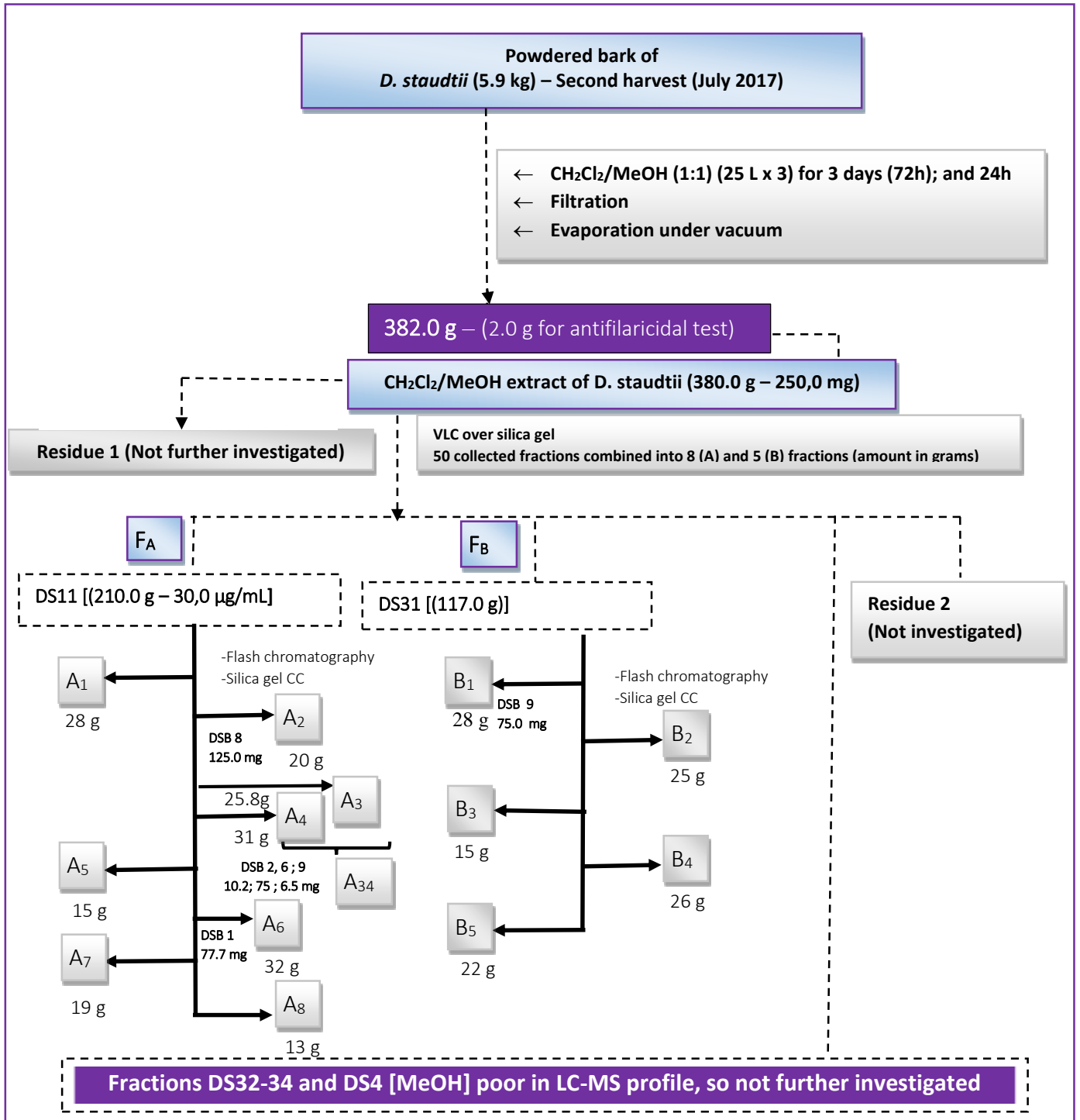
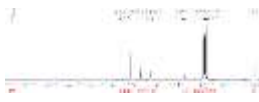
In addition to this first study, part of the second extract (380.0 g) was successively fractionated by a vacuum liquid chromatography (VLC) with dichloromethane (DCM) and methanol (MeOH) to give the soluble-DCM (**F_A**, 210.0 g) and methanol (**F_B**, 117.0 g) fractions.

Extract and fractions were assessed at 250 µg/mL along with fractions **F_A** and **F_B** which were separately assessed at 30 and 250 µg/mL respectively for their antifilaricidal activity on *O. ochengi* mf, resulting to 100% activity on mf for both fractions and further submitted to LC-MS analysis.

Part of the filaricidal fraction **F_A** (210.0 g) was subjected to LC-ESI-MS analysis (**Figure 27-31**) for the detection of new entities and their isolation through flash silica gel (230–400 mesh) column chromatography using a stepwise gradient of *n*-Hex/EtOAc (ranging from 0 to 100% of EtOAc, v/v). Afterwards, a total of 150 fractions (*fr*_{1–150}) of ca. 500 mL each were collected and combined on the basis of the TLC analysis to yield 8 main sub-fractions A_{1–8}. These sub-fractions were named A₁ (pure Hex), A₂ (Hex/ EtOAc, 20%), A₃ (Hex/ EtOAc, 30%), A₄ (Hex/ EtOAc, 40%), A₅ (Hex/ EtOAc, 50%), A₆ (Hex/ EtOAc, 60%), A₇ (Hex/ EtOAc, 70%), A₈ (pure EtOAc); with A₃ and A₄ combined later into A₃₄, as shown in **Scheme 14** below.

Some of these sub-fractions were also separately assessed for their LC-MS and antifilaricidal analyses. The biological experiment was done on any of the three parasite stages (mf, *O. ochengi* adult male and female worms) for further fractionation. Some compounds were detected through LC-MS analysis (**Figures 27-31, Table 25-27**) including **DSB 1, 2, 6, 8, 9** and obtained from these sub-fractions.

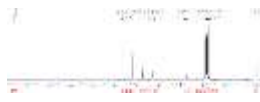
Part of the soluble-methanol fraction **F_B** (117.0 g) was also subjected to the flash chromatography over silica gel and eluted with a gradient of *n*-Hex/EtOAc (ranging from 6:4 to MeOH, v/v) to afford five sub-fractions (**B_{1–5}**) from which one compound labelled **DSB 9** were isolated as shown in **Scheme 14** below.



Scheme 14. Extraction and isolation flowchart of compounds from the bark of *D.staudtii*

II.1.2. LC/MS DETECTION OF COMPOUNDS OF *DUGUETIA Staudtii*

From the study of the stem bark of *D. staudtii*, with regard to the two harvest, some compounds have been isolated among which 10 (DSB 1-10; Table 27) were detected through LC-MS analysis and fully characterized. These structures were elucidated by means of



spectroscopic data analysis with the help of literature review and completed via LC-MS and XRD analysis. Prior to this, the LC-MS analysis help for detection of known compounds and fractions containing unknown compounds were scrutinized on the basis of their molecular profiles (Figures 27-31). So, the LC-MS analysis of the filaricidal (DCM/MeOH (1:1, v/v - 250 μ g/mL) extract DS02 (Figure 27) and DS11 (30 μ g/mL) active fraction (Figure 28) of the barks of *D. staudtii* led to a non-exhaustive detection of peaks with the retention time ranging respectively from 1.00 to 10.00 min (A, C, D and E) and from 1.00 to 27.50 min (B). The LC-MS spectrums interpretation was performed using database for organic compounds and Scifinder tool.

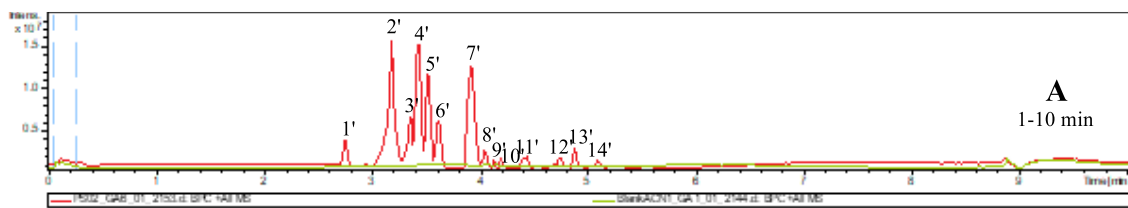


Figure 27. LC-MS chromatogram of the active (DCM/MeOH (1:1, v/v - 250 μ g/mL) extract of *D. staudtii* (A)

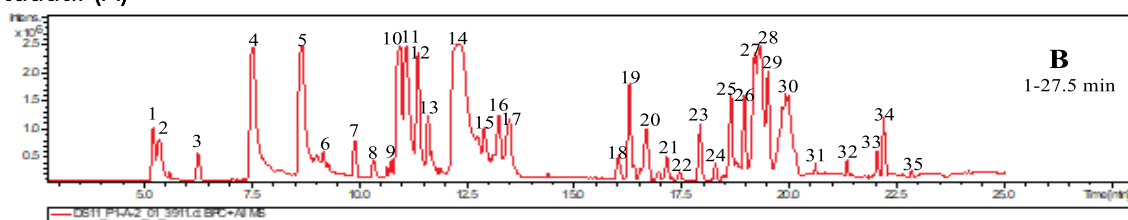


Figure 28. LC-MS chromatogram of the active DS11 (30 μ g/mL) fraction of *D. staudtii* (B)

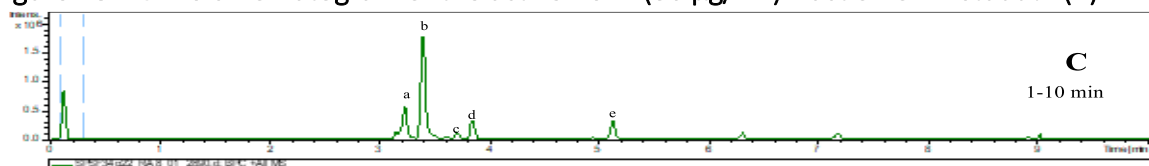


Figure 29. BPC of two unknown compounds (Rt: 3.3 and 3.4 min) and two known (Rt: 3.7 and 3.9 min) detected from the sub-fraction C

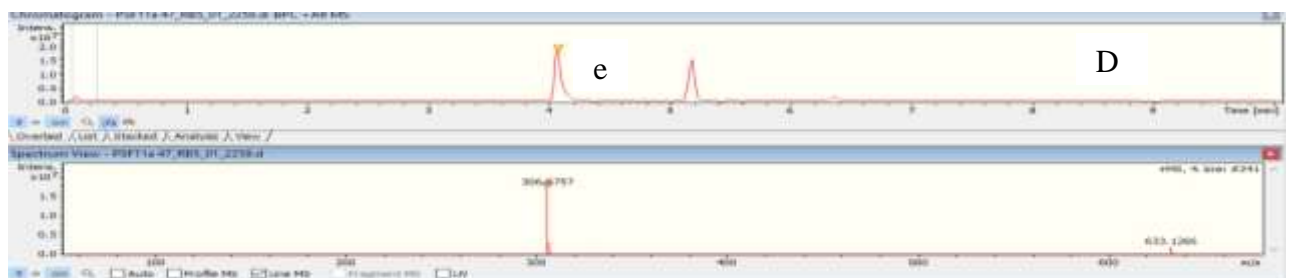


Figure 30. BPC of one unknown compound detected from the sub-fraction D of *D. Staudtii* respectively at Rt: 4.1 min (e)

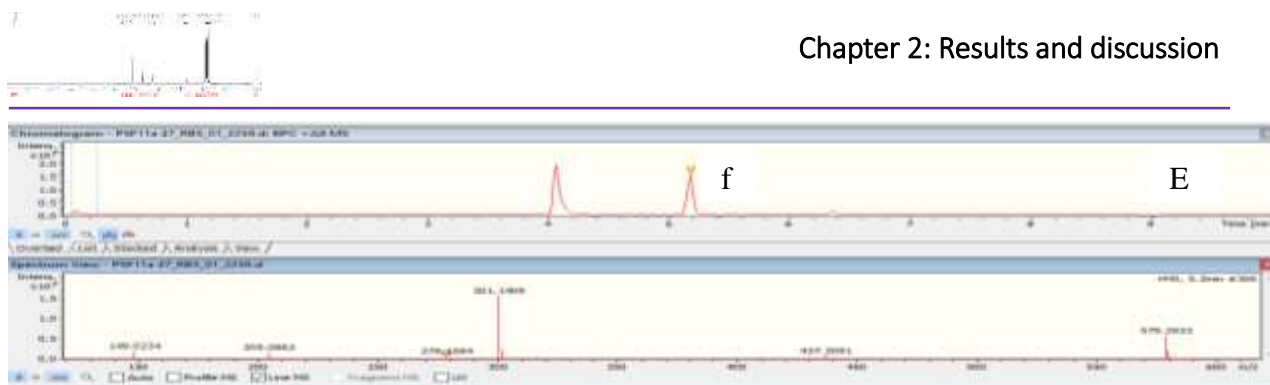


Figure 31. BPC of one unknown compound detected from the sub-fraction E of *D. Staudtii* respectively at Rt: 5.2 (f) min

Table 25. Peak list with mass-to-charge ratio (m/z) values, retention times of some detected compounds (1-30) from (DCM/MeOH (1:1, v/v) extract and DS11 (30 $\mu\text{g}/\text{mL}$) fraction of *D. staudtii*

Peak n°	R _t (min)	[M+H] ⁺		Hyp. Mol. formulae	Name of compounds	Chr. n°
		Exp.	Calcd.			
1'	3.2	342.1704	342.1700	C ₂₀ H ₂₄ NO ₄	Corypalmine 5 , Isocorypalmine and Discretine	
2'	3.4	233.1527	233.1536	C ₁₁ H ₂₁ O ₂	Costunolide 110	
3'	4.1	306.0757	306.0763	C ₁₈ H ₁₂ NO ₄	Atherospermidine or Lanuginosine	A
4'	4.3	322.1068	322.1074	C ₁₉ H ₁₆ NO ₄	O-Methylmoschatoline	
5'	4.4	345.0958	345.0969	C ₁₈ H ₁₆ O ₇	Pachypodol 16	
6'	5.0	539.1903	539.1912	C ₂₉ H ₃₁ O ₁₀	New –Pachypodostyflavone 105	
1	5.1	427.2497	427.2479	C ₂₆ H ₃₅ O ₅	N. I.	
3	6.3	211.0987	211.0965	C ₁₁ H ₁₅ O ₄	2',4',5'-Trimethoxyacetophenone 103	
4-1	7.50	195.1037	195.1016	C ₁₁ H ₁₅ O ₃	2,4,5-trimethoxystyrene 104	
4-2	7.59	323.9487	323.9470	C ₁₉ H ₁₉ N ₂ O ₃	Spiguetidine	
5	8.7	197.1094	197.1020	C ₇ H ₁₇ O ₆	N. I.	
9	11.0	407.2055	407.2064	C ₂₂ H ₃₀ O ₇	New – Pachypolignan 109	
10	11.1	395.3675	395.3672	C ₂₉ H ₄₇	N. I.	
12	11.4	219.1767	219.1743	C ₁₅ H ₂₃ O	N. I.	
13	11.6	389.1997	389.1959	C ₂₂ H ₂₉ O ₆	Pachypophyllin 13	B
18	16.0	445.2780	445.2796	C ₂₃ H ₄₁ O ₈	N. I.	
20	16.7	447.2937	447.2952	C ₂₃ H ₄₃ O ₈	N. I.	
21	17.1	369.2826	369.2788	C ₂₅ H ₃₇ O ₂	N. I.	
23	17.9	391.2848	391.3121	C ₂₁ H ₄₃ O ₆	N. I.	
25	18.6	457.3123	457.3101	C ₃₂ H ₄₁ O ₂	N. I.	
26	19.0	391.2881	391.2843	C ₂₄ H ₄₃ O ₈	N. I.	
27	19.3	437.3455	437.3473	C ₂₃ H ₄₉ O ₇	N. I.	
28	19.5	297.2818	297.2788	C ₁₉ H ₃₇ O ₂	N. I.	
30	20.0	419.3197	419.3156	C ₂₆ H ₄₃ O ₄	N. I.	

N.I.: Not identified – Chr.: Chromatogram – Hyp. Mol. : Hypothetical Molecular

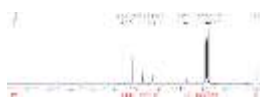


Table 26. Peak list with listed m/z values and retention times of some compounds detected from a sub-fraction A34 of *D. staudtii*

Peak n°	R _t (min)	[M+H] ⁺		[2M+H] ⁺	Molecular formulae	Name of compounds	Chr. n°
		Exp.	Calcd.				
a	3.3	358.1657	358.1649	715.3231	C ₂₀ H ₂₄ NO ₅	N.I	
b	3.4	372.1813	372.1805	743.3547	C ₂₁ H ₂₆ NO ₅	N.I	
c	3.7	326.1389	326.1387	651.2693	C ₂₀ H ₂₀ NO ₄	N-Methylcalycinine, Guatterine, Oliveridine or Buxifoline	C
d	3.9	338.1387	338.1387	–	C ₂₀ H ₂₀ NO ₄	N-Acetylpachypodanthine	
e	4.1	306.0757	306.0761	633.1266	C ₁₈ H ₁₂ NO ₄	N.I	D
f	5.2	279.1594	279.1591	579.2933	C ₁₆ H ₂₃ O ₄	N.I	E

N.I.: Not identified – Chr.: Chromatogram

The isolated compounds were sorted into flavonoids, lignans, alkaloids, triterpens and steroid (Table 27).

Table 27. Isolated Compounds from *D. staudtii* sorted by Class and Retention Time

Codes	Name of compounds	Class	[M+H] ⁺	RT (min)
DSB 1	Pachypodostyflavone <u>105</u> (New)	Flavonoid	539.1903	5.0
DSB 2	Pachypodol <u>16</u> (Known)	Flavonoid	345.0958	4.4
DSB 3	Kumatakenin <u>106</u> (Known)	Flavonoid	315.1825	4.8
DSB 4	5,4'-dihydroxy-3,7,3'5'-tetramethoxyflavone <u>107</u> (Known)	Flavonoid	375.1805	4.2
DSB 5	Pachypolignan <u>109</u> (New)	Lignan	407.2055	11.0
DSB 6	Pachypostaudin-B <u>11</u> (Known)	Lignan	387.1805	4.8
DSB 7	Pachypophyllin <u>13</u> (Known)	Lignan	389.1932	0.5
DSB 8	Costunolide (6R,7S) <u>110</u> (Known)	Sesquiterpenoid	233.1527	3.4
DSB 9	Corypalmine <u>5</u> (Known)	Alkaloid	342.1704	3.2
DSB 10	Polycarpol <u>111</u> (Known)	Terpenoid	441.1524	3.8

II.1.3. CHARACTERISATION AND IDENTIFICATION OF ISOLATED COMPOUNDS OF *DUGUETIA STAUDTII*

From the chemical study of the active fraction DS11 of *D. staudtii* active extract, several compounds were identified by LC-ESI-MS analysis and ten of these have been isolated. Their structures were elucidated by spectroscopic data and XRD analyses. In addition the microfilaricidal and Cytotoxicity activities were performed. These compounds belong to various classes of compounds.

II.1.3.1. Flavonoids

II.1.3.1.1. Identification of DSB 1

DSB 1 was obtained as an orange solid (m.p. 181–183 °C; $[\alpha]_D^{20} = 0$ (c 0.5); UV [MeOH, λ_{\max} nm (log ϵ): 229 (1.08), 269 (0.73), 293 (0.56), 354 (0.85) nm; IR [KBr, ν_{\max} (cm⁻¹): 3660 (OH stretching), 1738 (C=O), 1655 and 1595 (aromatic ring), 1489 and 1345 (CH₃ and CH₂), 1205 (aliphatic C–O), 1038 (aromatic C–O) (**Figure 33**). It reacted positively to the shinoda test and its phenolic nature was confirmed by the FeCl₃ reagent. Moreover, its molecular formula C₂₉H₃₀O₁₀ was established from the positive ion mode HR-ESI-MS, which showed the quasi-molecular ion peak $[M+Na]^+$ at m/z 561.1723 (calcd. for C₂₉H₃₀O₁₀Na, 561.1731) (**Figure 32**).

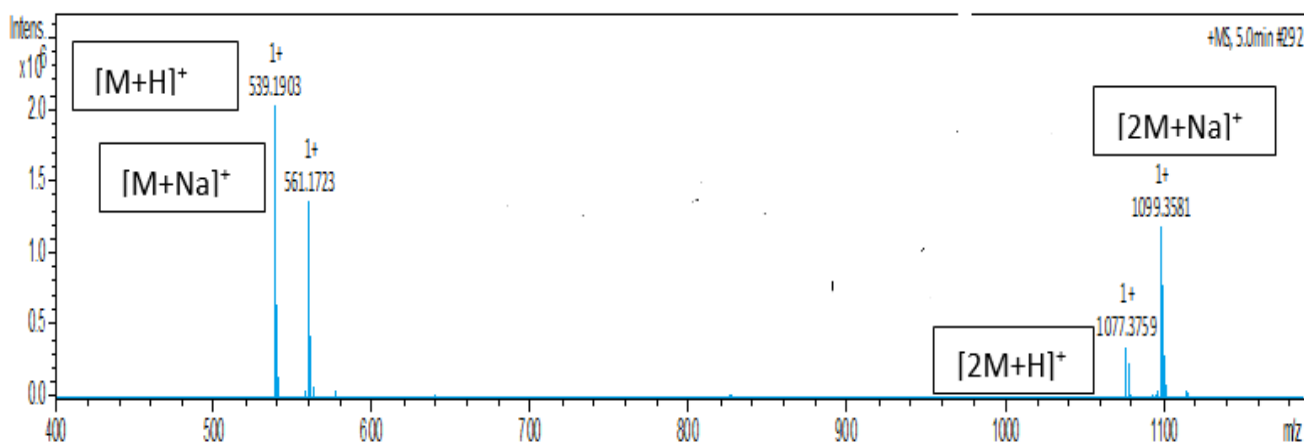
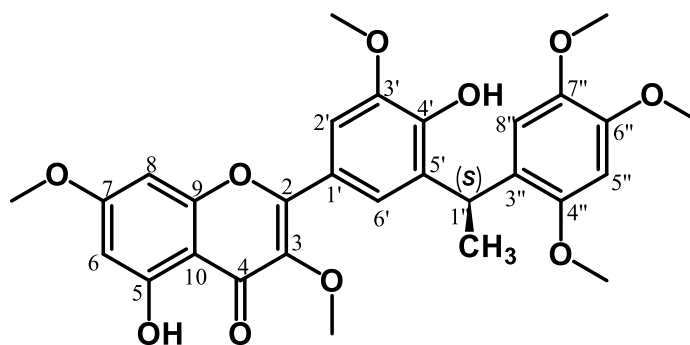
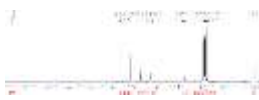


Figure 32. HR-ESI-MS spectrum of DSB 1

Based on the physical and spectroscopic data coupled with the analysis of the X-ray crystallography (**Scheme 15**) the structure of **DSB 1** was finally determined as mentioned below **105**:



105

In fact, the FT-IR spectrum (Figure 33) showed characteristic vibration bands for hydroxyl group, a conjugated carbonyl group and aromatic double bonds, while the experimental UV-vis spectrum of DBS 1 in methanol contains four electronic absorption bands with maxima all together as illustrated above (Figure 34), suggesting a flavone skeleton (Markahm, 1982).

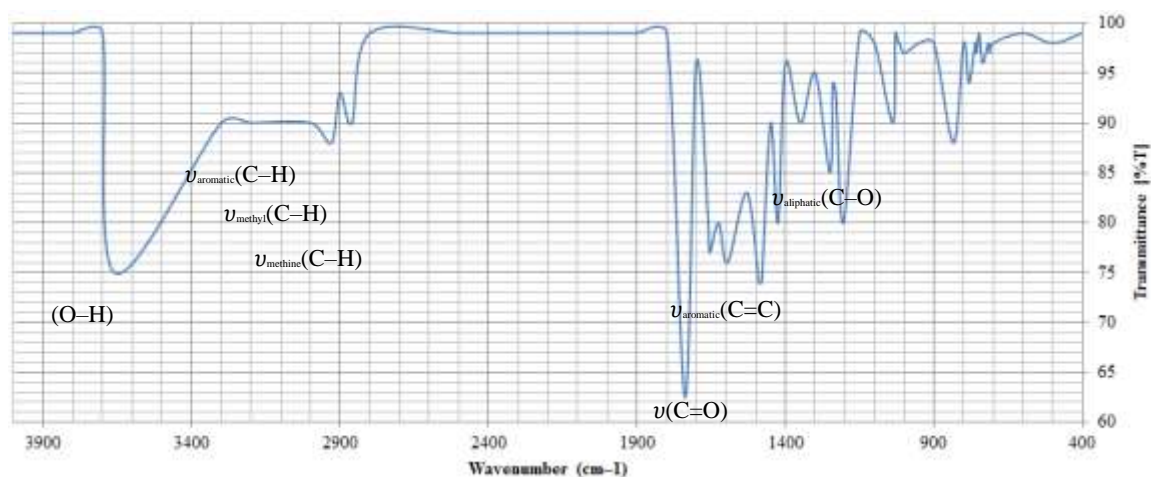


Figure 33. Experimental FT-IR spectrum of DSB 1 in methanol

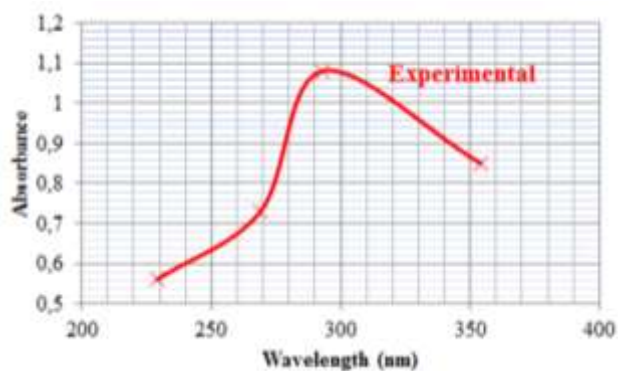


Figure 34. Experimental UV-vis spectra of DSB 1 in methanol

The ^{13}C NMR spectrum (Figure 35; Table 28) displayed 29 carbon signals which were sorted by DEPT (Figure 37) and HMQC (Figure 38) experiments into one methyl, six methoxyl,

seven methines and fifteen quaternary carbons including a characteristic flavone carbonyl group at δ_c 178.7 (Markham, 1990; Fang, 2006).

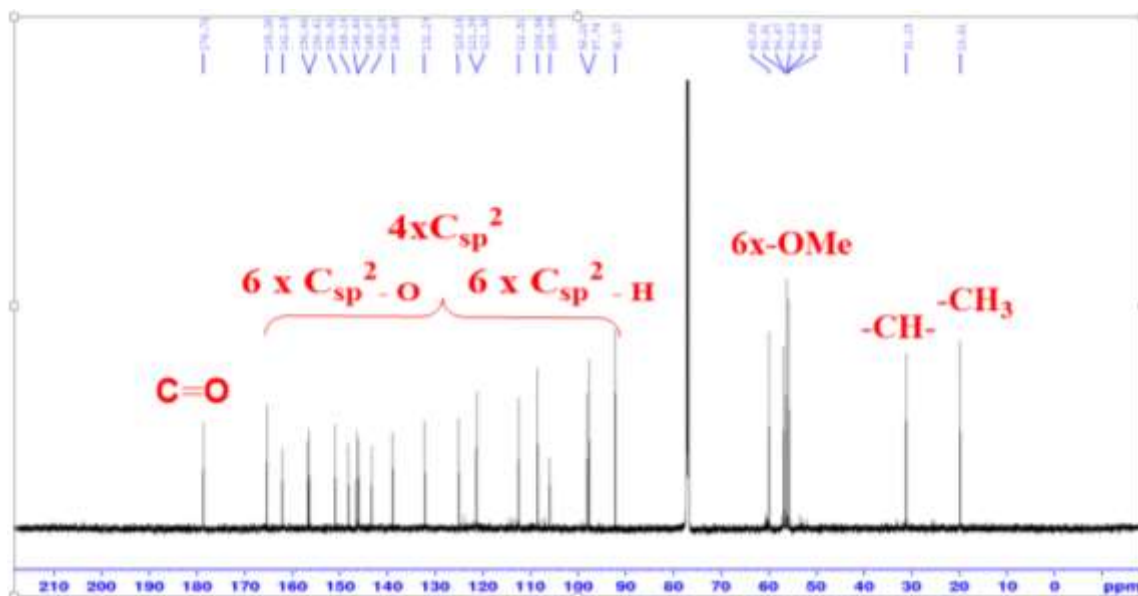


Figure 35. ^{13}C NMR (125 MHz, CDCl_3) spectrum of DSB 1

The ^1H NMR spectrum (Figure 36; Table 28) exhibited a signal of a chelated hydroxyl group (δ_{H} 12.69), the resonances of aromatic protons observed in the deshielded region (δ_{H} 7.70–6.40), and the signals of two sets of aliphatic protons in the up-field region at δ_{H} 4.85–1.60 which included six sharp 3-proton singlets at δ_{H} 3.98–3.80 for methoxyl groups.

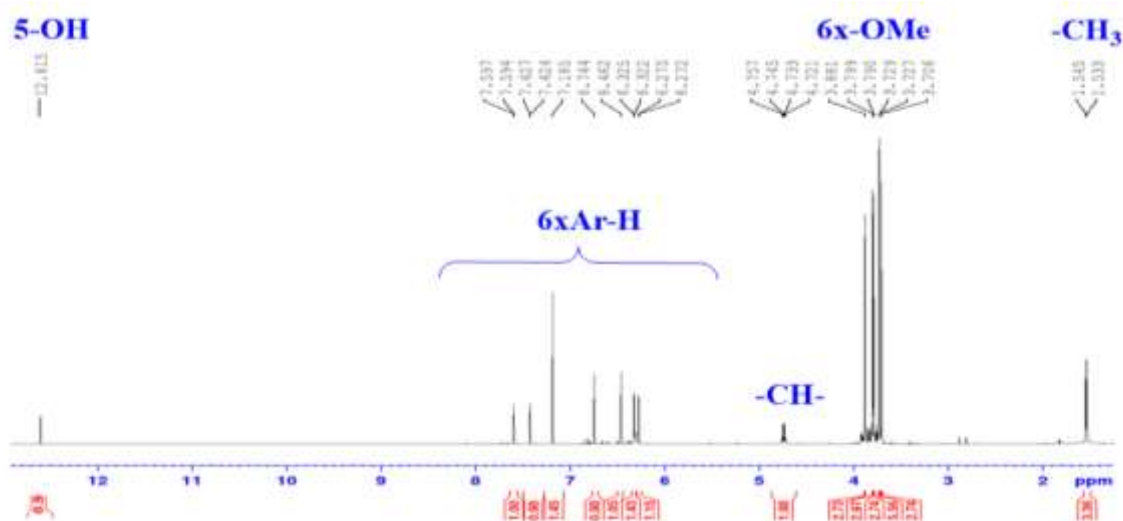


Figure 36. ^1H NMR (500, CDCl_3) spectrum of DSB 1

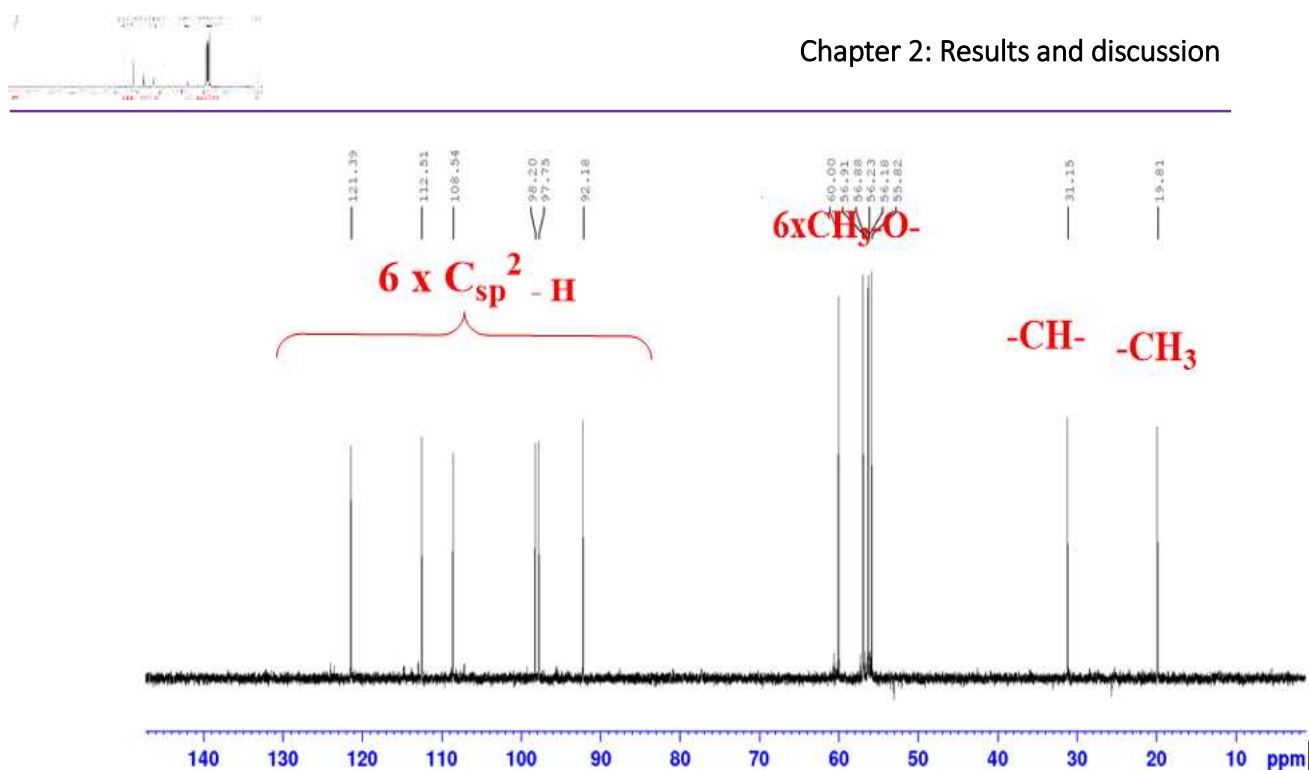


Figure 37. DEPT 135 spectrum of DSB 1

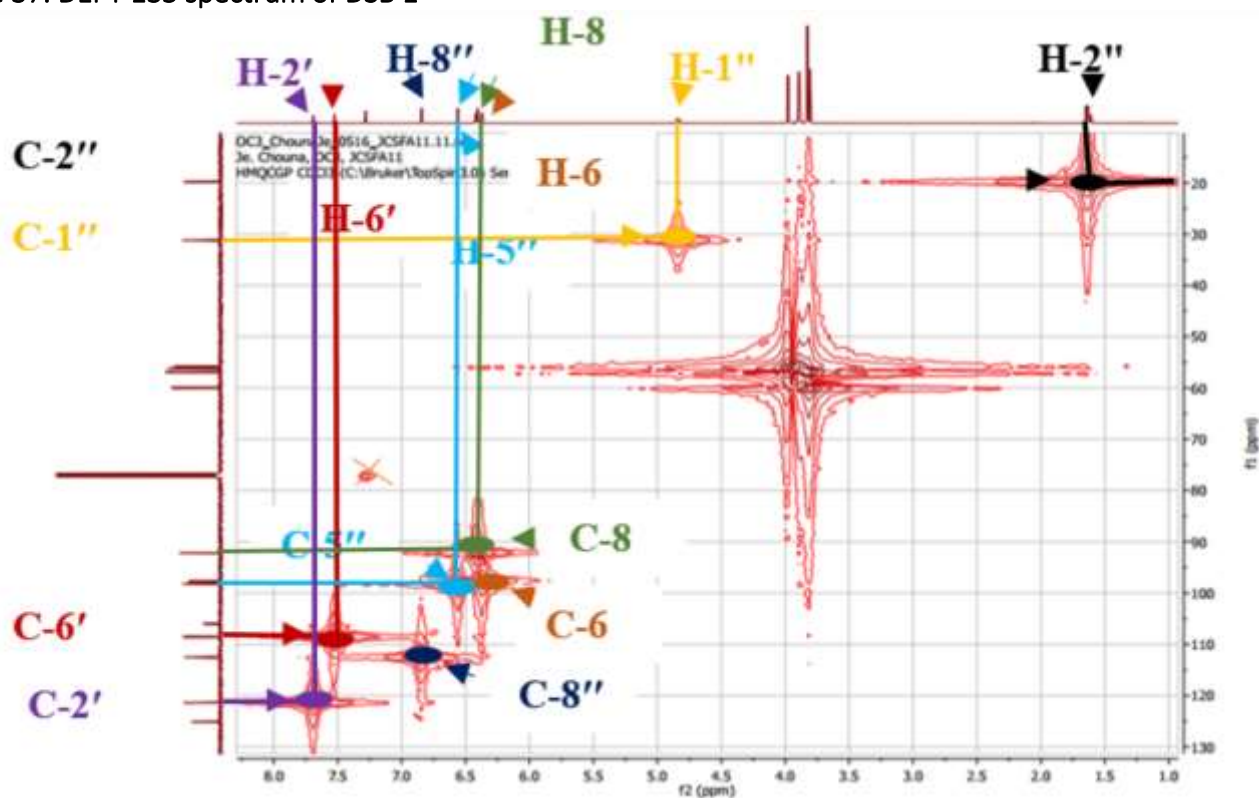
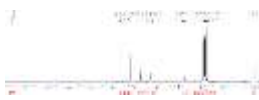


Figure 38. HMQC spectrum of DSB 1

However, the aromatic proton signals were sorted on the basis of their coupling constants, into three separate benzene ring systems as follows: (a) The meta-coupled aromatic proton signals at δ_H 6.42 and 6.37 (1H each, d , 2.2 Hz, H-6, H-8) set the presence of a tetra-



substituted benzene ring, characteristic for A-ring of flavones with the oxygenation at positions 5 and 7 (Waterman et al. 1976). Thus, the chelated hydroxyl group was attached at C-5 of the flavone skeleton, as illustrated by HMBC cross peaks (Figure 39) observed between the proton signal at δ_{H} 12.69 (5-OH) with the carbon signals at δ_{C} 165.4 (C-7), 162.0 (C-5), 106.0 (C-10) and 97.7 (C-6). (b) The presence of another tetra-substituted benzene ring was also set by the meta-coupled aromatic proton signals at δ_{H} 7.69 and 7.52 (1H each, *d*, 2.0 Hz, H-6', H-2'), characteristic for B-ring in the flavone unit. The flavone moiety was further confirmed by HMBC correlations (Figure 39) observed between the proton signal at δ_{H} 7.69 (H-6') with the carbon signals at δ_{C} 156.4 (C-2), 146.0 (C-4'), 108.5 (C-6') and 31.2 (C-1''), and also between the proton at δ_{H} 7.52 (H-2') with the carbon signals at δ_{C} 156.4 (C-2), 146.0 (C-4') and 121.4 (C-2'). (c) The 1,2,4-trioxygynated 1-phenylethyl group (a styrene derivative moiety), was deduced from the signals of two aromatic proton singlets at δ_{H} 6.84 and δ_{H} 6.56 (1H each, H-8'', H-5''), along with two sets of aliphatic protons at δ_{H} 4.84 (1H, *q*, 7.2 Hz, H-1'') and 1.63 (3H, *d*, 7.2 Hz, H-2''), which were further supported in the ^{13}C NMR (Figure 35) and HMQC (Figure 38) spectra with resonances at δ_{C} 112.5 (C-8''), 98.2 (C-5''), 31.2 (C-1'') and 19.8 (C-2''), respectively. Thus, the proton signal at δ_{H} 4.84 (H-1'') displayed HMBC correlations with the carbon signals at δ_{C} 150.9 (C-4''), 146.0 (C-4'), 132.3 (C-5'), 125.2 (C-3''), 121.4 (C-2'), 112.5 (C-8''), 19.8 (C-2''), which therefore suggested that the linkage was *via* the C-5' position of B-ring of the flavone unit. Additionally, both proton signals at δ_{H} 6.84 (H-8'') and 6.56 (H-5'') displayed HMBC cross peak correlations with the carbon signals at δ_{C} 150.9 (C-4''), 148.2 (C-6''), 143.2 (C-7''), 125.2 (C-3'') and 31.2 (C-1''), which further confirmed the presence of the 1,2,4-trioxygynated 1-phenylethyl group. Furthermore, the ^1H NMR spectrum (Figure 36) in combination with the ^{13}C NMR (Figure 35) and HMQC (Figure 38) spectra displayed six sharp 3-proton singlets at $\delta_{\text{H/C}}$ 3.98/56.2, 3.90/55.8, 3.89/56.1, 3.83/56.9, 3.83/56.8 and 3.81/60.0 which suggested the presence of six methoxyl groups. These methoxyl groups were respectively attached at C-3 (146.5), C-7 (165.4), C-6'' (148.2), C-4'' (150.9), C-7'' (143.2) and C-3' (138.8) as illustrated by HMBC correlations (Figure 39).

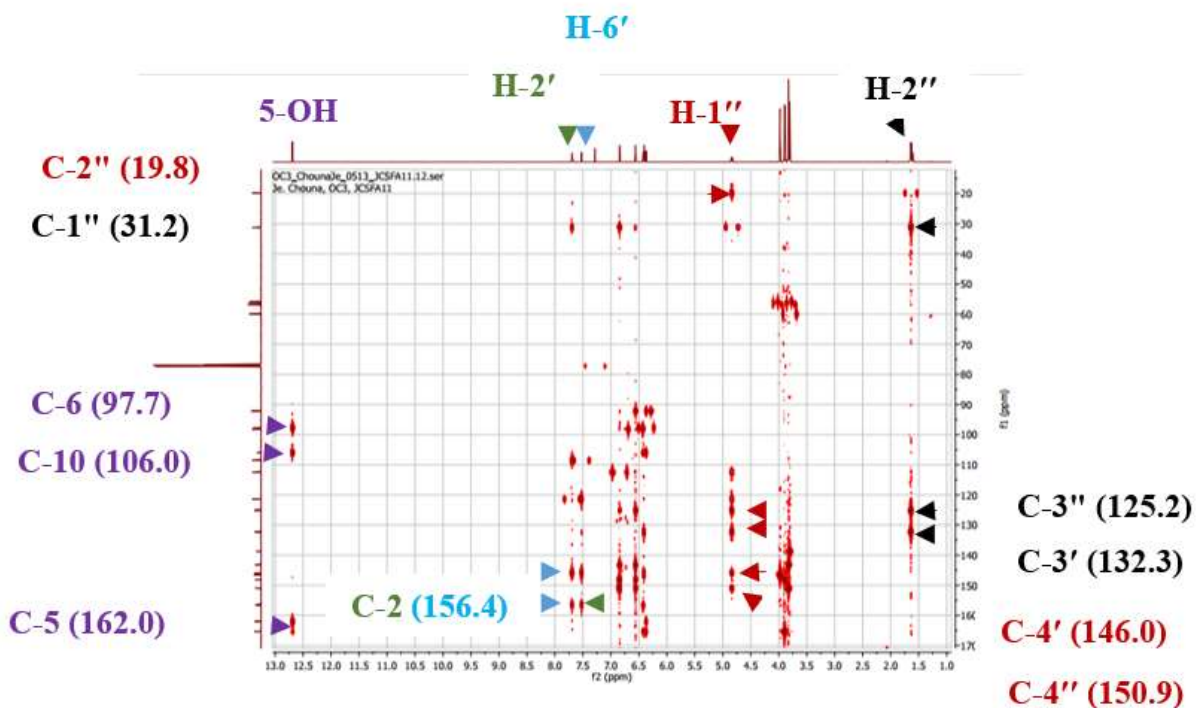
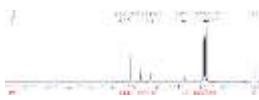


Figure 39. HMBC spectrum of DSB 1

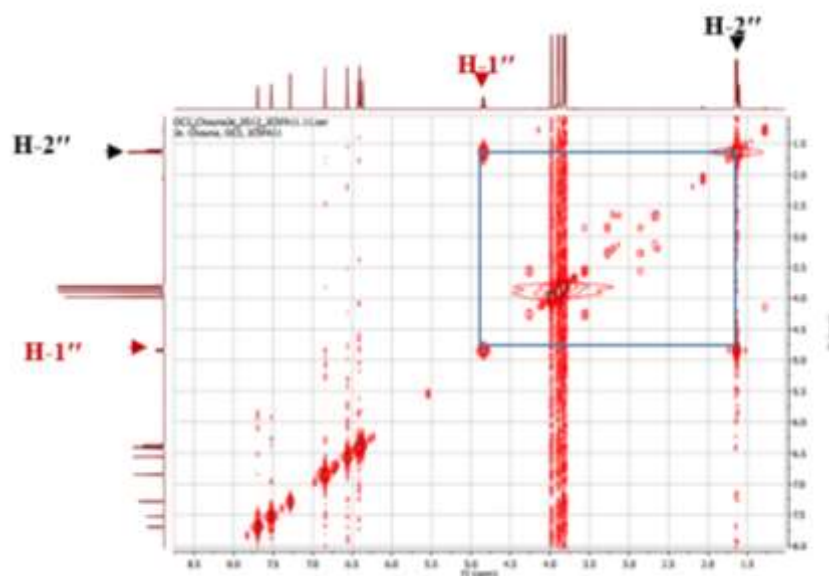
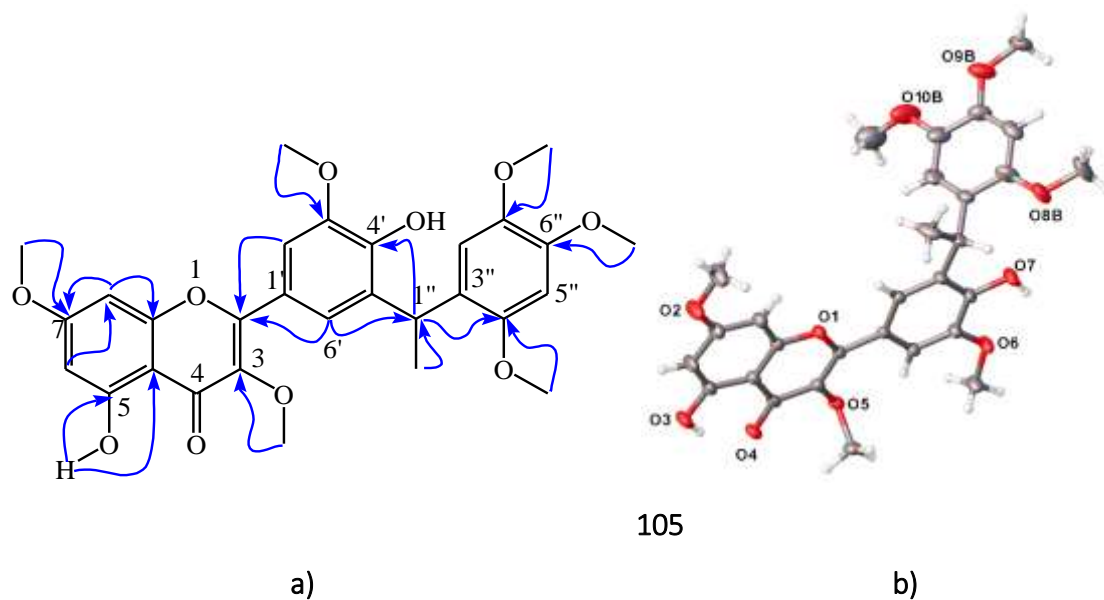


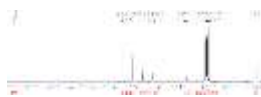
Figure 40. COSY spectrum of DSB 1

In addition, to confirm the structure of the solid **DSB 1**, its X-ray crystallography was carried out by a Rigaku Supernova diffractometer. Therefore, due to the Cahn-Ingold-Prelog sequence rules, the gem-carbon 1'' carrying the flavone and styrene moieties in the 3D structure of **DSB 1** (Scheme 15) was assigned the absolute configuration (1''S). Based on the above spectroscopic and spectrometric analyses, the structure of **DSB 1** was found to be (S)-5-

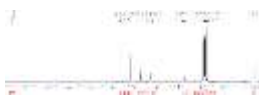
hydroxy-[4-hydroxy-3-methoxy-5-(1-(2,4,5-trimethoxyphenyl) ethyl)] flavone, trivially named as pachypodostyflavone **105**. The proposed structure was fully supported in **Table 28** and by HMBC (**Figure 39**) and COSY (**Figure 40**) spectra. Below are key HMBC correlations of **DSB 1** illustrated in **Scheme 15** and the X-ray structure **105**.



Scheme 15. Keys HMBC correlations (a) and a view of the XRD (b) of DSB 1


Table 28. ^1H - and ^{13}C -NMR data of compound DSB 1 in CDCl_3

C and H no.	^1H (500 MHz)	^{13}C (125 MHz)
	δ_{H} (<i>m</i> , J in Hz)	δ_{C}
2	–	156.4
3	–	146.5
4	–	178.7
5	–	162.0
6	6.37 (d, 2.2)	97.7
7	–	165.4
8	6.42 (d, 2.2)	92.2
9	–	156.7
10	–	106.0
1'	–	121.3
2'	7.69 (d, 2.0)	121.4
3'	–	132.3
4'	–	146.0
5'	–	138.8
6'	7.52 (d, 2.0)	108.5
1''	4.84 (q, 7.2)	31.2
2''	1.63 (d, 7.2)	19.8
3''	–	125.2
4''	–	150.9
5''	6.56 s	98.2
6''	–	148.2
7''	–	143.2
8''	6.84 s	112.5
3-OCH ₃	3.98 s	56.2
7-OCH ₃	3.90 s	55.8
5'-OCH ₃	3.81 s	60.0
4''-OCH ₃	3.83 s	56.8
6''-OCH ₃	3.89 s	56.1
7''-OCH ₃	3.83 s	56.8
5-OH	12.69 s	–
4'-OH	6.41 s	–



II.1.3.1.2. Structural Identification of DSB 2

DSB 2 was obtained as yellow crystal (mp 167-169 °C). It reacted positively with both ferric chloride (blue colour) and the mixture of magnesium with hydrochloride acid (red colour), indicating its phenolic nature and suggest that **DSB 2** is a flavonoid. Its molecular formula was established from the positive ion mode HR-ESI-MS, which showed the quasi-molecular ion peak $[M+H]^+$ at m/z 345.1134 (Calcd. 345.0969 for $C_{18}H_{16}O_6$) (**Figure 41**) and implying eleven degrees of unsaturation.

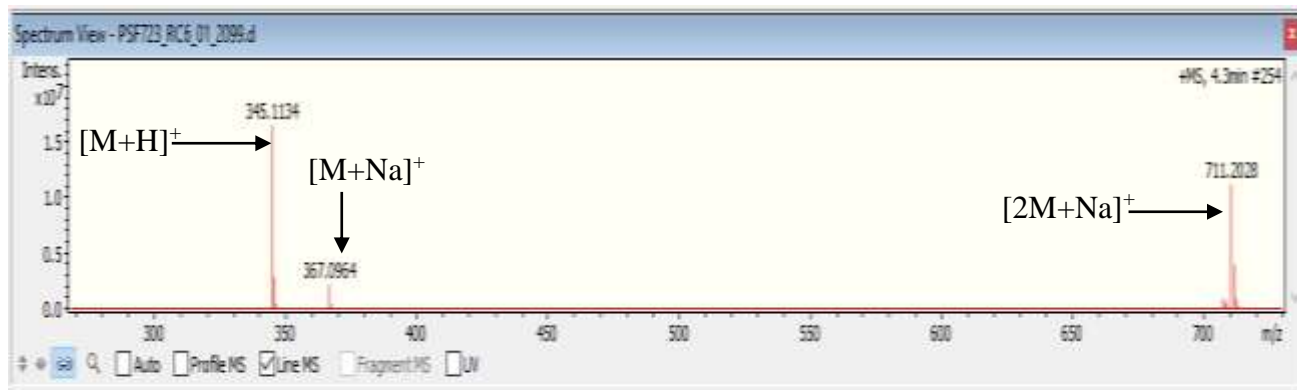
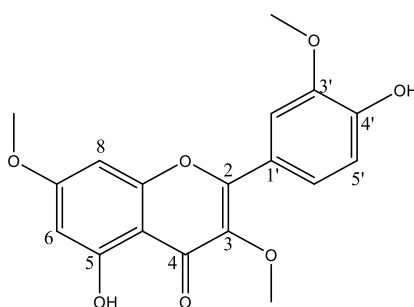


Figure 41. HR-ESI-MS spectrum of **DSB 2**

In addition, the UV spectrum showed absorptions bands at λ_{max} 365 and 265 nm suggesting a flavone nucleus (**Agrawal, 1989**). The analysis of its spectroscopic data coupled with those published in the literature allow us to attribute to **DSB 2** the following structure **16**.



16

In fact, the 1H -NMR spectral (500 MHz, $CDCl_3$) data (**Table 29**) of compound **DSB 2** were very similar to those of the methoxyflavonoid pachypodol described by **Citoğlu et al. (2003)**. This spectrum (**Figure 42**) exhibited two sets of signals, on ABX-type of three aromatic protons at δH 6.98 (1H, *d*, 8.2 Hz, H-5'), 7.61 (1H, *dd*, 2.1; 8.2 Hz, H-6') and 7.64 (1H, *d*, 2.1 Hz, H-2') assignable to tri-substituted ring B protons, and two doublets of one proton each at δH 6.29 (1H, *d*, 2.0

Hz, H-6), 6.38 (1H, *d*, 2.0 Hz, H-8) indicative of two *meta*-coupled aromatic protons of ring A belonging to flavone skeleton.

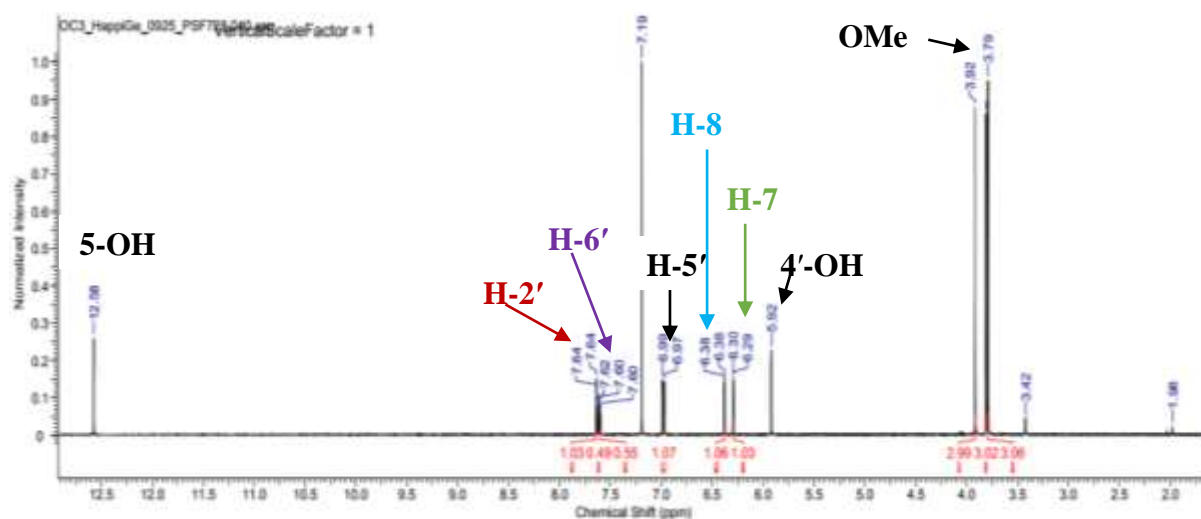


Figure 42. ^1H NMR spectrum of DSB 2 (500 MHz, CDCl_3)

These assumptions were fully confirmed in the HMQC spectrum (Figure 43) with the presence of five aromatic protons on two benzene rings linked through a heterocyclicpyrone nucleus of a polyoxygenated flavonoid. This spectrum also showed a chelated hydroxyl at δ_{H} 12, 58 (5-OH) along with another one at δ_{H} 5.92 (4'-OH) and three singlets of three protons each belonging to methoxyl groups and respectively 3.79 (3H, *s*), 3.81 (3H, *s*) and 3.92 (3H, *s*).

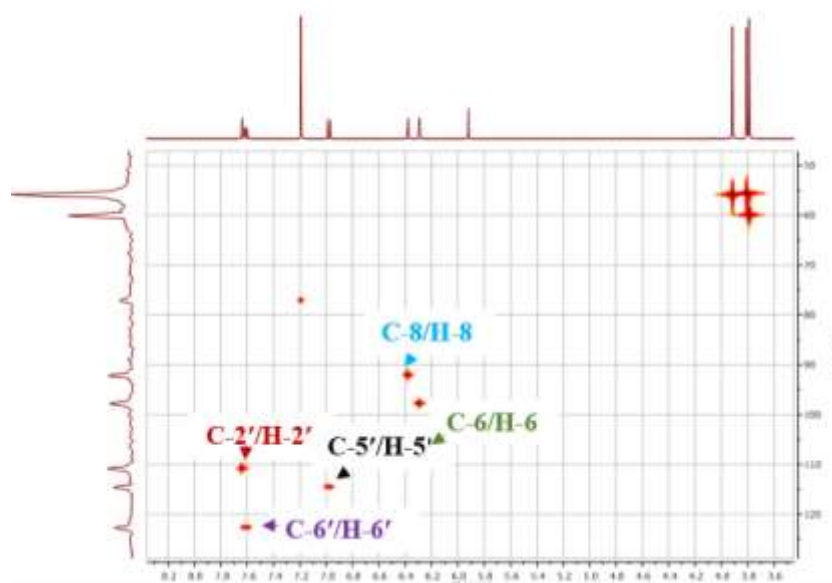
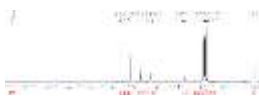


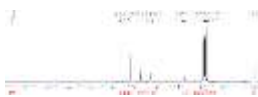
Figure 43. HMQC spectrum of DSB 2



Based on these physical and spectroscopic data coupled with the published values (Citoğlu et al. 2003; Cavé et al. 1980), DSB 2 was previously reported as 4',5-dihydroxy-3, 3', 7 trimethoxyflavone a chemical constituent from *Ballota glandulosissima* also known as Pachypodol **16**

Table 29. Comparative $^1\text{H-NMR}$ data of DSB 2 (500, CDCl_3) with Pachypodol **16** (500, CDCl_3)

H no.	DSB 2	Pachypodol
	^1H (500 MHz)	^1H (500 MHz)
	δ_{H} (m, J in Hz)	δ_{H} (m, J in Hz)
2	—	—
3	—	—
4	—	—
5	—	—
6	6.29 (d, 2.0)	6.34 (d, 2.0)
7	—	—
8	6.38 (d, 2.0)	6.43 (d, 2.0)
9	—	—
10	—	—
1'	—	—
2'	7.64 (d, 2.1)	7.68 (d, 1.6)
3'	—	—
4'	—	—
5'	6.98 (d, 8.2)	7.04 (d, 8.4)
6'	7.61 (dd, 2.1; 8.2)	7.64 (dd, 1.6, 8.4)
3-OCH ₃	3.79 (s, 3H)	3.85 (s, 3H)
7-OCH ₃	3.81 (s, 3H)	3.86 (s, 3H)
3'-OCH ₃	3.92 (s, 3H)	3.97 (s, 3H)
5-OH	12.58 (brs)	12.62 (brs)



II.1.3.1.3. Structural Identification of DSB 3

DSB 3 was obtained as yellow needle (mp 220-222°C). It reacted positively with both ferric chloride suggesting its phenolic nature (blue colour) and to the mixture of magnesium with hydrochloride acid (red colour), indicating that **DSB 3** is a flavonoid. Its molecular formula was established from the positive ion mode HR-ESI-MS, which showed the quasi-molecular ion peak $[M+H]^+$ at m/z 315.1825 (**Figure 44**) (Calcd. 315.0863 for $C_{17}H_{15}O_6$) implying eleven degrees of unsaturation.

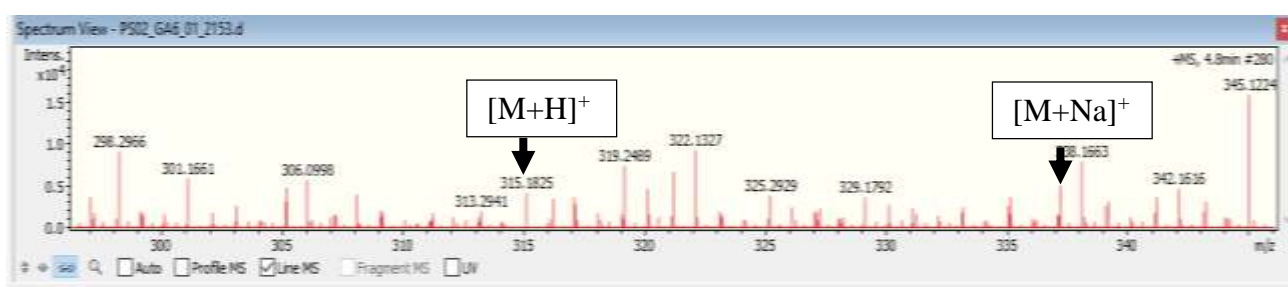
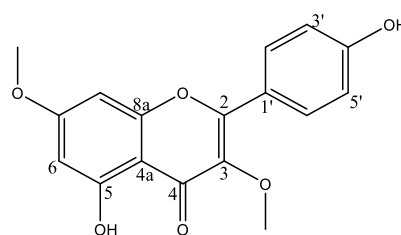


Figure 44. HR-ESI-MS spectrum of DSB 3

The UV spectrum showed absorptions bands at λ_{max} 340 and 269 nm suggesting a flavone skeleton (**Agrawal, 1989**).

The analysis of its spectroscopic data coupled with those published in the literature allow us to attribute to **DSB 3** the following structure **106**.



106

Its 1H -NMR spectrum (500 MHz, $CDCl_3$) (**Figure 45**) exhibited signals for two sets of aromatic protons with AA'-BB' spin system at δ_H 6.94 (2H, *d*, 8.5 Hz; H-3'), and 7.93 (2H, *dd*, 2.5; 8.5 Hz; H-2') assigned to *para*-substituted ring; and two *meta*-coupled aromatic protons at δ_H 6.37 (1H, *d*, $J = 2.5$ Hz, H-6), and δ_H 6.42 (1H, *d*, 2.5 Hz, H-8) which were diagnostic for a C-5 and C-7 oxygenated ring A. The 1H - and ^{13}C - NMR data were very similar to those of **DSB 2**. The only

difference was the substitution of the methoxy functional group (3.92/ 56.1) at δ_c [146.3 (C-3')] by a doublet of one aromatic proton at δ_H 6.94 (2H, *d*, 8.5 Hz, H-3';H-5') on the AA'BB' system of ring B of DSB 3.

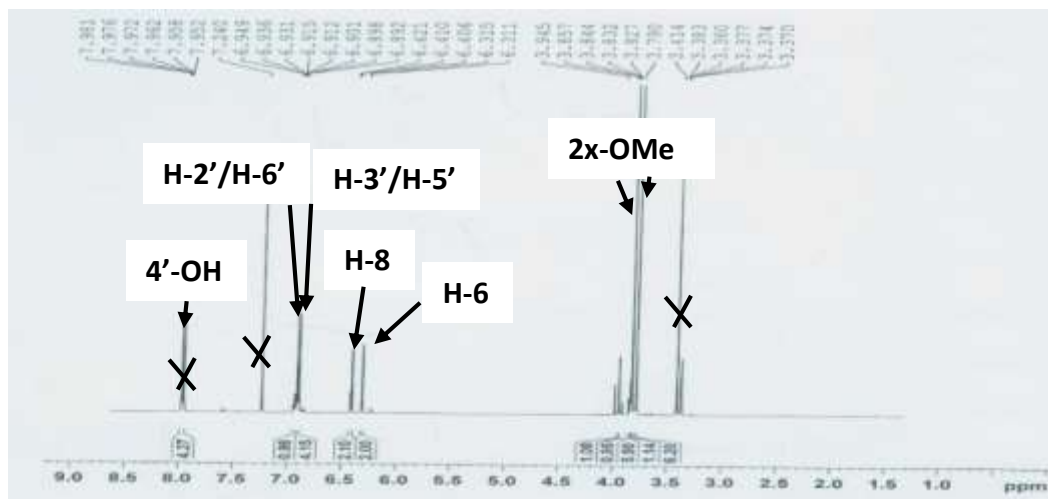


Figure 45. ^1H NMR spectrum (500 MHz, CDCl_3) of DSB 3

The broad band decoupled ^{13}C -NMR spectrum (Figure 46) displayed fifteen carbon signals instead of seventeen as expected from the molecular formulae. These signals were sorted by DEPT (90 and 135) spectra into four aromatic methines at δ_c 98.3 (C-6), 92.4 (C-8), 116.5 (C-3'/C-5') and 131.0 (C-2'/C-6'); four oxygenated aromatic carbons δ_c 165.8 (C-7), 162.4 (C-5), 161.9 (C-4') and 138.8 (C-3); five other quaternary carbons at δ_c 121.5 (C-1'), 156.6 (C-2), 138.8 (C-3), 157.1 (C-4a) 106.4 (C-8a) (Doan et al. 2019). The signal of the latter group being of a characteristic carbonyl of a flavone skeleton at δ_c 179.1 (C-4) (Agrawal, 1989).

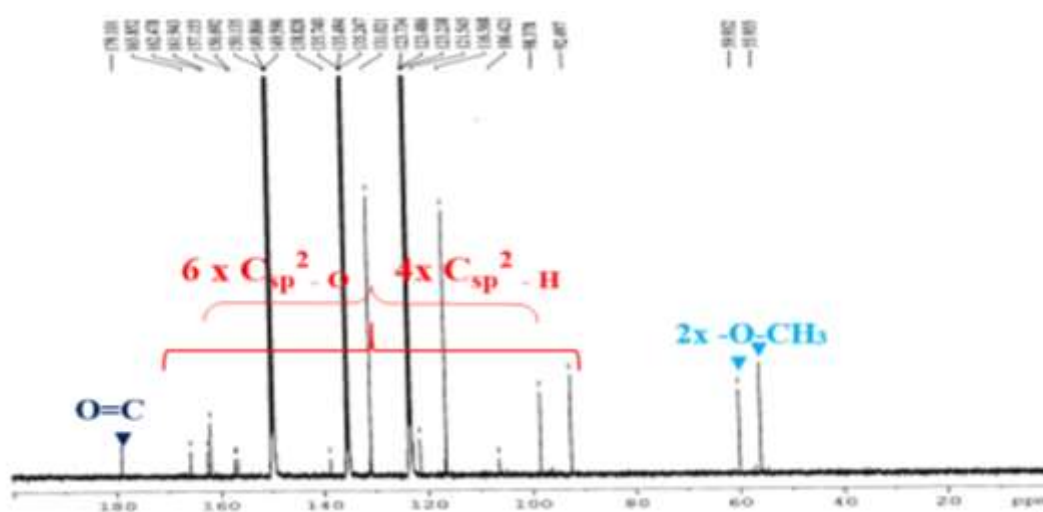
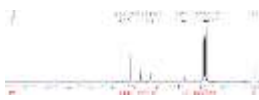


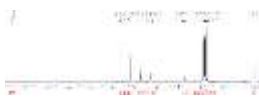
Figure 46. ^{13}C NMR spectrum (100 MHz, Pyridine-d_5) of DSB 3



On the basis of the interpretation of the above spectroscopic data, compound **DSB 3** was concluded to be 5,4'-dihydroxy 3,7-dimethoxyflavone, known as Kumatakenin **106** also previously isolated from *Ballota glandulosissima* (Citoğlu et al. 2003).

Table 30. Comparative ^1H -, ^{13}C -NMR data of DSB 3 with Kumatakenin **106**

C and H no.	DSB 3		Kumatakenin
	(CDCl_3)	(Pyridine- d_5)	(CDCl_3)
	^1H (500 MHz)	^{13}C (100 MHz)	^1H (500 MHz)
	δ_{H} (m , J in Hz)	δ_{C}	δ_{H} (m , J in Hz)
2	–	156.6	–
3	–	138.8	–
4	–	179.1	–
5	–	162.4	–
6	6.37 (d , 2.5)	98.3	6.22 (d , 2.5)
7	–	165.8	–
8	6.42 (d , 2.5)	92.4	6.41 (d , 2.5)
8a	–	157.1	–
4a	–	106.4	–
1'	–	121.5	–
2'	7.93 (1H, dd , 2.5 ; 8.5)	131.0	7.91 (dd , 2.5 ; 9.0)
3'	6.94 (1H, d , 8.5)	116.5	6.89 (d , 9.0)
4'	–	161.9	–
5'	6.94 (1H, d , 8.5)	116.5	6.89 (d , 9.0)
6'	7.93 (1H, dd , 2.5 ; 8.5)	131.0	7.91 (dd , 2.5 ; 9.0)
3-OCH ₃	3.98 (s , 3H)	56.2	3.82 (s , 3H)
7-OCH ₃	3.90 (s , 3H)	55.8	3.81 (s , 3H)
5-OH	12.69 (brs)	–	12.58 (brs)



II.1.3.1.4. Structural Identification of DSB 4

DSB 4 was obtained as yellow crystal (mp 173-175 °C). It is soluble in the DCM and reacted positively both with ferric chloride (blue colour) and the mixture of magnesium with hydrochloride acid (red colour), indicating its phenolic nature and suggest that **DSB 4** is a flavonoid. Its molecular formula was established from the positive ion mode HR-ESI-MS, which showed the quasi-molecular ion peak $[M+H]^+$ at m/z 375.1805 (Calcd. 375.1802 for $C_{19}H_{18}O_8$) (**Figure 47**) and implying eleven degrees of unsaturation.

The UV spectrum showed absorptions at λ_{max} 365 and 265 nm suggesting a flavone nucleus (**Agrawal, 1989**).

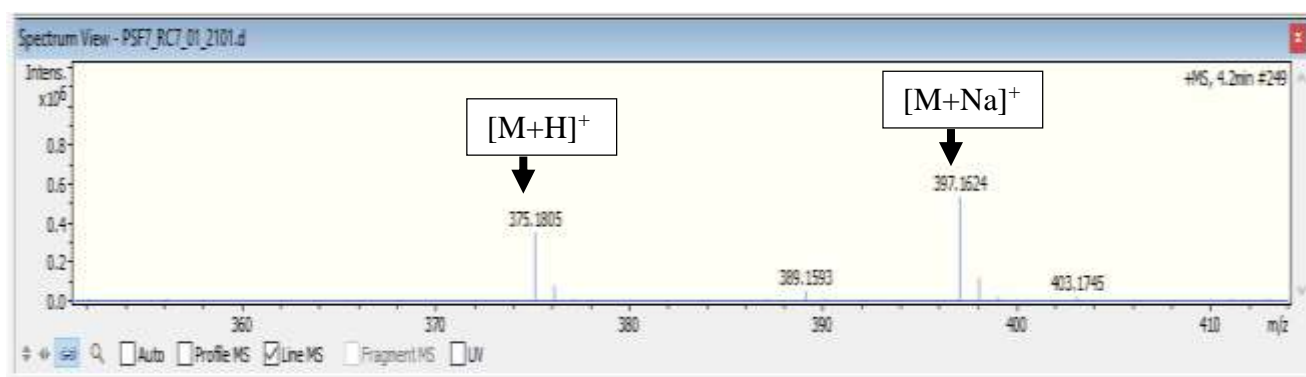
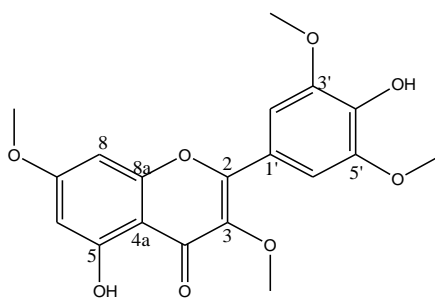


Figure 47. HR-ESI-MS spectrum of **DSB 4**

The analysis of its spectroscopic data coupled with those published in the literature allow us to attribute to **DSB 4** the following structure **107**.



107

The 1H -NMR spectrum (500 MHz, $CDCl_3$) and data of compound **DSB 4** were very similar to those of the methoxyflavonoid pachypodol described by **Citoğlu et al. (2003)**. In fact, the difference between **DSB 3** and **DSB 4** was indicative by the distribution of one additional

methoxyl groups in ring B of **DSB 4** compared to **DSB 3**. The 3'- and 5'-substitution of the two aromatic and *meta*-symmetrical protons at δ_H 6.94 (2H, d, 8.5) in B-ring by the signal of two others symmetrical methoxyl group at δ_H 3,86 (3'-, 5'-OMe) confirmed the difference observed. Furthermore, the two others methoxyl-group at δ_H 3,82 (3-OMe) and 3,84 (7-OMe) was almost closer to their corresponding position in ring A. The $^1\text{H-NMR}$ spectrum (**Figure 48**) exhibited also signals of two *meta*-coupled aromatic protons at δ_H 6.93 (1H, s, H-8) and 6.79 (1H, s, H-6) attributable to ring A and at δ_H 7.01 (2H, s, H-2', H-6') for B-ring. All these spectroscopic and spectrometric data were closely comparable to the published data of 4',5-dihydroxy-3,3',5',7-tetramethoxyflavone or Myricetin 3,7,3',5'-tetramethyl ether (Ariyanathan et al. 2010).

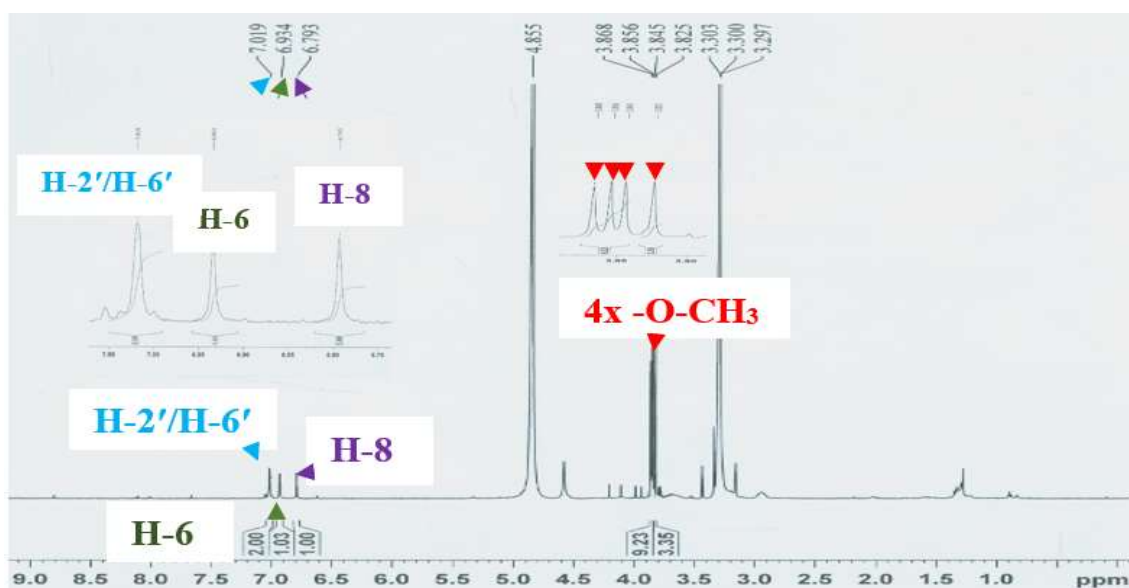
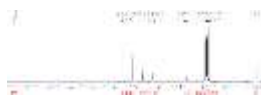
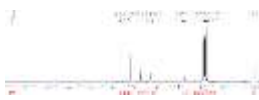


Figure 48. $^1\text{H-NMR}$ spectrum (500 MHz, MeOH) of DSB 4


Table 31. Comparative ¹H-NMR data of DSB 4 with Myricetin 3, 7, 3', 5'-tetramethyl ether

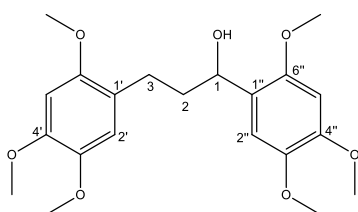
H no.	DSB 4	Myricetin 3, 7, 3',5'-tetramethyl ether
	¹ H (500 MHz, MeOH)	¹ H (400 MHz, CDCl ₃) (Ariyanathan et al. 2010)
	δ_H (m, J in Hz)	δ_H (m, J in Hz)
2	—	—
3	—	—
4	—	—
5	—	—
6	6.79 (s, 1H)	6.38 (d, 2.2)
7	—	—
8	6.93 (s, 1H)	6.48 (d, 2.2)
8a	—	—
4a	—	—
1'	—	—
2'	7.01 (s, 1H)	7.46 (1H, s)
3'	—	—
4'	—	—
5'	—	—
6'	7.01 (s, 1H)	7.46 (1H, s)
3-OCH ₃	3.82 (s, 3H)	3.82 (s, 3H)
7-OCH ₃	3.84 (s, 3H)	3.81 (s, 3H)
3', 5'-OMe	3,86 (s, 3H)	3.85 (s, 3H)



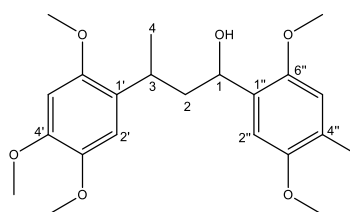
II.1.3.2. Bisnorlignans

II.1.3.2.1. Identification of DSB 5

DSB 5 was obtained as inactive colorless oil. Its molecular formula was found to be $C_{22}H_{30}O_7$ from its HR-ESI-MS at m/z 407.2055 ($[M+H]^+$), (calcd. for $C_{22}H_{30}O_7$, 406.2025), showing eight degrees of insaturation. The UV spectrum of **DSB 5** showed maxima at λ_{max} 229, 243 and 283 nm, characteristic of a benzene chromophore substituted by electron donor groups (**Mayo, 1968**). Its IR spectrum displayed absorption bands for aromatic rings (1609 and 1515 cm^{-1}), and hydroxyl group (3476 cm^{-1}). The NMR spectrum (400 MHz, CD_3OD) and data (**Table 32**) of compound **DSB 5** were very similar to those of the synthesized compound **108** described by **Sanchez-Viesca and Gomez, (1973)**. Due to the spectroscopic and spectrometric data along with those published in the literature, the structure of **DSB 5** was found to be the new compound characterized as 1, 3-bis (2, 4, 5-trimethoxyphenyl)-butan-1-ol and trivially named as pachypolignan **109**.



108



109

The information mentioned above were suggestive of two benzene rings system of a biphenylbutane skeleton. In fact, the 1H -NMR data of **109** (**Figure 50 and Table 32**) exhibited four aromatic H-atom signals at δ_H 6.56 (s), 6.60 (s), 6.80 (s), and 6.99 (s) which were confirmed in the ^{13}C NMR spectrum (100 MHz, CD_3OD) (**Figure 49**) indicating twelve aromatic C-atom signals among which, four aromatic methine (δ_C 114.5; 112.7; 100.0; and 99.1) bearing those latter protons. In addition we observed in the 1H -NMR spectrum six methoxyl substituents at δ_H 3.70 (s), 3.74 (s), 3.76 (s), 3.77 (s), 3.81 (s), and 3.82 (s) with 3J correlations respectively to the signals at δ_C 152.0, 153.3, 144.45, 144.45, 150.0 and, 149.3 attributed to C-2', C-2'', C-5'', C-5', C-4' and C-4''. The 1H -NMR spectrum showed also protons H-4, H-2a and H-2b assignable respectively to one methyl signal at δ_H 1.17 (d, 6.8.), one methylene signal at δ_H 2.02 (1H, ddd, 4.4; 4.8; 9.6)

and 1.77 (1H, *ddd*, 5.2; 8.4; 9.6) along with the signals of protons H-1 and H-3 attributable respectively to one hydroxymethine at δ_{H} 4.76 and one methine at δ_{H} 3.30.

The ^{13}C NMR spectrum (100 MHz, CD_3OD) (Figure 49 and Table 32) indicated other aromatic C-atom signals sorted into eight quaternary (δ_{C} 153.3; 152.0, 150.0; 149.3; 144.4; 144.4; 128.3; and 127.0), as well as one methyl carbon signal at δ_{C} 22.38 (C-4), one methylene carbon signal at δ_{C} 46.4 (C-2), and two aliphatic methine groups at δ_{C} 67.2 (C-1), and 30.5 (C-3).

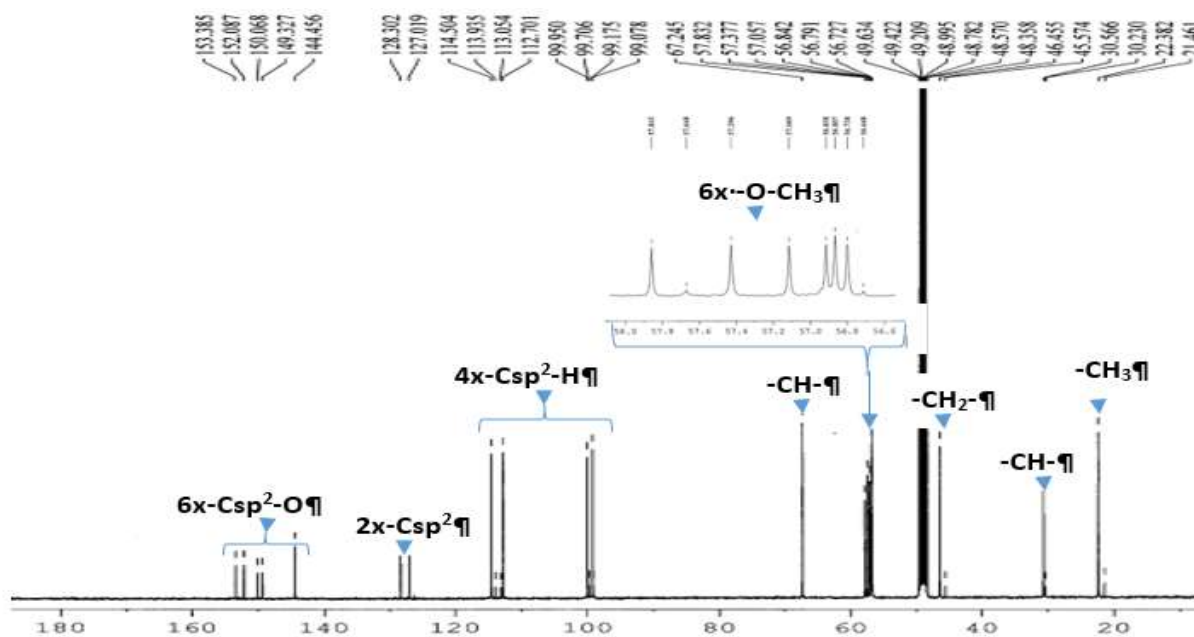


Figure 49. ^{13}C NMR spectrum of DSB 5 (100 MHz, CD_3OD)

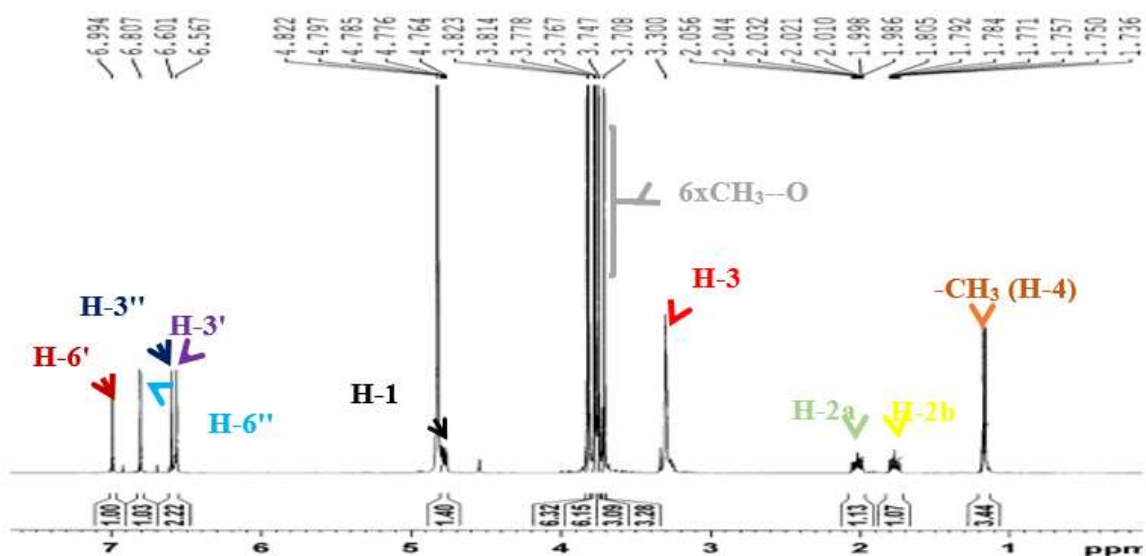
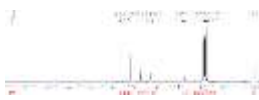


Figure 50. ^1H NMR spectrum of DSB 5 (400 MHz, CD_3OD)



The HMBC spectrum (**Figure 51**) showed 3J correlations between the oxymethine proton signal at δ_H 4.76 and the C-atom signals at δ_C 152.0 (C-2''), 112.7 (C-6'') and 30.5 (C-3), confirming its C-1 position. In addition, further correlations were observed between the methyl group at δ_H 1.17 (CH₃-4) and C-atom signals at δ_C 128.3 (C-1'), 46.4 (C-2) and 30.5 (C-3), whereas the proton δ_H 6.99 (H-6') showed 3J correlations with signals at δ_C 153.3 (C-2'), 150.0 (C-4') and 30.5 (C-3). Moreover the signal at δ_H 3.30 (H-3) displayed strong correlations with carbon signals at δ_C 114.5 (C-6'), 153.3 (C-2') and 67.2 (C-1). Other correlations were also observed between proton signal at δ_H 6.80 (H-6'') with δ_C 152.0 (C-2''), 149.3 (C-4'') and 67.2 (C-1) which further supporting the proposed lignan structure.

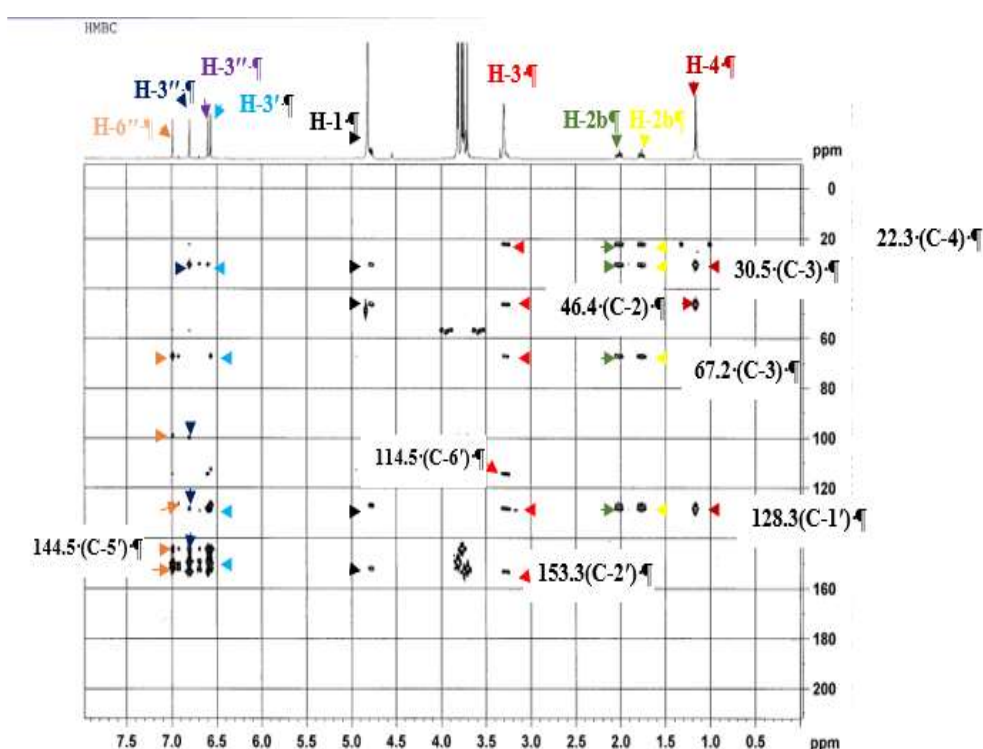


Figure 51. HMBC spectrum of DSB 5

Additionally, the NOESY spectrum (**Figure 52**) exhibited correlations between H-1 and H-3, and between H-2a and H-3'' and showed that the methyl group (CH₃-4) has the same orientation with the OH-1. The relative configuration of the acyclic part of compound **DSB 5** was determined based on the coupling constants as demonstrated by **Matsumori et al. (1999)**. The large vicinal coupling constants ($J = 8.4$ Hz and $J = 5.2$ Hz) between H-1 and H2b, and H2b and H-3 respectively indicate the anti-orientation of H2b with the two protons. However, it was not possible to determine the absolute configuration of these stereogenic centers due to the lack of material. In addition, the proposed and illustrated (**Table 32**) structure was fully

supported by key HMBC (Figure 51) correlations, DEPT-HSQC (Figure 53) and COSY (Figure 54) spectra.

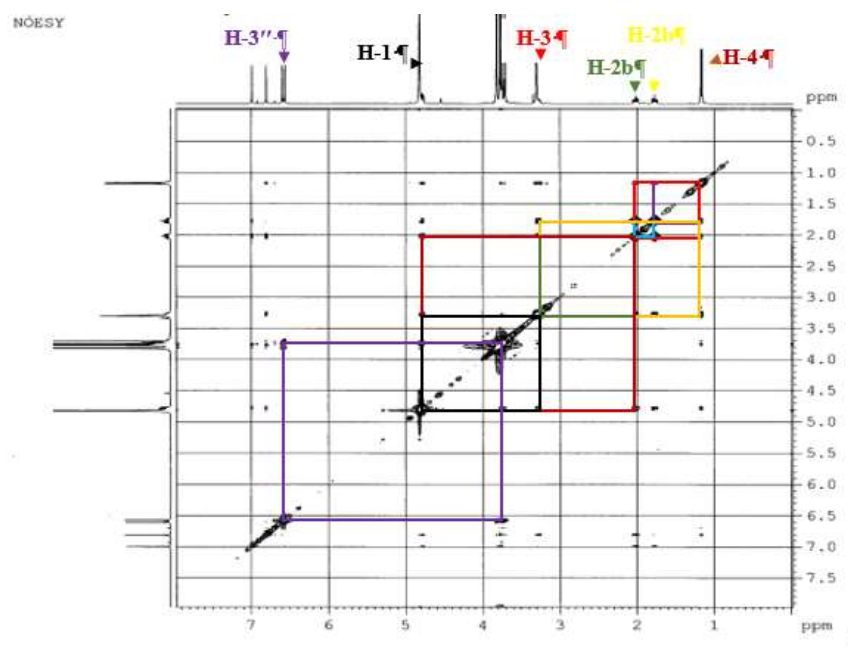


Figure 52. NOESY spectrum of DSB 5

From the above evidence, the structure of the new compound was characterized as 1, 3-bis (2, 4, 5-trimethoxyphenyl)-butan-1-ol and trivially named as pachypolignan 109.

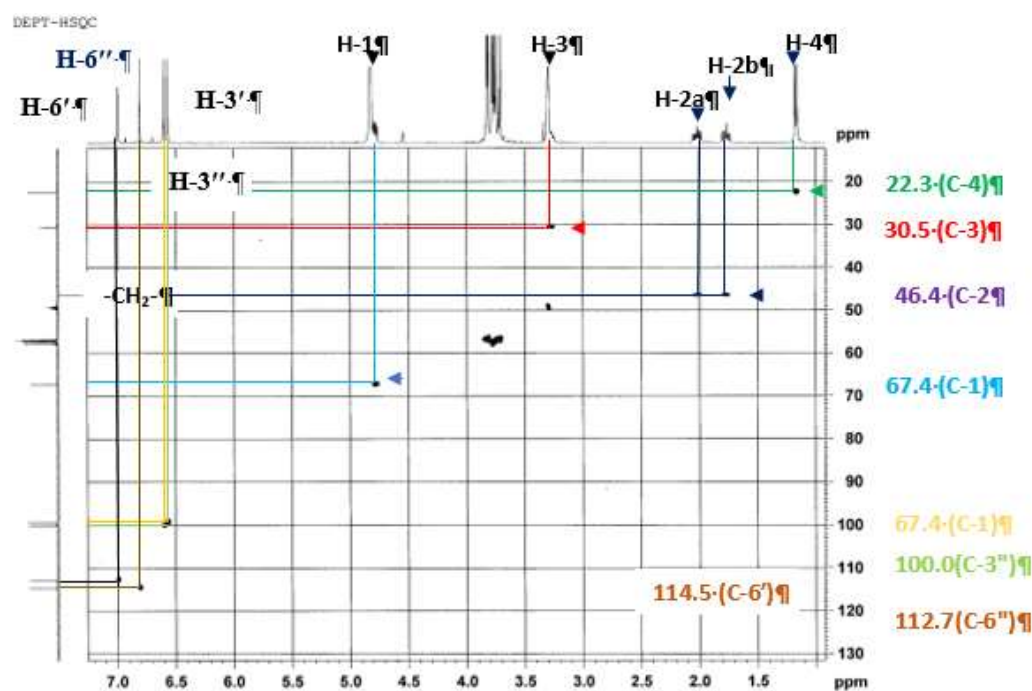


Figure 53. DEPT - HSQC spectrum of DSB 5

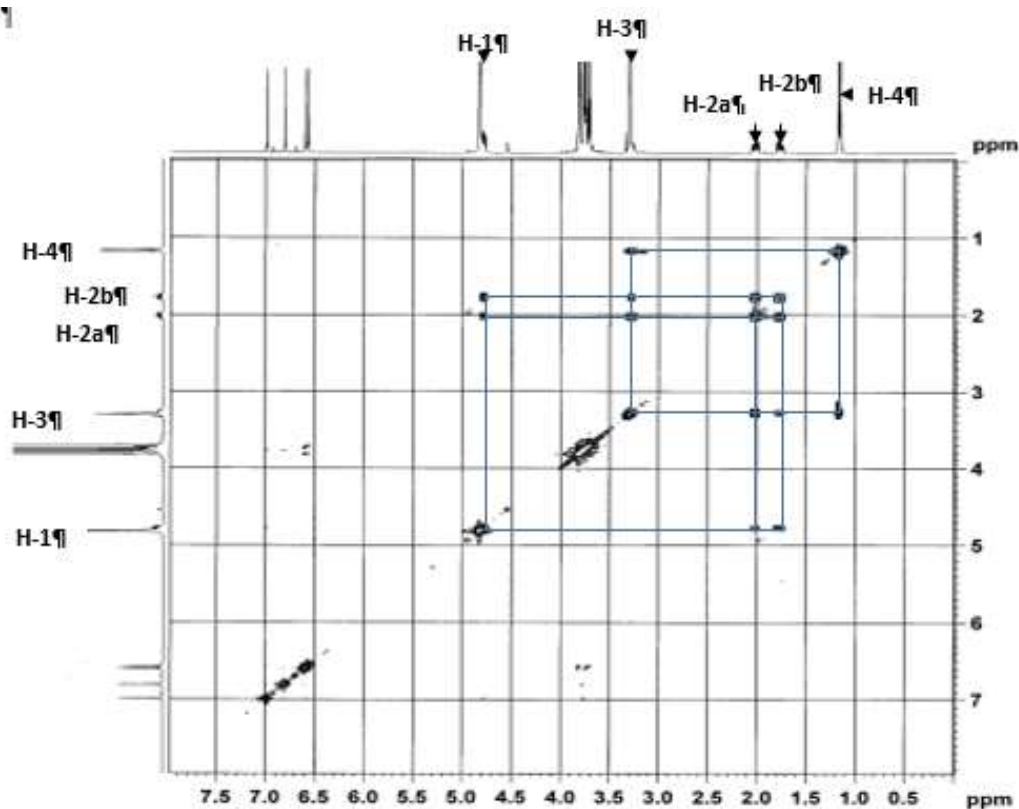
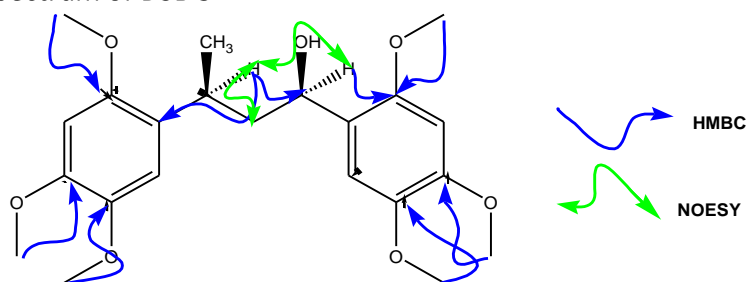
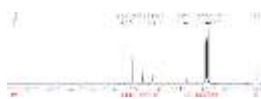


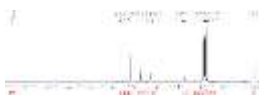
Figure 54. COSY spectrum of DSB 5



Scheme 16. Key NOESY and HMBC correlations of compound DSB 5


Table 32. NMR spectral data (400 MHz, CDCl₃) of DSB 5

C and H no	¹ H (400 MHz, CDCl ₃) δ _H (J in Hz)	¹³ C (100 MHz, CDCl ₃) δ _C	Key HMBC
1	4.76 (1H, <i>dd</i> , 4.8; 8.4)	67.2	C-3; C-2''; C-6''
2a	2.02 (1H, <i>ddd</i> , 4.4; 4.8; 9.6)	46.4	C-1; C-3; C-4; C-1'; C-1''
2b	1.77 (1H, <i>ddd</i> , 5.2; 8.4; 9.6)		
3	3.30 (1H, <i>m</i>)	30.5	C-1; C-2; C-2'; C-6'
4	1.17 (3H, <i>d</i> , 6.8)	22.3	C-2; C-3; C-1'
1'	-	128.3	
2'	-	153.3	
3'	(6.56, <i>s</i>)	99.1	C-1'; C-5'
4'	-	150.0	
5'	-	144.4	
6'	(6.99, <i>s</i>)	114.5	C-3; C-2'; C-4'
1''	-	127.0	
2''	-	152.0	
3''	(6.60, <i>s</i>)	100.0	C-1''; C-5''
4''	-	149.3	
5''	-	144.4	
6''	(6.80, <i>s</i>)	112.7	C-1; C-2''; C-4''
2'OCH ₃	(3.70, <i>s</i>)	56.7	C-2'
4'OCH ₃	(3.81, <i>s</i>)	56.7	C-4'
5'OCH ₃	(3.77, <i>s</i>)	57.8	C-5'
2''OCH ₃	(3.74, <i>s</i>)	57.0	C-2''
4''OCH ₃	(3.82, <i>s</i>)	56.8	C-4''
5''OCH ₃	(3.76, <i>s</i>)	57.3	C-5''



II.1.3.2.2. Structural identification of DSB 6

DSB 6 was obtained as colourless, mp 125-127°C and was soluble in the DCM. Its molecular formula was determined as C₂₂H₂₆O₆ on the basis of NMR data and the ESI-MS (Figure 55) which showed the pseudo-molecular ion peak at *m/z* 387.1805, and implying nine degrees of unsaturation.

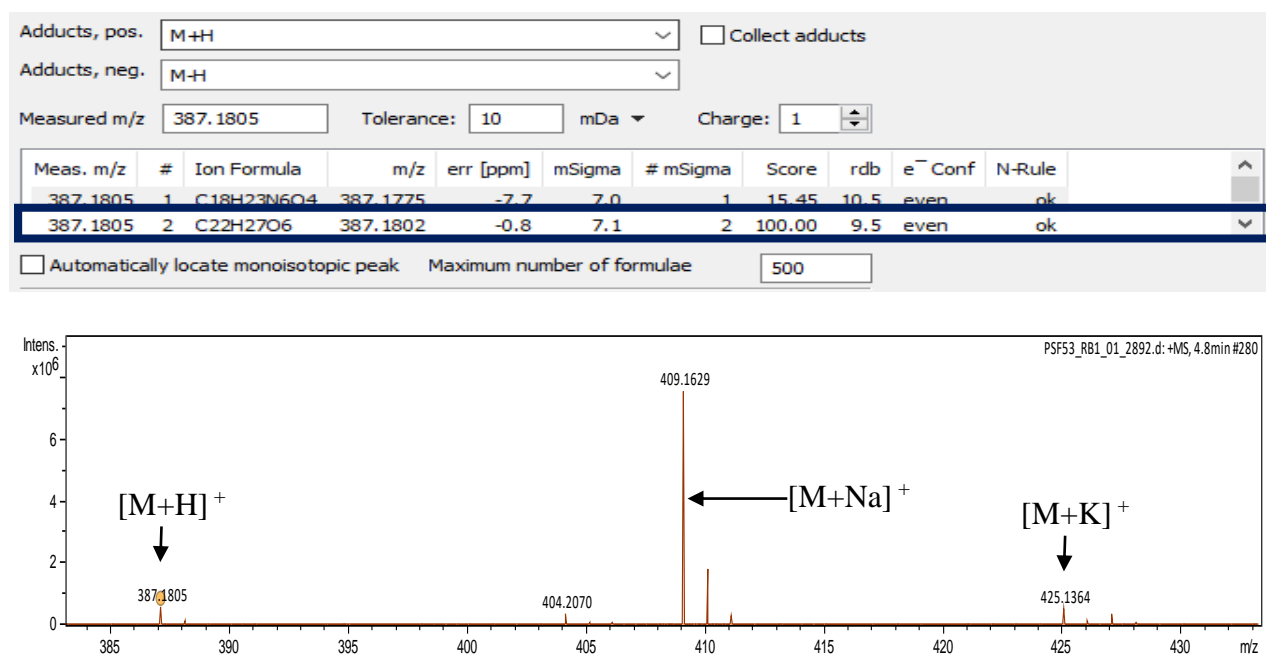
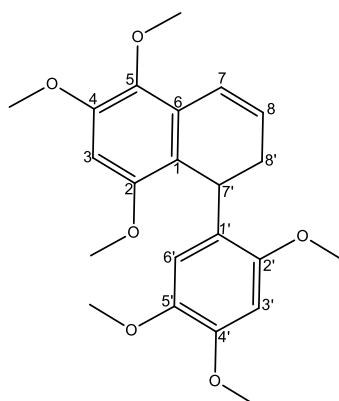
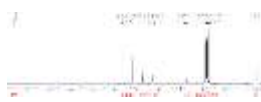


Figure 55. HR-ESI -Mass spectrum of DSB 6

DSB 6 was firstly compared through TLC technique to an authentic sample in the laboratory and by means of spectroscopic data (¹H-; ¹³C- NMR and 1-D and 2-D dimensional (COSY, HSQC, HMBC and NOESY) it has been found to be Pachypostaudin-B **11**.



11



The broad band decoupled ^{13}C NMR spectrum (**Figure 56**; **Table 33**) of compound **DSB 6** displayed C-signal, which were sorted by HMQC spectrum into nine quaternary carbons, with six linked to an O-atom; six methoxyl groups; one methine and one methylene.

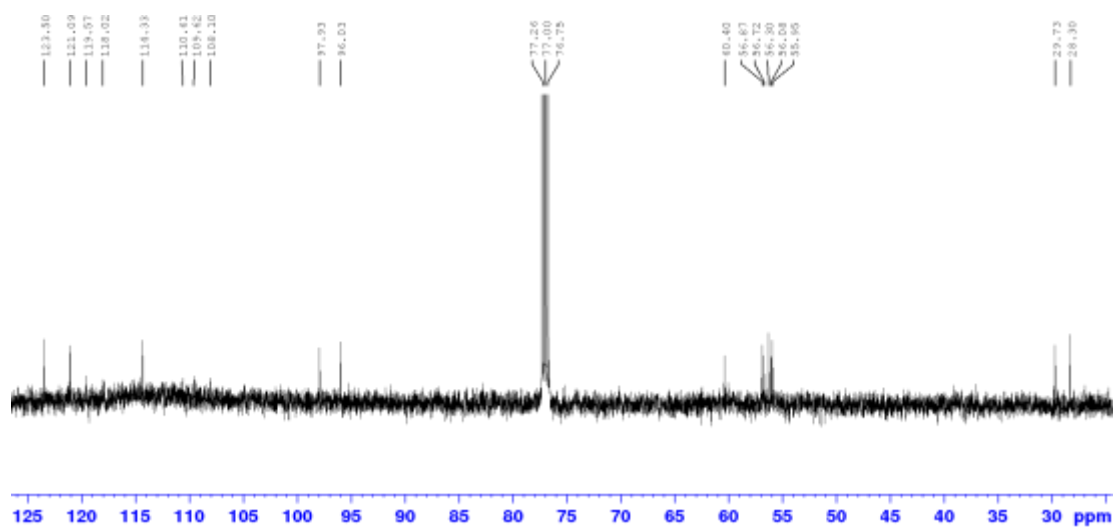


Figure 56. ^{13}C - NMR spectrum (125 MHz, CDCl_3) of **DSB 6**

The ^1H -NMR (**Figure 57**) spectrum exhibited two olefinic signals at δ_{H} 5.66 (1H, *d*, 8.6Hz, H-8) and 6.78 (1H, *dd*, 3.1, 9.7Hz, H-7). These observations were also made in the ^{13}C NMR spectrum (**Figure 56**) presenting the two olefinic carbons at δ_{C} 123.5 (C-8) and 121.1 (C-7) similar to those reported by **Ngadjui et al. (1989)** and bearing the two deshielded protons previously mentioned. In addition, the ^1H -NMR spectrum (**Figure 57**) showed three aromatic signals of protons respectively at δ_{H} 6.41 (H-3), 6.27 (H-6') and 6.50 (H-3') which were also closed to the described ones by **Ngadjui et al. (1989)**. The three sets of aromatic carbon signals at δ_{C} 96.0 (C-3); 114.3 (C-6') and 152.5 (C-2') bearing these latter signals were confirmed in the ^{13}C NMR spectrum (**Figure 56**). The olefinic signals previously mentioned in the ^1H -NMR spectrum were confirmed in the Noesy spectrum (**Figure 58**) through cross peaks observed due to the magnetization transfer via space-dipolar interactions between the two groups in close proximity.

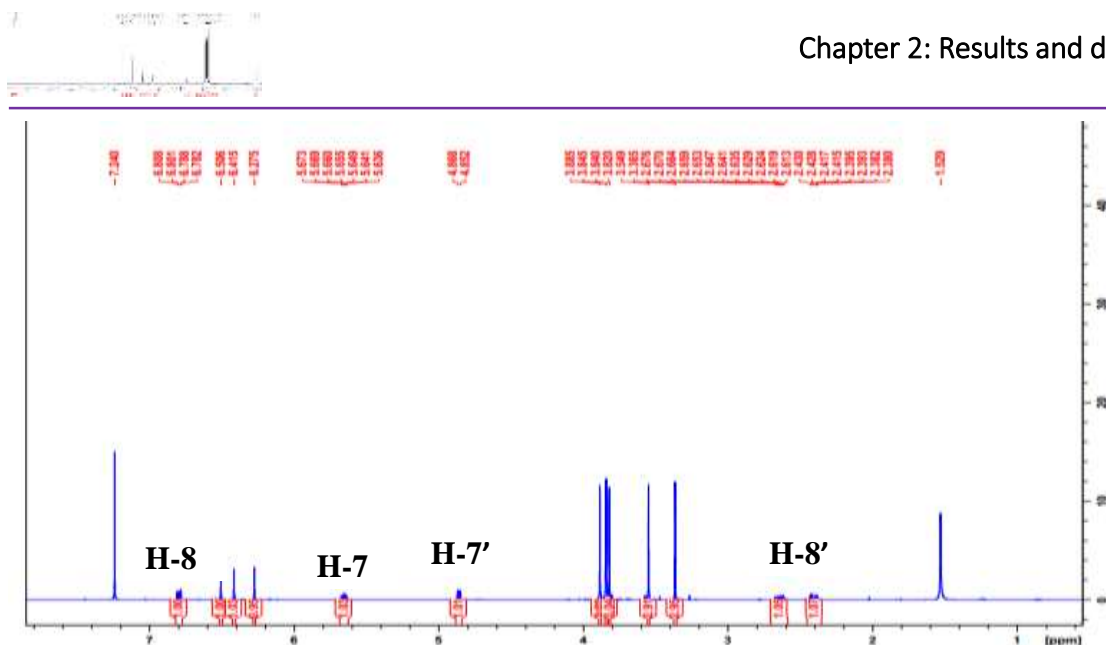


Figure 57. ^1H -NMR spectrum (500 MHz, CDCl_3) of DSB 6

Furthermore, the ^1H NMR spectrum (Figure 57) in combination with the ^{13}C NMR spectrum (Figure 56) displayed six sharp 3-proton singlets at $\delta_{\text{H/C}}$ 3.36/60.2, 3.54/57.7, 3.80/56.9, 3.83/56.7, 3.84/57.2 and 3.88/55.9 which suggested the presence of six methoxyl groups. These methoxyl groups were respectively attached at C-2 (142.2), C-5 (148.2), C-4 (140.5), C-5' (148.2), C-2' (152.5) and C-4' (151.2) as illustrated by HMBC correlations (Table 27). The ^{13}C NMR spectrum (Figure 56) displayed in addition two sets of aliphatic protons in the up-field region at δ_{H} 4.86–2.41. This information was further confirmed in the Noesy spectrum (Figure 58) with exhibited some significant cross peaks between the multiplet at δ_{H} 4.86 (H-7') and the doublet at δ_{H} 2.65 (H-8').

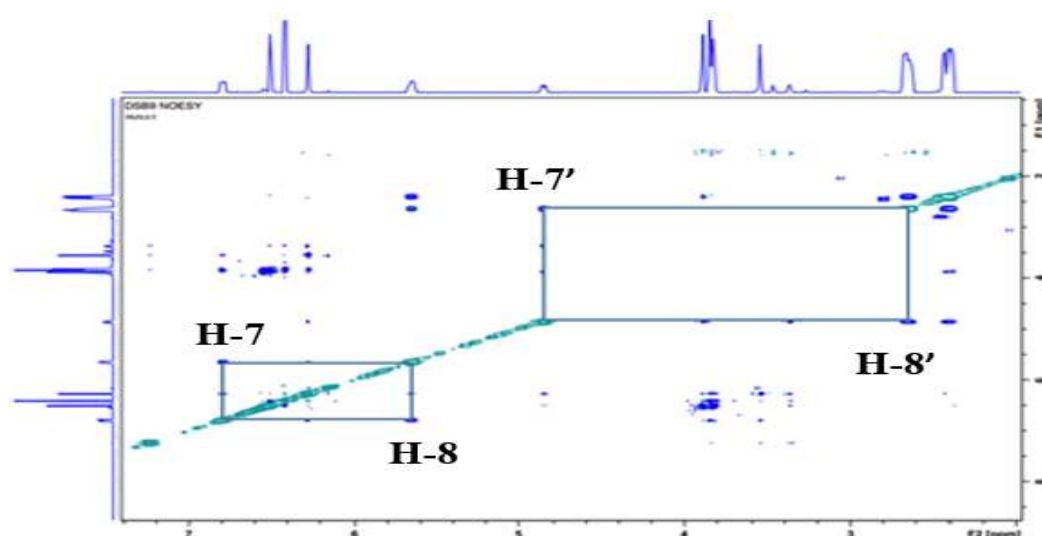
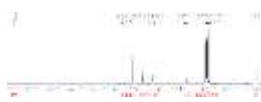


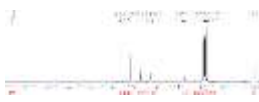
Figure 58. NOESY spectrum of DSB 6



All these information were further supported by the HMBC data (Table 33) which showed multiple keys correlations. On the basis of the above data, the structure of DSB 6 was concluded to be 1,2-Bis (2,4,5-trimethoxyphenyl) cyclobutane or 5, 6, 8-trimethoxy-1-(2, 4,5-trimethoxyphenyl)-1,2-dihydronaphthalene also known as Pachypostaudin B **11**, which was previously isolated from *Pachypodanthium staudtii* (Ngadjui et al. 1989).

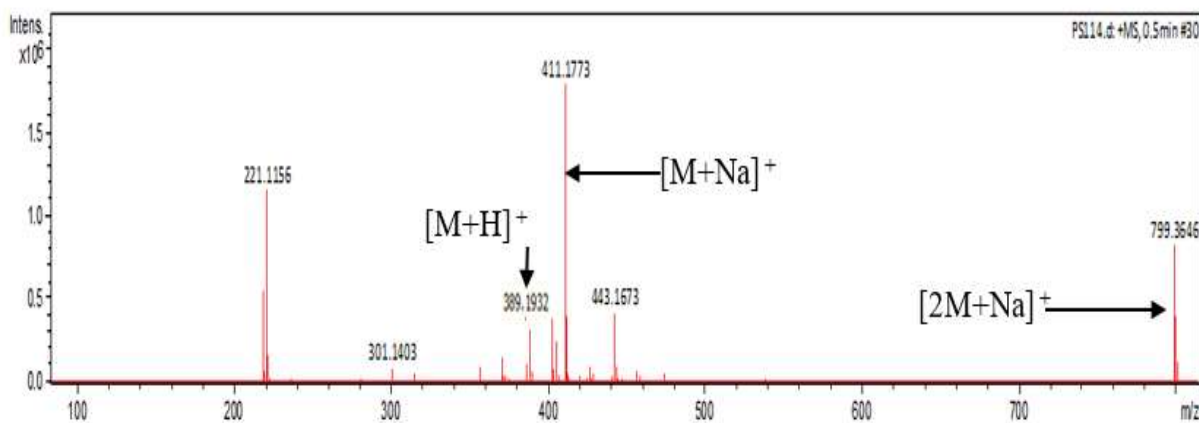
Table 33. Comparative ^{13}C -NMR spectral data of DSB 6 (CDCl_3) with Pachypostaudin B

C and H no.	^1H (500 MHz)	^{13}C (125 MHz)	HMBC	^1H (80 MHz)	^{13}C (20 MHz)
	δ_{H} (m , J in Hz)	δ_{C}	H \rightarrow C	δ_{H} (m , J in Hz)	δ_{C}
	DSB 6			(Ngadjui et al. 1989)	
1	-	118.0	-	-	-
2	-	142.2	-	-	142.5
3	6.41 (1H, <i>s</i>)	96.0	C-2	6.50 (1H, <i>s</i>)	96.1
4	-	140.5	-	-	150.7
5	-	148.2	-	-	-
6	-	132.5	-	-	-
1'	-	119.5	-	-	-
2'	-	152.5	-	-	152.5
3'	6.50 (1H, <i>s</i>)	97.9	C-4'	6.60 (1H, <i>s</i>)	98.1
4'	-	151.2	-	-	151.6
5'	-	148.2	-	-	148.0
6'	6.27 (1H, <i>s</i>)	114.3	C-5'	6.30 (1H, <i>s</i>)	114.5
7'	4.86 (1H, <i>m</i>)	28.3	C-2';C-6	4.90 (1H, <i>dd</i> , 2;8)	28.4
8'	2.41 (1H, <i>m</i>) 2.65 (1H, <i>d</i> , 2.9)	29.7	C-6; C-7; C-8	2.55 (2H, <i>m</i>)	29.8
7	6.78 (1H, <i>dd</i> , 3.1, 9.7)	121.1	C-6	6.80 (1H, <i>dd</i> , 2 ; 10)	121.2
8	5.66 (1H, <i>d</i> , 8.6)	123.5	C-2	5.70 (1H, <i>ddd</i> , 2;5;10)	123.5
2-OCH ₃	3.36	60.2	C-4	3.40	60.4
4-OCH ₃	3.80	56.9	C-5	3.90	56.9
5-OCH ₃	3.54	57.7	C-4	3.60	55.9
2'-OCH ₃	3.84	57.2	C-2'	3.90	56.3
4'-OCH ₃	3.88	55.9	C-4'	3.90	56.1
5'-OCH ₃	3.83	56.7	C-5'	3.90	56.7



II.1.3.2.3. Structural identification of DSB 7

DSB 7 was obtained as colourless crystal, mp 160-162°C and soluble in the DCM. The LC-ESI-MS showed the pseudo-molecular ion peak $[M+H]^+$ at m/z 389.1932 (**Figure 59**), compatible



with the molecular formula $C_{22}H_{28}O_6$ (Calcd. 388.1924) and implying nine degrees of unsaturation. Its UV spectrum showed also maxima at λ_{max} 229, 243 and 283 nm, characteristic of a benzene chromophore substituted by electron donor groups (**Mayo, 1968**).

Figure 59. HR-ESI-MS spectrum of DSB 7

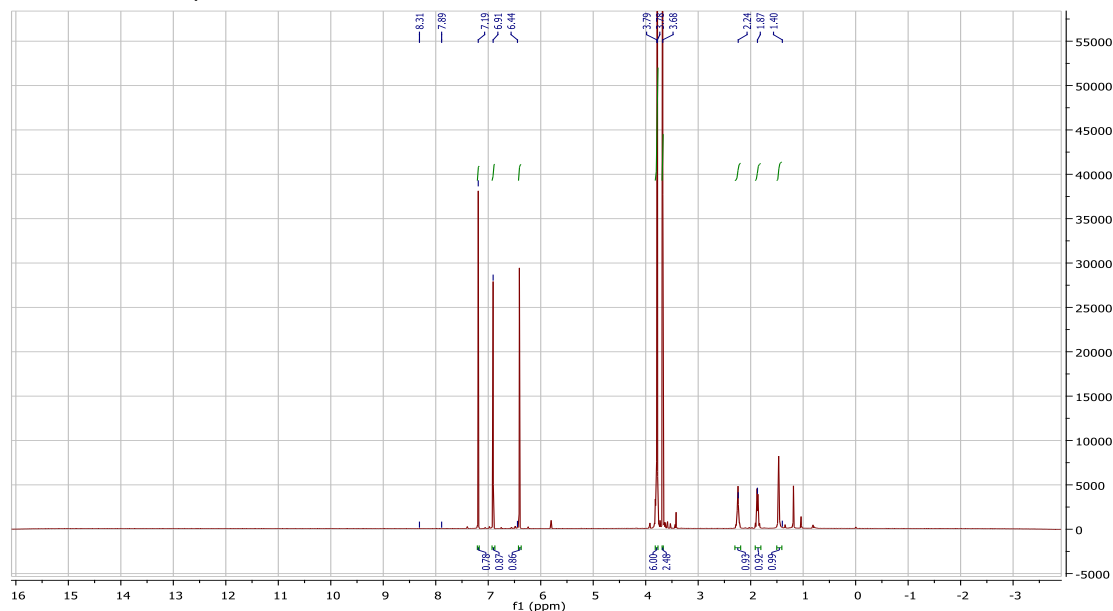
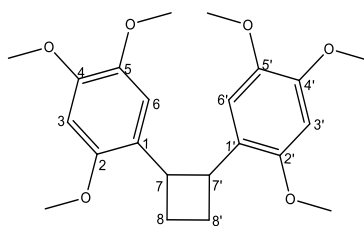
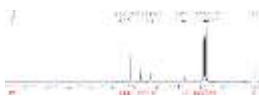


Figure 60. 1H - NMR spectrum (500 MHz, $CDCl_3$) of DSB 7

The interpretation of its NMR data (1H -NMR, DEPT) (**Figures 60, 61; Table 28**) prompted us to compare **DSB 7** to an authentic sample of Pachypophyllin **13**.

**13**

The $^1\text{H-NMR}$ spectrum (500 MHz, CDCl_3) (**Figure 60**) exhibited two sets of signal of the latter aromatic protons at δ_{H} 6.44 (2H, s, H-3 and H-3'); and 6.91 (2H, s, H-6 and H-6') integrating each for two symmetrical atom carbon signals. This information was confirmed in the broad band decoupled $^{13}\text{C-NMR}$ (125 MHz, CDCl_3) (**Table 34**) spectrum which showed only 11 out of the 22 carbon signals observed consisting of the two methine carbon signals at δ_{C} 124.6 (C-3; C-3') and 111.8 (C-6; C-6') observed in the HMQC spectrum and bearing the aforementioned aromatic proton signals. In addition this spectrum exhibited also three symmetrical methoxylated signals at δ_{C} 56.5 (C-2; C-2'); 56.6 (C-4; C-4'); and 56.2 (C-5; C-5'); resonances for two aliphatic carbon signals at δ_{C} 40.4 (C-7; C-7') and 27.0 (C-8; C-8') as exhibited also in upfield of the DEPT spectrum (**Figure 61**); three aromatic and oxygenated carbon atoms at δ_{C} 151.1 (C-2; C-2'); 147.6 (C-4; C-4') and 143.1 (C-5; C-5') and one quaternary carbon atom at δ_{C} 97.8 (C-1; C-1'). In addition, the $^1\text{H-NMR}$ spectrum (**Figure 60**) also showed three sets of methoxyl-group respectively at δ_{H} 3.79 (6H, s, 2xOMe), 3.68 (6H, s, 2xOMe) and 3.78 (6H, s, 2xOMe); an upfield complex multiplets of aliphatic methine at δ_{H} 3.84 (2H, m), and methylene groups 1.97 (2H, m, H-8a and H-8'a) and 2.31 (2H, m, H-8b and H-8'b). The COSY spectrum showed correlation between the multiplet of two protons at δ_{H} 3.84 and these two latter methylene groups respectively at δ_{H} 1.97 and 2.31. The mass of the base peak being (m/z : 194) exactly equals half of pachypophyllin and corresponds to 2, 4, 5-trimethoxystyrene, the major constituent of *D. staudtii* (**Ngadjui et al. 1989**), former *pachypodanthium staudtii*. Thus, **DSB 7** could be a symmetrical dimer of 2, 4, 5-trimethoxystyrene. These latter information as well as those aforesaid were in agreement with those published by **Ngadjui and coworkers (1989)**. Based on these evidences, **DSB 7** could be assigned the structure Pachypophyllin **13**.

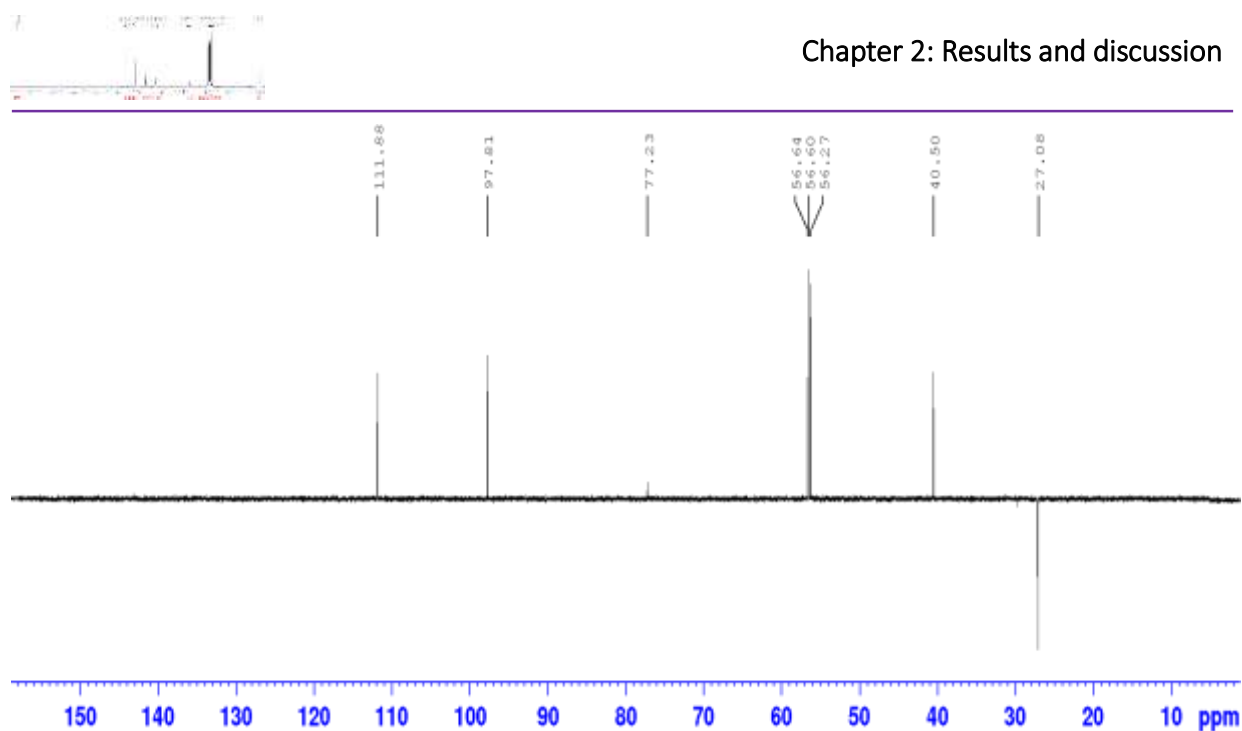
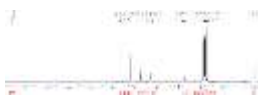


Figure 61. DEPT spectrum of DSB 7

Table 34. Comparative ^1H -, ^{13}C -NMR spectral data of DSB 7 (125 MHz, CDCl_3) with Pachypophyllin 13 (75 MHz, CDCl_3)

C and H n°	DSB 7		Ngadjui et al. 1989	
	^1H	^{13}C (125 MHz)	^1H	^{13}C (75 MHz)
	δ_{H} (m, J in Hz)		δ_{H} (m, J in Hz)	
1, 1'	-	97.8	-	98.0
2, 2'	-	151.1	-	151.3
3, 3'	6.44 (2H, s)	124.6	6.47 (2H, s)	124.8
4, 4'	-	147.6	-	147.8
5, 5'	-	143.1	-	143.3
6, 6'	6.91 (2H, s)	111.6	6.97 (2H, s)	112.1
2-2'-OCH ₃	3.79 (6H, s)	56.5	3.85 (6H, s, 2xOMe)	56.7
4-4'-OCH ₃	3.68 (6H, s)	56.6	3.74 (6H, s, 2xOMe)	56.8
5-5'-OCH ₃	3.78 (6H, s)	56.2	3.83 (6H, s, 2xOMe)	56.3
7, 7'	3.84 (2H, m)	40.4	3.85 (2H, m)	40.6
8, 8'	1.97; 2.31 (2H, m) each	27.0	1.95 ; 2.31 (2H, m) each	27.1



II.1.3.3. Sesquiterpene

II.1.3.3.1. Structural identification of DSB 8

DSB 8 was obtained as colourless needle, mp 109-111°C and soluble in the DCM. The HR-ESI-MS (Figure 62) showed the pseudo-molecular ion peak $[M+H]^+$ at m/z 233.1527, compatible with the molecular formula $C_{15}H_{21}O_2$ (Calcd. For $C_{15}H_{20}O_2$: 232.1536) and implying six degrees of unsaturation.

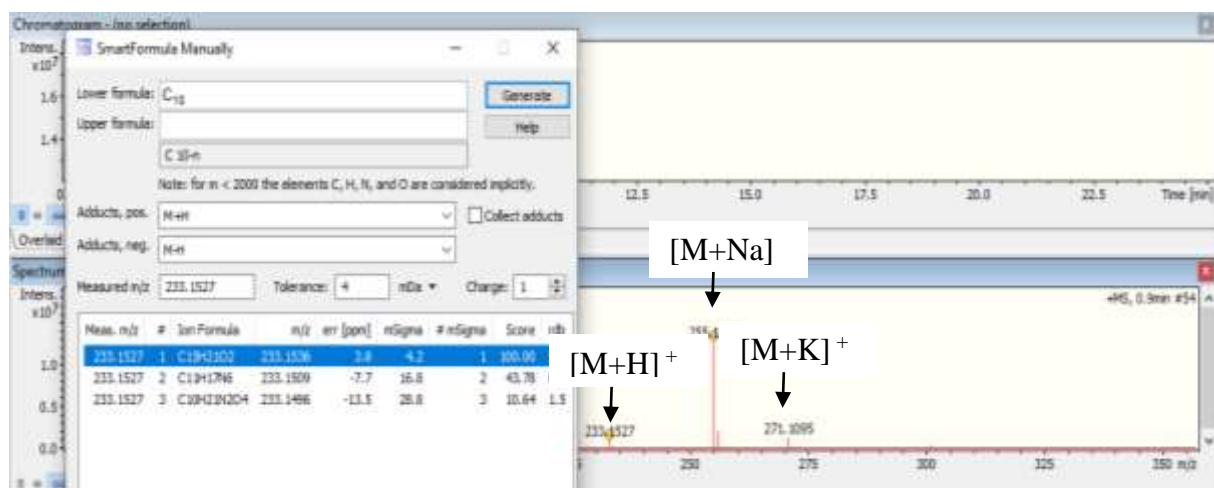
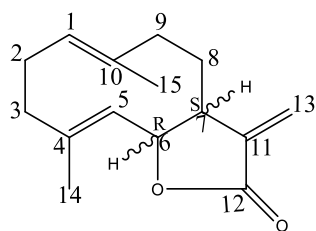
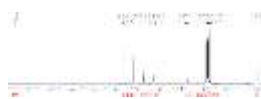


Figure 62. HR-ESI-MS spectrum of DSB 8

Although its IR spectrum exhibited no hydroxyl absorption its rather showed an α, β -unsaturated- γ -lactone carbonyl band at λ_{max} (CHCl₃) 1777 cm^{-1} with the C=C absorption band at 1670 cm^{-1} . The UV spectrum showed absorptions at λ_{max} 210 nm suggesting a germacranolide sesquiterpene- γ -lactone (Li et al. 2005). DSB 8 was characterized by direct comparison with an authentic sample on TLC and by the interpretation of its spectroscopic data (¹H- and ¹³C-NMR, DEPT). Its NMR data were almost identical to those of costunolide 110 (Li et al. 2005).



110



In fact, the broad band decoupled ^{13}C NMR spectrum of compound **DSB 8** (Figure 63; Table 35) displayed fifteen carbon signals sorted by DEPT and HMQC spectra into four quaternary carbons, four methines, two methyl groups and five methylene among which the one at δ_{C} 118.1 (C-13) bearing a pair of doublets typical for the two exocyclic methylene signals.

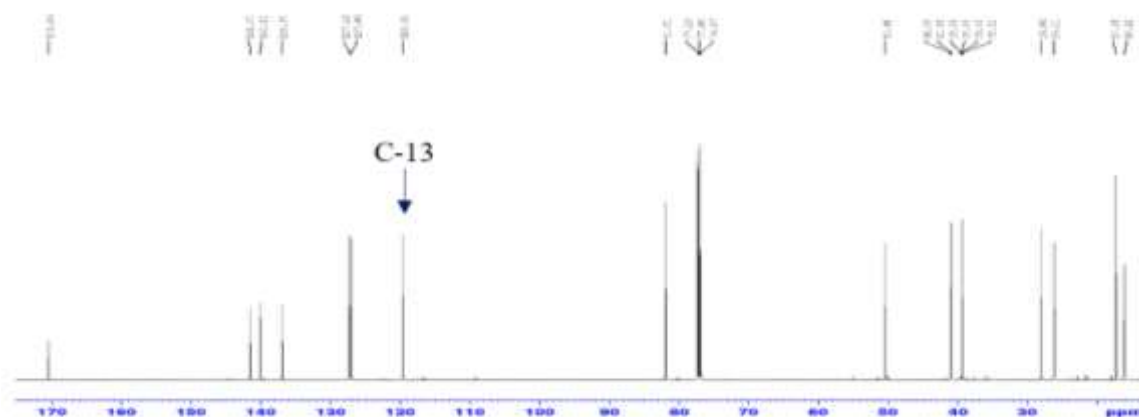


Figure 63. ^{13}C -NMR spectrum (125 MHz, Acetone- d_6) of **DSB 8**

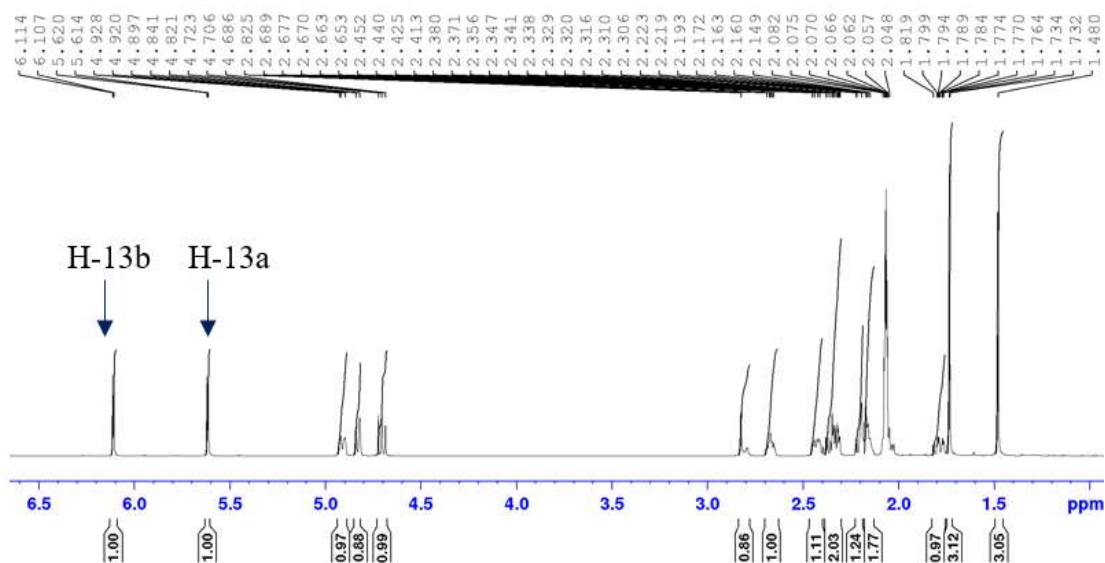


Figure 64. ^1H -NMR spectrum (500 MHz, Acetone- d_6) of **DSB 8**

This latter information was later confirmed in the ^1H -NMR spectrum (500 MHz, Acetone- d_6) (Figure 64) of **DSB 8** which exhibited a pair of doublets at δ_{H} 5.62 (1H, *d*, 3.2) and 6.08 (1H, *d*, 3.6) typical for this aforementioned exocyclic methylene protons H-13a, and H-13b associated with the α,β -unsaturated- γ -lactone group of **DSB 8**.

Moreover in this ^1H -NMR spectrum (Figure 64), two sharp singlet of olefinic methyl groups observed at δ_{H} 1.48 (H-14) and 1.73 (H-15) were assigned due to the HMBC spectrum

to correlate with the signal of quaternary carbons at δ_C 141.0 (C-4) and 137.1 (C-10) respectively. In the olefinic proton region, were centered at δ_H 4.91 (H-1) and 4.71 (H-5) a collection of multiplets of peaks integrating each for one proton and correlating with olefinic methyl groups respectively at δ_C 15.4 (C-14) and 16.4 (H-15) following the HMBC spectrum (Figure 67). The $^1\text{H-NMR}$ spectrum showed finally the presence of a bunch of four sets of multiplets of methylene protons at δ_H 2.16 (H-2a), 2.35 (H-2b), 2.04 (H-3a), 2.31 (H-3b), 1.77 (H-8a), 2.17 (H-8b), 2.18 (H-9a) and 2.42 (H-9b) along with the methine proton signals at 4.83 (H-6) and 4.71 (H-5). This latter information was further confirmed in the COSY spectrum (Figure 65) which showed correlations between these two signals.

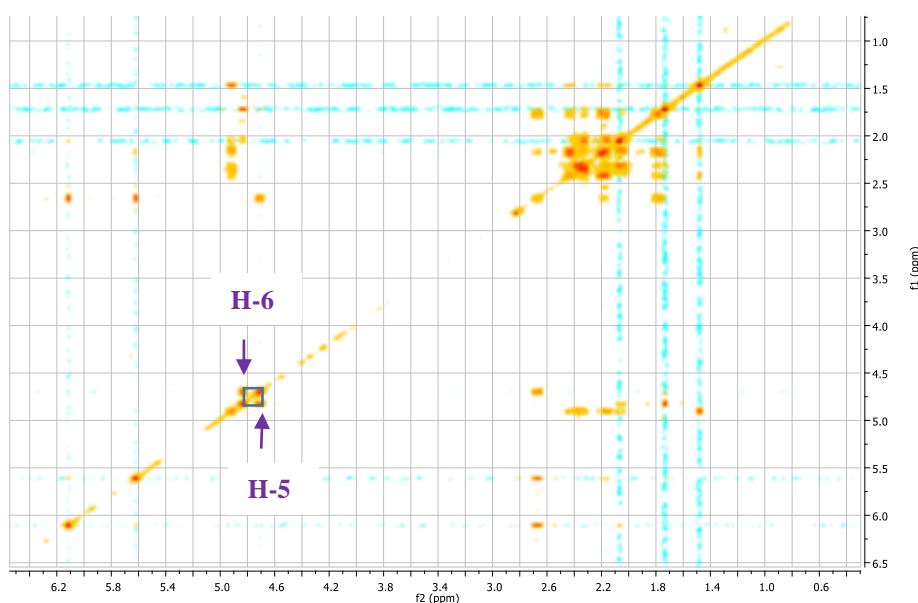


Figure 65. COSY spectrum of DSB 8

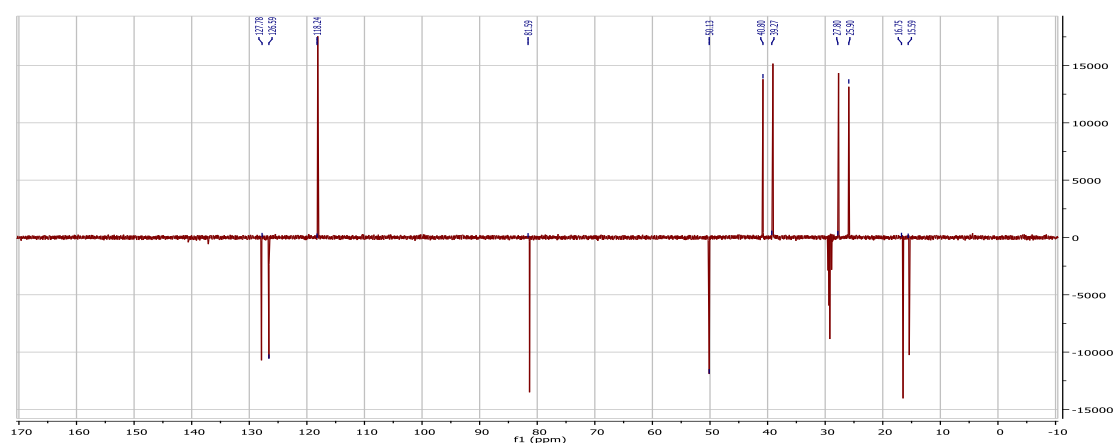


Figure 66. DEPT 135 spectrum of DSB 8

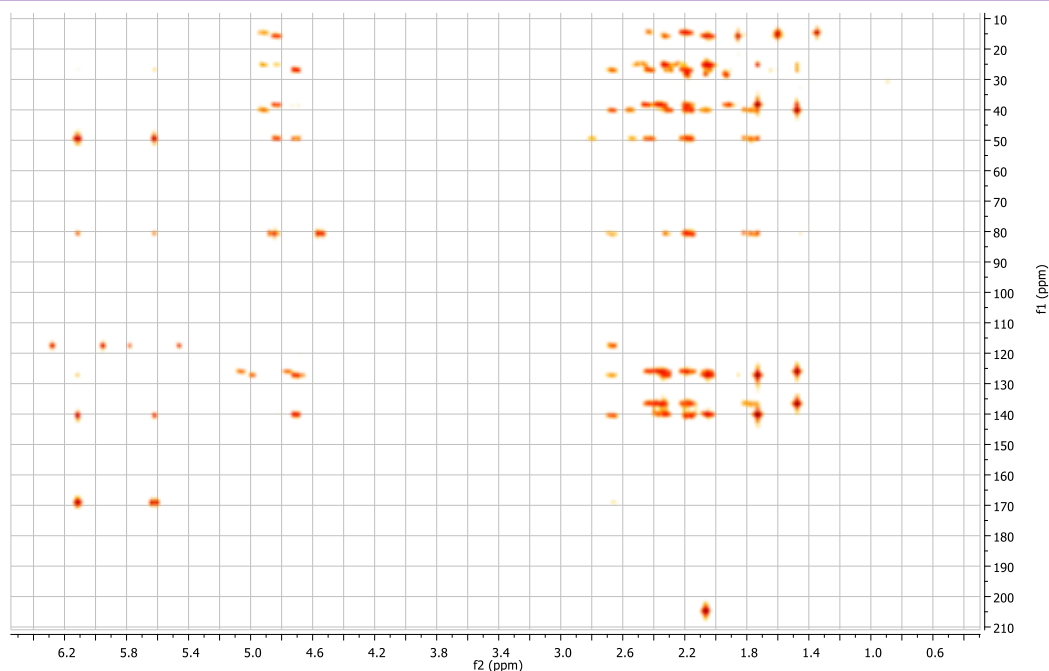
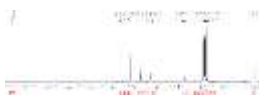
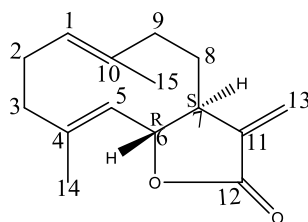


Figure 67. HMBC spectrum of DSB 8

In addition the presence of two chiral centers in position 6 and 7 indicated that **DSB 8** could exist in one of the four possible absolute configurations. The XRD analysis was done using a Rigaku supernova diffractometer which gave a 3D structure that verified the trans - orientation of the two vicinal protons on the fused bicyclic ring (**Scheme 25**). Based on these physical, crystal and spectroscopic data coupled with the published values (**Table 35**) (**Li et al. 2005**), **DSB 8** previously isolated from the roots of *Saussurea lappa* was reported as costunolide **110** and the absolute configuration of its two chiral centre assigned as (6R, 7S) and determined here for the first time and confirmed by **Mountessou et al. 2023a**.



110

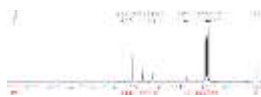
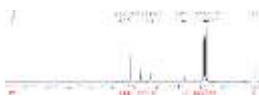


Table 35. Comparative ^{13}C (125 MHz, CDCl_3) NMR spectral data of DSB 8 with Costunolide 110
 ^{13}C (100 MHz, CDCl_3) NMR

C and H no.	^{13}H (500 MHz)	^{13}C (125 MHz)	^{13}C (100 MHz)
	δ_{H} (<i>m</i> , J in Hz)	δ_{C}	δ_{C}
	DSB 8		(Li et al. 2005)
1	4.91 (1H, <i>m</i>)	126.5	127.1
2	2.16 (1H, <i>m</i> , H-2a)	25.9	27.9
	2.35 (1H, <i>m</i> , H-2b)		
3	2.04 (1H, <i>m</i> , H-3a)	39.0	40.8
	2.31 (1H, <i>m</i> , H-3b)		
4	–	141.0	139.9
5	4.71 (1H, <i>m</i>)	81.3	81.8
6	4.83 (1H, <i>m</i>)	127.8	127.0
7	2.68 (1H, <i>m</i>)	50.1	50.3
8	1.77 (1H, <i>m</i> , H-8a)	27.5	26.1
	2.17 (1H, <i>m</i> , H-8b)		
9	2.18 (1H, <i>m</i> , H-9a)	40.8	39.4
	2.42 (1H, <i>m</i> , H-9b)		
10	–	137.1	136.9
11	–	140.6	141.5
12	–	169.6	170.5
13	5.62 (1H, <i>d</i> , 3.2, H-13a)	118.1	119.7
	6.08 (1H, <i>d</i> , 3.6, H-13b)		
14	1.48 (3H, <i>s</i>)	15.4	16.1
15	1.73 (3H, <i>s</i>)	16.4	17.3



II.1.3.4. Alkaloid

II.1.3.4.1. Structural identification of DSB 9

DSB 9 was obtained as an amorphous yellow powder. It is soluble in the Pyridine- d_5 and reacted positively with Dragendoff test, indicating its alkaloid nature. Its molecular formula was found to be $C_{20}H_{23}NO_4$ (Calcd. for 342.1700) established from the positive ion mode HR-ESI-MS, and showing the quasi-molecular ion peak $[M+H]^+$ at m/z 342.1711, implying nine degrees of unsaturation along with an important fragment ion signal at 178.0855 (**Figure 68**).

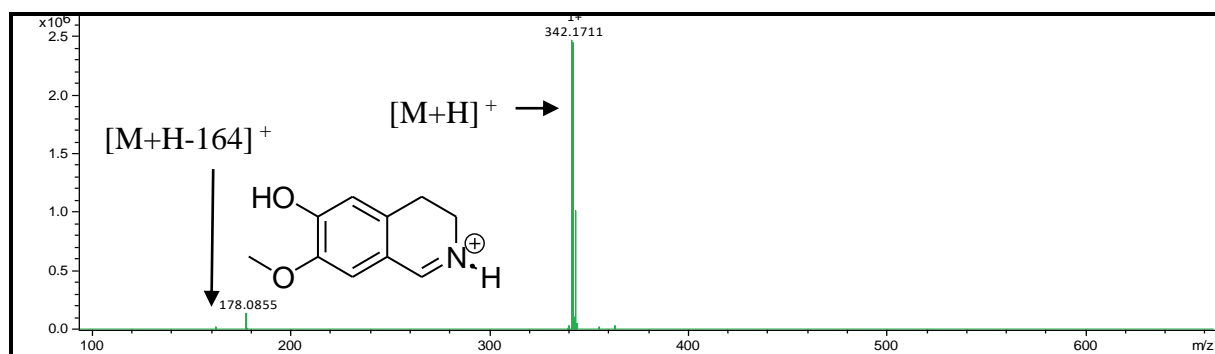
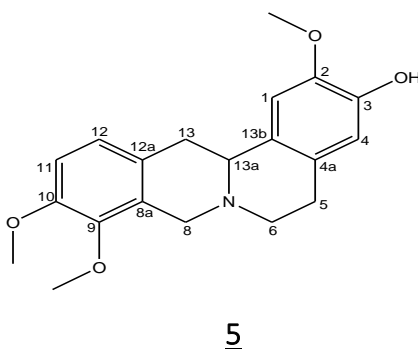
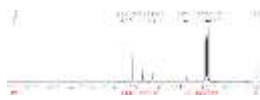


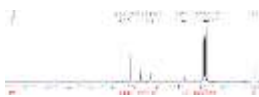
Figure 68. HR-ESI-MS spectrum of DSB 9



The broad band decoupled ^{13}C -NMR spectrum (**Figure 69**) of compound **DSB 9** displayed twenty carbon signals, which were sorted by DEPT and HSQC spectra into eight non-protonated carbons; three methoxyls and four methylene groups. This spectrum not only exhibited the signal of four aromatic methines at 109.7 (C-1), 116.0 (C-4), 145.4 (C-11) and 123.9 (C-12), but also the signal at δ_c 59.8 (C_{13a-N}) closed to the one at δ_c 59.4 (C_{13a-N}) of the tetrahydroajrorrhizine unit **De Castro Rodrigues et al. (2016)**. This latter information was confirmed in the 1H -NMR spectrum (**Figure 70**) of **DSB 9** which exhibited two sets of aromatic doublet protons. The first one appeared at δ_H 7.05-7.03 (H-1 and H-4) in ring A and the latter at δ_H 6.87 (H-11) and 6.95 (H-12) in ring D. Also in this spectrum, we observed the signal of protons belonging to four methylene groups at δ_H 3.14 (1H, *dd*, 10.5, 5.4; H-5_{ax}) and 2.56 (1H,

**Table 36.** Comparative ^1H -NMR spectral data of DSB 9 in Pyridine- d_5 with Corypalmine 5

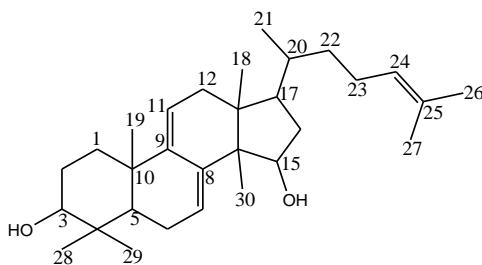
C and H n°	DSB 9		Corypalmine <u>5</u> (De Castro Rodrigues et al. 2016)	
	^1H (500 MHz, Pyridine- d_5)	^{13}C (125 MHz, Pyridine- d_5)	^{13}C (150 MHz, CDCl_3)	^1H (600 MHz, CDCl_3)
	δ_{H} (m, J in Hz)	δ_{C}	δ_{C}	δ_{H} (m, J in Hz)
1	7.05 (1H, d, 9)	109.7	108.7	6.73 (1H, s)
2	–	147.2	147.5	–
3	–	146.8	147.6	–
4	7.03 (1H, d, 9)	116.0	111.4	6.62 (1H, s)
4a	–	127.7	126.7	–
5 _{ax}	3.14 (1H, dd, 10.5, 5.4)	29.5	29.0	3.14 (1H, dd, 11.7; 5.0)
5 _{eq}	2.56 (1H, dd, 10.7, 3.0)	-	-	2.65 (1H, dd, 11.1; 3.4)
6 _{ax}	2.47 (1H, m)	51.1	51.5	2.69 (1H, m)
6 _{eq}	3.09 (1H, dd, 5.6; 3.5)	-	-	3.21 (1H, dd, 5.1; 3.5)
8 _{ax}	3.60 (1H, d, 15.6)	54.0	53.8	3.59 (1H, d, 15.3)
8 _{eq}	4.39 (1H, d, 15.6)	-	-	4.21 (1H, d, 15.4)
8a	–	128.5	127.3	–
9	–	111.3	114.0	–
10	–	146.1	146.5	–
11	6.87 (1H, d, 8.5)	145.4	143.2	6.81 (1H, d, 8.3)
12	6.95 (1H, d, 8.5)	123.9	124.9	6.84 (1H, d, 8.3)
12a	–	128.8	127.2	–
13 _{ax}	3.00 (1H, dd, 15.4, 11.7)	36.5	36.2	2.82 (1H, dd, 15.4, 11.7)
13 _{eq}	3.47 (1H, dd, 15.4, 3.5)	-	-	3.26 (1H, dd, 15.8, 3.8)
13a	3.57 (1H, dd, 11.5, 3.5)	59.8	59.4	3.58 (1H, dd, 11.5, 3.8)
13b	–	129.2	129.7	–
2-OCH ₃	3.87 (s)	55.7	56.3	3.91 (s)
9-OCH ₃	3.88 (s)	59.0	60.7	3.85 (s)
10-OCH ₃	3.73 (s)	55.3	55.7	3.90 (s)



II.1.3.5. Triterpenoids

II.1.3.5.1. Structural identification of DSB 10

DSB 10 was obtained in the system hexane-EtOAc as brown crystal, mp. 215–217 °C and soluble in the DMSO. It was positive to the Liebermann-Buchard (red-violet coloration) indicating its triterpene nature (Ngangoue et al. (2020)). Its molecular formula, implying seven degrees of unsaturation, was deduced from a pseudo-molecular ion peak $[M+H]^+$ at m/z 441.1524 (calcd. 440.1519 for $C_{30}H_{48}O_2$). The interpretation of its spectroscopic data 1H -; ^{13}C -NMR and 1-D and 2-D dimensional (COSY, HMQC, HMBC and DEPT 135) along with its comparison with an authentic sample allowed us to conclude that **DSB 10** was identical to polycarpol **111** (Pereira et al. 2003).



111

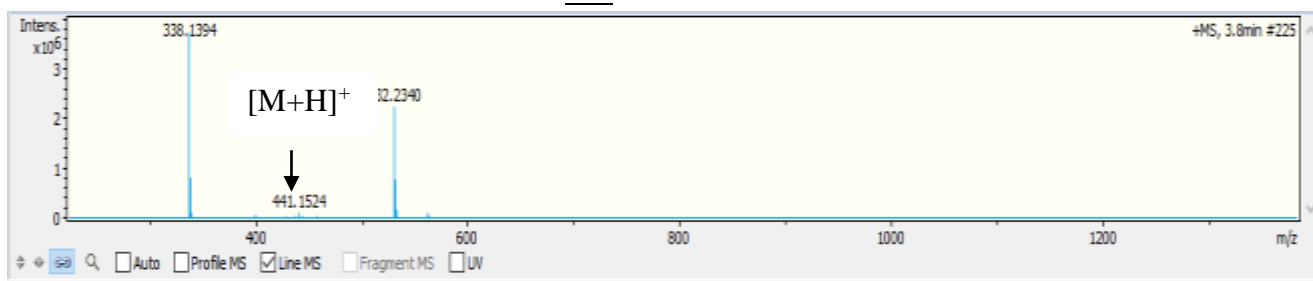


Figure 71. HR-ESI-Mass spectrum of DSB 10

The broad band decoupled ^{13}C -NMR spectrum (Figure 72) in conjunction with DEPT (90 and 135) and DEPT-HSQC revealed the presence of thirty carbon atoms among which six olefinic carbon atoms at δ_c 115.3 (C-11), 120.6 (C-7), 124.3 (C-24), 140.4 (C-8), 130.3 (C-25) and 145.6 (C-9); twenty-four sp^3 carbons attributed to eight methyls observed at δ_c 15.2 (C-18), 22.3 (C-19), 18.6 (C-21), 17.4 (C-26), 24.2 (C-27), 27.3 (C-28), 15.2 (C-29) and 36.9 (C-30); seven methylenes at δ_c 35.7 (C-1), 27.3 (C-2), 22.3 (C-6), 38.7 (C-12), 38.7 (C-16), 36.8 (C-22), 24.7 (C-23), three methines at δ_c 48.1 (C-5), 48.1 (C-17), 35.3 (C-20), along with two oxymethines at δ_c

76.9 (C-3), 73.5 (C-15), and four quaternary carbon at δ_c 38.7 (C-4), 37.9 (C-10), 43.6 (C-13) and 51.3 (C-14).

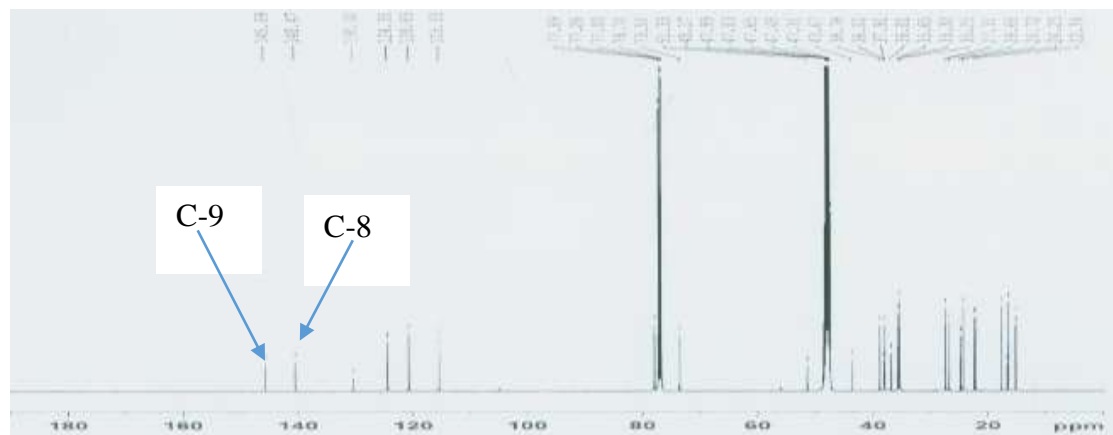


Figure 72. ¹³C-NMR (125 MHz, CDCl₃ and CD₃OD) of DSB 10

The ¹H-NMR spectrum (Figure 73) indicated the presence of three olefinic proton signals at δ_H 5.83 (1H, d, 5.3 Hz, H-7), 5.27 (1H, d, 4.9 Hz, H-11) and 5.04 (1H, m, H-24); two oxymethines at δ_H 4.20 (1H, m, H-15) and 3.16 (1H, m, H-3); one secondary and seven tertiary methyls respectively at δ_H 0.85 (H-21) and 0.57 (H-18), 0.94 (H-19), 0.84 (H-28), 0.88 (H-30), 1.02 (H-29), 1.59 (H-26) and 1.65 (H-27).

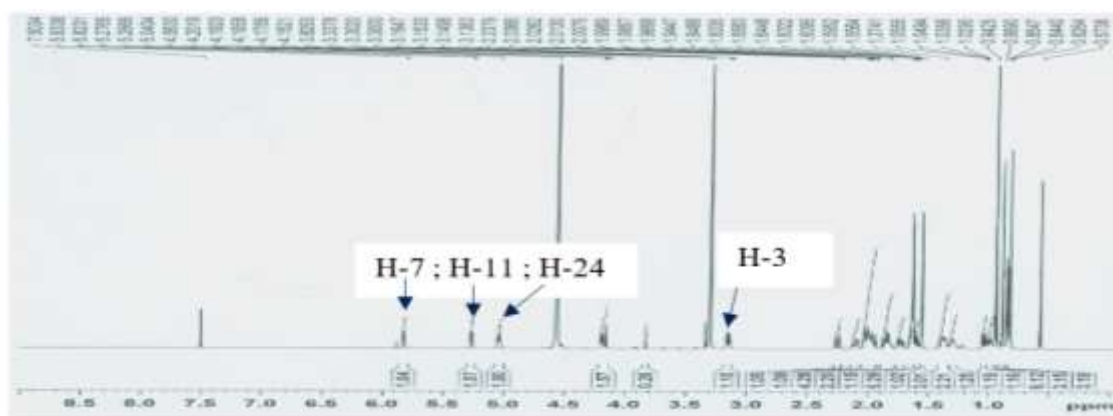
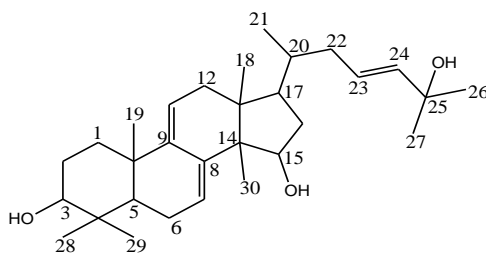
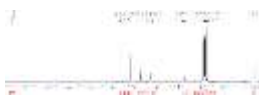


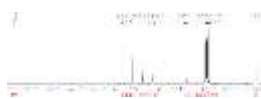
Figure 73. ¹H-NMR (500 MHz, CD₃OD) of DSB 10

DSB 10 spectral data were comparable to polycarpol (Pereira et al. 2003) and almost to those of Anomanol A [112](#), a lanosta-7, 9, 23-triene derivatives reported by Ngangoue et al. (2020).

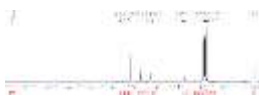


112

The HMBC spectrum showed correlations between the protons of the methyl C-30 at δ_{H} 0.91 with carbons at δ_{C} 43.6, (C-13) 51.3 (C-14) and 140.9 (C-8); methyl proton at δ_{H} 0.85 (H-21) correlated with carbons at δ_{C} 35.3 (C-20) and 36.8 (C-22). In addition, the signal proton at δ_{H} 1.59 (H-26) correlated also with carbons at 124.3 (C-24) and 130.3 (C-25). This latter information allowed us to identify **DSB 10** as polycarpol


Table 37. Comparative ^{13}C -NMR spectral data of DSB 10 with Polycarpol and Anomanol A.

C no.	^{13}C (125 MHz, CDCl_3 and CD_3OD)	^{13}C (75 MHz, CDCl_3)	^{13}C (150 MHz, DMSO)
	δ_{C} DSB 10	δ_{C} Polycarpol (Pereira et al. 2003)	δ_{C} Anomanol A (Ngangoue et al. 2020)
1	35.7	35.7	35.4
2	27.3	27.8	27.6
3	76.7	78.9	76.8
4	38.7	38.7	38.3
5	48.1	48.9	48.8
6	22.3	22.9	22.5
7	120.8	121.3	120.9
8	140.4	140.9	140.9
9	145.6	146.1	146.0
10	37.9	37.4	37.8
11	115.3	116.1	115.3
12	38.7	38.5	38.5
13	43.6	44.3	43.6
14	51.3	51.9	51.4
15	73.5	74.7	72.4
16	38.7	40.1	36.2
17	48.1	48.9	47.9
18	15.2	15.8	15.8
19	22.3	22.8	22.7
20	35.3	35.8	35.9
21	18.6	18.4	18.3
22	36.8	36.2	39.2
23	24.7	24.9	123.1
24	124.3	124.9	140.8
25	130.3	131.2	68.9
26	17.4	17.6	30.2
27	24.2	25.7	30.2
28	27.3	28.1	28.3
29	15.2	15.0	16.1
30	36.9	35.7	17.4

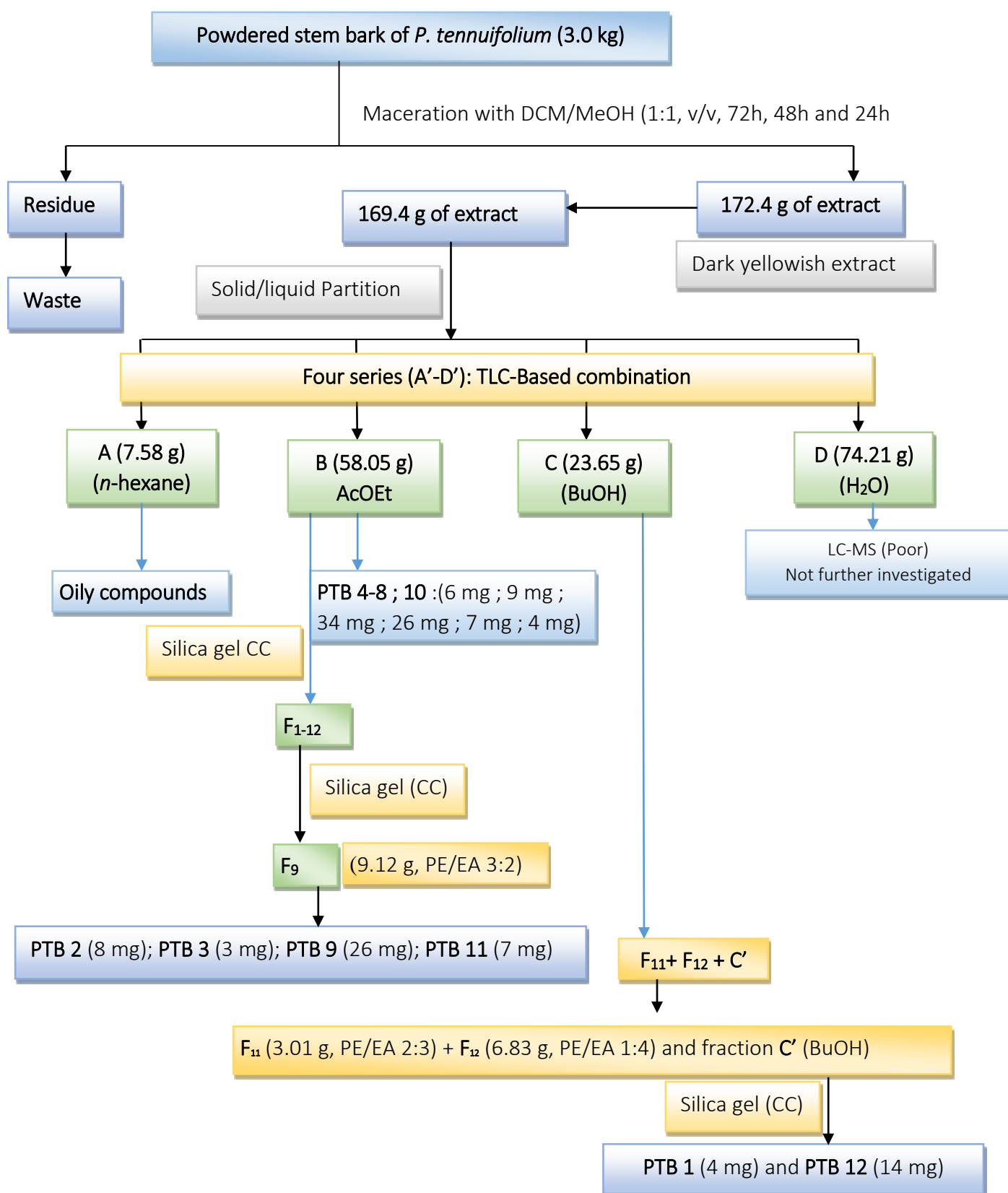
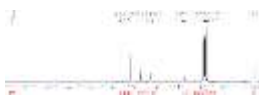


II.2. PLANT MATERIAL, EXTRACTION, ISOLATION, LC-MS DETECTION AND STRUCTURAL IDENTIFICATION OF COMPOUNDS OF *PSOROSPERMUM Tenuifolium*

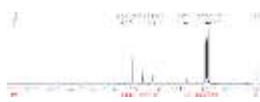
II.2.1. PLANT MATERIAL, EXTRACTION AND ISOLATION OF COMPOUNDS OF *PSOROSPERMUM Tenuifolium*

The stem bark of *P. tenuifolium* (Hypericaceae) was collected in April 2017, in the village Nkol-Afamba (GPS coordinates: Latitude 3°51'32"N, Longitude 11°39'53"E), near Yaounde, Centre Region of Cameroon. The plant material was authenticated with the help of Mr Victor Nana, a well-known botanist of the National Herbarium of Cameroon, where a voucher specimen was deposited and registered under the number 43860 HNC.

The air-dried and powdered stem bark (~3.0 kg) of *P. tenuifolium* was consequently extracted three times with the mixture of dichloromethane/methanol (1:1, v/v) for 72 h, 48 h and 24 h, respectively. After filtration and evaporation of solvent under reduced pressure, 172.46 g of crude extract were obtained, dissolved later on in water and successively partitioned with *n*-hexane (Hex), ethyl acetate (EtOAc), and *n*-butanol (BuOH) to give three solvent-soluble fractions labelled **A'** (7.58 g), **B'** (58.05 g), **C'** (23.65 g), respectively, as well as the remaining water soluble fraction **D'** (74.21 g) (**Scheme 18**). Twelve compounds labelled **PTB 1-12** were isolated. In continuation of our search for cytotoxic compounds from the genus *Psorospermum*, the potency of ten among the twelve (**Table 39**) of these isolated compounds was carried out on KB-3-1 cell lines with griseofulvin as reference ($IC_{50} = 17-21 \mu M$).



Scheme 17. Extraction and isolation flowchart of compounds from the stem bark of *P. tenuifolium*



From the study of the stem bark of *P. tenuifolium*, twelve compounds have been isolated. Their structures were elucidated by means of spectroscopic data analysis with the help of literature review one hand, and completed with the aid of LC-ESI-MS on the other hand. They comprise seven classes of compounds namely: phenylpropanoid glucoside, anthraquinones, bianthrone, flavonoids, triterpens, anthrone, steroid glycoside and steroid (Table 39).

II.2.2. LC-MS DETECTION OF COMPOUNDS OF *PSOROSPERMUM TENUIFOLIUM*

The crude hydro-alcoholic extract of the barks of *P. tenuifolium* was also successively subjected to LC-MS analysis (Figures 74; 74a; 74b; 75; 76 and Tables 38; 39) as well as through solid/liquid partition technique (Table 61).

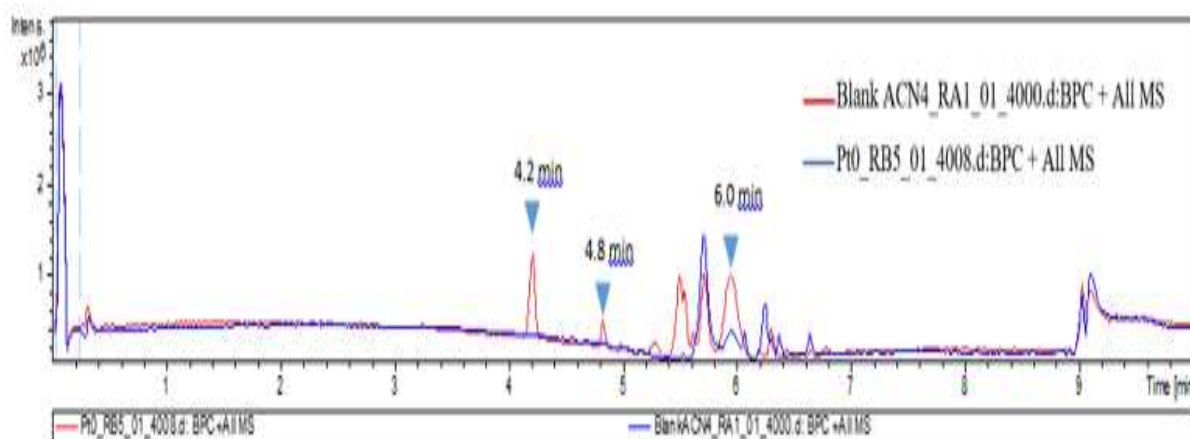
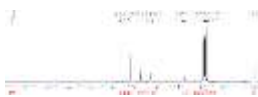


Figure 74. BPC of two unknown compounds (R_t : 4.2 and 6.0 min) and Vismione D (R_t : 4.8 min) detected from the crude extract of *P. tenuifolium* – Below 74a. Chromatogram of the crude extract of *P. tenuifolium* for the detection of Emodin and 74b. BPC of the pur compound Emodin (R_t : 3.8 min) detected through the LC-MS guided isolation from the crude extract of *P. tenuifolium*



From the LC-MS guided isolation of the crude extract, **PTB 2** (R.T. 3.8 min) was identified.

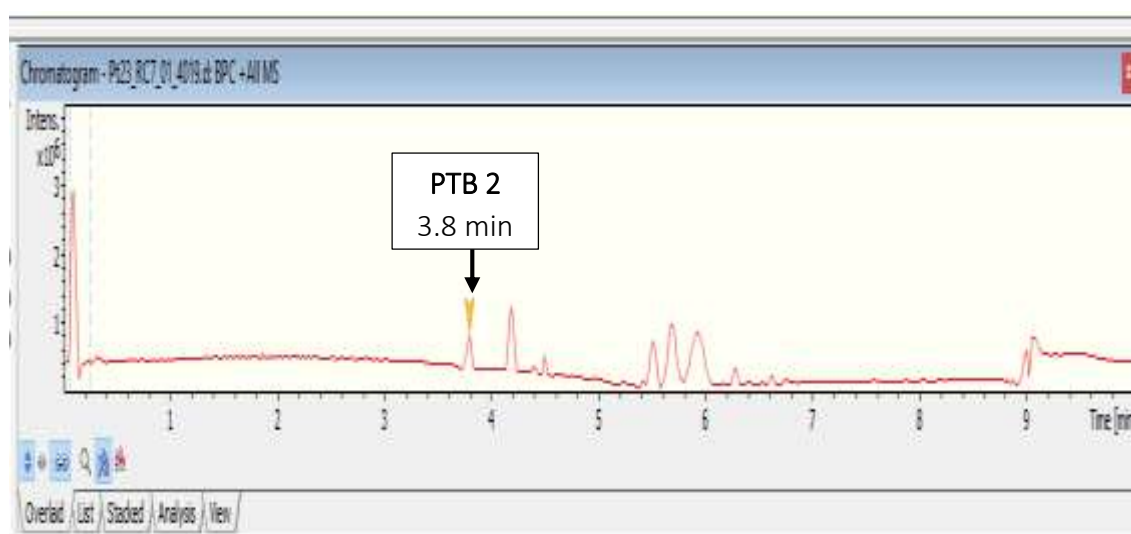


Figure 74a. Chromatogram of the crude extract of *P. tenuifolium* for the detection of Emodin

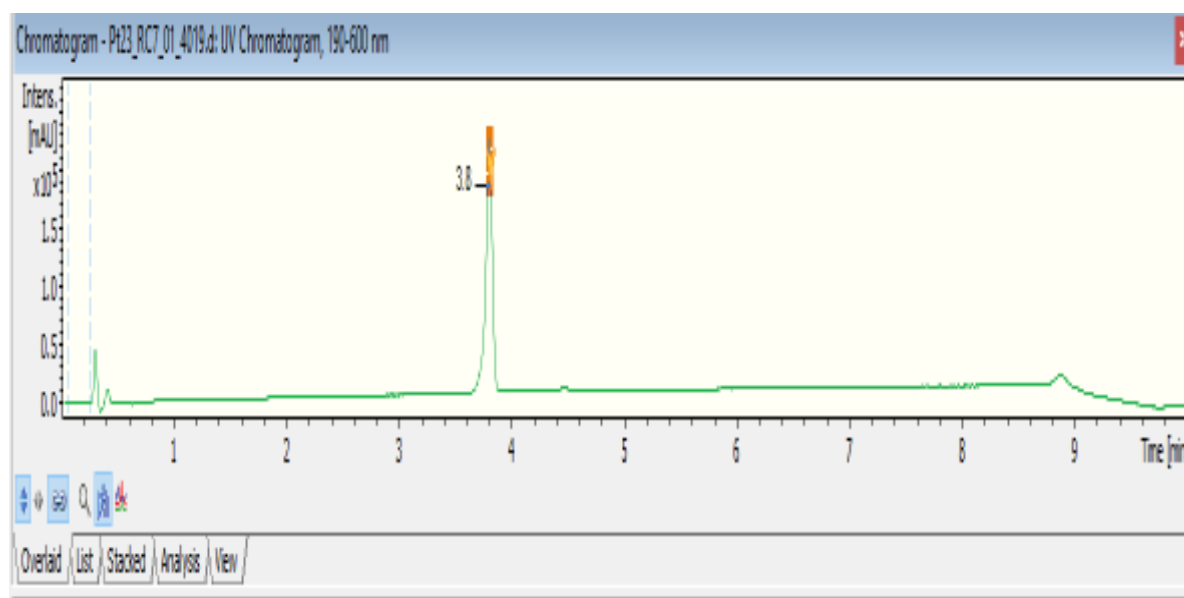


Figure 74b. BPC of the pur compound Emodin (R_t : 3.8 min) detected through the LC-MS guided isolation from the crude extract of *P. tenuifolium*

From the LC-MS guided isolation of the sub-fraction B', **PTB 8** (R.T. 1.5 min) was identified.

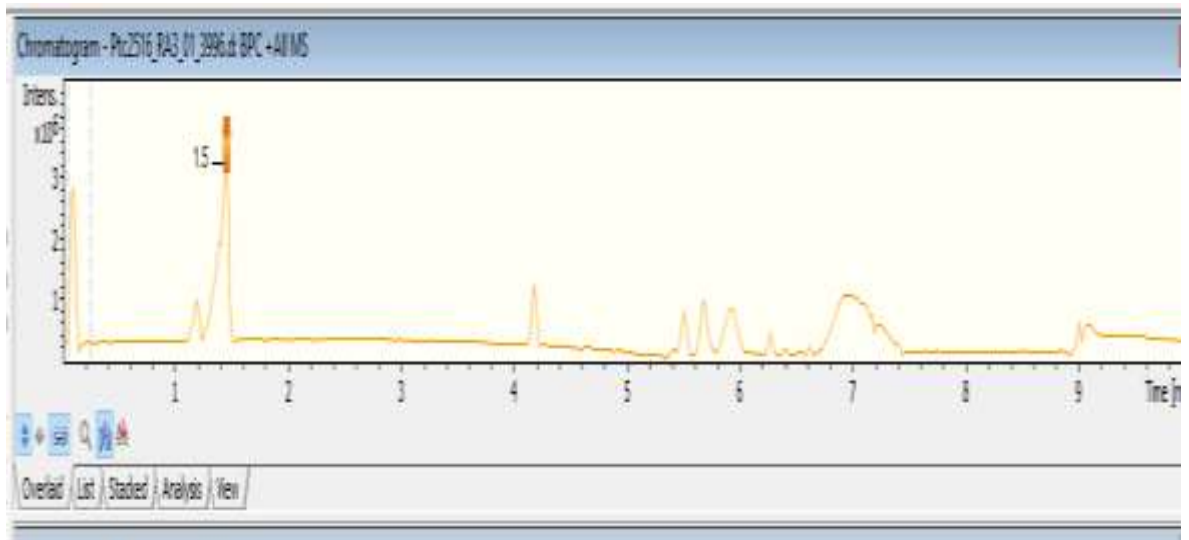
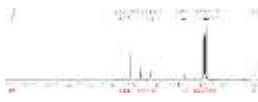


Figure 75. Chromatogram of the sub-fraction B' of the crude extract of *P. tenuifolium*

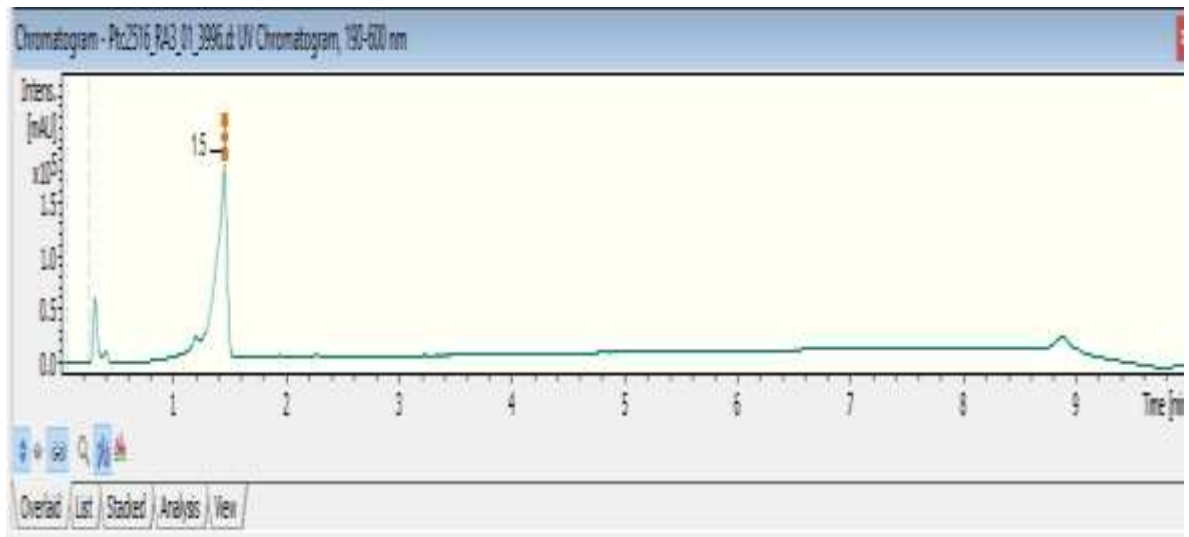
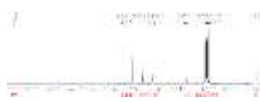


Figure 76. BPC of the pur compound (+)-Catechin (R_t : 1.5 min) detected through the LC-MS guided isolation from the sub-fraction B' of the crude extract of *P. tenuifolium*


Table 38. Non exhaustive peak list for detected compounds with listed m/z value and retention time from *Psorospermum* sp.

Peak n°	R _t (min)	[M+H] ⁺		Molecular formulae	Name of compound
		Exp.	Calcd.		
1''	4.2	439.1713	439.1711	C ₂₀ H ₂₇ N ₂ O ₉	N.I.
2''	4.8	411.2171	411.2166	C ₂₅ H ₃₁ O ₅	Vismione D <u>76</u>
3''	5.7	338.3430	338.3417	C ₂₂ H ₄₄ NO	N.I.
4''	6.0	425.3615	425.3625	C ₂₆ H ₄₉ O ₄	N.I.

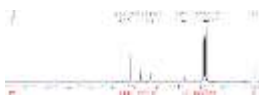
N.I. : Not Identified

The isolated compounds were sorted into Phenylpropanoid glucoside, Anthraquinones, Bianthrone, Flavonoid, Triterpenoids, Steroid glycoside and Steroid glycoside (**Table 39**).

Table 39. Compounds isolated per class from the stem bark of *P. tenuifolium*

Codes	Name of compounds (Number)	Class (Observation)	[M+H] ⁺	RT (min)
PTB 1	Psorospermoside <u>113</u>	Phenylpropanoid glucoside (New)	515.1521	N.d.
PTB 2	Emodin <u>77</u>		271.1017	3.8
PTB 3	Physcion <u>79</u>		285.1123	4.0
PTB 4	2-prenylemodin <u>78</u>	Anthraquinones (Known)	339.3911	6.3
PTB 5	2-geranylemodin <u>114</u>		407.1852	5.9
PTB 6	3-geranyloxyemodin <u>55</u>		N.d.	N.d.
PTB 7	Bianthrone A3a/3b <u>115</u>	Bianthrone (Known)	N.d.	N.d.
PTB 8	(+)- Catechin <u>64</u>	Flavonoid (Known)	291.0968	1.5
PTB 9	Betulinic acid <u>60</u>		-	N.d.
PTB 10	Lupeol <u>116</u>	Triterpenoids (Known)	-	N.d.
PTB 11	Lupeol acetate <u>117</u>		-	N.d.
PTB 12	Daucosterol <u>118</u>	Steroid glycoside (Known)	-	N.d.

N.d.: not determined – Poor ionization of samples



II.2.3. CHARACTERIZATION AND STRUCTURAL IDENTIFICATION OF COMPOUNDS OF *PSOROSPERMUM TENUIFOLIUM*

II.2.3.1. Phenylpropanoid glucoside

II.2.3.1.1. Identification of PTB 1

Compound **PTB 1** was obtained as a white amorphous powder [$\alpha_D^{20} +5.8$ (c 0.5, MeOH)]. Its UV (MeOH) spectrum exhibited absorption band at λ_{\max} (log ϵ) 312 nm suggesting the presence of α,β -Unsaturated Ketones (**Woodward, 1941**). The IR (KBr) spectrum showed absorption band for hydroxyl (3317 cm^{-1}), conjugated carbonyl (1699 cm^{-1}) and aromatic system (1599 cm^{-1}) functionalities (**Figure 78**). Its HR-ESI-Mass spectrum exhibited $[M+Na]^+$ ion peak at m/z 515.1521 (calcd. for $C_{24}H_{28}O_{11}Na$, 515.1524) as illustrated below (**Figure 77**).

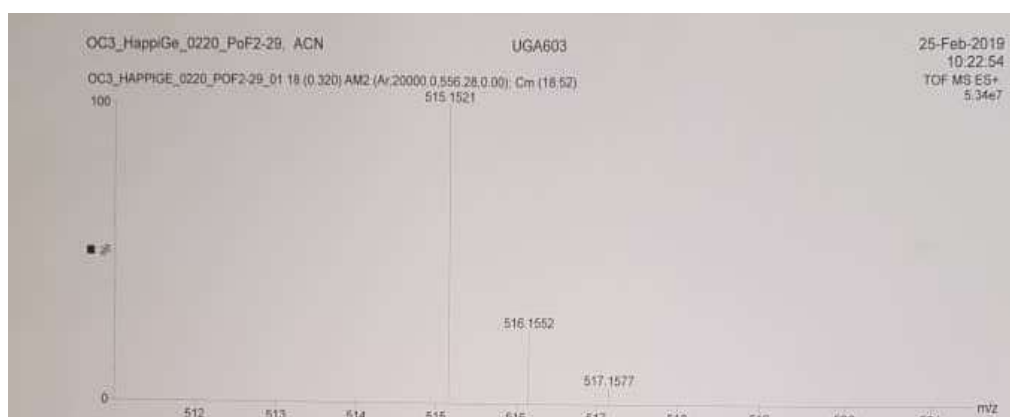
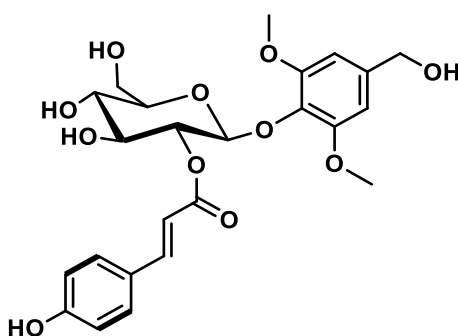


Figure 77. HR-ESI-Mass spectrum of PTB 1



113

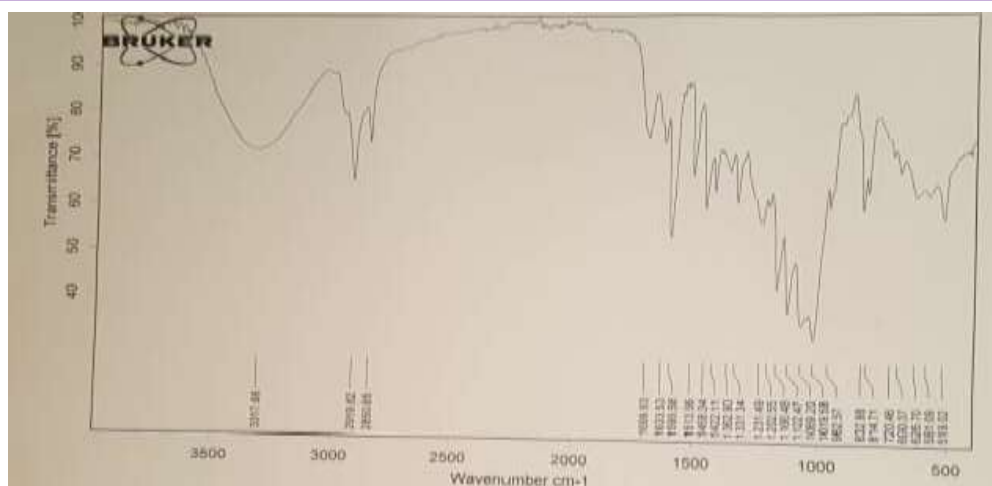
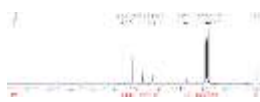


Figure 78. IR spectrum of PTB 1 in KBr

The broad band decoupled ^{13}C NMR (Figure 79) and HMQC (Figure 84) spectra exhibited signals of 24 carbon atoms including signals of a glucosyl unit at δ_{C} 102.9, 78.6, 76.3, 75.7, 71.5 and 62.3, signals of an α,β -unsaturated carbonyl group at δ_{C} 166.5; two methoxy groups at δ_{C} 56.2 (x 2); one oxymethylene at δ_{C} 64.1; as well as fourteen sp^2 carbon signals in the range of δ_{C} 104.5–161.1.

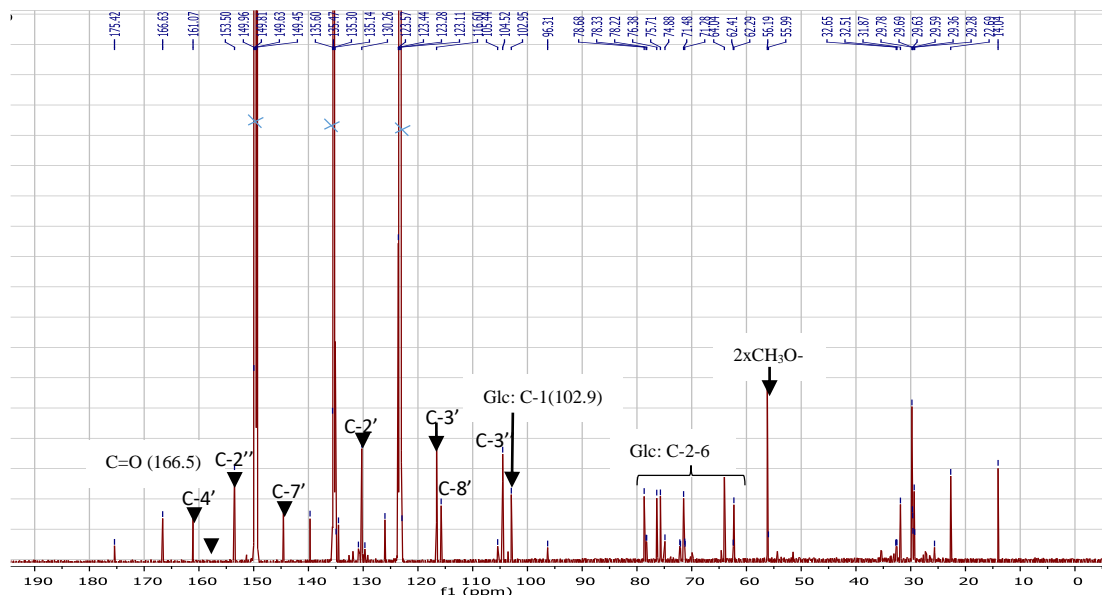


Figure 79. ^{13}C NMR spectrum (125 MHz, Pyridine- d_5) of PTB 1

All these findings were in accordance with the ^1H NMR spectrum (Figure 80) of compound **PTB 1** which showed the AA'BB'-type proton signals at δ 7.52 (d, $J = 7.9$ Hz, 2H) and δ 7.12 (d, $J = 7.9$ Hz, 2H), as well as an AA' system at δ 6.90 (brs, 2H). This observation suggested

the presence of a 1,4-disubstituted and a 1,2,4,6-tetrasubstituted benzene rings in **PTB 1**. Additionally, signals corresponding to an α,β -unsaturated carbonyl group at δ_{H} 6.67 and 7.94 (d, $J = 15.9$ Hz, 1H each), two methoxy signals at δ_{H} 3.71 (6H, s), one highly deshielded oxymethylene signal at δ_{H} 4.88 (2H, s) and one signal at δ_{H} 5.79 (d, $J = 8.0$ Hz, 1H) corresponding to an anomeric proton were also observed. The large $^3J_{\text{H-1,H-2}}$ coupling constant suggested a β -glucosidic linkage in **PTB 1**. All these spectroscopic data indicated that compound **PTB 1** is a phenylpropanoid glucoside containing one glucopyranosyl (unit I); one *trans-p*-coumaroyl (unit II) and one 1,2,3,5-tetrasubstituted benzene (unit III) groups.

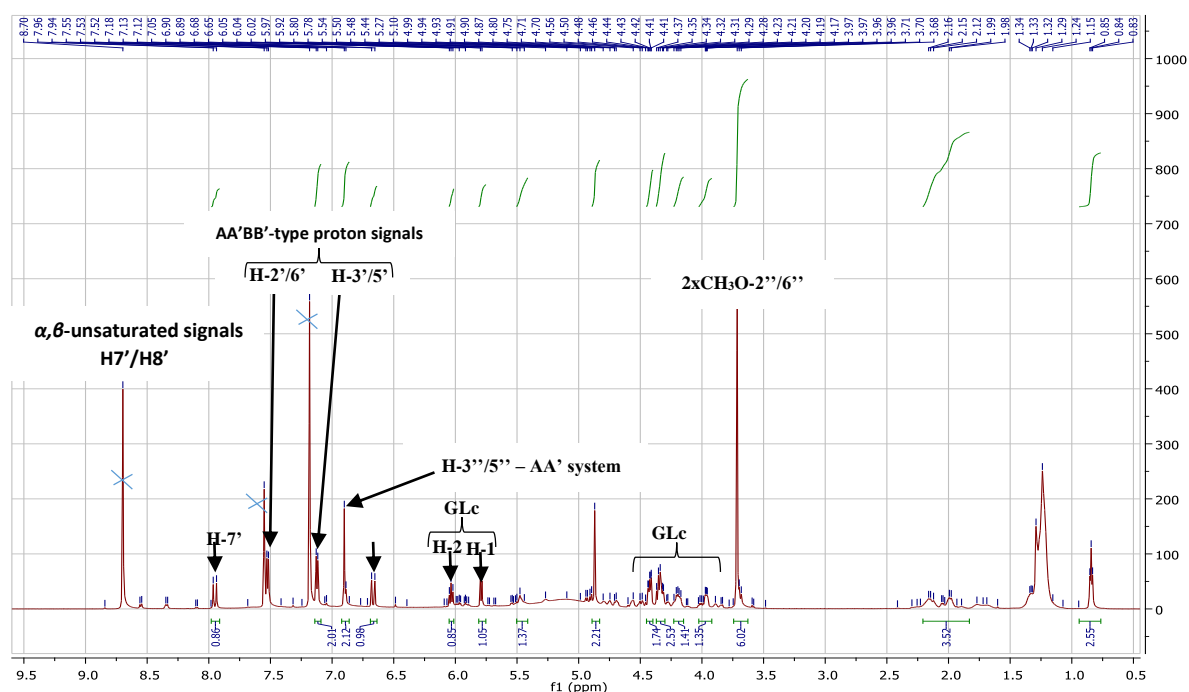


Figure 80. ^1H NMR spectrum (500 MHz, Pyridine- d_5) of **PTB 1**

Careful analysis of the ^1H NMR spectrum indicated signals of six protons at δ_{H} 6.03 (1H, *dd*, 1.6, 8.0, H-2), 5.79 (1H, *d*, 8.0, H-1), 4.43 (1H, *m*, H-3), 4.42 (1H, *m*, H-6b), 4.34 (1H, *m*, H-4), 4.33 (1H, *m*, H-6a), 3.96 (1H, *ddd*, 2.4, 4.9, 9.4, H-5) assignable to the glucopyranose moiety. The COSY spectrum (**Figure 82**) exhibited the correlations between H-1/H-2, H-2/H-3, H-3/H-4, H-4/H-5 and a cluster of correlation spots corresponding to correlations between the protons H-3, H-4 and H-6a/b. All these evidence easily allowed to build and assign the glucose scaffold from C-1 to C-6 (**Figure 81**).

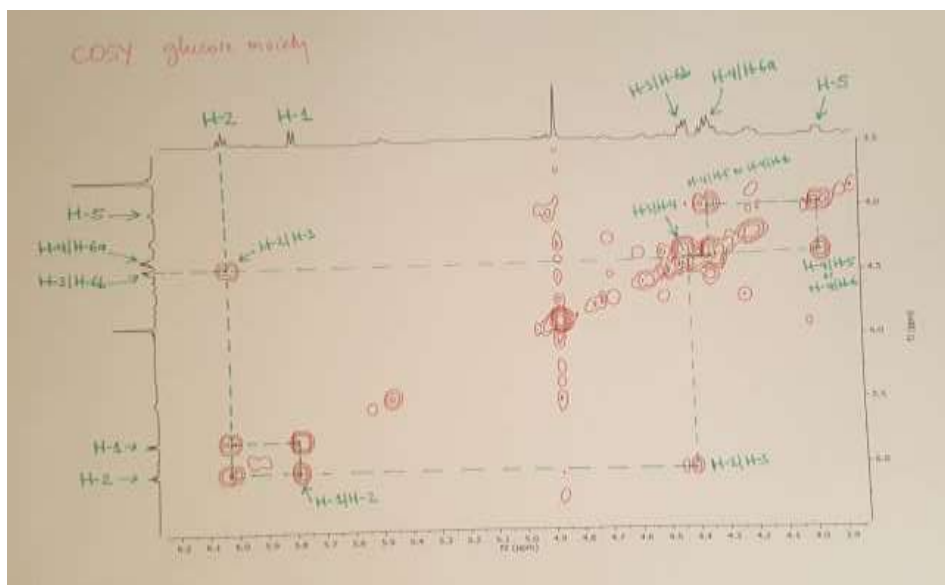
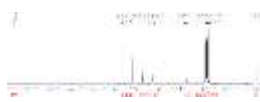


Figure 81. COSY spectrum of the glucose moiety of PTB 1

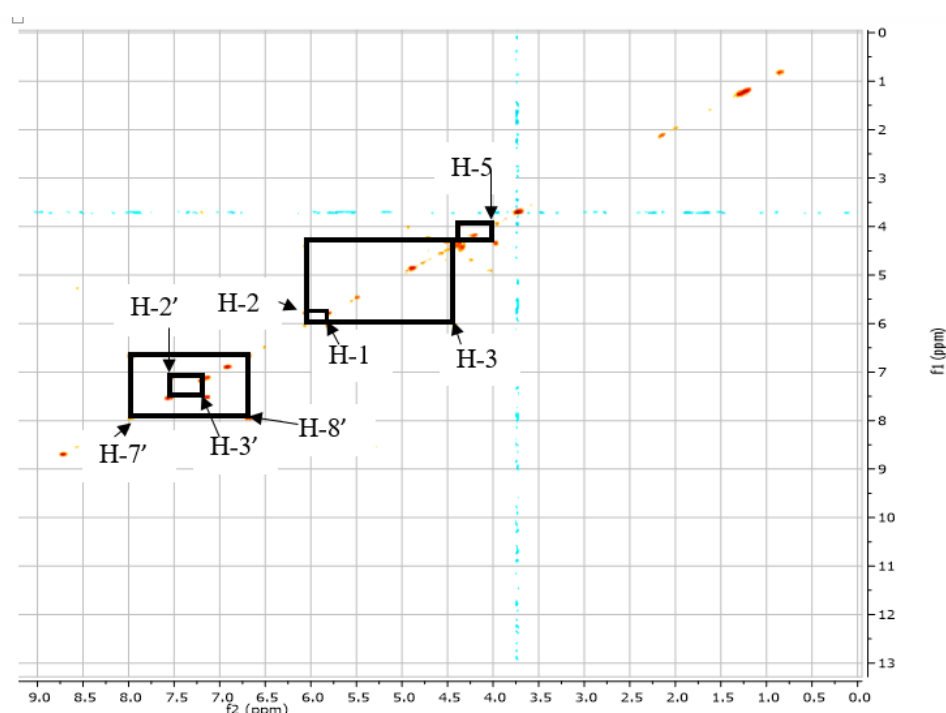


Figure 82. COSY spectrum of the AA'BB' and AA' moieties of PTB 1

The deshielded proton signal observed at δ_{H} 6.03 (H-2) indicated an esterification of C-2 (connection with unit II), while the carbon signal at δ_{C} 102.9 (C-1) suggested another substitution at C-1 (connection with unit III). The connections between units I–III were established on the basis of the HMBC correlations. Consequently, a long-range cross-peak was observed between the highly deshielded proton signal of unit I at δ_{H} 6.03 (H-2) and the carbon signal at δ_{C} 166.5 (C-9') of unit II, supporting the connection through the oxygen bond in-

between units I and II. The HMBC spectrum (**Figure 83**) exhibited some correlations from δ_{H} 6.90 (H-3''/H-5'') to δ_{C} 64.1 (C-7'') and from δ_{H} 3.71 (OCH₃-2''/OCH₃-6'') to δ_{C} 153.7 (C-2''/C-6''), allowed to set up the unit C (1,2,3,5-tetrasubstituted benzene group) as a 4''-(hydroxymethyl)-2'',6''-dimethoxyphenolate moiety. It appears evident that the only position to link unit C is at position 1''. This proposition was confirmed by the observed HMBC long range correlation from the anomeric proton at δ_{H} 5.79 (H-1) to the carbon signal at δ_{C} 134.5 (C-1'') establishing the connection C-1/C-1'' between units I and III. Based on all this evidence, **PTB 1** was found to be a new compound and trivially named as psorospermoside **113**.

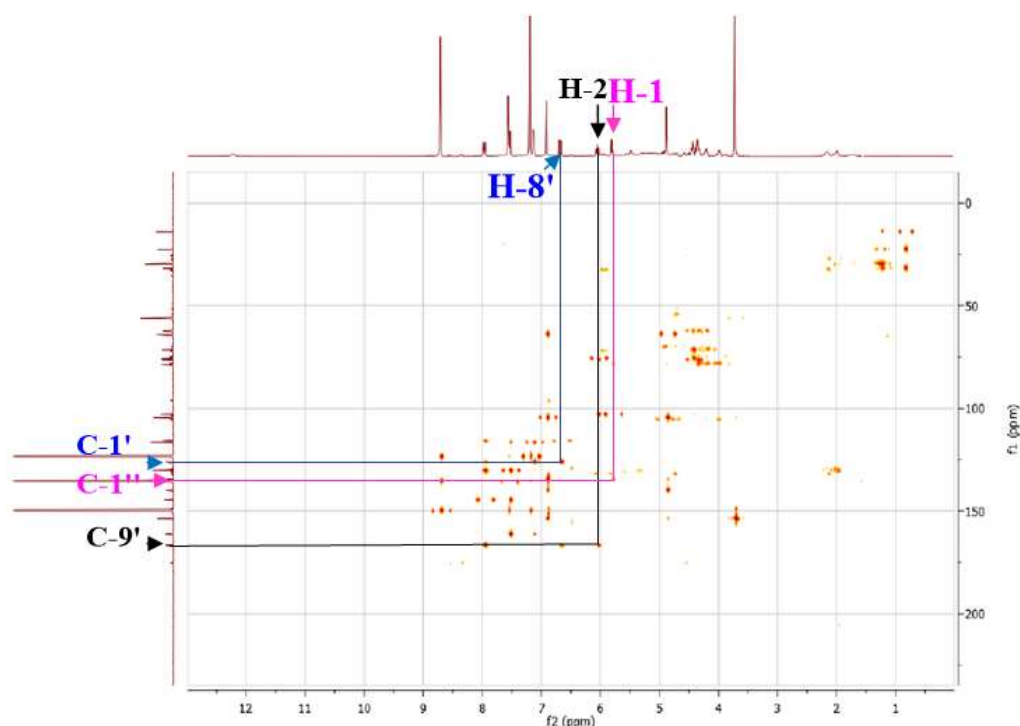


Figure 83. Key cross peaks on HMBC spectrum of PTB 1

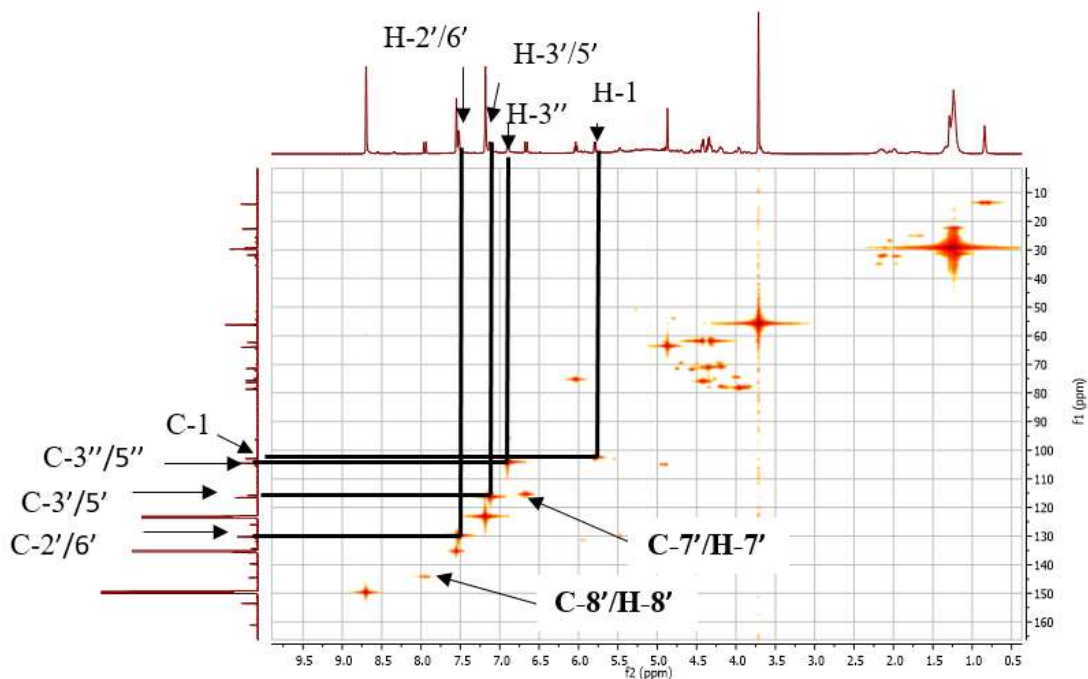
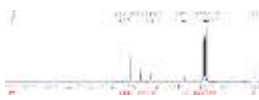
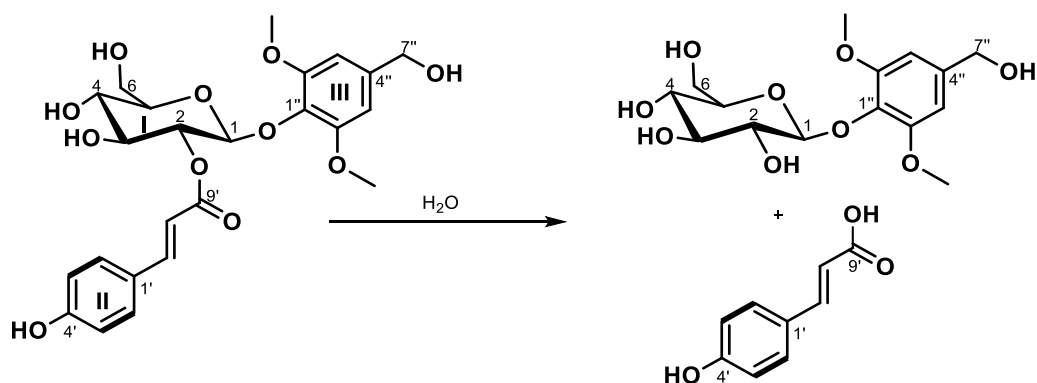
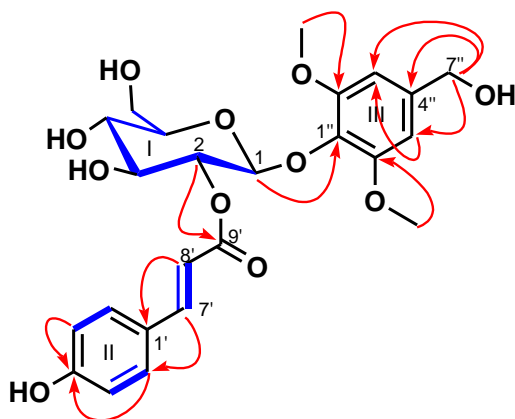


Figure 84. HMQC spectrum of PTB 1

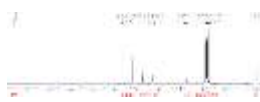
A possible hydrolysis reaction of PTB 1 might allow us to get the following substrates (Scheme 18a)



And some Key COSY (blue) and selected HMBC (red) correlations as shown in Scheme 18b.



Scheme 18. Hydrolysis reaction (a) and Key COSY (blue) and selected HMBC (red) correlations (b) of PTB 1


Table 40. ^1H (500 MHz) and ^{13}C (125 MHz) NMR assignments of PTB 1 in Pyridine- d_5

Unit	C and H no	PTB 1	
		δ_{C}^a	δ_{H} (mult., J in Hz) ^a
I	1	102.9	5.79 (1H, <i>d</i> , 8.0)
	2	75.7	6.03 (1H, <i>dd</i> , 1.6, 8.0)
	3	76.3	4.43 (1H, <i>m</i>)
	4	71.5	4.34 (1H, <i>m</i>)
	5	78.6	3.96 (1H, <i>ddd</i> , 2.4, 4.9, 9.4)
	6	62.3	4.33 (1H, <i>m</i>) 4.42 (1H, <i>m</i>)
II	1'	125.9	–
	2'/6'	130.1	7.52 (2H, <i>d</i> , 7.9)
	3'/5'	116.6	7.12 (2H, <i>d</i> , 7.9)
	4'	161.1	–
	7'	144.5	7.94 (1H, <i>d</i> , 15.9)
	8'	115.7	6.67 (1H, <i>d</i> , 15.9)
	9'	166.5	–
III	1''	134.5	–
	2'', 6''	153.7	–
	3'', 5''	104.5	6.90 (2H, <i>brs</i>)
	4''	139.6	–
	7''	64.1	4.88 (2H, <i>brs</i>)
	CH ₃ O-2'', 6''	56.2	3.71 (6H, <i>s</i>)

^aThe chemical shifts are in δ values (ppm) from TMS. ¹³C multiplicities were determined through HSQC experiment

II.2.3.2. Anthraquinones

II.2.3.2.1. Structural identification of PTB 2

PTB 2 was obtained as red powder and gave a positive result to the Borntrager test characteristic of anthraquinones. Its HR-ESI-MS spectrum (Figure 85) exhibited a pseudo-molecular ion peak $[M+H]^+$ at m/z 271,1017 (calculated for 271,1024) compatible with the molecular formula $C_{15}H_{11}O_5$ corresponding to eleven degree of insaturations.

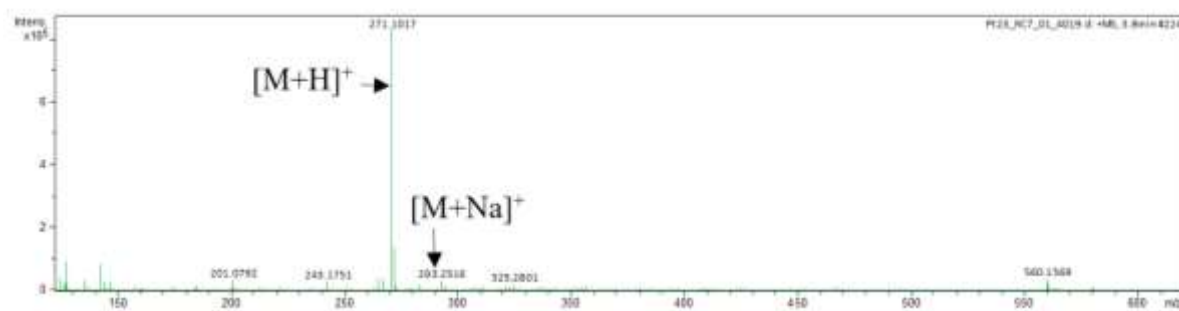
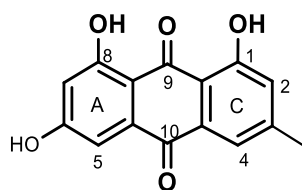


Figure 85. HR-ESI-Mass spectrum of PTB 2

The analysis of the NMR data (1H -, ^{13}C -NMR, HMQC and HMBC) of PTB 2 and those reported in the literature permit us to assign structure numbered 77 to emodin.



77

In fact, the broad band decoupled ^{13}C -NMR spectrum (Figure 86) of PTB 2 displayed 15 carbon resonances which were sorted partly by HMQC spectrum into 10 quaternary carbons at δ_c 165.3 (C-1), 148.4 (C-3), 161.5 (C-6), 165.4 (C-8), 190.8 (C-9), 181.3 (C-10), 135.7 (C-10a), 113.5 (C-9a), 108.7 (C-8a) and 133.3 (C-4a); four methines aromatic carbons at δ_c 120.6 (C-2), 124.2 (C-4), 107.9 (C-5) and 109.6 (C-7) and the presence of the methyl was further confirmed by the carbon signal at δ_c 21.1 (CH_3). The exact location of the substituents was established after careful examination of the NMR pattern of the aromatic protons using HMQC and HMBC spectra. In fact the position of methyl was assigned based on the HMBC correlations of the proton at δ_H 2.33 (CH_3) with carbon signals at δ_c 124.2 (C-4), 148.4 (C-3) and 120.6 (C-2).

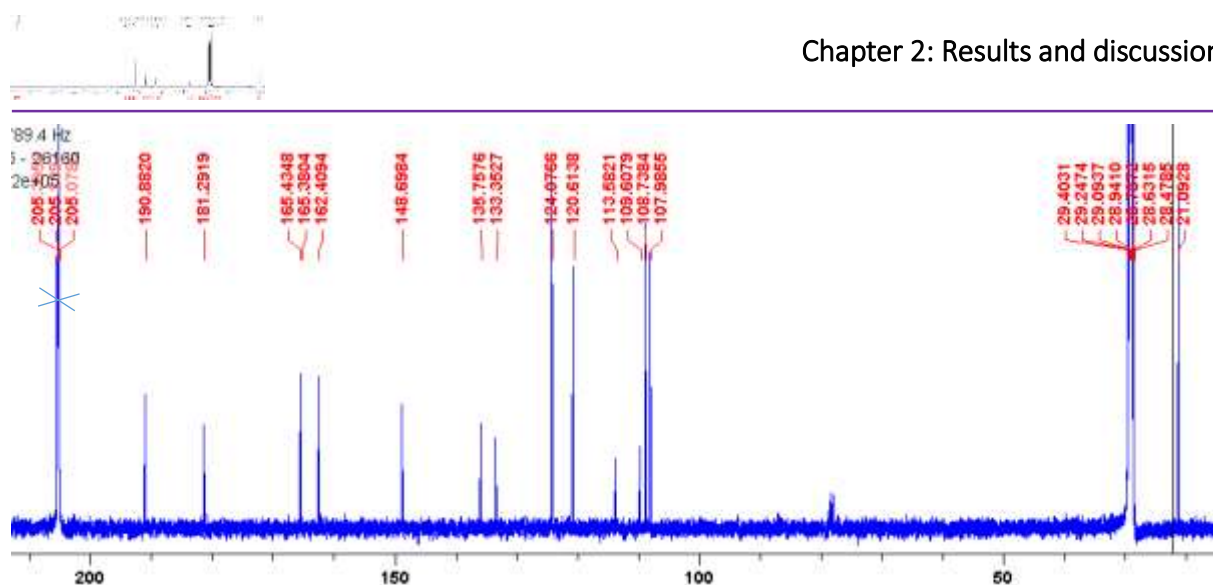


Figure 86. ^{13}C NMR spectrum (125 MHz, Acetone- d_6) of PTB 2

the ^1H -NMR spectrum below (Figure 87) exhibited the signals of four aromatic *meta*-protons in A- and C-rings sorted into two doublets of one proton each at δ_{H} 7.12 (1H, d, 2.4 Hz) and 6.53 (1H, d, 2.4 Hz) and also two broad singlets of one proton each not well resolved at δ_{H} 7.43 (1H, brs) and 7.01 (1H, brs).

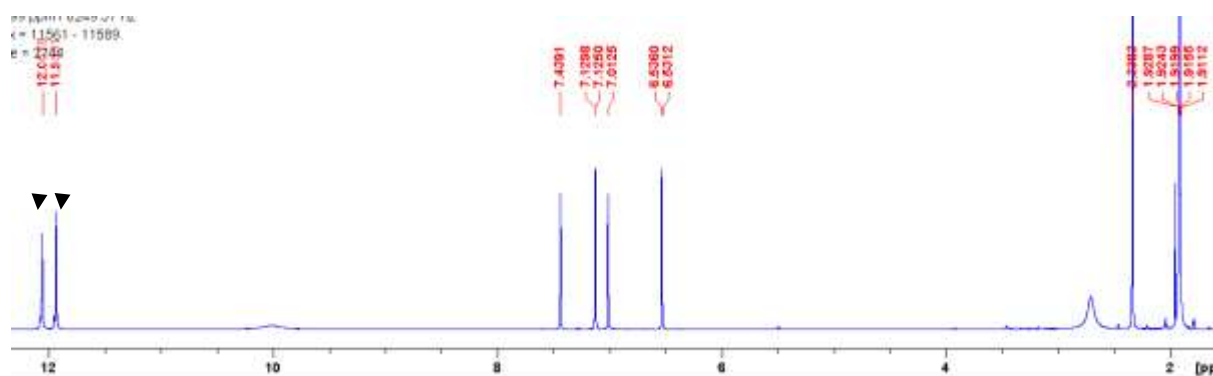
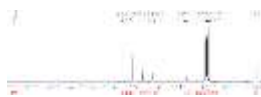
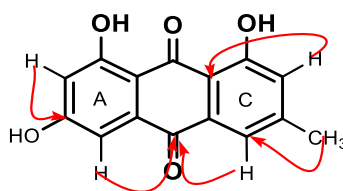


Figure 87. ^1H NMR spectrum (500 MHz, Acetone- d_6) of PTB 2

These four signals were further confirmed in the HMQC spectrum where four ^1J correlations between these aromatic protons and the methines respectively at 7.12/107.9 (C-5), 6.53/109.6 (C-7), 7.43/120.6 (C-2) and 7.01/124.2 (C-4) were observed. In addition, the positions of the aromatic signal were deduced through the cross peaks observed in the HMBC spectrum between the signal of the proton at δ_{H} 6.53 and the signals of the carbons at 107.9 (C-5) and 165.4 (C-8); the proton at δ_{H} 7.01 and the signal of carbons at 120.6 (C-2) and 113.5 (C-9a); the proton at δ_{H} 7.12 and the signal of carbons at 109.6 (C-7) and 181.3 (C-10) and finally the latter signal of the proton at δ_{H} 7.43 and the signal at 113.5 (C-9a). These physical and



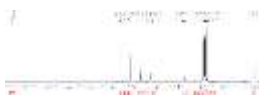
spectroscopic data were in agreement with those previously reported for 6-methyl-1,3,8-trihydroxyanthraquinone (emodin) **77** (Dar Ar et al. 2017).



Scheme 19. Selected HMBC correlations of PTB 2

Table 41. ^{13}C -NMR data of PTB 2 and Emodin **77**

C no.	PTB 2	Emodin (Dar Ar et al. 2017)
	^{13}C (125 MHz, Acetone- d_6)	^{13}C (100 MHz, CDCl_3)
	δ_{C}	δ_{C}
1	165.3	164.4
2	120.6	120.5
3	148.4	148.3
4	124.2	124.2
5	109.6	108.9
6	161.5	161.4
7	107.9	107.9
8	165.4	165.6
9	190.8	189.9
10	181.3	181.5
10a	135.7	135.2
9a	113.5	113.4
8a	108.7	108.8
4a	133.3	132.9
3- CH_3	21.1	21.8



II.2.3.2.2. Structural identification of PTB 3

PTB 3 was obtained as an amorphous reddish powder and gave also a positive result to the Borntrager test, characteristic of anthraquinones. Its HR-ESI-MS spectrum (**Figure 87**) exhibited a pseudo-molecular ion peak $[M+H]^+$ at m/z 285,1120 (calculated for 285,0685) compatible with the molecular formula $C_{16}H_{13}O_5$ and corresponding to eleven degree of insaturations.

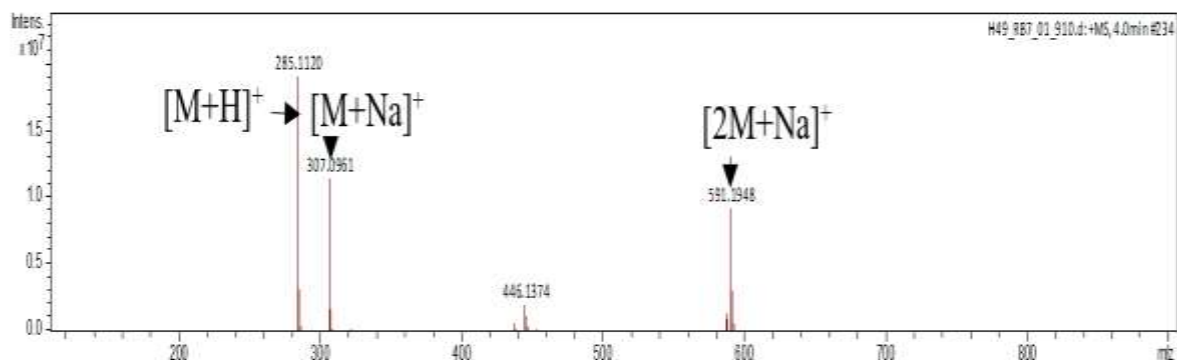
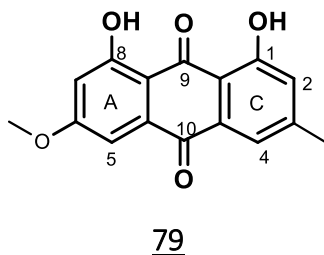


Figure 88. HR-ESI-Mass spectrum of PTB 3

The analysis of the 1H -NMR data of **PTB 3** and the published ones in the literature as well as those of **PTB 2** permit us to assign to **PTB 3** the structure of Physcion **79**.



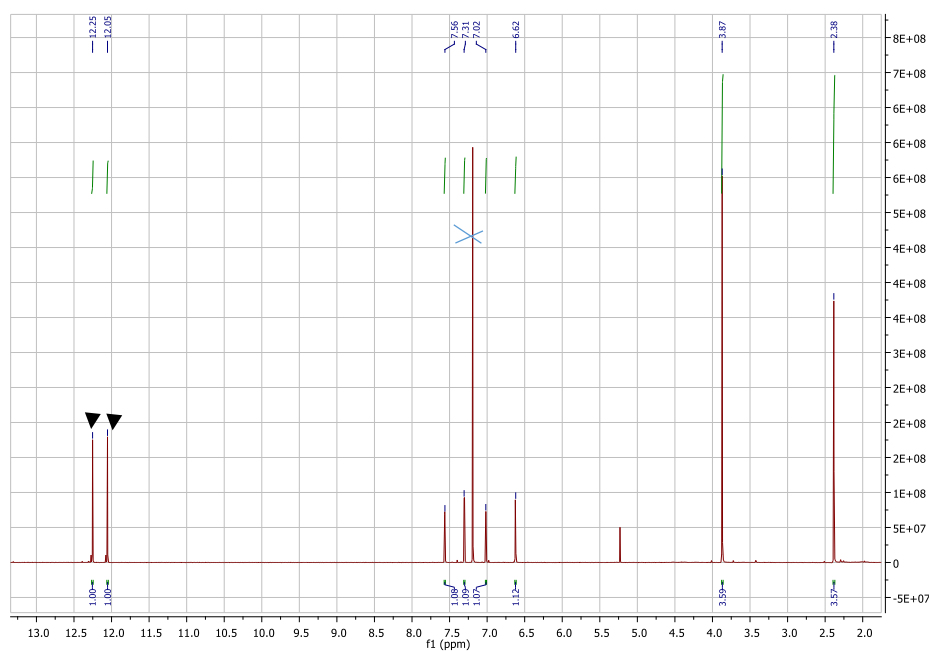
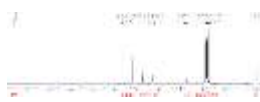
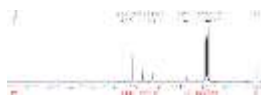


Figure 89. ^1H NMR spectrum (500 MHz, CDCl_3) of PTB 3

In fact, the ^1H -NMR spectrum (Figure 88) of PTB 3 displayed also four aromatic signal protons respectively at δ_{H} 7.56 (1H, d, 1.1 Hz), 7.30 (1H, d, 2.5 Hz), 7.02 (1H, d, 0.7 Hz) and 6.62 (1H, d, 2.5 Hz) along with the signal of a singlet of three protons at δ_{H} 2.38 (s, 3H). The only difference with PTB 2 was the presence of a methoxyl signal at δ_{H} 3.87 (s, 3H). These physical and spectroscopic data were in agreement with those previously reported for 3-methoxyl-6-methyl-1,8-dihydroxyanthraquinone trivially called physcion 79 (Moreira et al. 2018).


Table 42. ^1H -NMR data of PTB 3 and of Phycion 79 in CDCl_3

H no.	PTB 3	Phycion (Moreira et al. 2018)
	^1H (500 MHz, CDCl_3)	^1H (400 MHz, CDCl_3)
	δ_{H}	δ_{H}
1	-	-
2	6.62 (1H, d, 2.5 Hz)	6.67 (1H, d, J = 2.6 Hz)
3	-	-
4	7.30 (1H, d, 2.5 Hz)	7.35 (1H, d, J = 2.6 Hz)
5	7.56 (1H, d, 1.1 Hz)	7.62 (m, 1H)
6	-	-
7	7.02 (1H, d, 0.7Hz)	7.07 (m, 1H)
8	-	-
9	-	-
10	-	-
10a	-	-
9a	-	-
8a	-	-
4a	-	-
3- CH_3	2.38 (s, 3H)	2.45 (s, 3H)
11- CH_3O	3.87 (s, 3H)	3.93 (s, 3H)

II.2.3.2.3. Structural identification of PTB 4

PTB 4 was obtained as red powder and gave a positive result to the Borntrager test characteristic of anthraquinones. Its HR-ESI-MS spectrum (Figure 89) exhibited a pseudo-molecular ion peak $[M+H]^+$ at m/z 339.3911 (calculated for 339.3924) compatible with the molecular formula $C_{20}H_{19}O_5$ corresponding to eleven degree of insaturations.

The analysis of its NMR data were in agreement with those (1H -, ^{13}C -NMR, HMQC and HMBC) of emodin 77 and enabled us to assign structure 78 to 2-prenylemodin.

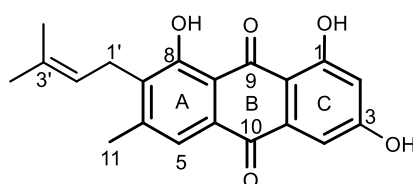
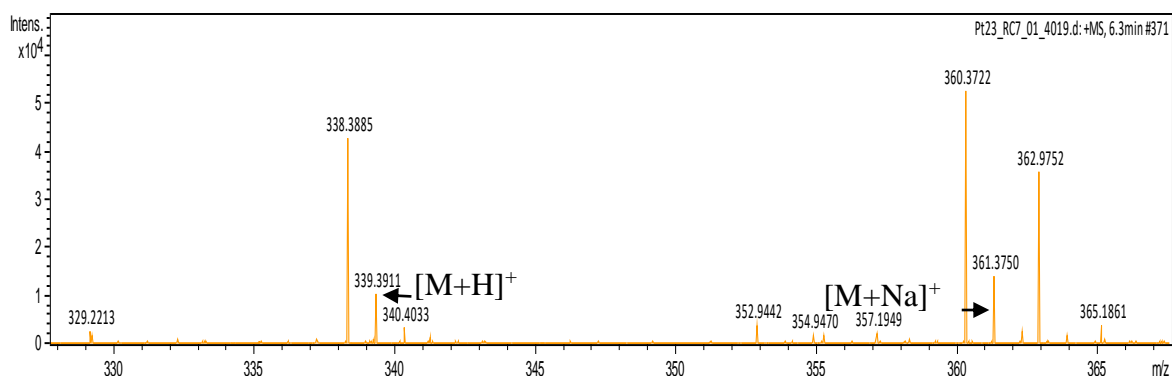
78

Figure 90. HR-ESI-MS of PTB 4

The 1H -NMR spectrum (Figure 90) below exhibited three aromatic signal protons instead of four sorted into three broad singlets of one proton each at δ_H 7.23 (1H, *brs*), 7.43 (1H, *brs*) and 7.00 (1H, *brs*). The signal of the proton at δ_H 6.53 (1H, *d*, 2.4 Hz, H-2) present in emodin 77 was absent here and substituted by proton resonance signals of prenyl moiety which appeared at [δ_H 5.16 (1H, *tt*, 7.5 Hz, olefinic proton); 3.46 (2H, *brd*, 7.5 Hz, methylene protons); 1.67 and 1.53 (3H each)].

This information was further confirmed in the HMBC spectrum where the γ,γ -dimethylallyl group is located at C-7 in A-ring. The position of the methyl group at δ_H 2.33 (3H, *s*) was equivalent to that described in the literature (Gallé, 2015). Moreover, two broad singlets were observed within the range δ_H 10–14, suggesting the presence of one chelated hydroxyl at

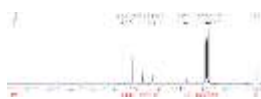
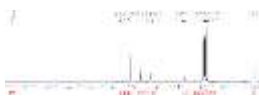


Table 43. Comparison of ^1H - (500 MHz) NMR data of PTB 4 in Acetone- d_6 and of 2-prenylemodin in DMSO- d_6 .

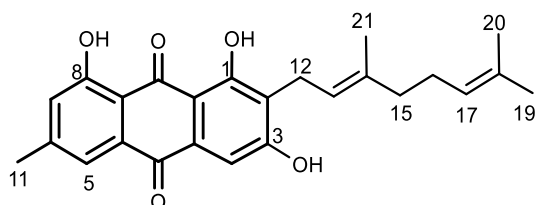
H no.	PTB 4	Botta et al. 1983
	^1H (500 MHz, Acetone- d_6)	^1H (60 MHz, DMSO- d_6)
	δ_{H} (m, J in Hz)	δ_{H} (m, J in Hz)
1	–	–
2	7.00 (1H, <i>brs</i>)	7.13 (1H, <i>brd</i> , 7)
3	–	–
4	7.43 (1H, <i>brs</i>)	7.46 (1H, <i>brd</i> , 2.0)
5	7.23 (1H, <i>brs</i>)	7.23 (1H, <i>s</i>)
6	–	–
7	–	–
8-13	–	–
14	–	–
15	2.33 (3H, <i>s</i>)	2.43 (3H, <i>s</i>)
16	3.46 (2H, <i>brs</i>)	3.34 (2H, <i>d</i> , 7)
17	5.16 (1H, <i>tt</i> , 7)	5.34 ((1H, <i>t</i> , 7)
18	–	–
19	1.67 (3H, <i>s</i>)	1.82 (3H, <i>s</i>)
20	1.53 (3H, <i>s</i>)	1.72 (3H, <i>s</i>)
OH-1	12.44 (1H, <i>s</i>)	12.40 (1H, <i>s</i>)
OH-8	11.96 (1H, <i>s</i>)	12.00 (1H, <i>s</i>)
OH-6	10.07 (1H, <i>s</i>)	-



II.2.3.2.4. Structural identification of PTB 5

PTB 5 was obtained as orange crystal and gave a positive result to the Borntrager test characteristic of anthraquinones. Its HR-ESI-MS spectrum (**Figure 92**) exhibited a pseudo-molecular ion peak $[M+H]^+$ at m/z 407.1852 (calculated for 407.1853) compatible with the molecular formula $C_{25}H_{26}O_5$ corresponding to thirteen degree of insaturations. Its UV spectrum showed absorptions at λ_{max} 225, 263 and 281 nm which closely resembled those of the previously known Emodin **77** confirming an 1,8- dihydroxyanthraquinone skeleton (**Botta et al. 1983**).

The analysis of its NMR data were in agreement with those (1H -, ^{13}C -NMR, HMQC and HMBC) of Emodin except the substitution of the singlet signal proton at δ_H 7.00/(C-2) by the geranyl moiety which enabled us to assign structure **114** to **PTB 5**.



114

This is confirmed in the HMBC spectrum which showed cross peaks between the multiplet at 3.44 (C-12) of the geranyl unit respectively with aromatic carbon signals at δ_c 162.7 (C-1), 113.6 (C-2) and 148.5 (C-3). The 1H NMR (**Figures 94**), ^{13}C NMR (**Figures 93**) spectral data and **Table 44** of geranyl- moiety observed in **114** were similar to those described by **Botta et al. (1985)**. In fact, the DEPT 135 spectrum of **PTB 5** exhibited the signal of three sets of methylene respectively at δ_c 21.7 (C-12), 39.4 (C-15) and 26.4 (C-16); it displayed also three singlets of methyls and two multiplets of olefinic proton respectively at δ_H 5.31 (C-13) and 5.08 (C-17) attributed to the same geranyl unit. On the basis of these evidences, **PTB 5** was found to be 2-geranylemodin **114** already isolated from the berries of *Psorospermum febrifugum* (**Botta et al. 1985**).

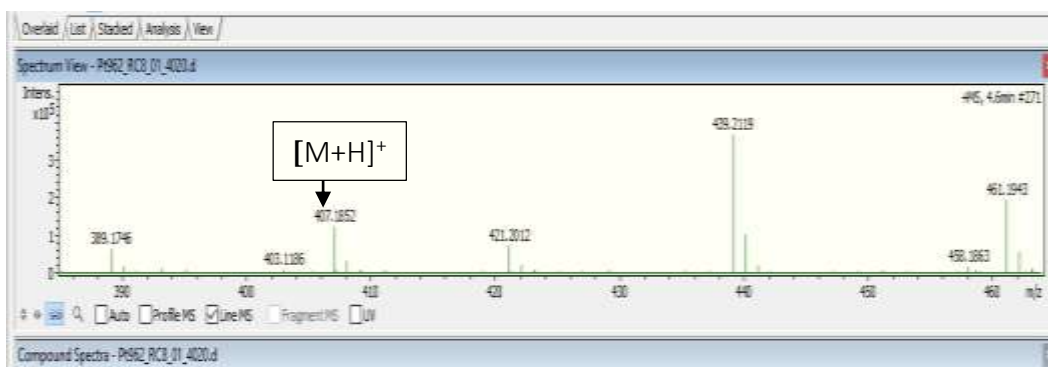
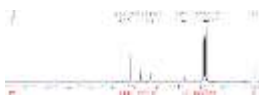


Figure 92. HR-ESI-MS of PTB 5

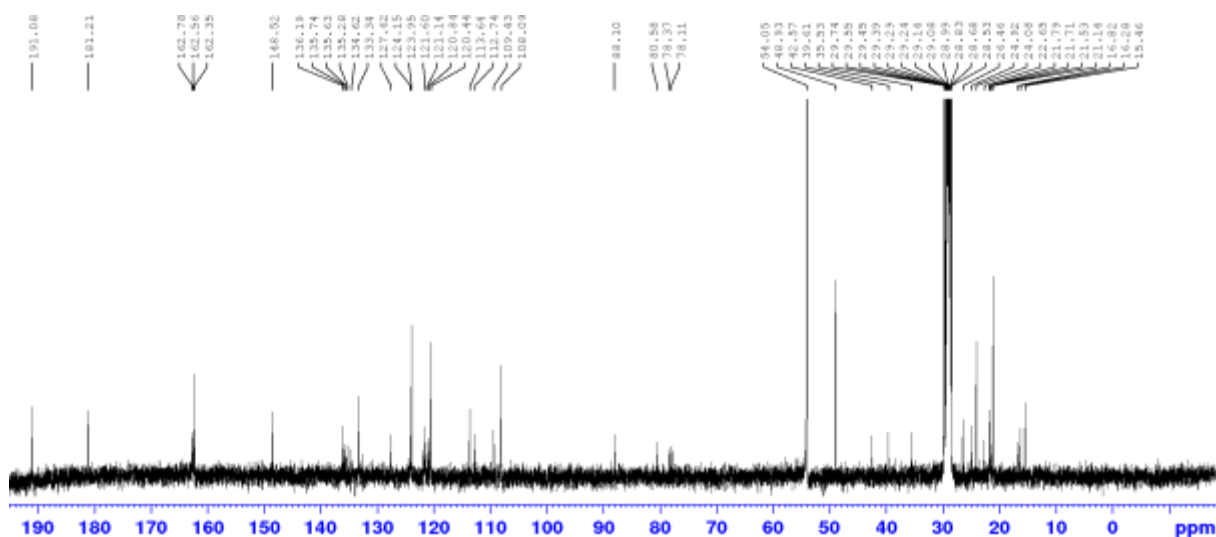


Figure 93. ¹³C- NMR spectrum of PTB 5 (125 MHz, Acetone -d₆)

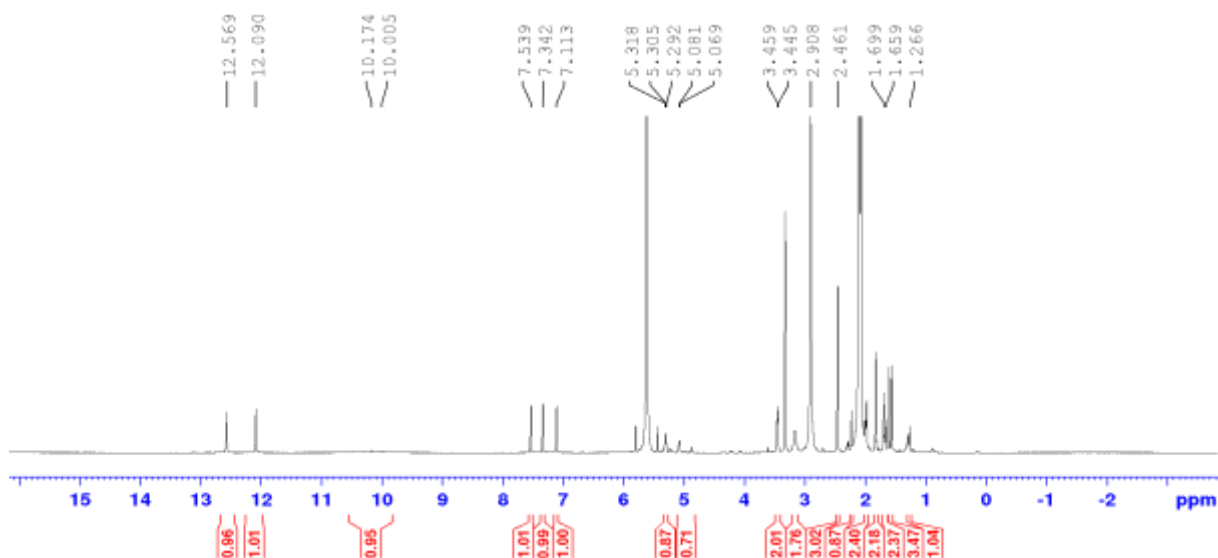


Figure 94. ¹H NMR spectrum of PTB 5 (500 MHz, Acetone -d₆)

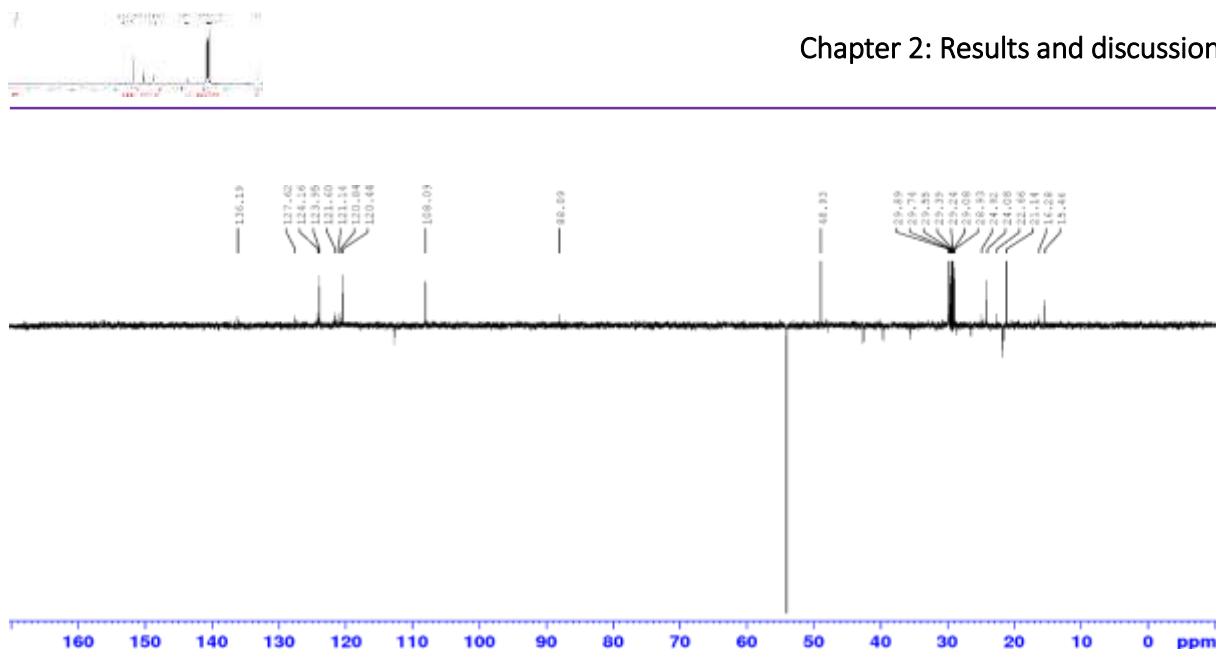
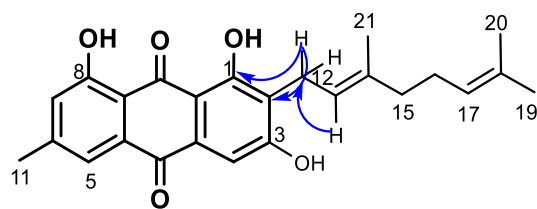
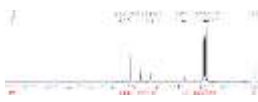


Figure 95. DEPT 135 spectrum of PTB 5

Table 44. Comparison of ^1H - (500 MHz) NMR data of PTB 5 in Acetone- d_6 and ^1H - (60 MHz) NMR data of 2-geranylemodin in DMSO- d_6 .

H no.	PTB 5		Botta et al. 1985	
	^1H (500 MHz, Acetone- d_6)		^1H (60 MHz, DMSO- d_6)	
	δ_{H} (m, J in Hz)		δ_{H} (m, J in Hz)	
1	—	—		
1a	—	—		
2	—	—		
3	—	—		
4	7.53 (1H, <i>brs</i>)	7.20 (1H, <i>s</i>)		
4a	—	—		
5	7.34 (1H, <i>brs</i>)	7.40 (1H, <i>d</i> , 2)		
5a	—	—		
6	—	—		
7	7.11 (1H, <i>brs</i>)	7.06 (1H, <i>d</i> , 2)		
8-9	—	—		
10	—	—		
11	2.45 (3H, <i>s</i>)	2.35 (3H, <i>s</i>)		
12	3.44-2.47 (2H, <i>m</i>)	3.40 (2H, <i>brd</i> , 7)		
13	5.31 (1H, <i>m</i>)	5.30 (1H, <i>m</i>)		
14	—	—		
15	2.00-1.82 (4H, <i>m</i>)	2.10-1.95 (4H, <i>m</i>)		
16	—	—		
17	5.08 (1H, <i>m</i>)	4.90 (1H, <i>s</i>)		
18	—	—		
19	1.83 (3H, <i>s</i>)	1.76 (3H, <i>s</i>)		
20	1.69 (3H, <i>s</i>)	1.57 (3H, <i>s</i>)		
21	1.58 (3H, <i>s</i>)	1.50 (3H, <i>s</i>)		
OH-1	12.44 (1H, <i>s</i>)	12.30 (1H, <i>s</i>)		
OH-8	11.96 (1H, <i>s</i>)	11.90 (1H, <i>s</i>)		
OH-3	10.17 (1H, <i>s</i>)	—		

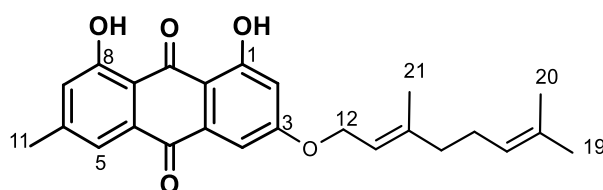


Scheme 20. Key HMBC (blue) correlations of PTB 5

II.2.3.2.5. Structural identification of PTB 6

PTB 6 was obtained as orange powder and gave a positive result to the Borntrager test characteristic of anthraquinones and ferric chloride test, indicating its phenolic nature. The UV spectrum showed absorptions at λ_{\max} 225, 263 and 281 nm which closely resembled those of the previously known Emodin **77** indicating an 1,8- dihydroxyanthraquinone skeleton (Botta et al. 1983).

The analysis of its NMR data (^1H -, ^{13}C -NMR, HMQC and HMBC) were in agreement with those of Emodin. The only difference was the substitution of the hydroxyl group at δ_{H} 10, 17 (3-OH) by a geranyloxy moiety. So PTB 6 was found to be structure **55** below.



55

In fact, the ^1H - NMR spectrum of **PTB 6** (500 MHz, CDCl_3) (Figure 97) exhibited one set of signals [δ_{H} 4.60 (1H, *brd*, 6.4 Hz, H-12)/ δ_{C} 67.4; δ_{H} 5.01 (1H, *m*, H-17)/ δ_{C} 122.8; δ_{H} 5.42 (1H, *t*, 6.55 Hz, H-13)/ δ_{C} 118.4; δ_{H} 2.05-2.08 (4H, *m*, H-15, H-16); δ_{H} 1.51 (3H, *s*, H-19), and δ_{H} 1.61 (3H, *s*, H-20)] corresponding to one geranyloxy moiety. This unit was supported by analysis of the HMBC spectrum of **PTB 6** which showed three sets of cross peaks at δ_{H} 4.60 (H-12)/C-13 (118.4) and C-14 (143.4); at δ_{H} 5.42 (H-13)/C-21(17.9) and C-15 (39.6); and at δ_{H} 1.51 (H-19) and 1.61 (H-20)/ C-17 (122.8) and C-18 (131.8). These information were further confirmed by The ^{13}C NMR (Figure 96) and DEPT 135 spectra (Figure 98) of **PTB 6** which exhibited the signals of two methylene carbons at δ_{C} 26.8 (C-16), 39.6 (C-15) and the oxymethylene signal at δ_{C} 65.7 (C-12). The HMBC spectrum also showed a cross peak between the latter oxymethylene signal at δ_{H} 4.62 (H-12) with the aromatic carbon at δ_{C} 165.7 (C-3) which confirmed clearly its

attachment to that position of the 1,8-dihydroxyanthraquinone moiety. On the basis of the above results, **PTB 6** was identified as 3-geranyloxyemodin and isolated from *Psorospermum febrifugum* by (Botta et al. 1983).

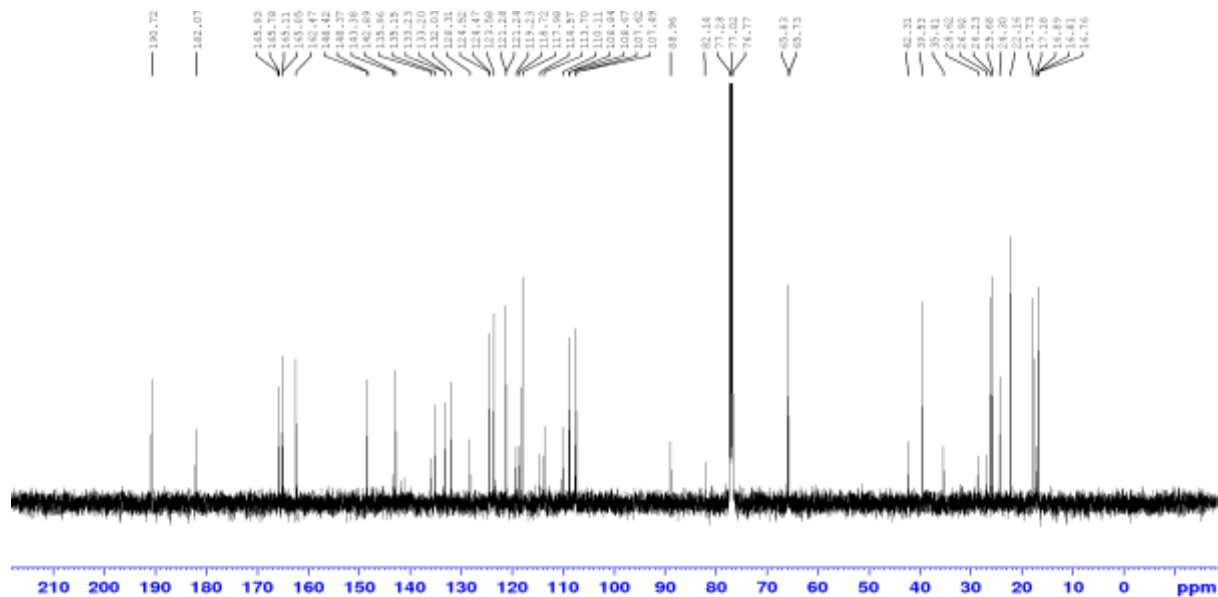


Figure 96. ^{13}C - NMR spectrum (125 MHz, CDCl_3) of PTB 6

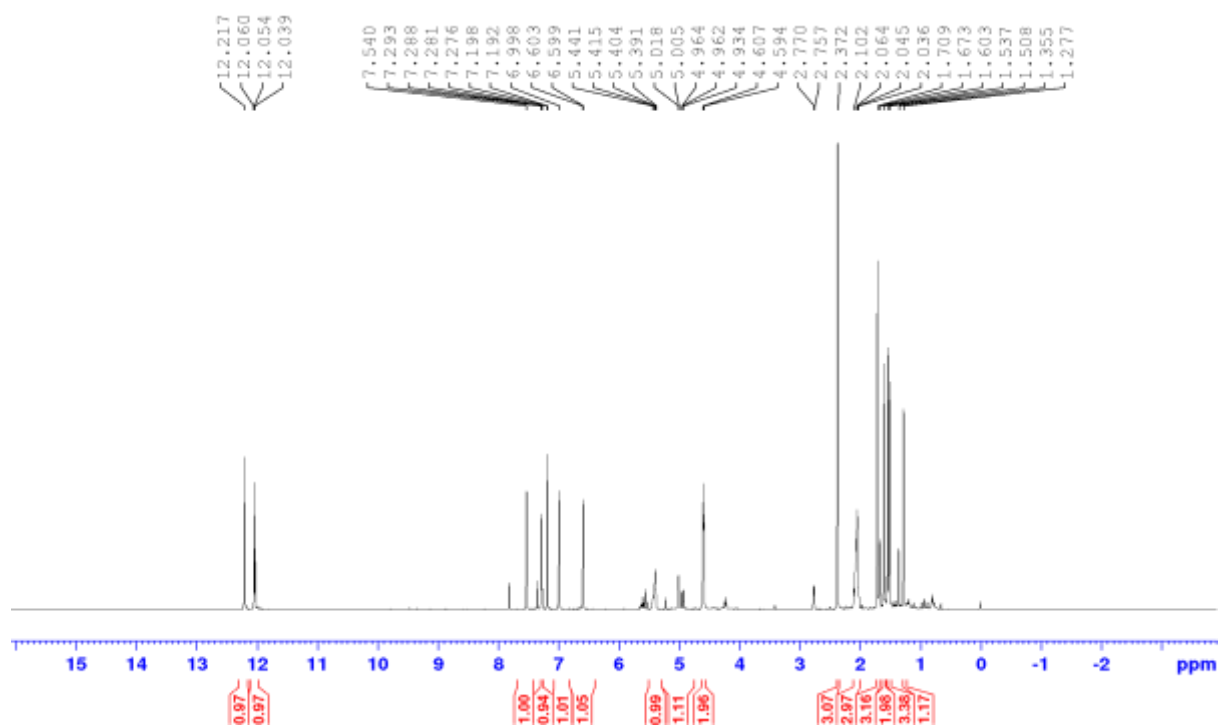


Figure 97. ^1H - NMR spectrum (500 MHz, CDCl_3) of PTB 6

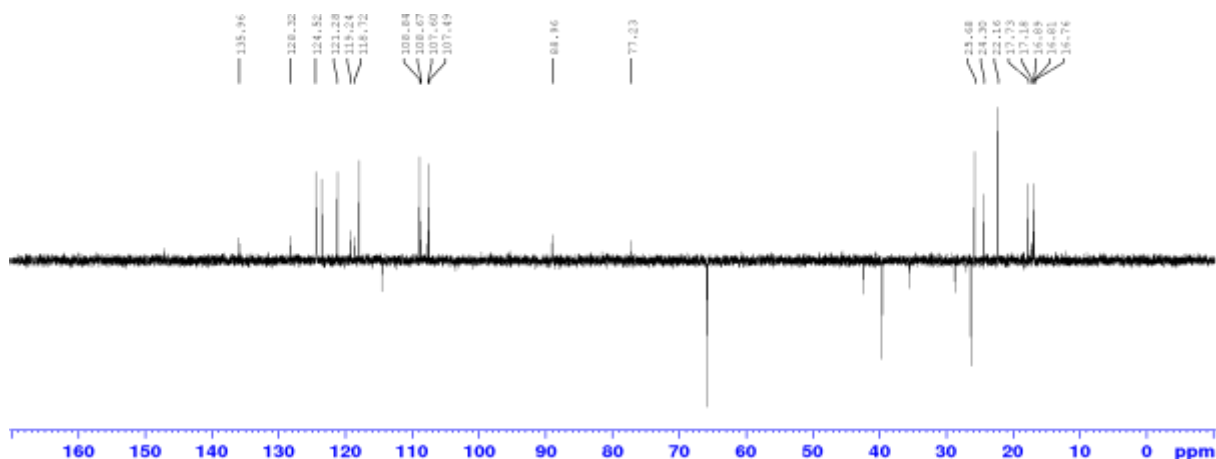
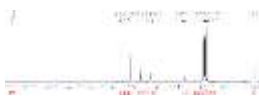
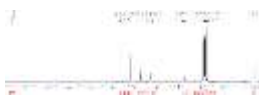


Figure 98. DEPT 135 spectrum of PTB 6

Table 45. Comparison of ^1H - (500 MHz) NMR data of PTB 6 and ^1H - (60 MHz) NMR data of 3-geranyloxyemodin in CDCl_3 .

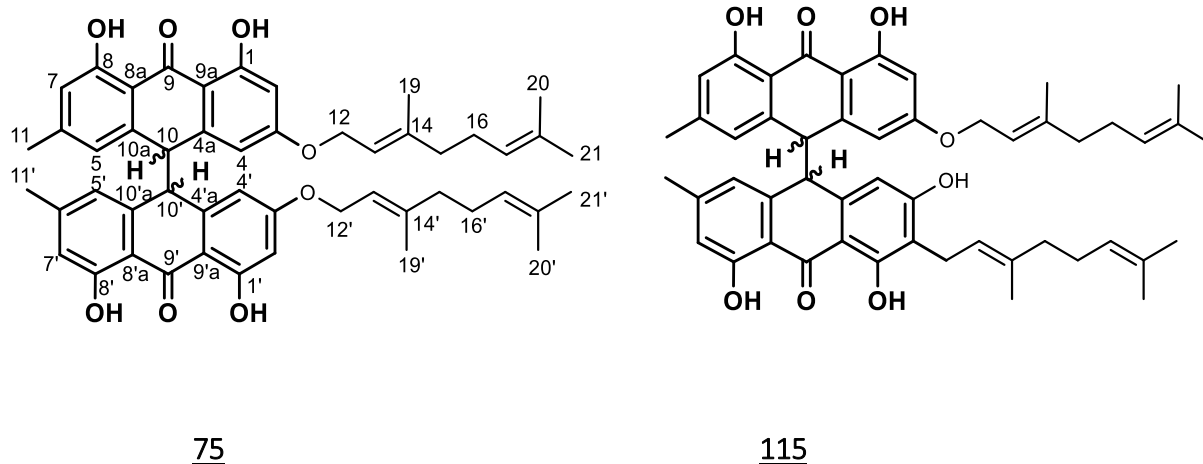
H no.	PTB 6	Botta et al. 1983
	^1H (500 MHz, CDCl_3)	^1H (60 MHz, CDCl_3)
	δ_{H} (m, J in Hz)	δ_{H} (m, J in Hz)
1-1a	—	—
2	6.60 (1H, <i>brs</i>)	6.60 (1H, <i>d</i> , 2.5)
3	—	—
4	7.29 (1H, <i>brs</i>)	7.27 (1H, <i>d</i> , 2.5)
4a	—	—
5	7.54 (1H, <i>brs</i>)	7.50 (1H, <i>brd</i> , 1.8)
5a-6	—	—
7	6.99 (1H, <i>brs</i>)	7.00 (1H, <i>brd</i> , 1.8)
8-8a	—	—
9-10	—	—
11	2.39 (3H, <i>s</i>)	2.40 (3H, <i>s</i>)
12	4.60 (2H, <i>brd</i> , 6.4)	4.60 (2H, <i>d</i> , 7)
13	5.40 (1H, <i>brd</i> , 6.5)	5.43 (1H, <i>t</i> , 7)
14	—	—
15	2.05-2.08 (4H, <i>m</i>)	2.10 (4H, <i>m</i>)
16	—	—
17	5.01 (1H, <i>m</i>)	5.05 (1H, <i>m</i>)
18	—	—
19	1.51 (3H, <i>s</i>)	1.77 (3H, <i>s</i>)
20	1.61 (3H, <i>s</i>)	1.67 (3H, <i>s</i>)
21	1.74 (3H, <i>s</i>)	1.60 (3H, <i>s</i>)
OH-1	12.21 (1H, <i>s</i>)	12.23 (1H, <i>s</i>)
OH-8	12.06 (1H, <i>s</i>)	12.08 (1H, <i>s</i>)



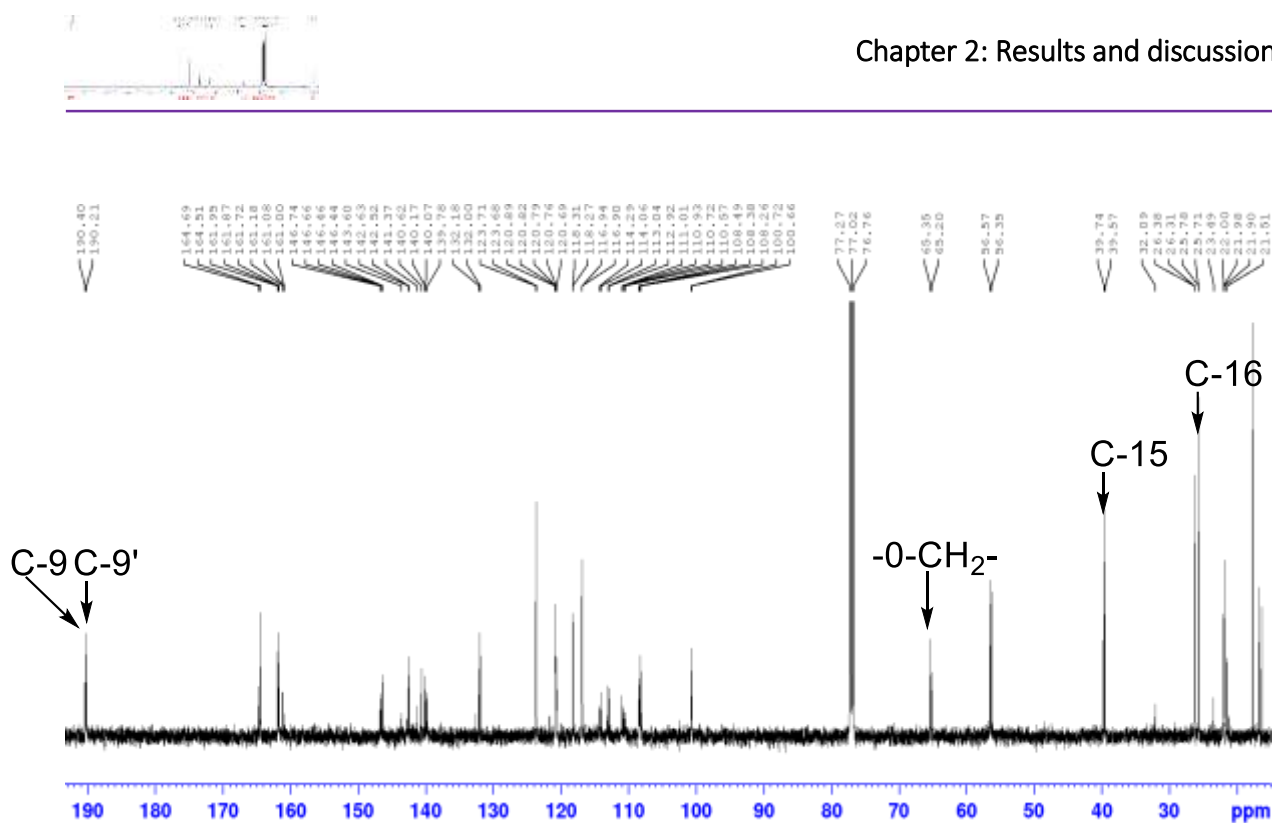
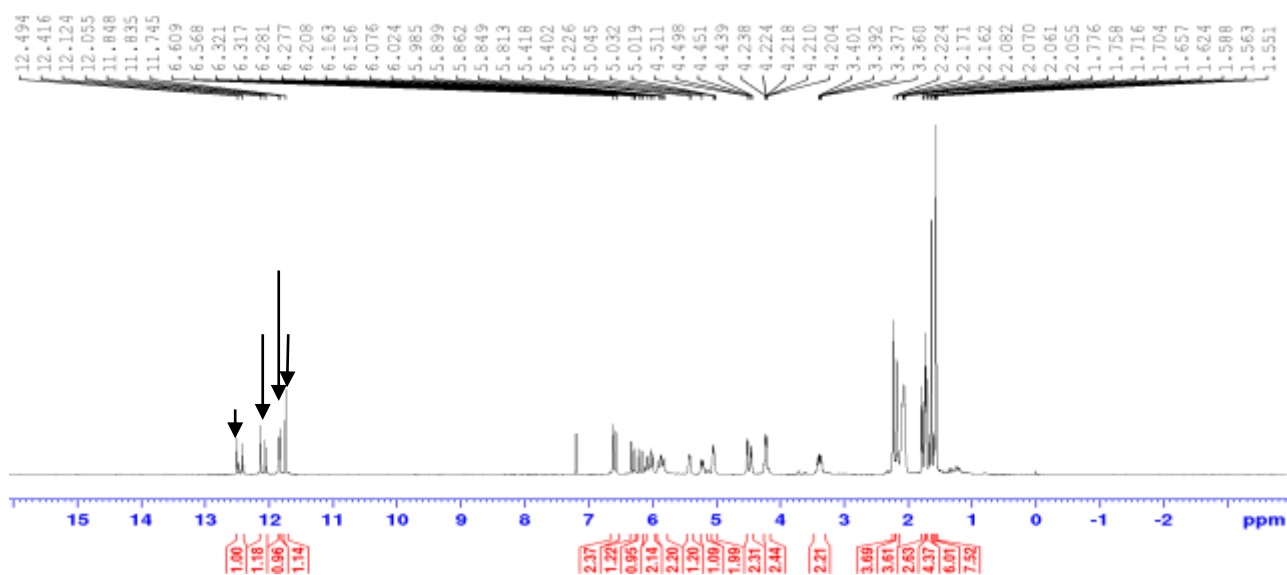
II.2.3.3. Bianthrone

II.2.3.3.1. Structural identification of PTB 7

PTB 7 was obtained as yellow powder and reacted positively to the FeCl_3 reagent suggesting its phenolic nature. Also, its positive reaction to magnesium acetate indicated a 1,8-dihydroxyanthraquinone chromophore (Botta et al. 1985). Its HR-ESI-MS spectrum exhibited a protonated molecule $[\text{M}+\text{H}]^+$ at m/z 783.3812 (calcd. for 783.3819) compatible with the molecular formulae $\text{C}_{50}\text{H}_{54}\text{O}_8$ and corresponding to twenty-three degree of insaturations. The IR spectrum exhibited strong absorption bands due to carbonyl groups at 1716 and 1619 cm^{-1} , and chelated hydroxyl groups at 3397 cm^{-1} . The UV spectrum showed absorption bands at λ_{max} 278, 363 and 370 nm, which were very close to those of bianthrone A₁ 75 (Tsaffack et al. 2009) and bianthrone A_{3a/3b} 115 derivatives (Botta et al. 1985).



In fact, the major differences between the two compounds above appeared in the ^1H -NMR spectrum (500 MHz, CDCl_3) (Figure 100) of PTB 7 which, showed one set of signals [δ_{H} 4.51 (1H, m, H-12); δ_{H} 5.04 (1H, m, H-17); δ_{H} 5.43 (1H, t, 6.55 Hz, H-13); δ_{H} 2.06-2.16 (4H, m, H-15, H-16); δ_{H} 1.73 (3H, s, H-19), δ_{H} 1.62 (3H, s, H-20) and at δ_{H} 1.56 (3H, s, H-21)], corresponding to one O-geranyloxy group, instead of two as in bianthrone A₁. This information was further confirmed in the DEPT 135 spectrum (Figure 101) which exhibited the signal of only the oxymethylene at δ_{C} 65.3 (C-12) and two others signals of two methylene respectively at 39.5 (C-15) and 26.3 (C-16).

Figure 99. ^{13}C NMR spectrum (125 MHz, CDCl_3) of PTB 7Figure 100. ^1H - NMR spectrum (500 MHz, CDCl_3) of PTB 7

Also in the ^1H -NMR spectrum (Figure 100), the presence of one additional geranyl moiety signals is observed in substitution of the proton normally around δ_{H} 6.35 (H-2') of Bianthrone derivative (Tsaffack et al. 2009). The ^{13}C NMR (Figure 99) displayed resonances that supported the presence of these units in PTB 7 along with the presence of two quaternary carbons at δ_{C} 190.4 (C-9) and 190.2 (C-9') (carbonyl groups). In addition, this spectrum showed

the signals of other quaternary sp^2 carbon; methyl carbons; two aliphatic methines of the anthronyl nucleus such as those at δ_c 56.5 (C-10) and 56.3 (C-10'). This latter information prompted us to assign to **PTB 7** the structure Bianthrone A_{3a} which was isolated from *Psorospermum febrifugum* by Botta et al. (1987).

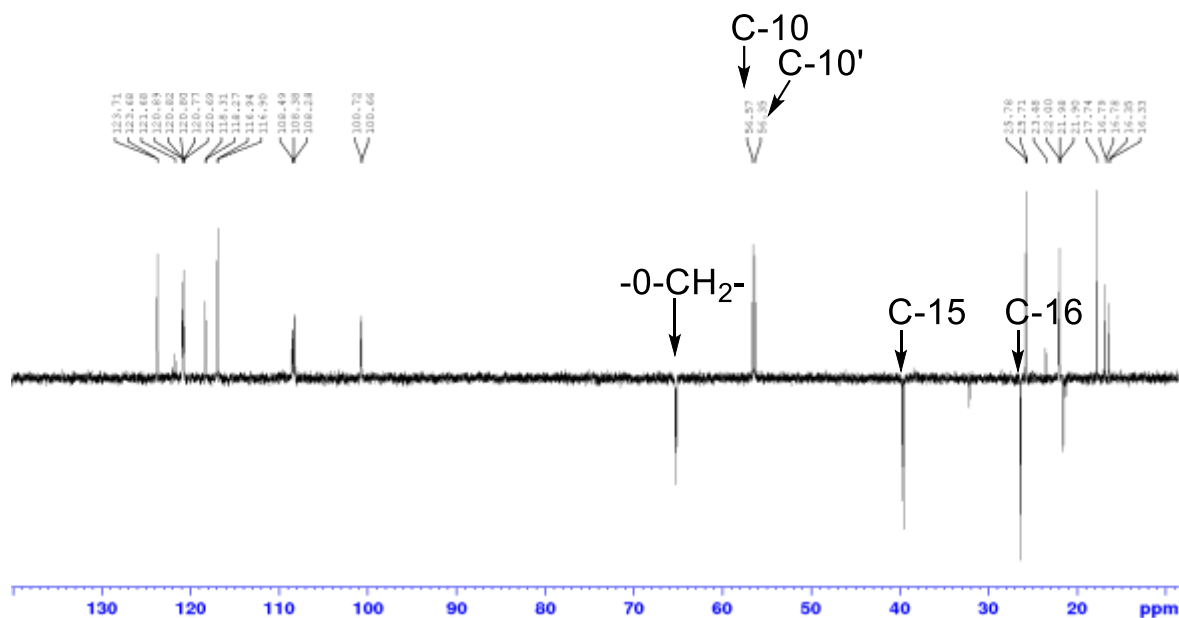
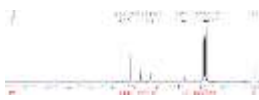


Figure 101. DEPT 135 spectrum of PTB 7


Table 46. Comparison of ^1H - (500 MHz) NMR data of PTB 7 and ^1H - (400 MHz) NMR data bianthrone A3a/3b in CDCl_3

H no.	PTB 7	(Botta et al. 1985)
	^1H (500 MHz, CDCl_3)	^{13}C (400 MHz, CDCl_3)
	δ_{H} (m, J in Hz)	δ_{H} (m, J in Hz)
1-OH; 1'-OH	12.49, 12.12 (1H, s)	12.40, 12.03 (1H, s)
2; 2'	6.03 (1H, m)	6.03 (1H, m)
4; 4'	6.35 (1H, m)	6.30 (1H, m)
4a; 4'a	-	-
5; 5'	6.58 (1H, m)	6.52 (1H, m)
6; 6'	-	-
7; 7'	5.84 (1H, m)	5.80 (1H, m)
8-OH; 8'-OH	11.84 (2H, s)	11.66 (2H, s)
8a ; 8'a; 9; 9'	-	-
9a; 9'a	-	-
10; 10'	4.21 (1H, s)	4.13 (1H, m)
10a; 10'a	-	-
11; 11'	2.22 (3H, s)	2.25 (3H, s)
12; 12'	4.51, 3.41 (2H, m)	4.50 , 3.35 (2H, brd, 7 Hz)
13; 13'	5.43, 5.22 (2H, m)	5.40, 4.90 (2H, m)
14; 14'	-	-
15; 15'	2.06 (4H, m)	2.15-2.00 (8H, m)
16; 16'	2.16 (4H, m)	
17; 17'	5.04, 5.01 (2H, m)	4.90 (2H, m)
18; 18'	-	-
19; 19'	1.73 (6H, s)	
20; 20'	1.62 (6H, s)	1.85-1.55 (18H, s)
21; 21'	1.56 (6H, s)	

II.2.3.4. Flavonoid

II.2.3.4. 1. Structural identification of PTB 8

PTB 8 obtained as a white powder, was soluble in methanol. It reacted positively with the Shinoda test (Mg/HCl) to yield a reddish colour indicating the presence of flavonoid along with phenol test (1% FeCl₃), indicating its phenolic nature. Its HR-ESI-MS spectrum (Figure 102) exhibited a pseudo-molecular ion peak [M+H]⁺ at *m/z* 291.0968 (calcd. for C₁₅H₁₄O₆; 291.0969) compatible with the molecular formula C₁₅H₁₄O₆ implying nine degrees of unsaturation. The LC-ESI-MS of PTB 8 coupled with its UV absorption band (λ_{max} 278 nm) suggested a flavan skeleton (Hye et al. 2009; Hummer et Schreier, 2008).

In addition the ¹H NMR (500 MHz, acetone-*d*₆) spectrum (Figure 103) of compound PTB 8 were identical to those of authentic (+)-catechin (Davis et al. 1996). In fact, the characteristic signals of H-2, H-3 and H-4 of a (+)-catechin residue (δ_{H} 4.89, *brs*, H-2; δ_{H} 4.22, *brs*, H-3; δ_{H} 2.77, *ddd*, H-4_{ax}, *J* = 3.1, 15.4 Hz and δ_{H} 2.90, *dd*, H-4_{eq} *J* = 4.4, 16.6 Hz, ring C) were detected in the ¹H-NMR experiment and confirmed by Hye et al. (2009). Moreover, this ¹H-NMR spectrum (Figure 103) of PTB 8 also revealed on the one hand a AX system, a *meta*-coupled protons [H-6 (δ_{H} 5.93) and H-8 (δ_{H} 6.03) (*J* = 2.2 Hz)] for ring A, and on the other hand a ABX system of three protons [H-2' (δ_{H} 7.07, 1H, 1.8 Hz); H-5' (δ_{H} 6.84, 1H, 8.1 Hz); H-6' (δ_{H} 6.86 (1H, 1.8, 8.1 Hz)] in ring B. The COSY (Figure 104) spectrum exhibited the correlation between the signals of H-2 and H-3. The relative stereochemistry of these two signals was not determined. But, the signals of protons H-2 and H-3 in 2,3-*trans* configuration were also observed following (Davis et al. 1996). The comparison of these data with the published ones in the literature led to the identification of PTB 8 as (+)-catechin 64 (Hye et al. 2009).

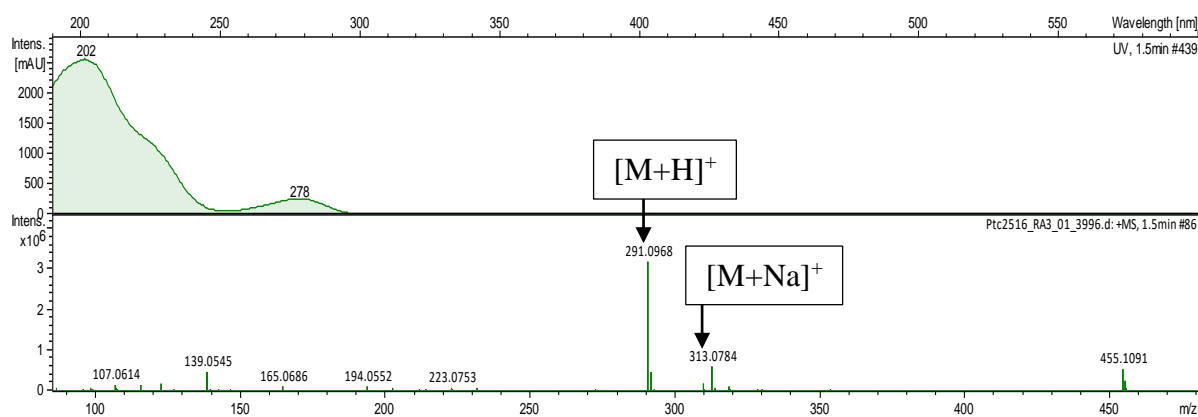
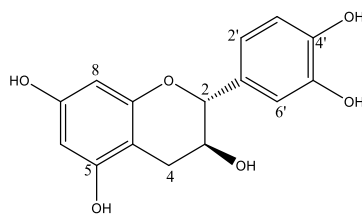
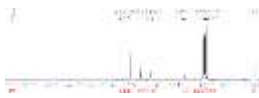


Figure 102. HR-ESI-MS spectrum of PTB 8



64

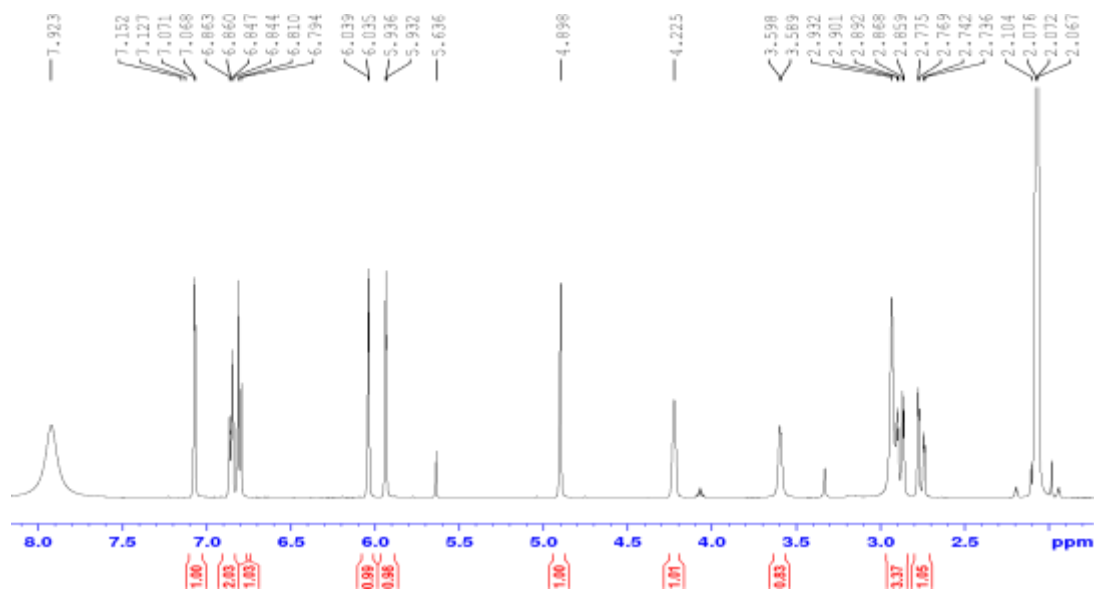


Figure 103. ¹H NMR spectrum of PTB 8

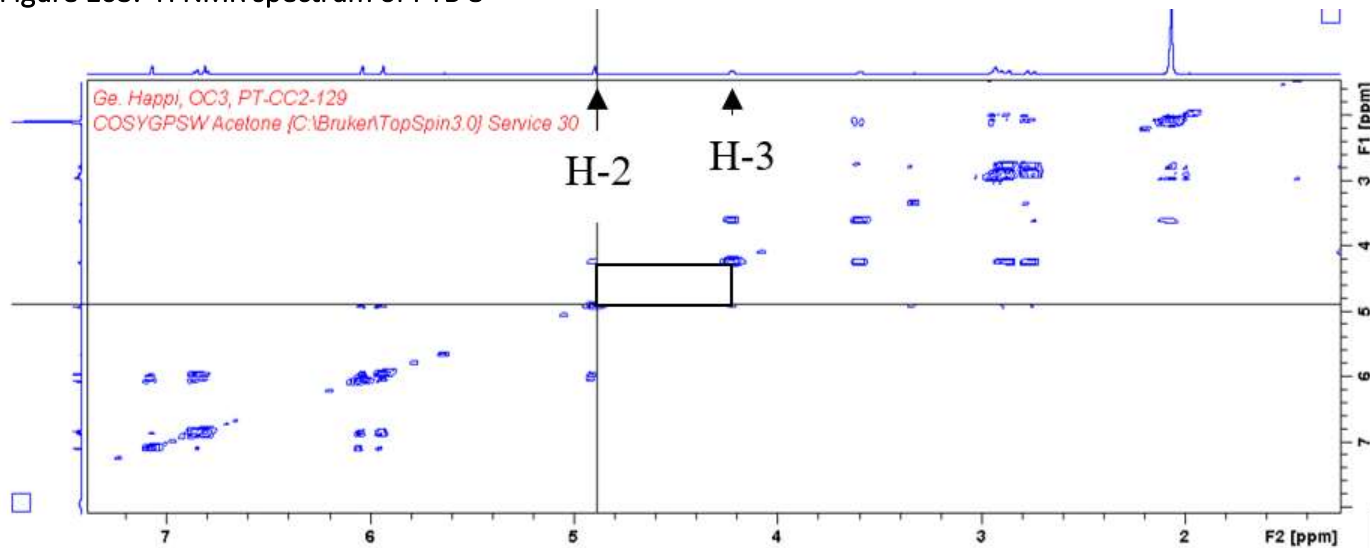
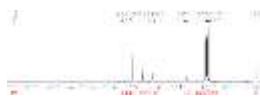


Figure 104. COSY spectrum of PTB 8


Table 47. Comparative ^1H (500 MHz, acetone- d_6) NMR data of PTB 8 with those of (+)-catechin 64

H no.	PTB 8	(+)-catechin
	δ_{H} (500 MHz, acetone- d_6)	δ_{H} (400 MHz, acetone- d_6) (Hye et al. 2009)
	δ_{H} (m, J in Hz)	δ_{H} (m, J in Hz)
2	4.89 (1H, <i>brs</i>)	4.56 (1H, <i>d</i> , 7.8 Hz)
3	4.22 (1H, <i>brs</i>)	4.00 (1H, <i>ddd</i> , 5.5, 7.8, 8.5 Hz)
4ax	2.77 (1H, <i>dd</i> , 15.4, 3.1 Hz)	2.54 (1H, <i>dd</i> , 16.1, 8.5 Hz)
4eq	2.90 (1H, <i>dd</i> , 16.6, 4.4 Hz)	2.90 (1H, <i>dd</i> , 16.1, 5.5 Hz)
4a	-	-
5	-	-
6	5.93 (1H, <i>d</i> , 2.2 Hz)	5.87 (1H, <i>d</i> , 2.3 Hz)
7	-	-
8	6.03 (1H, <i>d</i> , 2.2 Hz)	6.01 (1H, <i>d</i> , 2.3 Hz)
8a	-	-
1'	-	-
2'	7.07 (1H, <i>d</i> , 1.8 Hz)	6.89 (1H, <i>d</i> , 1.9 Hz)
3'	-	-
4'	-	-
5'	6.84 (1H, <i>d</i> , 8.1 Hz)	6.79 (1H, <i>d</i> , 8.1 Hz)
6'	6.86 (1H, <i>dd</i> , 1.8, 8.1 Hz)	6.73 (1H, <i>dd</i> , 1.9, 8.2 Hz)

II.2.3.5. Triterpenoids

II.2.3.5.1. Structural identification of PTB 9

PTB 9 was obtained from the barks of *P. tenuifolium* as a colourless amorphous powder. It was soluble in chloroform and reacted positively to the Liebermann-Burchard test, typical for triterpenoids (violet colour). The analysis of the NMR data (^1H -, ^{13}C -NMR, DEPT 135) of PTB 9 and those reported in the literature permit us to assign structure numbered 60 as betulinic acid (Siddiqui et al. 1988; Mahato et al. 1994).

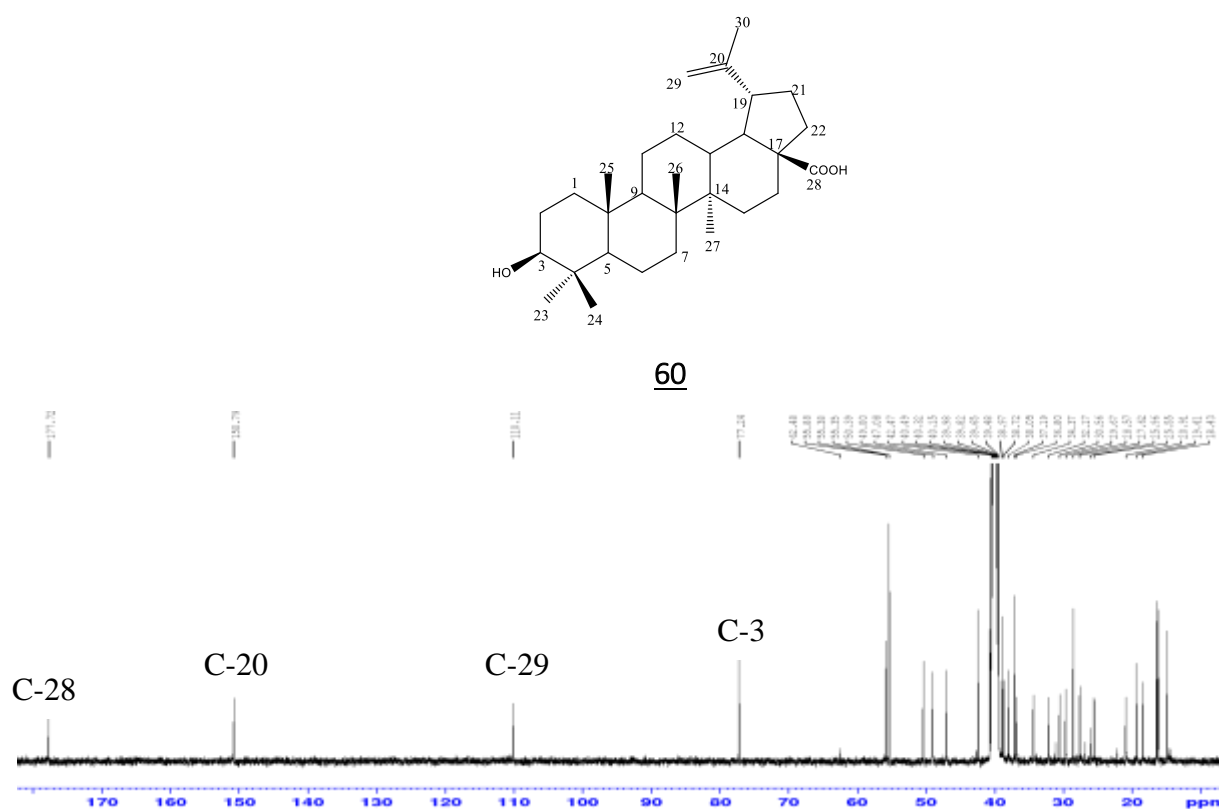


Figure 105. ^{13}C NMR spectrum of PTB 9

In fact, the broad band decoupled ^{13}C - NMR (500 MHz, $\text{DMSO}-d_6$) spectrum (Figure 105) of PTB 9 exhibited thirty carbons signal among which an exocyclic double bond at δ_{C} 150.7 ppm and 110.1 ppm which was assigned respectively to C-20 and C-29 and suggesting that compound PTB 9 was a triterpenic acid having five rings of a lupane-type skeleton (Table 48) (Siddiqui et al. 1988; Mahato et al. 1994).

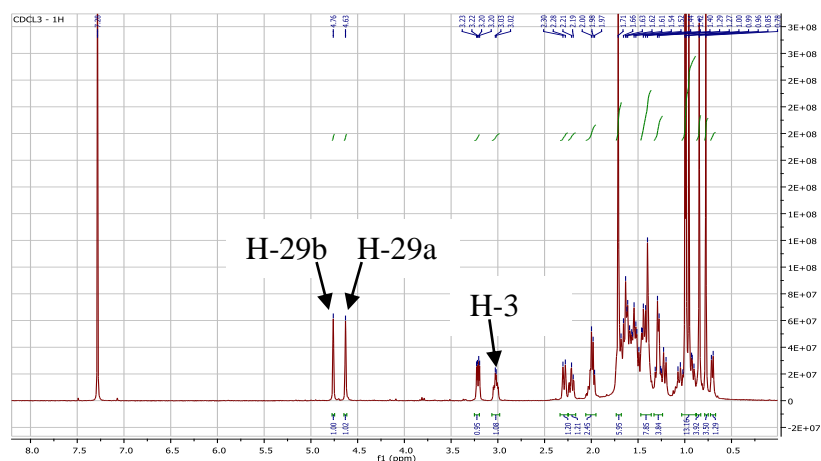
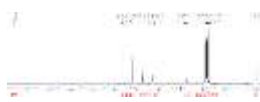


Figure 106. ^1H -NMR spectrum of PTB 9

In confirmation of this latter exocyclic double bond signal, the ^1H -NMR spectrum (Figure 106) of PTB 9 showed two H-atom signals corresponding to the signals of an exocyclic moiety at δ_{H} 4.63 (H-29a) and 4.76 (H-29b). Furthermore, this spectrum exhibited five tertiary methyl signals at δ_{H} 0.78 (H-23), 0.85 (H-24), 0.93 (H-25), 0.96 (H-26) and 0.99 (H-27), and a deshielded one at 1.64 (H-30) confirming that PTB 9 was a lupane type triterpenoid compound. This latter information allowed us to identify PTB 9 with the reported values (Table 48) as betulinic acid 60 (Siddiqui et al. 1988).

Also in ^{13}C -NMR (500 MHz, $\text{DMSO}-d_6$) spectrum (Figure 105) were exhibited other carbon resonances assigned through DEPT 135 spectrum (Figure 107) into ten methylenes, six methines, five quaternary carbons, one carboxylic acid and six methyls.

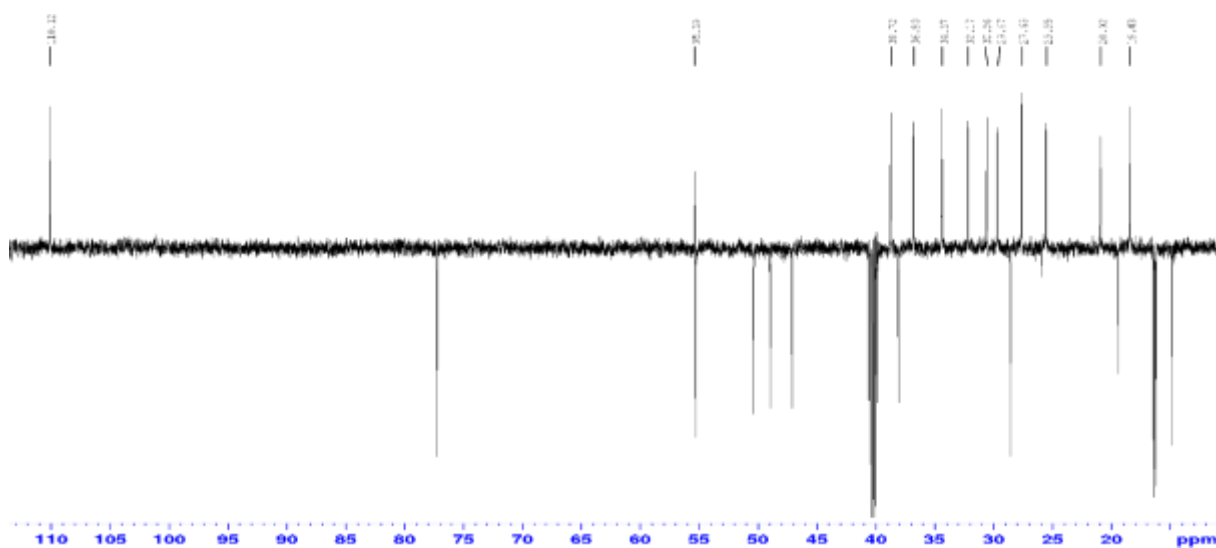
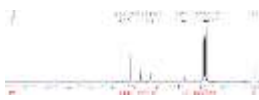
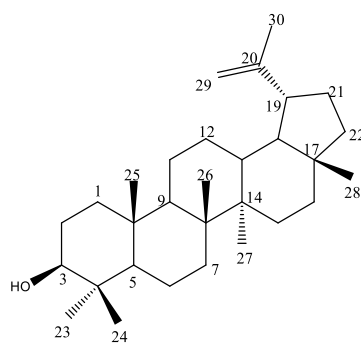


Figure 107. DEPT 135 NMR spectrum of PTB 9



II.2.3.5.2. Structural identification of PTB 10

PTB 10 was obtained from the bark of *P. tenuifolium* as a colourless crystal. It was soluble in chloroform; mp 218-220 °C and reacted positively to the Liebermann-Burchard test with a red colouration that turned to violet, typical for triterpenoids. The broad band decoupled ¹³C-NMR spectrum of **PTB 10** was similar with ¹³C- NMR data (**Figure 105; Table 48**) of the previous **PTB 9** except for the disappearance in the downfield region of the carboxylic acid group of **PTB 9** at (C-28) substituted in the same position by one methyl at δ_C 18.6. This was confirmed in the ¹H- NMR spectrum (**Figure 108**) of **PTB 10** which showed in upper field area the presence of the signal of a broad singlet of three protons at δ_H 1.94 (H-28). These data were in agreement with those reported for Lupeol (**Table 48**) (**Mahato et al. 1994**). The analysis of its NMR data (¹H-NMR, DEPT 135) enabled us to assign the structure **PTB 10** to lupeol **116**.



116

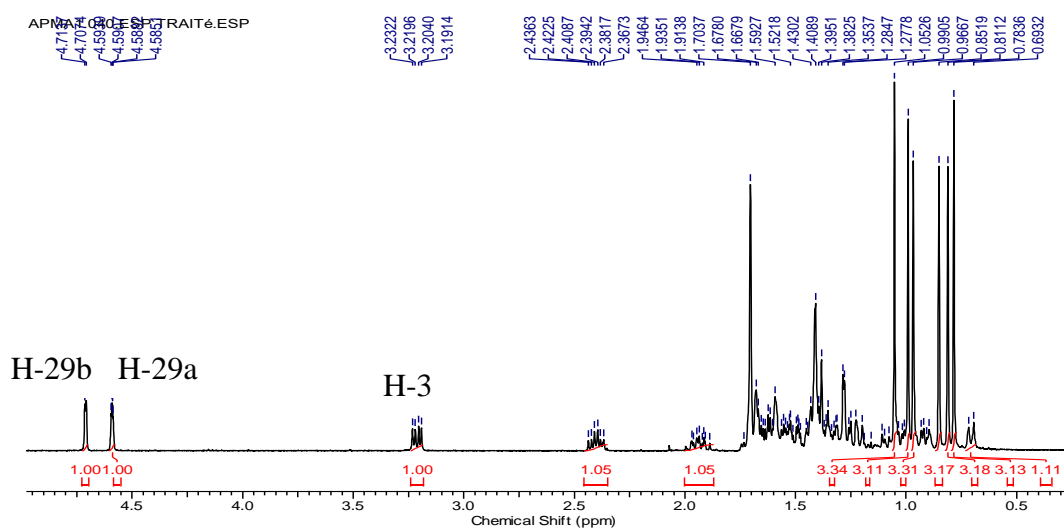


Figure 108. ¹H-NMR spectrum of PTB 10

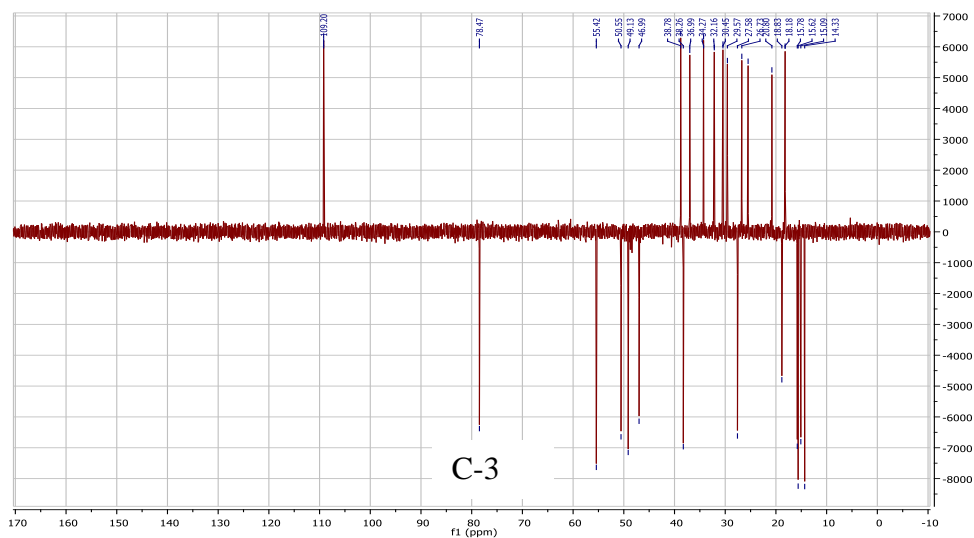
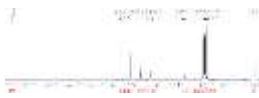
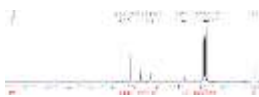
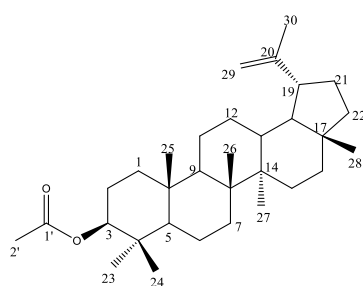
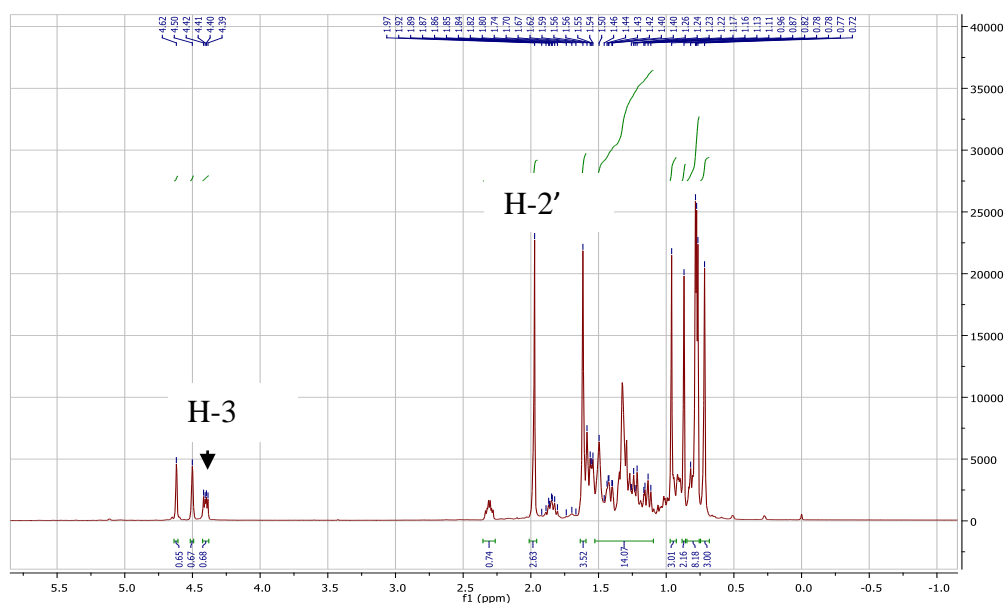


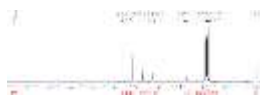
Figure 109. DEPT 135 spectrum of PTB 10



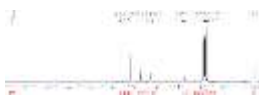
II.2.3.5.3. Structural identification of PTB 11

PTB 11 was obtained as a white powder. The NMR data of PTB 11 were almost similar to those of compound PTB 10 (Figure 108; Table 48) except the two additional carbon signals at δ_C 171.3 and 28.2. In addition, the ^1H -NMR spectrum (Figure 110) exhibited a deshielded methyl signal at δ_C 2.05 (3H, s, H'-2) in α -position of the latter carbonyl group and a much more deshielded methine proton signal at δ_H 4.42 (H-3) compare to the same signal of compounds PTB 9 and PTB 10. These NMR data of PTB 11 were thus in agreement with those of lupeol acetate 117 previously reported from the n-Hexane extract of *Tapinanthus globiferus* (Table 48) (Jamal et al. 2008).

117Figure 110. ^1H -NMR spectrum of PTB 11


Table 48. Comparative ^{13}C -NMR data of PTB 9 (DMSO- d_6) with Betulinic acid (BA); PTB 10 (CDCl_3) with Lupeol and PTB 11 (CDCl_3) with Lupeol acetate (LA)

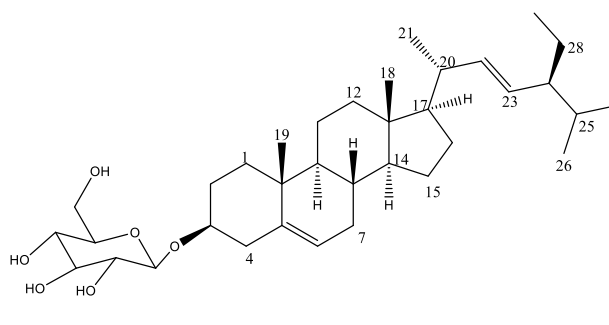
C and H no.	PTB 9	BA	PTB 10	Lupeol	PTB 11 (CDCl_3 , 500 MHz)	LA (CDCl_3 , 400 MHz)
	δ_{C}	$^a\delta_{\text{C}}$	δ_{C}	$^b\delta_{\text{C}}$	δ_{H}	δ_{H}
1	38.9	39.1	38.7	38.7	-	-
2	27.3	28.1	26.7	26.4	-	-
3	77.2	78.1	78.4	78.9	4.42 (1H, <i>d</i> , 5 Hz)	4.47 (1H, <i>dd</i> , 4.4, 12.8 Hz)
4	38.7	39.4	38.8	38.8	-	-
5	55.3	55.7	55.4	55.3	-	-
6	18.2	18.6	18.1	18.3	-	-
7	34.4	34.7	34.2	34.2	-	-
8	40.5	40.9	40.2	40.8	-	-
9	50.4	50.8	50.5	50.4	-	-
10	37.2	37.3	36.9	37.1	-	-
11	20.8	21.1	20.8	20.9	-	-
12	25.4	25.9	25.4	25.1	-	-
13	38.3	38.4	38.2	38.0	-	-
14	42.4	42.4	42.3	42.8	-	-
15	30.5	31.1	30.4	27.4	-	-
16	32.1	32.7	32.1	35.5	-	-
17	55.8	56.3	55.4	43.0	-	-
18	46.8	47.6	46.9	48.2	-	-
19	49.2	49.5	49.1	47.9	-	-
20	150.7	150.7	150.6	150.9	-	-
21	29.7	30.1	29.5	29.8	-	-
22	37.2	37.5	36.9	40.0	-	-
23	27.6	28.5	27.5	28.0	0.87 (3H, <i>s</i>)	0.85 (3H, <i>s</i>)
24	15.3	16.3	15.1	15.4	0.82 (3H, <i>s</i>)	0.84 (3H, <i>s</i>)
25	16.0	16.3	15.6	16.1	1.10 (3H, <i>s</i>)	1.03 (3H, <i>s</i>)
26	16.1	16.2	15.7	15.9	0.77 (3H, <i>s</i>)	0.83 (3H, <i>s</i>)
27	14.7	14.8	14.3	14.5	0.78 (3H, <i>s</i>)	0.79 (3H, <i>s</i>)
28	177.7	178.7	18.2	18.0	0.96 (3H, <i>s</i>)	0.94 (3H, <i>s</i>)
29	110.1	110.3	109.2	109.3	4.50 (1H, <i>s</i> , H-29a), 4.62 (1H, <i>s</i> , H29b)	4.57 (1H, <i>s</i> , H-29a), 4.69 (1H, <i>s</i> , H-29b)
30	19.4	19.4	18.8	19.3	1.70 (3H, <i>s</i>)	1.69 (3H, <i>s</i>)
1'	-	-	-	-	-	-
2'	-	-	-	-	1.97 (3H, <i>s</i>)	2.05 (3H, <i>s</i>)



II.2.3.6. Steroid

II.2.3.6.1. Structural identification of PTB 12

PTB 12 was obtained as colourless crystals, mp 258-260 °C. It reacted positively to the Liebermann-Burchard test for steroids (blue -violet colour). Its HR-ESI-MS spectrum exhibited a pseudo-molecular ion peak $[M+H]^+$ at m/z 577.4475 compatible with the molecular formula $C_{35}H_{61}O_6$ corresponding to six (06) degree of unsaturated bonds. This spectrum also exhibited two other fragments at m/z 414 and 396 which suggested that compound **PTB 12** contained a β -sitosterol moiety together with sugar moiety. This information was confirmed in the 1H NMR spectrum (**Figure 111**) of **PTB 12** which showed clusters signals among which one proton with olefinic substitution at δ_H 5.34 (H-6), two protons with substituted olefinic at δ_H 5.18 (H-22) and 5.04 (H-23) and one anomeric proton at δ_H 4.39. These observations were in agreement with an authentic sample of the isolated compound in the laboratory. Thus, **PTB 12** was identified as Daucosterol **118**, (Mouffok, 2012) previously reported from the roots of *Calliandra portoricensis* (Table 49) by (Nvau et al. 2020).



118

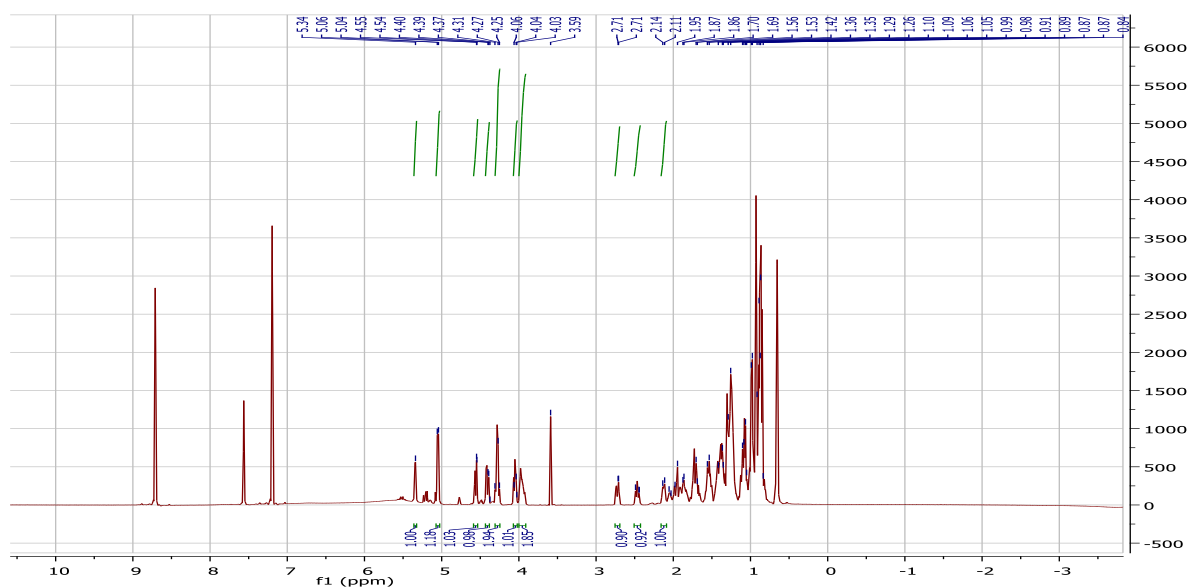
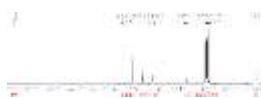
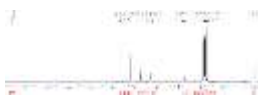


Figure 111. 1H NMR spectrum of PTB 12 (500 MHz, Pyridine- d_5)


Table 49 : Comparative ^1H -NMR data of PTB 12 with Daucosterol 118

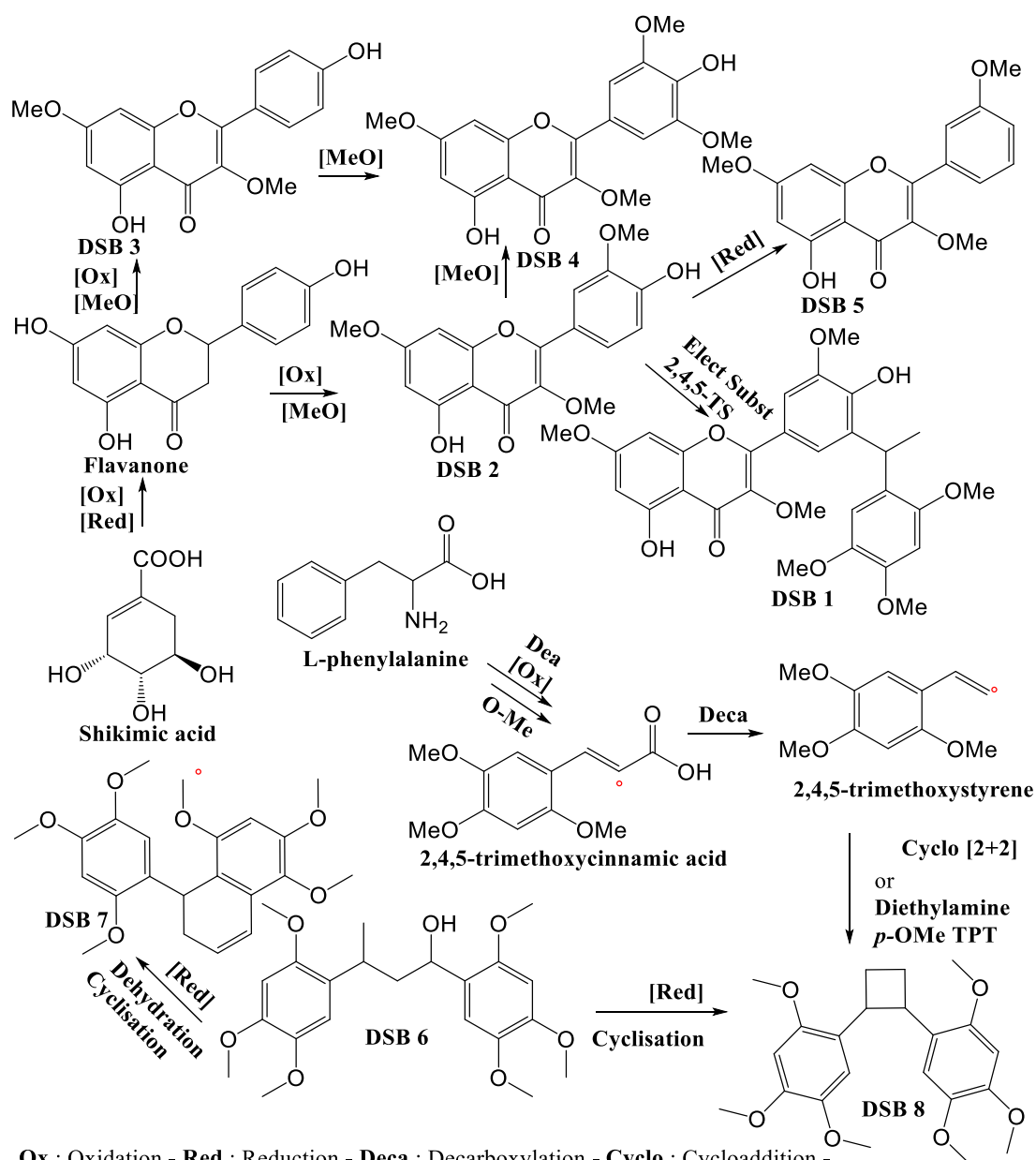
PTB 12 [^1H (500 MHz, Pyridine- d_5)]				Daucosterol [^1H -NMR (400 MHz, CDCl_3)]			
H no.	δ_{H} (m, J in Hz)	H no.	δ_{H} (m, J in Hz)	H no.	δ_{H} (m, J in Hz)	H no.	δ_{H} (m, J in Hz)
1	1.53; 1.95	15	1.52; 1.73	1	1.47; 2.12	15	1.56; 1.75
2	2.11	16	1.30; 1.70	2	2.22	16	1.29; 1.67
3	3.58 (1H, <i>m</i>)	17	1.37	3	-	17	1.30
4	2.11; 2.14	18	0.87 (3H, <i>s</i>)	4	2.23	18	0.68
5	-	19	0.95 (3H, <i>s</i>)	5	-	19	0.97
6	5.34 (<i>brs</i>)	20	2.11	6	5.18	20	2.05
7	1.98	22	5.18 (1H, <i>s</i>)	7	1.83	22	5.16
8	1.95	23	5.04 (1H, <i>d</i> , 10 Hz)	8	1.81	23	5.02
9	-	1'	4.39 (1H, <i>m</i>)	9	-	1'	4.41
10	-	2'	3.57	10	-	2'	3.26
11	1.56; 1.73	3'	3.59	11	1.56; 1.75	3'	3.44
12	1.24; 2.11	4'	4.03	12	1.27; 2.04	4'	3.42
13	-	5'	4.04	13	-	5'	3.30
14	1.82	6'	4.57	14	1.83	6'	4.51



II.2.4. BIOGENETIC RELATIONSHIP OF ISOLATED COMPOUNDS

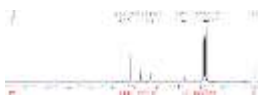
 II.2.4.1. Biogenetic relationship of compounds isolated from *D. staudtii*

The structural identification of secondary metabolites isolated from the stem bark of *Duguetia staudtii* showed that these compounds belong mainly to alkaloids, flavonoids, as well as binorlignans compounds. **Scheme 21** displays only a hypothesis of what could possibly be the biosynthetic pathway of the major isolated classes of compounds cited above.



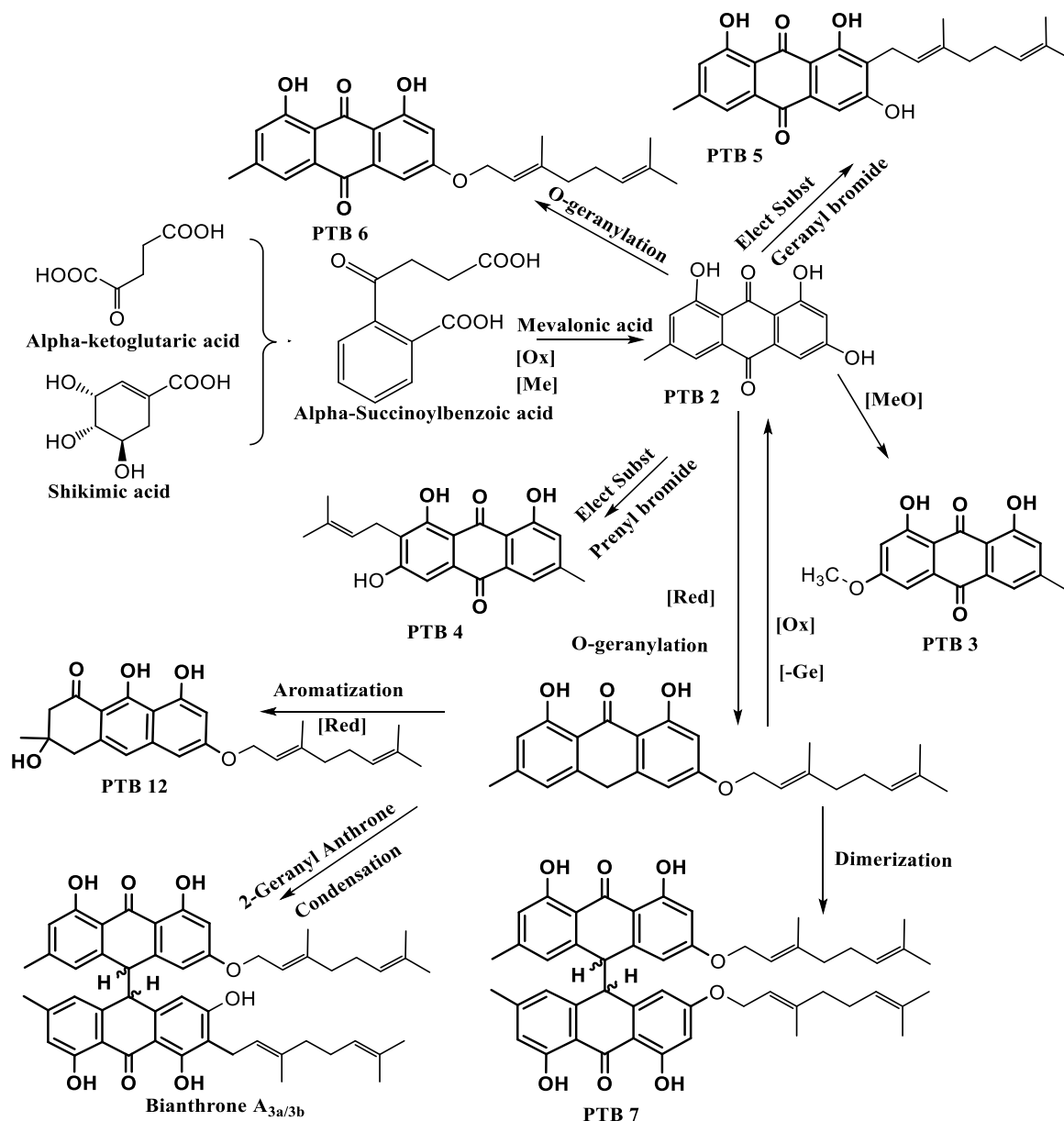
Ox : Oxidation - **Red** : Reduction - **Deca** : Decarboxylation - **Cyclo** : Cycloaddition - **Elect Subst** : Electrophilic Substitution - **OMe** : O-methylation - **MeO** : Methoxylation - **2,4,5-TS** : 2,4,5-Trimethoxystyrene - **Dea** : Deamination - **TPT** : 2,4,6-Triphenylpyrylium tetrafluoroborate

Scheme 21. Hypothetical biosynthetic pathway leading to main isolated compounds from *D. staudtii*

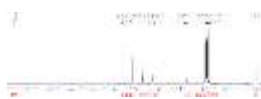


II.2.4.2. Biogenetic relationship of compounds isolated from *P. tenuifolium*

Likewise, the structural identification of secondary metabolites isolated from the stem bark of *Psorospermum tenuifolium* showed that these compounds belong mainly to anthraquinones, bianthrone and steroids compounds. **Scheme 22** displays only a hypothetical biosynthetic pathway of the major isolated classes of compounds from this specie.



Scheme 22. Hypothetical biosynthetic pathway leading to isolated compounds from *P. tenuifolium*



II.3. BIOLOGICAL ACTIVITIES

II.3.1. Main target: Microfilaricidal activity

II.3.1.1. Biological screening of crude extracts

The crude extract of *D. staudtii* (DCM/MeOH, 1:1, v/v) was 100% active on microfilariae at 250µg/mL. This means that the extract completely inhibited the mf motility at this concentration.

Medicinal plant preparations have been identified as alternative remedies for several diseases. Titanji et al (1990) reported the filaricidal activities on *D. staudtii* this is why our focus prior to the isolation of compounds was to perform the primary screen on *Onchocerca ochengi* microfilariae as shown in Table 50.

Table 50. *Onchocerca ochengi* microfilariae (mf) primary screen

Sample codes and compounds	Conc. (µg/mL)	% inhibition of mf motility										Remarks	
		Time (h)											
		24	48	72	96	120	24	48	72	96	120		
DS 33 (E ₁)	250	100	100	100	100	100	100	100	100	100	100	100	✓
DS 32 (E ₂)	250	100	100	100	100	100	100	100	100	100	100	100	✓
DS 31 (E ₃)	250	100	100	100	100	100	100	100	100	100	100	100	✓
DS 11 (A ₁)	30	100	100	100	100	100	100	100	100	100	100	100	✓
<u>105</u>	250	100	100	100	100	100	100	100	100	100	100	100	✓
<u>16</u>	250	0	0	50	50	50	50	50	50	50	50	50	~
<u>110</u>	30	50	50	100	100	100	100	100	100	100	100	100	✓
<u>5</u>	250	0	0	25	25	50	50	50	50	50	50	50	~
Neg. control: 2%													
DMSO	30	0	0	0	0	0	0	0	0	0	0	0	✓
Pos. control													
(Auranofin)	10	50	50	50	50	50	50	100	100	100	100	100	✓
		✓ Active	~	Moderately active									

II.3.1.2. Biological Screening on *O. ochengi* adult worms

On *O. ochengi* adult worms, the crude extract was 100% active on adult female worms at 250µg/mL. This has completely inhibited the conversion of MTT to formazan. Live worms are coloured blue (due to conversion of MTT to formazan) while dead worms are not coloured. An illustration of this is shown on Figure 112 below.

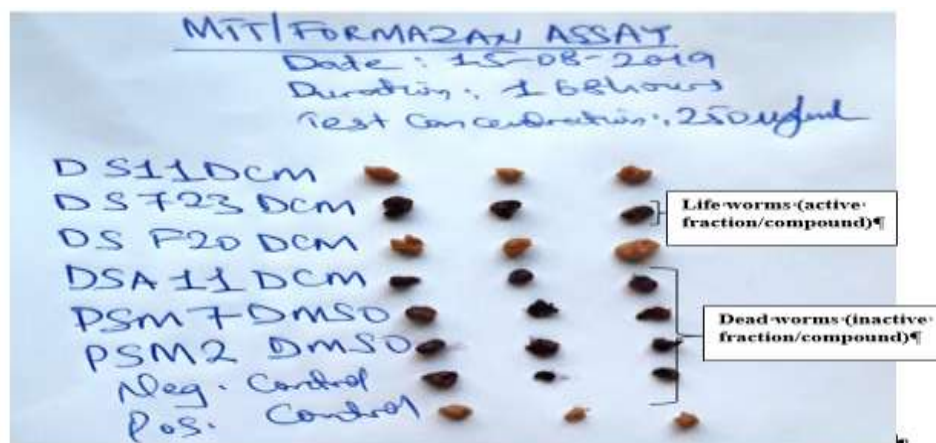
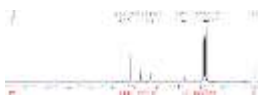


Figure 112. MTT formazan staining of adult female worms

II.3.1.3. Biological Screening of fractions

Since the crude extracts of *D. staudtii* showed 100% activity on both mf and adult worms, they were fractionated and the resulting fractions were also screened.

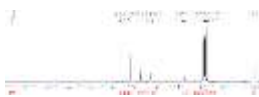
II.3.1.4. Biological Screening on *O. ochengi* adult worms

Out of the 6 fractions tested from *D. staudtii*, 4 fractions had 100% activity on adult male worms while 3 had 100% on adult female worms. All 6 fractions tested showed 100% activity on the mf as shown in Table 51 below.

Table 51. Screening of fractions on *O. ochengi* adult worms and (mf) of *D. staudtii*

S/N	CODE	Concentration (µg/mL)	Activity on male	Activity of female		Activity on mf
				% inhibition of motility		
1	DS11 DCM	250	100	100	100	100
2	DS31 MeOH	250	100	100	100	100
3	DS32 MeOH	250	100	0.00	100	100
4	DS33 MeOH	250	100	50	100	100
5	DS34 MeOH	250	33.3	100	100	100
6	DS4 MeOH	250	nd	0.00	100	100

nd :Not determined



II.3.2. Others activities

II.3.2.1. Cytotoxic Assay of some compounds from *P. tenuifolium*

Previous cytotoxic compounds have been isolated from *Psorospermum* plants (Amonkar et al. 1981). As continuity in search for cytotoxic compounds from the genus *Psorospermum*, the potency of some isolated compounds PTB 1–12 was carried out on KB-3-1 cell lines with griseofulvin as reference ($IC_{50} = 17\text{--}21 \mu\text{M}$). The results obtained (Table 52) showed that emodin (77, $IC_{50} = 11.4 \mu\text{M}$, was most active than the used standard; while 2-geranylemodin (114, $IC_{50} = 19 \mu\text{M}$, Figure 113 exhibited a moderate potency close to griseofulvin. All the results were obtained at a concentration of 0.2 mM for each sample. Although *P. tenuifolium* extract did not show any cytotoxicity, its components 77 and 114 showed moderate activities IC_{50} values of 11.4 and 19 μM respectively. This observation may indicate the synergistic effect of the compounds contained in *P. tenuifolium* extract.

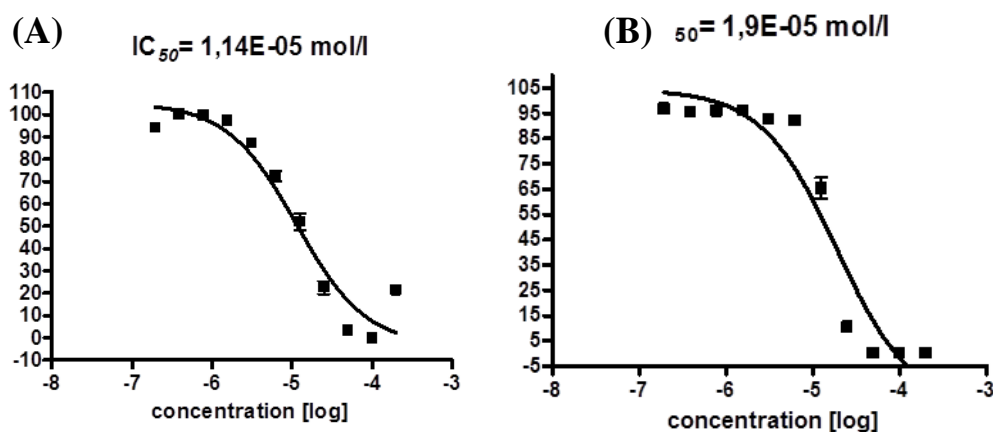
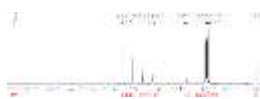


Figure 113. Cytotoxic activity of emodin 77 [A] and 2-geranylemodin 114 [B] on KB-3-1 cell lines


Table 52. Cytotoxic potencies of some compounds on KB3-1 cell lines

KB-3-1 cell lines	
Compound	IC ₅₀ (μM)
Crude extract	n.a
psorospermoside <u>113</u>	n.a
emodin <u>77</u>	11.4
2-geranylemodin <u>114</u>	19.0
3- <i>O</i> -geranylemodin <u>55</u>	>100
2-prenylemodin <u>78</u>	>100
bianthrone A1 <u>75</u>	>100
bianthrone A3a/3b <u>115</u>	>500
Lupeol <u>116</u>	n.a
betulinic acid <u>60</u>	n.a
Catechin <u>64</u>	n.a
Griseofulvin	17–21

n.a = not active

II.3.2.2. Urease inhibition

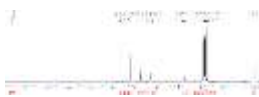
The new compound pachypolignan 109 and compounds 16, 106-107 and 5 were evaluated for their urease inhibitory potency. Compound 109 demonstrated a significant activity with IC₅₀ value of 20.2 μg/mL compared to the standard thiourea (IC₅₀ = 21.6 μg/mL). Whereas compounds 16, 106-107 and 5 exhibited potent urease inhibitory activity with IC₅₀ values ranging from 10.9 to 17.5 μg/mL (Table 53).

II.3.2.3. Antiinflammatory activity

Additionally, the inflammatory inhibitory activities of compounds 16, 106-107 and 5 were also evaluated. Only compounds 16, 106-107 exhibited potent anti-inflammatory activity on myeloperoxidase dependent (luminol/zymosan) and independent (lucigenin/PMA) oxidative burst with potencies expressed in IC₅₀ from 3.89 to 14.13 μg/mL (see Table 53).

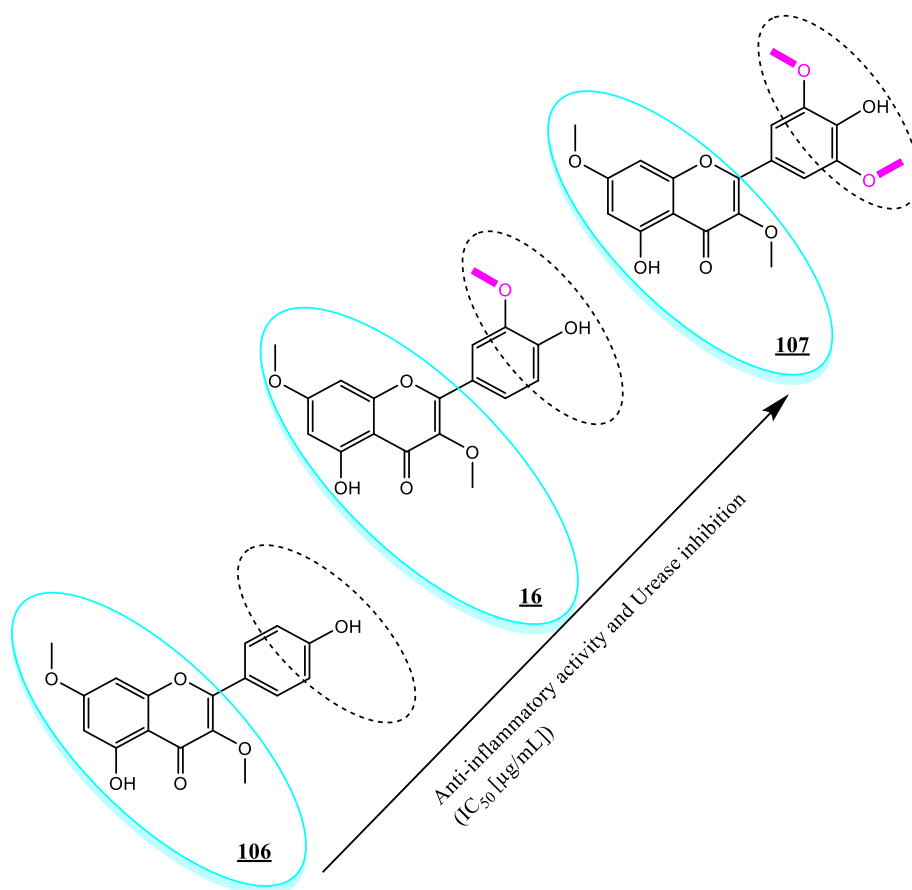
Table 53. IC₅₀ for some compounds isolated from *D. staudtii*

Compounds	Antiinflammatory activity (IC ₅₀ [μg/mL])					Urease inhibition (IC ₅₀ [μg/mL])
	Luminol			Lucigenin		
	Whole blood	PMNs	Macrophages	PMNs	Macrophages	
<u>109</u>	–	–	–	–	–	20.20
<u>106</u>	6.38	7.69	10.64	12.91	14.13	17.50
<u>16</u>	4.99	6.01	8.32	10.09	11.04	14.50
<u>107</u>	3.89	4.65	6.44	7.82	8.55	10.90
<u>5</u>	> 250	> 250	> 250	> 250	> 250	15.30
Ibuprofen	11.5	2.5	16.9	13.69	14.30	–
Thiourea	–	–	–	–	–	21.6±0.12



II.3.2.4. Hypothetical Structure–Activity Relationships (HSAR)

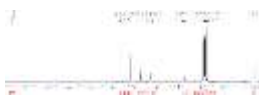
It's quite remarkable that the more a compound is substituted with methoxyl groups its potency gets better. From the previous result (**Table 53**) we can draw the conclusion that methoxylation might enhance the anti-inflammatory potential along with the potency of the urease inhibitory activity of the isolated flavonoids **DSB 2**, **DSB 3** and **DSB 4**.



Scheme 23. Hypothetical Structure–Activity Relationships of three isolated flavonoids

II.3.2.5. Methoxylation: A brief look!

It's the addition of one or more methoxy groups. In organic chemistry, a methoxy group is the functional group consisting of a methyl group bound to oxygen. This alkoxy group has the formula $R-O-CH_3$. Also, concerning Organic Methoxides, they are often produced by methylation of alkoxides (**Scarow and Allen 1933**). Whereas some aryl methoxides can be synthesized by metal-catalysed methylation of phenols or by methoxylation of aryl halides (**Cheung and Buchwald 2013**).



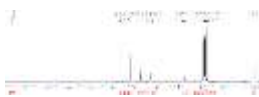
II.4. CHEMOTAXONOMIC AND CHEMOPHENETIC SIGNIFICANCE OF SOME COMPOUNDS ISOLATED RESPECTIVELY FROM *D. STAUDTII* AND *P.TENUIFOLIUM*

II.4.1. CHEMOTAXONOMIC SIGNIFICANCE OF SOME COMPOUNDS ISOLATED FROM *D. STAUDTII*

This chemical study from *Duguetia staudtii* yielded ten (10) chemical constituents including one new and one known bisnorlignans 109 and 11, resp, four flavonoids 105, 16, 106, 107, one alkaloid 5 and one triterpenoid 111. Notably, compound 111 is reported for the first time from the genus *Duguetia*, while this is the first report of compounds 109, 16, 106, 107 from the Annonaceae family. The other compounds 111 and 5, have been already reported from the species *D. staudtii*. Phenolic compounds including lignan and flavonoids have been reported from *Duguetia staudtii* and *Duguetia confne*, the two species already investigated in the literature. In the first plant of this study, four flavonoids and one triterpenoid were isolated for the first time from the genus *Duguetia* in addition to one new bisnorlignan. The systematic investigation of all the species of *Duguetia* could be helpful to identify the other classes of secondary metabolites present in this genus. With regards on the previous phytochemical works, lignans and flavonoids could be obviously considered as chemotaxonomic markers for the genus *Duguetia*.

II.4.2. CHEMOPHENETIC SIGNIFICANCE OF SOME COMPOUNDS ISOLATED *P.TENUIFOLIUM*

During this chemical investigation of the bark of *Psorospermum tenuifolium*, twelve compounds have been isolated and fully characterized (PTB 1-12) including one new phenylpropanoid glycoside (PTB 1), four anthraquinones 77, 55, 78 and 114; one bianthrone A3a/3b 115, two lupane-type triterpenoids 60; 116; , one flavonoid 64 and one steroid glycoside 118. Especially, emodin 77 and its derivatives 55, 78 and 114 are reported for the first time from the species *P. tenuifolium* but were already reported from other species of the genus *Psorospermum*. However, only the detected vismione D 76 (Table 38) and bianthrone A1 75 were previously isolated from *P. tenuifolium* (Delle Monache et al. 1987b). These observations provide important evidence on the plant taxonomy. Indeed, anthraquinone and anthrone derivatives represent the most encountered classes of metabolites in the family Hypericaceae (Happi et al. 2020) and especially in the genus *Psorospermum* (Epifano et al., 2013). Therefore, they can be considered as chemomarkers for the genus *Psorospermum*. Previous works on *P. tenuifolium* led to the isolation of a lupane-type triterpenoid betuline (Delle Monache et al. 1987a, b), whereas its derivative lupeol acetate where obtained from *P. androsaemifolium* (Poumale et al. 2011). In the same way, the isolation of lupeol PTB 10 and betulinic acid PTB 9



is more comprehensible and provides additional information to enrich the chemistry of the genus *Psorospermum*. Furthermore, lupane- type triterpenoids might represent a new significant chemotaxonomic finding for the Hypericaceae plants. **PTB 1** is reported for the first time from the family Hypericaceae, whereas the flavonoid catechin **PTB 8** and the steroid daucosterol **PTB 12** are commonly obtained from high plants.



GENERAL CONCLUSION AND PERSPECTIVES

Our walk across Natural products allow us to investigate on the subject intitled: “Chemical study of *Duguetia staudtii* Engl. & Diels Chatrou (Annonaceae) and *Psorospermum tenuifolium* Hook.f. (Hypericaceae): Microfilaricidal activities and LC-ESI-MS application”. Thus, by means of LC-ESI-MS guided isolation and using common chromatographic techniques, the chemical study of the CH₂Cl₂/MeOH (1/1, v/v) extracts of the stem bark of both plants enabled us to detect some known (DSB 2-4; 6-10; PTB 2-5; 8) and unknown (DSB 1, DSB 5 and PTB 1) compounds; to isolate and characterize twenty-two labelled (DSB 1 to DSB 10 ; PTB 1 to PTB 12); and to fully and structurally identified them by means of usual spectroscopic methods namely UV, IR, MS, XRD, 1D and 2D NMR; while some among the detected ones were confirmed by comparison of their NMR data with those previously reported in the literature.

The twenty-two isolated and fully characterized compounds were sorted into three known and nineteen unknown compounds. The three were found to be new derivatives viz., pachypodostyflavone, a new 3-methoxyflavone; pachypolignan, a lignan derivative, both from *D. staudtii* and the new phenylpropanoid glycoside, psorospermoside, a derivative from *P. tenuifolium*. Whereas the nineteen others, which have been previously isolated were identified as: pachypodol, kumatakenin, 5,4'-dihydroxy-3,7,3',5'-tetramethoxy flavone, (+)-catechin, pachypophillin, pachypostaudin-B, corypalmine, costunolide, 3-geranyloxyemodin, 2-geranylemodin, 2-prenyl emodin, emodin, physcion, lupeol, lupeol acetate, betulinic acid, polycarpol, Daucosterol, bianthrone A3a/A3b, The chemical study carried out on extracts from the bark of these two plants yielded seven active fractions. Following the method described by (Cho-Ngwa et al. 2010), fractions tested at 250 mg/mL and having 100% inhibition of microfilaria (mf) motility and adult male worm viability were screened at various concentrations to determine their inhibitory concentration (IC₅₀). The new 3-methoxyflavone, pachypodostyflavone, and the known sesquiterpenoid, costunolide, both isolated from the genus *Duguetia* from the active fraction DS11 (30 mg/mL), showed 100% activity on both mf and adult worms respectively at 250 and 30 mg/mL. These two compounds were obtained as crystals from *D. staudtii*. The XRD experiment using a Rigaku supernova diffractometer permitted first of all, to deduce for the first time the absolute configuration of the new compound, and therefore, to assign it as (S) (Mountessou et al. 2023b). While for the known



General Conclusion and Perspective

sesquiterpene costunolide, its X-ray crystallography carried out was assigned as (6R, 7S) (Mountessou et al 2023a). In the biological part of this work, several compounds were submitted to antiinflammatory tests. Thus 3, 7, 3', 5'-tetramethoxy-5, 4'-dihydroxy flavone **107**, pachypodol **16** and kumakatemin **106**, showed a good activity with IC₅₀ ranging from 3.89 to 14.13 µg/mL on luminol/zymosan and lucigenin, compared to the reference drug ibuprofen (14.30 µg/mL). In addition, others compounds were screened for their urease inhibitory activity. As the result, the new compound pachypolignan showed a notable urease inhibition with an IC₅₀ of 20.2 µg/mL compared to 21.6 µg/mL for the potent inhibitor Thiourea, with methoxylated flavone perhaps, being the key factor which might justify the enhancement of both the antiinflammatory and urease potential observed from the tested compounds. Thus, the systematic investigation of all the species of *Duguetia* could be helpful to identify the other classes of secondary metabolites present in this genus. With regards on the previous phytochemical works, lignans and flavonoids could be obviously considered as chemotaxonomic markers for the genus *Duguetia*. The extract and compounds of *Psorospermum tenuifolium* were subjected to cytotoxic activities on cell lines of human squamous cell carcinoma KB-3-1. Thus, emodin on the one hand exhibited an IC₅₀ value of (11.4 µM) more important than the standard drug griseofulvin (17-21 µM) whereas on the other hand, 2-geranylemodin (19.0 µM) showed a moderate activity. Indeed anthraquinone along with anthrone derivatives represent the most encountered classes of metabolites in the family Hypericaceae, therefore they can be considered as chemomarkers for the genus *Psorospermum*.

In addition, due to the acute toxicity of *D. staudtii* extract carried out in this thesis at a single dose of 2000 mg/kg of body weight, and to the successful in-silico results obtained later on by (Mountessou and coworkers 2023b) with pachypodostyflavone on *Onchocerca volvulus* main protease, along with the significant potential of the same compound to treat Onchocerciasis from a negative binding affinity (E_{binding}) of -7.00 kcal mol⁻¹, obtained for its docking against *Onchocerca volvulus* Pi-class Glutathione S-transferase binding pocket, we hope that these aforementioned results may provide insights into the development of a pre-formulation of a phytodrug to treat river blindness through this single plant or with the combination of two of the Cameroonian medicinal plants studied. We intend consequently for this latter objective, to assess the filaricidal potential of the plant *Psorospermum tenuifolium*



General Conclusion and Perspective

even up to at 30 $\mu\text{g/mL}$; to evaluate the *antionchocerca* activity of the extract, fractions and all the twelve compounds isolated along with the acute toxicity of *Psorospermum tenuifolium* extract at the same single dose of 2000 mg/kg of body weight.



CHAPTER 3: EXPERIMENTAL PART



CHAPTER 3: EXPERIMENTAL PART**III.1. MICROFILARICIDAL SCREENING OF CRUDE EXTRACTS****III.1.1. Preparation of stock solutions**

Stock solutions of 25 mg/mL were also prepared for each fraction and compound in dimethyl sulfoxide (DMSO, solvent grade >99.8%, from Sigma-Aldrich) and kept at -20° C until testing on worms and larvae.

III.1.2. Preparation of mammalian cells

LLC-MK2 cells obtained from American Type Culture Collection (ATCC, Virginia, USA) were proliferated in T-25 culture flask (Corning) in CCM (with 10% new born calf serum) at 37° C and 5% CO₂ in humidified air. The cells were dislodged with trypsin-EDTA (Sigma) and seeded in 96-well cell culture plates (flat bottom CELLSTAR®, greinerbio-one, Germany) at a density of 3000 cells/ 100 µL CCM / well and then incubated for 3 days to become fully confluent. When confluent, the cells served as feeder layer for the mf assays and were also used for cytotoxicity assays.

III.1.3. Isolation of *Onchocerca ochengi* microfilariae (mf) and screening

This was done as described by **Cho-Ngwa et al. (2010)** with slight modifications. Briefly, fresh pieces of cattle skin from the umbilical area with palpable nodules obtained from the slaughter house were cleaned, carefully shaved, and sterilized with 70% ethanol. Skin slivers were obtained using a sterile scalpel and incubated for 4-6 hours at room temperature in CCM (CCM, which is RPMI 1640 with NaHCO₃ and supplemented with 25 mM HEPES, 0.3g γ-irradiated L-glutamine powder, 5% new born calf serum, 200 units/mL penicillin, 200 µg/mL streptomycin and 0.25 µg/mL amphotericin B; pH 7.4) . The emerged and highly motile *O. ochengi* mf were concentrated by centrifugation (400xg, 10 minutes), re-suspended and distributed into wells (about 15 mf/100 µL of CCM/well) of the 96- well plates containing the feeder layer.

Primary of fractions screens were done in duplicates at 250µg/mL in order to eliminate inactive fractions. The mfs were incubated at 37° C under an atmosphere of 5% CO₂ in humidified air and mf viability assessed microscopically daily for 5 days. Viability scores were assigned based on percentage motility, using the following key: 100% (all mf immotile), 75%



(only head or tail of mf shaking, occasionally), 50% (whole body of mf motile but sluggishly or with difficulties), 25% (almost vigorous motility), and 0% (vigorous motility).

Fractions with 100% inhibition of mf motility were further screened at lower concentrations (right down to 3.9 $\mu\text{g}/\text{mL}$) to determine $\text{IC}_{50\text{s}}$. Active fractions were further fractionated following a bio-assay guided approach in view of obtaining pure compounds. These compounds were tested first at 30 $\mu\text{g}/\text{mL}$ and if active, then tested further at lower concentrations.

III.1.4. Isolation of *O. ochengi* adult worms and screening

Worms were isolated using the method described by (Cho-Ngwa et al. 2010). Briefly, pieces of umbilical cattle skin with palpable nodules collected from the slaughter houses in Douala and Buea Cameroon were thoroughly washed with soap and water. The inner and outer surfaces of the skin were sterilized with 70% ethanol and left in a lamina flow sterile hood for the ethanol to evaporate. Nodules were carefully excised and the recovered worm masses submerged in 2 mL of complete culture medium in 12-well culture plates (Corning, USA). The worm masses were incubated overnight at 37° C under an atmosphere of 5% CO_2 in humidified air (in a HERACELL-150i CO_2 incubator, USA). Male worms usually emerge from the worm masses while female worms remain in them. Viability of worms and sterility of cultures were evaluated using an inverted microscope (Nikon Eclipse TS100, China) prior to drug testing in primary and secondary screens. Primary screens were done in order to eliminate inactive fractions. The worms were treated in triplicates with fractions prepared 2X concentrated to give a test concentration of 250 $\mu\text{g}/\text{mL}$ in 4 mL of CCM final volume. Auranofin (Origin: Enzo Life Science, Farmingdale NY, USA. Purity 99.9%), previously shown to be active was used as positive control at 10 μM . Negative control wells received 2% DMSO, shown to be safe for worms. Viability of worms was assessed after an incubation period of 5 days.

Viability of adult male worms was assessed by evaluation of worm motility using an inverted microscope and viability scores ranging from 100% (complete inhibition of motility), 75% (only head or tail of worm shaking occasionally), 50% (whole worm motile, but sluggishly), 25% (only little change in motility), to 0% (no observable change in motility) were assigned. Also, adult female worms viability was assessed biochemically, by visual estimation of the percentage inhibition of formazan (blue colour) formation following incubation of the worm masses in 500 μL of 3-(4,5-dimethylthiazol-2-yl)-2,5-diphenyltetrazolium bromide (from Sigma)



dissolved in ICM (MTT solution, 0.5 mg/ml) for 30 minutes (Cho-Ngwa et al. 2016) Viability scores assigned ranged from 100%, parasite killing (no blue formazan coloration seen), 90%, 75%, 50%, 25% to 0% (entire worm appears blue as in negative control).

A fraction was considered active if there was $\geq 90\%$ inhibition of male worm motility or of formazan formation; moderately active if there was 50 - 89% inhibition of male worm motility or of formazan formation and inactive if there was $< 50\%$ inhibition of male worm motility or of formazan formation. All experiments were repeated at least once to confirm activity. Fractions with 100% activity at primary screens were treated as previously described above.

III.1.5. Isolation and screens on *Loa loa* microfilariae

III.1.5.1. Isolation of *Loa loa* microfilariae

Ethical clearance (2015/12/679/L/CE/CNERSH/SP) and administrative clearance (631-06.14) were obtained from the Cameroon National Ethical Committee for Research on Human Health and the Ministry of Public health, respectively. Local administrative clearances were given by the District Medical Officers of the Kribi and Akonolinga health districts where volunteers were recruited following parasitological screening. Only adults with *Loa loa* loads greater than 30,000 mf/mL of blood were recruited as voluntary donors after informed consent.

Whole blood (4 mL) was collected in an EDTA tube and transported to the laboratory for use within the next 24 hours. The blood was diluted with CCM by a factor determined by the initial mf load of the sample and distributed in wells of a 96 well plate (15 mfs/100 μ L). The mfs were monitored after 24 hours for viability and sterility prior to treatment with extracts. Fractions and compound with good activity against *O. ochengi* were counter screened on *L. loa* mf to determine IC_{50s}.

III.1.5.2. Cytotoxicity assessment of fractions

Cytotoxicity of extracts was evaluated by the MTT [3-(4,5-dimethylthiazol-2-yl)-2,5-diphenyl tetrazolium bromide] cell viability assay on LLCMK2 cells using protocol adapted from (Denizot et al. 1986; Wardihan et al. 2013). Summarily, confluent cell layers were prepared as described above and treated in duplicates with serial dilutions (250 - 3.91 μ g/mL) of extracts in CCM after refreshing the medium. Control wells received the vehicle, 0.5% DMSO. The cell cultures were thereafter incubated at 37°C under an atmosphere of 5% CO₂ in humidified air.



After 5 days of incubation, the entire supernatant over the cells was removed by inverting, flicking and blotting the plate. The plate was washed 2 times with ICM (100 μ L/well), and 100 μ L of MTT solution (1 mg/mL, dissolved in ICM) added into each well. The plate was incubated for 3 hours at 37 $^{\circ}$ C, and the untransformed MTT solution removed by gently inverting, flicking and blotting the plate. DMSO (100 μ L) was added to each well and the plate was shaken on a shaker (KS125 basic, IKA LABORTECHNIK, Germany) in order to dissolve the blue formazan crystals. Only living cells were able to reduce MTT to formazan. Optical densities were read using the E-max Molecular Devices Elisa plate reader with wavelength set at 595 nm and percentage inhibition of formazan formation calculated using the following formula:

$$\text{Percentage inhibition (\%)} = [(\text{OD of control} - \text{OD of treatment}) \times 100] / (\text{OD of control})$$

The 50 % cytotoxic concentration (CC₅₀ values) of extracts was used together with their IC_{50s} to compute the selectivity index (SI) of each extract, which is the ratio of CC₅₀ of the extract on the mammalian cells to the IC₅₀ of the extract on the parasites.

III.2. UREASE ASSAY

Exactly 25 μ L of enzyme (Jack Bean Urease) solution and 5 μ L of test compounds (0.5 mM concentration) were incubated for 15 min at 30 $^{\circ}$ C (Tariq et al. 2011). The aliquot was taken after 15 min and again incubated with 55 μ L of buffers containing 100mM urea for 15 min at 30 $^{\circ}$ C. Ammonia production was measured as a urease activity by indophenol method as described earlier (Khan et al. 2013). Final volumes were maintained as 200 μ L by adding 45 μ L phenol reagent (1% w/v phenol and 0.005% w/v sodium nitroprusside) and 70 μ L of alkali reagent (0.5% w/v NaOH and 0.1% active chloride NaOCl). The increase in absorbance was measured at 630nm after 50min at pH 8.2. The results (change in absorbance per min) were calculated spectrometrically on different concentrations of drugs in the absence and presence of ascorbic acid. The IC₅₀ values were calculated using statistical software, GraphPad PRISM 6. Thiourea was used as the standard inhibitor and percentage inhibitions were calculated as follows:

$$\% \text{ Inhibition} = 100 - [(\text{OD}_{\text{testwell}}) / (\text{OD}_{\text{control}})] \times 100$$

III.3. X-RAY CRISTALLOGRAPHY OF SOME COMPOUNDS ISOLATED

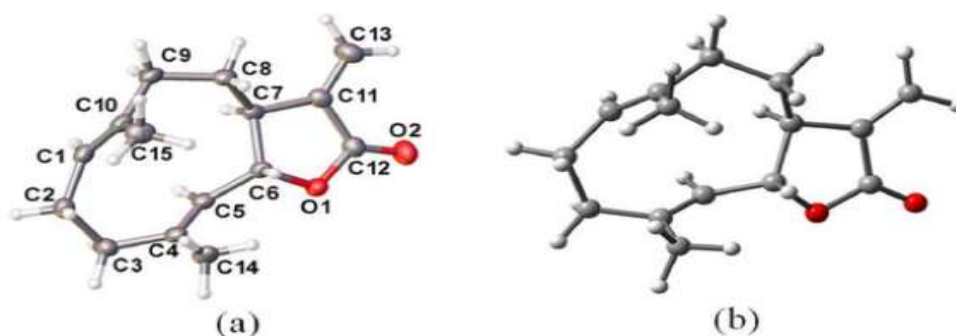
III.3.1. X-ray analysis of costunolide

A single crystal of C₁₅H₂₀O₂ was examined on a Rigaku Supernova diffractometer using Cu K α (λ = 1.54184 Å) radiation. The crystal was kept at 100.0 K during data collection



(Dolomanov et al. 2009). Using Olex (Sheldrick, 2015), the structure was solved with the ShelXT structure solution program using Intrinsic Phasing and refined with the ShelXL refinement package using Least Squares minimisation. Hydrogen atoms were refined isotropically. Chirality: C3 S, C4 R; Flack parameter 0.01(6).

Crystal Data for $C_{15}H_{20}O_2$ ($M = 232.31$ g/mol): orthorhombic, space group $P2_12_12_1$ (no. 19), $a = 7.84072(9)$ Å, $b = 11.06760(17)$ Å, $c = 15.09857(20)$ Å, $V = 1310.22(3)$ Å³, $Z = 4$, $T = 100.0(1)$ K, $\mu(\text{Cu K}\alpha) = 0.601$ mm⁻¹, $D_{\text{calc}} = 1.178$ g/cm³, 48168 reflections measured ($9.91^\circ \leq 2\theta \leq 153.142^\circ$), 2735 unique ($R_{\text{int}} = 0.0431$, $R_{\text{sigma}} = 0.0139$) which were used in all calculations. The final R_1 was 0.0247 for 2644 reflections with $I > 2\sigma(I)$ and wR_2 was 0.0614 for all data.



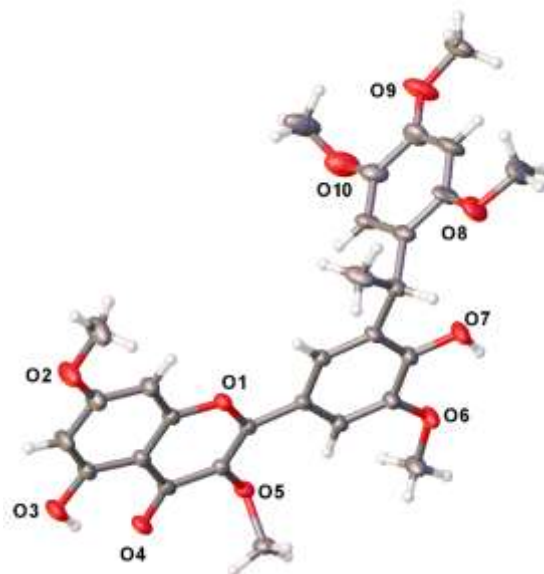
Scheme 24. (a) ORTEP representation as determined by X-ray, and (b) theoretically optimised structure of costunolide 110 through Rigaku Supernova diffractometer

**Table 54. Crystal data and structure refinement for costunolide 110**

Identification code	DSB 8
Empirical formula	C ₁₅ H ₂₀ O ₂
Formula weight	232.31
Temperature/K	100.0 (1)
Crystal system	orthorhombic
Space group	P2 ₁ 2 ₁ 2 ₁
a/Å	7.84072(9)
b/Å	11.06760 (17)
c/Å	15.09857 (20)
α/°	90
β/°	90
γ/°	90
Volume/Å ³	1310.22 (3)
Z	4
ρ _{calc} /g/cm ³	1.178
μ/mm ⁻¹	0.601
F(000)	504.0
Crystal size/mm ³	0.165 × 0.154 × 0.081
Radiation/Å	Cu Kα (λ = 1.54184)
2θ range for data collection/°	9.91 to 153.142
Index ranges	-9 ≤ h ≤ 9, -13 ≤ k ≤ 13, -19 ≤ l ≤ 19
Reflections collected	48168
Independent reflections	2735 [R _{int} = 0.0431, R _{sigma} = 0.0139]
Reflections with I > 2σ(I)	2644
Data/restraints/parameters	2735/0/235
Goodness-of-fit on F ²	1.056
Final R indexes [I > 2σ(I)]	R ₁ = 0.0247, wR ₂ = 0.0604
Final R indexes [all data]	R ₁ = 0.0260, wR ₂ = 0.0614
Largest diff. peak/hole / e Å ⁻³	0.16/-0.11
Flack parameter	0.01(6)

III.3.2. X-ray analysis of pachypodostyflavone

A single crystal of C₂₉H₃₀O₁₀ was examined on a Rigaku Supernova diffractometer using Mo Kα (λ = 0.71073 Å) radiation. The crystal was kept at 100.01(10) K during data collection. Using Olex2 (Dolomanov et al. 2009), the structure was solved with the ShelXS (Sheldrick, 2008) structure solution program using Direct Methods and refined with the ShelXL (Sheldrick, 2015) refinement package using Least Squares minimisation. Disorder of C22 to C29, O8, O9, and O10 over two sites (51:49).



Scheme 25. 3D structure of pachypodostyflavone 105 through Rigaku Supernova diffractometer

Crystal Data for $C_{29}H_{30}O_{10}$ ($M = 538.53$ g/mol): monoclinic, space group $P2_1/c$ (no. 14), $a = 23.9096(10)$ Å, $b = 13.2552(6)$ Å, $c = 8.0442(5)$ Å, $\beta = 94.961(5)^\circ$, $V = 2539.9(2)$ Å³, $Z = 4$, $T = 100.01(10)$ K, $\mu(\text{Mo K}\alpha) = 0.107$ mm⁻¹, $D_{\text{calc}} = 1.408$ g/cm³, 54964 reflections measured ($5.94^\circ \leq 2\theta \leq 60.158^\circ$), 7454 unique ($R_{\text{int}} = 0.0419$, $R_{\text{sigma}} = 0.0215$) which were used in all calculations. The final R_1 was 0.0816 for 6515 reflections with $I > 2\sigma(I)$ and wR_2 was 0.2173 for all data.

**Table 55. Crystal data and structure refinement for DSB 1**

Identification code	DSB 1
Empirical formula	C ₂₉ H ₃₀ O ₁₀
Formula weight	538.53
Temperature/K	100.01(10)
Crystal system	monoclinic
Space group	P2 ₁ /c
a/Å	23.9096 (10)
b/Å	13.2552 (6)
c/Å	8.0442 (5)
α/°	90
β/°	94.961 (5)
γ/°	90
Volume/Å ³	2539.9 (2)
Z	4
ρ _{calc} /g/cm ³	1.408
μ/mm ⁻¹	0.107
F(000)	1136.0
Crystal size/mm ³	0.366 × 0.297 × 0.06
Radiation/Å	Mo Kα (λ = 0.71073)
2θ range for data collection/°	5.94 to 60.158
Index ranges	-33 ≤ h ≤ 33, -18 ≤ k ≤ 18, -11 ≤ l ≤ 11
Reflections collected	54964
Independent reflections	7454 [R _{int} = 0.0419, R _{sigma} = 0.0215]
Reflections with I > 2σ(I)	6515
Data/restraints/parameters	7454/0/464
Goodness-of-fit on F ²	1.146
Final R indexes [I > 2σ(I)]	R ₁ = 0.0816, wR ₂ = 0.2122
Final R indexes [all data]	R ₁ = 0.0900, wR ₂ = 0.2173
Largest diff. peak/hole / e Å ⁻³	0.62/-0.34

III.4. PRE-FORMULATION OF A PHYTODRUG FROM ACTIVE FRACTION DS 11

III.4.1. Acute oral toxicity

The acute oral toxicity of the extract was assessed in rats according to OECD guideline 423 for chemical testing adopted in December 17, 2001.

III.4.2. Principle of the test

The principle of this test is that with a sequential process, using a minimum number of animals per stage, sufficient information on the acute toxicity of the substance can be obtained to allow its classification. The substance is tested in a sequential process in which three female



animals are used at each stage. The absence or manifestation of substance-related mortality in a group given a dose at a given stage determines the toxicity of the extract. If no dead of animal was recorded at the limit dose of 2000 mg/kg, the test was stopped and the LD50 considered to be high than 2000 mg/kg. The substance thus classified as less toxic.

III.4.3. Procedure

The test was done with 6 female rats (aged: 8-10 weeks; weight: 100-110 g), divided into 2 groups of 3 animals each: One control group receiving the vehicle at 10 mL/kg and test group receiving a single dose of 2000 mg/kg of body weight. All the substances were administered orally by gavage. Prior to the test, the animals were submitted to 12 hours fasting period.

III.4.4. Observation of animals and recording of the body weight.

Animals were observed individually after dosing, at least once during the first 30 minutes, periodically during the first 24 hours, with special attention given during the first 4 hours, and daily thereafter, for a total of 14 days. The times at which signs of toxicity appear and disappear were recorded for each animal. Observations included changes in skin and fur, eyes and mucous membranes, and also respiratory, circulatory, autonomic and central nervous systems, and somato-motor activity and behavior pattern.

Symptoms like tremors, convulsions, salivation, diarrhea, lethargy, sleep and coma were also recorded. The changes in body weight were recorded for the entire duration of the study.

III.5. GENERAL INSTRUMENTAL PROCEDURES

Optical rotation indices were determined in methanol on a JASCO DIP-3600 digital polarimeter (JASCO, Tokyo, Japan) using a 10 cm cell. IR spectra were determined on a JASCO Fourier transform IR-420 spectrometer (JASCO). Ultraviolet spectra were recorded on a Hitachi UV 3200 spectrophotometer in MeOH and infrared spectra on an ALPHA Platinum-ATR (Bruker, Rheinstetten, Germany). ESI-HR mass spectra were measured on Agilent Techn. 6220 TOF LCMS mass spectrometer (Agilent Technologies, Santa Clara, CA, USA) and EI-MS on a Finnigan MAT 95 spectrometer (70 eV) (Thermo Fischer Scientific, Darmstadt, Germany) with perfluorokerosene as reference substance for ESI-HR-MS. The ^1H - and ^{13}C -NMR spectra were recorded at 500 MHz and 125 MHz, respectively, on Bruker DRX 500 NMR spectrometers (Bruker Corporation, Brussels, Belgium) in CDCl_3 . Chemical shifts are reported in δ (ppm) using



tetramethylsilane (TMS) (Sigma-Aldrich, Munich, Germany) as internal standard, while coupling constants (J) were measured in Hz. Column chromatography was carried out on silica gel 230–400 mesh, Merck, (Merck, Bielefeld, Germany), silica gel 70–230 mesh (Merck), and sephadex LH-20 (Sigma-Aldrich). Thin layer chromatography (TLC) was performed on Merck precoated silica gel 60 F254 aluminum foil (Merck), and spots were detected using diluted sulfuric acid spray reagent before heating. The molecular composition of the isolated compounds was identified by exact mass determinations. All reagents used were of analytical grade.

III.5.1. Plant material

The sample bark of *D. staudtii* Engl & Diels were collected for the second time in the Dja forest at Lomié-Bertoua (GPS coordinates provided by system WGS8: Altitude 665 m; Latitude N 4°34'38''; Longitude E 13°41'04''), in the East Region of Cameroon, in July 2017. The botanical identification was done by Mr. Victor Nana, a botanist at the National Herbarium of Cameroon where the samples were registered under the voucher specimen 52711HNC.

The stem bark of *P. tenuifolium* was collected in April 2017, in the village Nkolafamba, (GPS coordinates: Latitude 3°51'32"N, Longitude 11°39'53"E), near Yaounde, Centre Region of Cameroon. The plant material was authenticated with the help of Mr Victor Nana, a well-known botanist of the National Herbarium of Cameroon, where a voucher specimen was deposited and registered under the number 43860 HNC. The two plants were air-dried to constant weight and then ground to fine powder.

III.5.2. Extraction of *D. staudtii* and *P. tenuifolium*

The air-dried and powdered stem bark of *D. staudtii* (~5.9 kg) [DCM/MeOH (1:1, v/v, 72h and 48h)] were consequently extracted separately at room temperature. Extracts were concentrated to dryness under vacuum at low temperature to give respectively 382.0 g (brownish extract) and 172.4 g (dark yellowish extract) of stem bark each.

Where as the air-dried and powdered stem barks (~3 kg) of *P. tenuifolium* were consequently extracted three times with the mixture of dichloromethane/methanol (1/1, v/v) for 72 h, 48 h and 24 h, respectively. After filtration and evaporation of solvent under reduced pressure, 172.4 g of crude extract were obtained, dissolved in water and successively partitioned with *n*-hexane (Hex), ethyl acetate (EtOAc), and *n*-butanol (BuOH) to obtain three



solvent-soluble fractions labelled **A'** (7.58 g), **B'** (58.05 g), **C'** (23.65 g), respectively, as well as the remaining water soluble fraction **D'** (74.21 g)

III.5.2.1. Fractionation of the crude extract of *D. staudtii*

The fractionation of the crude extract (C.E.) of *D. staudtii* carried out in two steps through Vacuum liquid chromatography (VLC) allowed us to get two sets of fractions.

III.5.2.1.1. Partition of 150.0 g of the first Crude extract of *D. staudtii*

The first set (**114.0 g**) of crude extract obtained after the partition via ethyl acetate from **150.0 g** of *D. staudtii* was subjected to silica gel column chromatography using a gradient of ethyl acetate in hexane (Hex), followed by pure dichloromethane (DCM), and finally through a gradient of methanol (MeOH) in dichloromethane, led to seven main fractions named F₁ (pure Hex), F₂ (Hex/ EtOAc, 10%), F₃ (Hex/ EtOAc, 30%), F₄ (Hex/ EtOAc, 50%), F₅ (pure DCM), F₆ (DCM/MeOH, 5%) and F₇ (DCM/MeOH, 10% and H₂O/ACN 5%) (Table 56).

Table 56. Chromatogram of the fractionation of 114.0 g after the partition of 150.0 g of the C.E. of *D. staudtii*

Eluents	Series N°	Observations	Fractions
100 % <i>n</i> -hexane	1-25	Non-polar mixture of compounds	F ₁ (17.5 g)
Hex-EtOAc (10-15%)	26-38	DSB 7 and DSB 10 and others	F₂ (10.4 g)
Hex-EtOAc (30%)	39-46	Mixture of close to 8 compounds	F ₃ (10.2 g)
Hex-EtOAc (50%)	47-67	Mixture of more than 9 compounds	F ₄ (11.5 g)
DCM	68-84	Mixture almost 4 compounds	F ₅ (14.5 g)
DCM/MeOH 5%	85-102	DSB 2-DSB 4 and four others	F₆ (22.2 g)
DCM/MeOH 10%	103-125	DSB 9 precipitated	F₇ (14.3g)
H ₂ O/ACN 5%		DSB 5 via prep. HPLC	

▪ Treatment of fractions 2, 6 and 7

Fraction F₂ [10.4 g - Hex-EtOAc 15%; from Hex-EtOAc 2.5% to Hex-EtOAc 45%] was subjected to a silica gel column chromatography using a gradient of *n*-Hex/EtOAc and monitored with TLC to afford compounds **DSB 7** (8 mg) and **DSB 10** (10 mg) both at Hex-EtOAc (10-15%).

Fraction F₆ [22.2 g - DCM/MeOH 5%; from 100 % DCM to DCM/MeOH 8%] was subjected to silica gel column chromatography using the gradient DCM/MeOH as mixture of solvents to afford at DCM/MeOH 5%) **DSB 2** (800 mg), **DSB 3** (6 mg), **DSB 4** (5 mg) and a flavonoid (11 mg; with poor NMR recording).



Compound **DSB 9** (1.5 g) precipitated from fraction F_7 (14.3 g) and the HPLC profile of the filtrate showed a mixture of compounds which was submitted to preparative HPLC using the UV wavelength 205 nm and the solvent system H_2O/ACN 5% to afford the new compound **DSB 5** (4 mg).



Scheme 26. HPLC columns

So, at least seven (07) compounds were isolated from the fractionation of 114.0 g of the first extract of *D. staudtii*.

III.5.2.1.2. VLC of 380.0 g of the active extract of the second harvest of *D. staudtii*

The second set of fractionation of *D. staudtii* crude extract (**380.0 g**) obtained after the second harvest was subjected to VLC using a gradient of DCM and MeOH (**Table 57**).

Table 57. VLC of the bioactive extract of the stem bark of *D.*

Eluents	Series N°	Fractions
DCM (A)	1-125	DCM soluble fraction (210.0 g)
MeOH (B)	126-230	MeOH soluble fraction (117.0 g)
		Residue 2

- **Chromatogram of the VLC of the DCM soluble fraction A of *D. staudtii***

The DCM fraction of the stem bark was once more subjected to VLC over silica gel (Merck, 230–400 mesh) eluting with *n*-hexane, *n*-hexane/EtOAc, EtOAc and EtOAc/MeOH, in increasing order of polarity. Sixty fractions, each containing almost 1000 mL, were collected and combined according to their TLC profiles on pre-coated silica gel 60 F254 plates developed with *n*-hexane/EtOAc and $CHCl_3/MeOH$ mixtures to give eight main fractions (A_{1-8}). The study of these fractions led to the isolation and characterization of five other compounds, with two (**DSB 2** and **DSB 9**) already isolated in the first extract.

Part of extract F_A (210.0 g) was subjected to flash silica gel (230–400 mesh) column chromatography (width 5.5 - 8.5 cm; depth 25.4 cm) using a stepwise gradient of *n*-Hex/EtOAc (ranging from 0 to 100% of EtOAc, *v/v*). Afterwards, a total of 150 fractions ($f_{r1}-f_{r150}$) of ca. 500 mL each were collected and combined on the basis of TLC analysis to yield 8 main fractions



(A₁–A₈) **Table 58.** Some of these fractions were also separately assessed for their antifilaricidal activity on any of the three parasite stages (mf, *O. ochengi* adult male and female worms) used in the bioassay for further fractionation. All the following fractions A₁ (*f*_{r1}–*f*_{r24}: 28.0 g; ~2000 mL); A₂ (*f*_{r25}–*f*_{r39}: 30.0 g; ~3500 mL); A₃₄ [(*f*_{r40}–*f*_{r76}: 55.8 g; ~4000 mL; VLC; from 100% *n*-hexane to 100% EtOAc; **DSB 2** (10.2 mg; mp: 167-169°C); **DSB 6** (75.0 mg) and **DSB 9** (6.5 mg)]; fraction A₄ [(*f*_{r62}–*f*_{r76}: 31.0 g, ~5000 mL *n*-Hex/EtOAc 6:4, v/v; fluorescent yellow crystal **DSB 2**); fraction A₅ [(*f*_{r77}–*f*_{r86}: 25.0 g, ~3500 mL; *n*-Hex/EtOAc 1:1, v/v)]; fraction A₆ [(*f*_{r87}–*f*_{r103}: 32.0 g, *n*-Hex/EtOAc 4:6; *n*-Hex/EtOAc (from 7:3, v/v – 3:7); orange needle-shaped crystal **DSB 1** (77.7 mg; Hex- EtOAc 60:40)], on the basis of the TLC were eluted on silica gel CC successively with *n*-hexane-ethyl acetate gradient of increasing polarity, starting from 100% *n*-hexane to 100% EtOAc. while fractions A₇ (*f*_{r104}–*f*_{r124}: 19.0 g, ~1500 ml; *n*-Hex/EtOAc 3:7) and A₈ (*f*_{r125}–*f*_{r150}: 13.0 g, ~5000 mL; pure EtOAc) were gummy and were not further investigated.

Table 58. Chromatogram of the DCM soluble and bioactive fraction A of *D. staudtii*

Eluents	Series N°	Observations	Sub-fractions
100 % <i>n</i> -hexane	1-24	Non polar mixture + DSB 8 (125.0 mg)	A ₁ (28.0 g)
Hex-EtOAc (90:10)	25-39	Mixture of nearly 5 along with DSB 8	A ₂ (20.0 g)
Hex-EtOAc (80:20)	40-46	Mixture of 7 compounds	A ₃ (25.8 g)
Hex-EtOAc (70:30 -60 :40)	47-76	(DSB 2, DSB 6, DSB 9 + a Mixture)	A ₄ (31.0 g)
Hex-EtOAc (50:50)	77-86	Mixture of complex compounds	A ₅ (15.0 g)
Hex-EtOAc (40:60)	87-103	Mixture of six compounds	A₆ (32.0 g)
Hex-EtOAc (20:80) -	104-124	More than 8 compounds	A ₇ (19.0 g)
Pur EtOAc	125-137	Complex mixture	A ₈ (13.0 g)
EtOAc/MeOH 10%	138-150		

Table 59. Chromatogram of the sub-fraction A34 from the DCM soluble fraction of *D. staudtii*

Eluents	Series n°	Observations	Compounds
100 % <i>n</i> -hexane	1-5	Oily mixture of almost 5 compounds	-
Hex-AcOEt (95:5)	6-13	Mixture of 3 compounds	-
Hex-AcOEt (90:10)	14-25	Mixture of 4 compounds	-
Hex-AcOEt (80:20)	26-37	Mixture of compounds	DSB 2 (10.2 mg)
Hex-AcOEt (75:25)	38-48	Mixture of 5 compounds	-
Hex-AcOEt (65:35)	49-55	Mixture of 2 compounds	-
Hex-AcOEt (60:40)	56-61	Mixture of 3 compounds	DSB 6 (75.0 mg) and DSB 9 (6.5 mg)
Pur AcOEt	62-66	Complex mixture	-



Part of the soluble-methanol extract **F_B** (Table 60) (117.0 g) was also subjected to flash chromatography over silica gel and eluted with a stepwise gradient of *n*-Hex/EtOAc and EtOAc/MeOH. Afterwards, fractions of ca. 500 mL each were collected and combined on the basis of TLC analysis to yield 5 main fractions (B₁–B₅). Only fraction B₁ (*f*_{r1}–*f*_{r32}: 28.0 g) obtained with *n*-Hex/EtOAc (6:4, v/v) was chromatographed over silica gel CC and eluted with a gradient of *n*-Hex/EtOAc (7:3–0:10, v/v) to afford a yellow amorphous powder **DSB 9** (75 mg).

Table 60. Chromatogram of the MeOH soluble fraction B of the stem bark of *D. staudtii*

Eluents	Series N°	Observations	Sub-fractions
<i>n</i> -Hex/EtOAc (7:3)	1-32	Mixture of compounds with DSB 9	B ₁ (28.0 g)
<i>n</i> -Hex/EtOAc (5:5)	33-75		
<i>n</i> -Hex/EtOAc (4:6)	76-123	Mixture of compounds	B ₂ (25.0 g)
<i>n</i> -Hex/EtOAc (3:7)	124-162		
<i>n</i> -Hex/EtOAc (2:8)	163-166	Mixture of compounds	B ₃ (15.0 g)
Pur EtOAc	167-174		
EtOAc/MeOH 5%	175-180	Mixture of compounds	B ₄ (26.0 g)
EtOAc/MeOH 10%	181-197		
EtOAc/MeOH 15%	198-201	Complex and gummy mixture	B ₅ (22.0 g)
EtOAc/MeOH 20%	202-230		

Overall, at least three (03) different compounds (**DSB 1**; **DSB 6** and **DSB 8**) from those obtained in the first harvest of *D. staudtii* were isolated from the fractionation of 380.0 g of extract of the second harvest.

III.5.2.2. Fractionation of the crude extract of *P. tenuifolium*

▪ Isolation of chemical constituents from *P. tenuifolium*

172.4 g of the crude extract from *P. tenuifolium* were obtained from which 169.4 g were dissolved in water and successively partitioned with *n*-hexane (Hex), ethyl acetate (EtOAc), and *n*-butanol (BuOH) to obtain three solvent-soluble fractions **A'**, **B'** and **C'** as well as the remaining water soluble fraction **D'** (Table 61).

Table 61. SLP of the bioactive extract of the stem bark of *P. tenuifolium*

Eluents	Fractions
<i>n</i> -Hex	Soluble fraction A' (07.58 g)
EtOAc	Soluble fraction B' (58.05 g)
<i>n</i> -BuOH	Soluble fraction C' (23.65 g)
H ₂ O	Soluble fraction D' (74.21 g)

▪ Column Chromatography (CC) of the EtOAc soluble fraction of *P. tenuifolium*

Fraction **B'** (58.05 g) was subjected to a silica gel column chromatography eluting with



a stepwise gradient of petroleum ether (PE)/ dichloromethane (3:1 → 1:3, v/v), followed by petroleum ether–ethyl acetate (7:3 → 0:1, v/v) to afford twelve sub-fractions labelled F₁–F₁₂ along with twelve compounds including 2-geranylemodin **114** (9 mg), 3-*O*-geranylemodin **55** (34 mg), 2-prenylemodin **78** (6 mg), bianthrone A3a/3b **115** (26 mg), lupeol **116** (4 mg), and catechin **64** (7 mg).

Table 62. Chromatogram of the sub-fraction B' from the EtOAc soluble fraction of *P. tenuifolium*

Eluents	Series N°	Observations	SFr.	Compounds
n-PE	1-8	Oily mixture of compounds	1	–
n-PE/DCM 3 :1	9-19	Mixture of 4 compounds	2	–
n-PE/DCM 2 :2	20-31	Mixture of compounds including	3	PTB 8; 10
n-PE/DCM 1 :3	32-39	Mixture of 5 compounds	4	–
DCM	40-51	Mixture of 6 compounds	5	–
n-PE/EtOAc 7:3	52-63	Mixture of less than 8 compounds	6	PTB 4-5
n-PE/EtOAc 6:4	64-71	Mixture of 7 compounds	7	–
n-PE/EtOAc 5:6	72-92	Mixture of 4 compounds	8	PTB 7
n-PE/EtOAc 3:2	93-107	Mixture of 5 compounds	9	PTB 6
n-PE/EtOAc 3:4	108-123	Mixture of 3 compounds	10	–
n-PE/EtOAc 2:3	124-131	Mixture of polar compounds	11	–
n-PE/EtOAc 1:4	132-150	Complex mixture	12	–

SFr. : Sub-fractions

▪ **Column chromatography (CC) of the EtOAc soluble fraction**

F₉ (9.12 g, PE/EA 3:2) was further purified by column chromatography on silica gel with a gradient of ethyl acetate in petroleum ether (9:1 → 3:2, v/v) to obtain **PTB 2** (8 mg) and **PTB 9** (26 mg) along with **PTB 3** (3mg) and **PTB 11** (10 mg).

Table 63. Chromatogram of the sub-fraction F9 from the EtOAc soluble fraction of *P. tenuifolium*

Eluents	Series N°	Observations	Compounds
n-PE/EtOAc 9:1	1-18	Mixture of almost 3 compounds	
n-PE/EtOAc 7:3	19-27	Mixture of 4 compounds	PTB 2-3
n-PE/EtOAc 5:5	28-39	Mixture of compounds including	PTB 9
n-PE/EtOAc 3:7	40-59	Mixture of 4 compounds	PTB 11
n-PE/EtOAc 1:9	60-78	Mixture of 5 compounds	–
Pur EtOAc	79-90	Mixture of 6 compounds	–

▪ **Column chromatography (CC) of the BuOH soluble fraction**

F₁₁ (3.01 g, PE/EA 2:3), F₁₂ (6.83 g, PE/EA 1:4) and fraction C' (BuOH) (23.65 g) were



combined and submitted to a column chromatography on silica gel using the gradient of methanol in ethyl acetate (0 to 20%) to yield **PTB 1** (4 mg) and **PTB 12** (14 mg).

Table 64. Chromatogram of the sub-fractions F11 and F12 from the EtOAc combined to fraction C' from BuOH soluble fraction of *P. tenuifolium*

Eluent	Series N°	Observations	Compounds
Pur EtOAc	1-5	Mixture of 5 compounds	-
EtOAc/MeOH 2.5%	6-21	Mixture of 4 compounds	PTB 12
EtOAc /MeOH 5%	22-34	Mixture of 5 compounds including	PTB 1
EtOAc/MeOH 7.5%	35-41	Mixture of 3 compounds	-
EtOAc /MeOH 10%	42-54	Mixture of 4 compounds	-
EtOAc/MeOH 12.5%	55-64	Mixture of 3 compounds	-
EtOAc /MeOH 15%	65-78	Mixture of 4 compounds	-
EtOAc/MeOH 17.5%	79-84	Mixture of gummy compounds	-
EtOAc /MeOH 20%	85-100	Complex compounds	-

The remaining hexane and water soluble fractions **A'** (7.58 g) and **D'** (74.21 g) were not further investigated due to some poor LC-MS profiles.

III. 6. CHARACTERISTIC TESTS OF CLASSES OF ISOLATED COMPOUNDS

III.6.1. Feric chloride (FeCl_3) test: characteristic for phenols

1 mg of a given compound was dissolved in a methanolic solution and a few drops of ferric chloride (FeCl_3) were added. The appearance of a purple colouration due to the formation of a complex ion $[\text{Fe}(\text{ArO})_6]^{3-}$ indicated that the compound is a phenolic derivative.

III.6.2. Shinoda test: characteristic for flavonoids

From the methanolic solution of a given compound, some drops of concentrated hydrochloric acid (HCl) and a few pieces of magnesium (Mg) chips were added. The appearance of effervescence followed by an abrupt change in colour of the solution into a pink colour indicated that the compound is a flavonoid.

III.6.3. Liebermann-Burchard test: characteristic for triterpenoids and steroids

Considering 1 mg of a given compound dissolved in 1 mL of chloroform. From the obtained solution, 1 mL of acetic anhydride was added with 0.5 mL of the concentrated sulphuric acid (H_2SO_4). Triterpenoids gave with this reagent a brown colour which became later on violet. Whereas steroids gave a blue colouration which quickly became dark green.



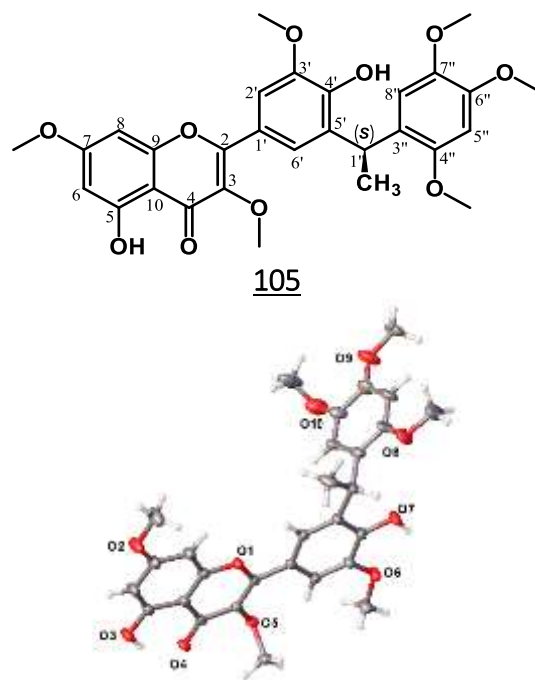
III.7. PHYSICAL AND SPECTROSCOPIC CHARACTERISTICS OF COMPOUNDS ISOLATED FROM BOTH PLANTS

III.7.1. Physical and spectroscopic characteristics of *D. staudtii*

Compounds

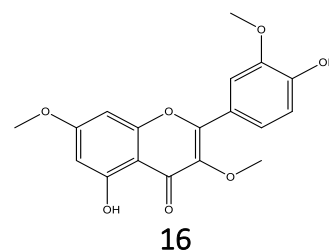
→ Pachypodostyflavone (DSB 1)

- Orange solid (CHCl₃);
- m.p. 181–183 °C;
- $[\alpha]_D^{20}$ 0 (c 0.5; CH₂Cl₂);
- UV (MeOH) λ_{\max} (log ϵ) 229 (1.08), 269 (0.73), 293 (0.56), 354 (0.85) nm
- IR (KBr) ν_{\max} 3660, 1738, 1655, 1595, 1489, 1345, 1205, 1038 cm⁻¹
- ¹³C and ¹H NMR data, see
- HR-ESI-MS: m/z 561.1723 [M+Na]⁺ (calcd. for C₂₉H₃₀O₁₀Na, 561.1731)
- Crystal Data



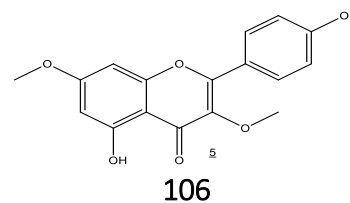
→ Pachypodol (DSB 2)

- Yellow crystal (CHCl₃);
- mp 167-169°C;
- HR-ESI-MS, [M+H]⁺ at m/z 345.0958. C₁₈H₁₆O₈
- UV : λ_{\max} 365 and 265 nm
- The ¹H-NMR (500 MHz, CDCl₃) data



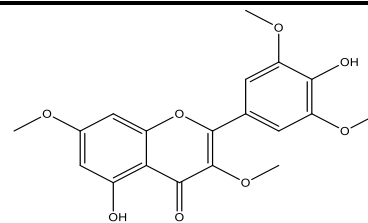
→ Kumatakenin (DSB 3)

- Yellow needles (Pyridine-*d*₅);
- mp 220-222°C - Ferric chloride test (+) ;
- HR-ESI-MS, [M+H]⁺ at m/z 315.1820 C₁₇H₁₅O₆ - UV at λ_{\max} 340 and 269 nm ;
- ¹H-NMR spectrum (400 MHz, Pyridine-*d*₅)
- ¹³C NMR spectrum (100 MHz, Pyridine-*d*₅)

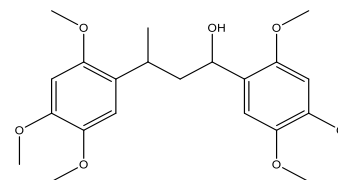


→ **3,7,3'-tetramethoxy-5,4'-dihydroxy flavone (DSB 4)**

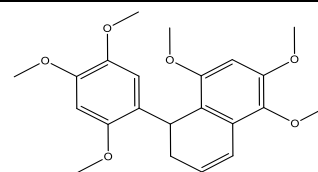
- Yellow crystal (CHCl₃) - UV at λ_{max} 365 and 265 nm;
- mp 173-175°C - Ferric chloride (blue colour) (+) ;
- HR-ESI-MS, [M+H]⁺ at *m/z* 375.1805 (C₁₉H₁₈O₈) ;
- ¹H-NMR (500 MHz, CDCl₃)

**107**→ **Pachypolignan (DSB 5)**

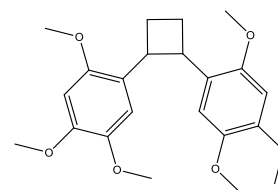
- Colorless oil. (CD₃OD) ;
- HR-ESI-MS at *m/z* 407.2055 [M+H]⁺, (calcd. for C₂₂H₃₀O₇, 406.2025), showing eight degrees of unsaturation;
- UV at λ_{max} 229, 243 and 283 nm;
- IR (1609 and 1515 cm⁻¹), and hydroxyl group (3476 cm⁻¹);
- ¹H-NMR (400 MHz, CD₃OD); ¹³C NMR (100 MHz, CD₃OD)

**109**→ **Pachypostaudin-B (DSB 6)**

- Colourless needle (CDCl₃.);
- mp 125-127°C HR ESI-MS [M+H]⁺ at *m/z* 387.1805, 355, 218, 194 (100) 151, and 136 (C₂₂H₂₆O₆);
- ¹³C NMR and ¹H NMR;

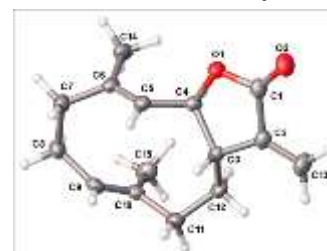
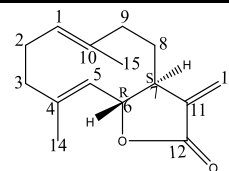
**11**→ **Pachyphyllin (DSB 7)**

- Colourless crystal (8.0:2.0 *n*-Hexane/EtOAc);
- mp 160-162°C HR-ESI-MS [M+H]⁺ at *m/z* 389.1932, C₂₂H₂₈O₆;
- UV spectrum showed also maxima at λ_{max} 229, 243 and 283 nm;
- ¹H- NMR (500 MHz, CDCl₃);

**13**



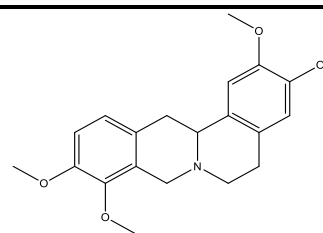
- **Costunolide (DSB 8)**
- Yellow needles (CDCl₃), mp 109-111°C ;
- HR-ESI-MS [M+H]⁺ at *m/z* 233.1534, C₁₅H₂₁O₂ for C₁₅H₂₀O₂);
- ¹H- NMR (500 MHz, CDCl₃);
- ¹³C NMR (125 MHz, CDCl₃);
- IR (α, β -unsaturated-γ-lactone carbonyl band at λ_{max} (CHCl₃) 1777 cm⁻¹ with the C=C absorption band at 1670 cm⁻¹. UV at λ_{max} 210 nm ;
- Crystal Data ;



110

→ **Corypalmine (DSB 9)**

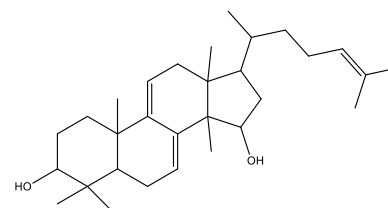
- Amorphous yellow powder (Pyridine-*d*₅);
- Draggendorf test (+) ;
- HR-ESI-MS [M+H]⁺ at *m/z* 342.1711 for C₂₀H₂₃NO₄ ;
- ¹H-NMR (500 MHz, Pyridine-*d*₅) - ¹³C- NMR (125 MHz, Pyridine-*d*₅);



5

→ **Polycarpol- (DSB 10)**

- Brown crystal (DMSO-*d*₆);
- mp. 215–217 °C ;
- Liebermann-Buchard Test (+) ;
- HR-ESI-MS [M+H]⁺ at *m/z* 441.1524 for C₃₀H₄₈O₂ ;
- ¹H-NMR (500 MHz, Pyridine-*d*₅) - ¹³C- NMR (125 MHz, Pyridine-*d*₅);



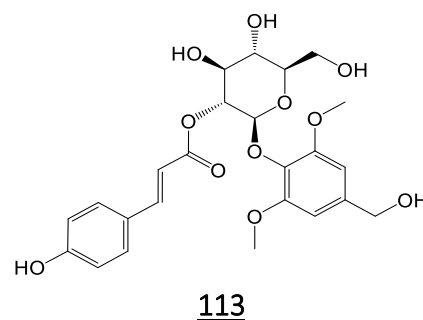
111

III.7.2. Physical and spectroscopic characteristics of *P. tenuifolium*

Compounds

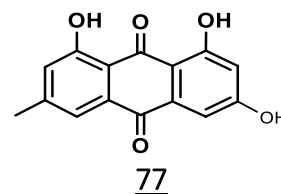
→ Psorospermoside (PTB 1)

- White amorphous powder (MeOH);
- HR-ESI-MS: m/z 515.1521 $[M + Na]^+$ (calcd for $C_{24}H_{28}O_{11}Na$, 515.1524);
- $\alpha_D^{20} +5.8$ (c 0.5, MeOH);
- m.p. 184–186 °C;
- UV (MeOH) λ_{max} (log ϵ) 312 (1.72), 226 (1.59), 212 (2.17) nm;
- IR (KBr) ν_{max} 3317, 2919, 2850, 1699, 1599, 1122, 1019, 832, 519 cm^{-1} ;
- 1H NMR (500 MHz, pyridine- d_5);
- ^{13}C NMR (125 MHz, pyridine- d_5);



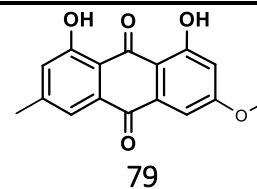
→ Emodin (PTB 2)

- Red powder - Borntrager test (+);
- HR-ESI-MS $[M+H]^+$ at m/z 271,1017 for $C_{15}H_{11}O_6$;
- ^{13}C -NMR (125 MHz, Acetone d_6);
- 1H NMR (500 MHz, Acetone d_6);



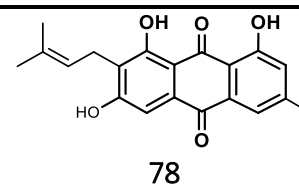
→ Physcion (PTB 3)

- Amorphous reddish powder - Borntrager test (+);
- HR-ESI-MS $[M+H]^+$ at m/z 285,1120 for $C_{16}H_{13}O_5$;
- 1H -NMR (500 MHz, Acetone d_6);



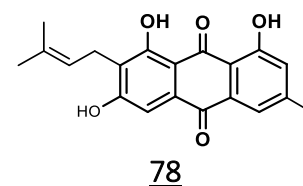
→ Isoprenylemodin (PTB 4)

- Red powder - Borntrager test (+);
- HR-ESI-MS $[M+H]^+$ at m/z 339.3911 for $C_{20}H_{19}O_5$ -
- 1H NMR spectrum (500 MHz, Acetone d_6)

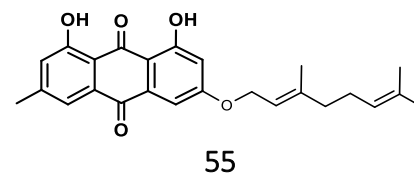


→ **2-geranylemodin (PTB 5)**

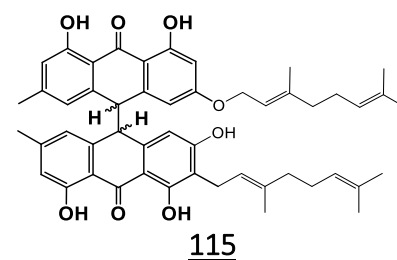
- Orange crystal (Acetone- d_6);
- m.p.122–124°C - Borntrager test (+) ;
- HR-ESI-MS $[M+H]^+$ at m/z 407.3678 for $C_{25}H_{26}O_5$; - UV at λ_{max} 225, 263 and 281 ;
- 1H NMR (500 MHz, Acetone d_6);
- ^{13}C - NMR (125 MHz, Acetone d_6) ;

→ **3-geranyloxyemodin (PTB 6)**

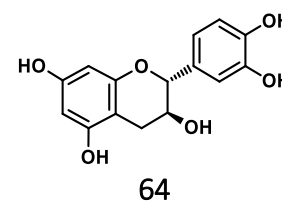
- Orange powder ($CDCl_3$);
- Borntrager test (+) ;
- UV : λ_{max} 225, 263 and 281 ;
- 1H - NMR (500 MHz, $CDCl_3$);
- ^{13}C (125 MHz, $CDCl_3$);

→ **Bianthrone $A_{3a/3b}$ (PTB 7)**

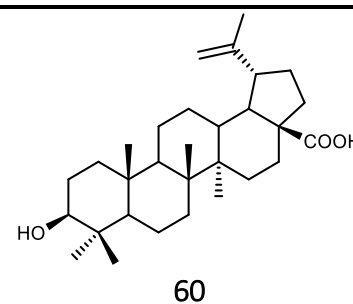
- Yellow powder $FeCl_3$ reagent and magnesium acetate (+) ;
- HR-ESI-MS $[M+H]^+$ at m/z 783.3812 for $C_{50}H_{54}O_8$;
- IR: 1716 and 1619 cm^{-1} , 3397 cm^{-1} . ;
- UV at λ_{max} 278, 363 and 370 ;
- 1H - NMR (500 MHz, $CDCl_3$);
- ^{13}C (125 MHz, $CDCl_3$) ;

→ **(+)-Catechin (PTB 8)**

- White powder (Acetone- d_6) - UV (λ_{max} 278 nm);
- Shinoda test (Mg/HCl) (+) and phenol test (1% $FeCl_3$) (+);
- HR-ESI-MS $[M+H]^+$ at m/z 291,0968 for $C_{15}H_{14}O_6$;
- 1H NMR (500 MHz, acetone d_6);

→ **Betulinic acid (PTB 9)**

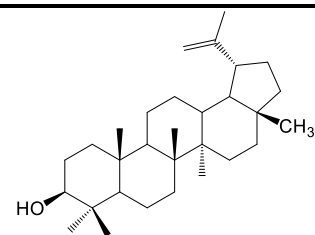
- Colourless amorphous powder;
- Liebermann-Burchard (+);
- 1H -NMR (500 MHz, $CDCl_3$) ;
- ^{13}C (125 MHz, $CDCl_3$);





→ **Lupeol (PTB 10)**

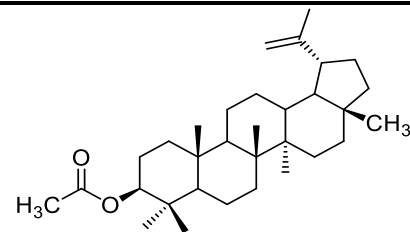
- Colourless crystal (chloroform);
- mp 218–220 °C;
- Liebermann-Burchard (+);
- ¹H-NMR (500 MHz, CDCl₃);



64

→ **Lupeol acetate (PTB 11)**

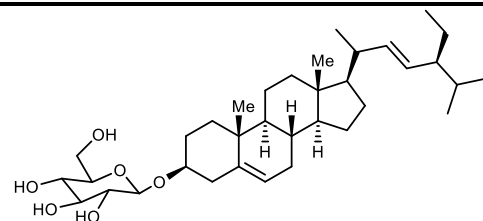
- White powder;
- ¹H-NMR (500 MHz, CDCl₃);



117

→ **Daucosterol (PTB 12)**

- Colourless crystals (CDCl₃)
- m p : 258-260°C
- Liebermann-Burchard test (+)
- ¹H NMR (500 MHz, CDCl₃);



118



REFERENCES



REFERENCES

- Abongwa, M., Samje, M., Ayimele, G., A., Babiaka, S., B., Bulman, C., Sakanari, J., Koszewski, N., J., Verma, S., Goff, J., Cho-Ngwa, F., Martin, R., J., Robertson, A., P., **2021**. Filaricidal activity of *Daniellia oliveri* and *Psorospermum febrifugum* extracts. *Parasites Vectors*. **14**. 305. Doi.org/10.1186/s13071-021-04759-6;
- Agrawal P., K., **1989**. Carbon-13 NMR of flavonoids. *Elsevier*, Netherlands;
- Ajaiyeoba, E., Falade, M., Ogbale, O., Okpak, L, and Akinboye, D., **2006**. *In vivo* antimalarial and cytotoxic properties of *Annona senegalensis* extract. *Afr. J. Trad. Cam.* **3**. 137 – 141;
- Allen J., S., **1947**. An improved electron multiplier particle counter. *Rev. Sci. Instrum.* **18**. 739-749. Doi:10.1063/1.1740838 ;
- Amonkar, A., Chang, C., J., Cassady, J., M., **1981**. 6-Geranyloxy-3-methyl-1,8-dihydroxanthone, a novel antileukemic agent from *Psorospermum febrifugum* Spach var. ferrugineum (Hook. fil). *Experientia*. **37**. 1138-1139;
- Annie Bligh, S.W., Ogegbo O., Wang Z.T., Flavonoids by HPLC. In: Ramawat, K.G., Merillon, J.M., **2013**. *Nat. Prod.* 2107-2144;
- Ariyanathan, S., Saraswathy, A., Rajamanickam, G., V., Connolly, J., D., **2010**; Polyphenols from roots of *Plumbago rosea*. *Ind. J. Chem.* **49B**. 386-389;
- Bankeu, K., J., J., **2011**. “Phytochemical and some pharmacological studies on the stem bark and the figs of *Ficus mucoso* Welw. (Moraceae)”. Doctorat/PhD en chimie Organique. Université de Yaoundé 1. 38-52 ;
- Barnes, J., H., Hieftje, G., M., **2004**. Recent advances in detector-array technology for mass spectrometry. *Int. J. Mass Spectrom.* **238**. 33-46. doi:10.1016/j.ijms.2004.08.004 ;
- Botta B., Monache F. D., Monache G. D., Bettolo G. B. M., Msonthi J. D., **1985**. Prenylated bianthrone and vismione F from *Psorospermum febrifugum*. *Phytochem.* **24**. 827- 830. Doi: 10.1016/S0031-9422(00)84902-X;
- Botta, B.; Monache, F., D., Monache, G., D., **1987**. A novel type of prenylated anthranoid from *Psorospermum glaberrimum*. *Tetrahedron Lett.* **28**. 567-570;
- Botta, B.; Monache, F.D.; Monache, G.D.; Bettolo, G.B.M.; Oguakwa, J.U., **1983**. 3-Geranyloxy-6-methyl-1,8-dihydroxyanthraquinone and vismiones C, D and E from *Psorospermum febrifugum*. *Phytochem.* **22**, 539–542;
- Brown, K., L., Tautfest, G., W., **1956**. Faraday-cup monitors for high-energy electron beams. *Rev. Sci. Instrum.* **27**. 696-702. Doi:10.1063/1.1715674 ;



- Burkill, H., M., **1985**. 2nd Ed. The Useful Plants of West Tropical Africa, vol. 1 *Roy. Bot. Gard. Kew*;
- Calvo-Flores, F., G., Dobado, J., A., Isac-García, J., Martín-Martínez, F., J., **2015**. Lignin and lignans as renewable raw materials: Chemistry, Technology and Applications ISBN: 978-1-118-59786-6. 506;
- Carollo, C., A., Hellmann-Carollo, A., R., De Siqueira, J., M., Albuquerque, S., **2006**. Alkaloids and Flavonoid from aerial parts (leaves and twigs) of *Duguetia furfuraceae* – Annonaceae. *J. Chil. Chem. Soc.* **51**. 837-841;
- Cavé, A., Kunesch, N., Leboeuf, M., Bevalot, F., Chiaroni, A., Riche, C., **1980** Alkaloids of Annonaceae. Staudine, a new isoquinoline alkaloids from *Pachypodanthium staudtii* Engl. and Diels. *J. Nat. Prod.* **43**. 103-111;
- Chatrou, L., W., Koek-Noorman, J., Maas, P., J., M., **2000**. Studies in Annonaceae XXXVI. The *Duguetia* Alliance: Where the Ways Part. *Ann. Miss. Bot. Gard.* **87**. 234-245;
- Chatrou, L.W., **2012**. The Linnean Society of London, *Bot. J. Linn. Soc.* **169**. 1-4;
- Chaturvedula, V., S., P., Prakash, I., **2012**. Isolation of Stigmasterol and β -Sitosterol from the dichloromethane extract of *Rubus suavissimus*, *Int. Curr. Pharm. J.* **1**. 239-242;
- Cheung, C., W., Buchwald, S., L., **2013**. "Mild and General palladium-catalyzed Synthesis of Methyl Aryl Ethers Enabled by the Use of a Palladacycle Precatalyst. *Organic Letters.* **15**. 3998-4001. Doi: 10.1021/ol401796v;
- Cheynier, V., Comte, G., Davies, K. M., Lattanzio, V., Martens, S., **2013**. Plant phenolics: Recent advances on their biosynthesis, genetics and ecophysiology. *Plant Physiol Biochem.* **72**.1-20;
- Chintamunnee V., Mahomoodally M. F., **2012**. Herbal medicine commonly used against infectious diseases in the tropical island of Mauritius. *J. Herb. Med.* **2**. 113–125;
- Cho-Ngwa F., Monya E., Azantsa B., K., Manfo F., P., T., Babiaka S., B., Mbah J., A., Samje M., **2016**. Filaricidal activities on *Onchocerca ochengi* and *Loa loa*, toxicity and phytochemical screening of extracts of *Tragia benthami* and *Piper umbellatum*. *BMC Complement Altern. Med.* **16**. 326. Doi.org/10.1186/s12906-016-1319-2;
- Cho-Ngwa, F., Abongwa, M., Ngemenya, M., N., Nyongbela, K., D., **2010**. Selective activity of extracts of *Margaritaria discoidea* and *Homalium Africanum* on *Onchocerca ochengi*. *BMC Complement. Altern. Med.* **10**. 1-7;



- Citoglu', G., S., Sever', B., Antus', S., Baitz-Gacs', E., and Altanlar, N., **2003**. Antifungal Flavonoids from *Ballota glandulosissima*. *Pharm. Biol.***41**. 483-486;
- Cronquist, A., **1981**. An integrated system of classification of flowering plants. New York: *Columbia University Press*. 248-250;
- Cupp, E. W., Sauerbrey, M., Richards, F., **2011**. Elimination of human onchocerciasis: History of progress and current feasibility using ivermectin monotherapy. *Acta Tropica*. **120**. 100-108;
- Cupp, E., W., Mackenzie, C., D., Unnasch, T., R., **2011**. Importance of Ivermectin to human Onchocerciasis: past, present, and the future. *Res. Rep. Trop Med*. **2**. 81-92;
- Cuyckens, F., Claeys, M., **2004**. Mass spectrometry in the structural analysis of flavonoids. *J. Mass. Spectrom*. **39**. 1-15;
- Dar, A., R., Majeed, R., Sheikh, A., A., Shakeel-u-Rehman, Hamid, A., Hassan, Q., P., **2017**. Emodin, isolated and characterized from an endophytic fungus *Polyporales* sp., induces apoptotic cell death in human lung cancer cells through the loss of mitochondrial membrane potential. *J. Phytopharm*. **6**. 288-292;
- Dave, H., Ledwani, L., **2012**. A review on anthraquinones isolated from *Cassia* species and their applications. *Indian J. Nat. Prod. Resour*. **3**. 291-319 ;
- Davis, A.L., Cai, Y., Davies, A.P., Lewis, J.R., **1996**. ¹H and ¹³C assignments of some green tea polyphenols. *Magn. Res. Chem*. **34**, 887-890 ;
- De Castro Rodrigues, C., M., S., Dutra, L., M., Barison, A., Costa, E., V., & da Silva Almeida, J., R., G., **2016**. Isoquinoline alkaloids from the leaves of *Annona leptopetala* (Annonaceae). *Biochem. Syst. Ecol*. **69**. 223-224. Doi:10.1016/j.bse.2016.10.002;
- De Rijke, E., Out, P., Niessen, W.M.A., **2006**. Analytical separation and detection methods for flavonoids. *J. Chromatogr. A*. **1112**. 31-63 ;
- De Villiers, A., Venter, P., Pasch, H., **2016**. Recent advances and trends in the liquid chromatography-mass spectrometry analysis of flavonoids. *J. Chromatogr. A*. **1430**.16-78;
- Delle Monache, G., Botta, B., Oguakwa, J., U., Delle Monache, F., **1987a**. New vismiones from *Psorospermum tenuifolium*. *Bull. Chem. Soc. Ethiop*. **1**. 42-46;
- Delle Monache, G., Delle Monache, F., Di Benedetto, R., Oguakwa, J., U., **1987b**. New metabolites from *Psorospermum tenuifolium*. *Phytochem*. **26**. 2611-2613;



- Denizot, F., Lang R., **1986**. Rapid colorimetric assay for cell growth and survival. Modifications to the tetrazolium dye procedure giving improved sensitivity and reliability. *J. immunol. Methods*, **89**. 271-277;
- Dieter, N., **1996**. African Ethnobotany: Poisons and Drugs: Chemistry, *Pharmacol. Toxicol. CRC press*. 57-59;
- Dikti, V., J., Kalmobe, J., Djafsia, B., Schmidt, T., J., Liebau, E., & Ndjonka, D., **2017**. Anti-onchocerca and anti-caenorhabditis activity of a hydro-alcoholic extract from the fruits of *Acacia nilotica* and some proanthocyanidin derivatives. *Mol.* **22**. 748. Doi: 10.3390/molecules22050748;
- Djafsia, B., Ndjonka, D., Dikti, J.,V., and Van Hoorn, S., **2015**. Immune recognition of excretory and secretory products of the filarial nematode *Onchocerca ochengi* in cattle and human sera. *J. Helminthol.* **94**. Doi: Doi.org/10.1017/S0022149X15000796;
- Doan, T., D., C., Ha, T., D., Nguyen, T., D., Pham, D., T., Nguyen, T., P., Mai, D., T., Dang, V., S., Nguyen, T., H., Pham, N., K., T., Nguyen, K., P., P., **2019**. Isolation and characterization of six flavonoids from the leaves of *Sterculia foetida*. *Vietnam J. Chem.*, **57**. 438-442. Doi: 10.1002/vjch.201900084;
- Dolomanov, O.V., Bourhis, L.J., Gildea, R.J., Howard, J.A.K. and Puschmann, H. **2009**. OLEX2: A Complete Structure Solution, Refinement and Analysis Program. *J. Appl. Crystallogr.*, **42**, 339-341. Doi.org/10.1107/S0021889808042726;
- Duval, J., Pecher, V., Poujol, M., and Lesellier, E., **2016**. Research advances for the extraction, analysis and uses of anthraquinones: A review. *Ind. Crop. Prod.* **94**. 812–833;
- Epifano, F., Fiorito, S. & Genovese, S. **2013**. Phytochemistry and pharmacognosy of the genus *Psorospermum*. *Phytochem. Rev.* **12**. 673-684. Doi.org/10.1007/s11101-013-9274-8;
- Fang, Q., C., **2006**. Research of Natural Pharmaceutical Chemistry. *Pecking Union medical College Press*. Beijing, China;
- Farnsworth, N., R., Akerele, R., O., Bingel, A., S., Soejarto, D., D., Guo, Z., **1985**. Medicinal Plants in Therapy. *Bull. WHO.* **63**. 965-981;
- Fosso, M., Y., Chan, K., Y., Gregory, R., Chang, C.,-W.T., **2012**. *ACS Comb. Sci.* **14**. 231-235;
- Galle, J., B., **2015**. “Pharmacochimie d’anthranoïdes issus du genre *Psorospermum* (Hypericaceae): Isolement, activités antiparasitaires et synthèse d’analogues structuraux”. Thèse de doctorat en Pharmacognosie à l’Université de Strasbourg, France. 1-337 ;



- Gaspar Diaz-Mun˜oz, Izabel Miranda, L., Suelen Sartori, K., Daniele de Rezende C., and Marisa Diaz, A.N., **2018**. Anthraquinones: An Overview Studies in *Nat. Prod.Chem.* **58**. Doi.org/10.1016/B978-0-444-64056-7.00011-8;
- Global Health, Division of Parasitic Diseases. **2019**;
- Happi, G., M., Tiani, G., L., M., Gbetnkom, B., Y., M., Hussain, H., Green, I., R., Ngadjui, B., T., Kouam, S., F., **2020**. Phytochemistry and pharmacology of *Harungana madagascariensis*: mini review. *Phyto. Lett.* **35**, 103-112;
- Hendy, A., **2018**. “Thesis for the degree of Doctor in Biomedical Sciences at the University of Antwerp. Belgium”;
- <https://plants.jstor.org/compilation/pachypodanthium.staudtii>, accessed in April 21, 2021;
- <https://www.perkinelmer.com/fr/category/lc-instruments?> Accessed online in April 6, 2023, 8 PM;
- https://www.wildflowers-and-weeds.com/Plant_Families/Hypericaceae.htm accessed April 8, 2020;
- Hummer, W., Schreier P. **2008**. Analysis of proanthocyanidins. *Mol. Nutr. Food Res.* **52**. 1381-1398. Doi:10.1002/mnfr.200700463;
- Hye, M., A., Taher, M., A., Ali, M., Y., Ali, M., U., and Shahed Zaman. **2009**. Isolation of (+)-Catechin from *Acacia Catechu* (Cutch Tree) by a Convenient Method *J. Sci. Res.* **1**. 300-305;
- Jamal, A., K., Yaacob W., A., Din, L., B., **2008**. A chemical study on *Phyllanthus columnaris*. *Eur. J. Sci. Res.* **28**. 76-81;
- James, J. P., **2009**. Principles and applications of Liquid chromatography Mass Spectrometry in clinical biochemistry. *Clin. Biochem. Rev.* **30**. 19-34;
- Kaufmann, B., Souverain, S., Cherkaoui, S., Christen, P., Veuthey, J., L., **2002**. Rapid liquid chromatography-Mass spectrometric analysis of withanolides in crude plant extracts by use of a monolithic column *Chromatographia*; **56**. 137-41;
- Khan, H., Saeed, M., Muhammad, N., **2013**. Lipoxigenase and urease inhibition of the aerial parts of the *Polygonatum verticillatum*. *Toxicol. Ind. Health.* 1-6. DOI: 10.1177/0748233713483197;
- Koonan, P., Bouda, H., **2004**. Activity of 2,4,5-trimethoxystyrene from *Pachypodanthium staudtii* against two stored product pests. *Trop. Sci.* **44**. 120 -123;
- Koppenaal D., W., Barinaga, C., J., Denton, M., B., **2005**. MS detectors. *J. Am. Chem. Soc.* 418-427;



- Korfmacher, W., A., **2005**. Foundation review: Principles and applications of LC-MS in new drug discovery. *Drug Discov. Today*. **10**. 1357-67;
- Kouam S., F., Ngadjui B., T., Krohn K., Wafo P., Ajaz A., Choudhary M., I., **2005**. Prenylated anthronoid antioxidants from the stem bark of *Harungana madagascariensis*. *Phytochem.* **66**. 1174-1179;
- Kouam, S., F., Njonkou, Y., L., N., Kuigoua, G., M., Ngadjui, B., T., Hussain, H., Green, I., R., Schulz, B., Krohn, K., **2010**. Psorantin, a unique methylene linked dimer of vismin and kenganthranol E, two anthranoid derivatives from the fruits of *Psorospermum aurantiacum* (Hypericaceae). *Phytochem. Lett.* **3**. 185-189;
- Kurkin, V., A., **2002**. Modern aspects of chemical classification of biologically active compounds of medicinal plants. *Pharm.* **50**. 8-16;
- Kurkin, V., A., **2003**. Phenylpropanoids from medicinal plants: distribution, classification, structural analysis, and biological activity. *Chem. Nat. Compd.* **39**. 123-153;
- Kurkin, V., A., Zapesochnaya, G., G., Dubichev, A., G., Vorontsov, E., D., **1991**. *Khim. Prir. Soedin.* 481;
- Lefoulon, E., Giannelli, A., Makepeace, B., L., Mutafchiev, Y., Townson, S., Uni, S., Verocai, G., G., Otranto, D., Martin, C., **2017**. Whence river blindness? The domestication of mammals and host-parasite co-evolution in the nematode genus *Onchocerca*. *Int. J. Parasitol.* **47**. 457-470;
- Li, A., Sun, A., Liu, R., **2005** Short communication Preparative isolation and purification of costunolide and dehydrocostuslactone from *Aucklandia lappa Decne* by high-speed counter-current chromatography *J. Chr. A.* **1076**. 193-197;
- Lim, C. K., Lord G., **2002**. Current development in LC-MS for pharmaceutical analysis. *Bio. Pharm. Bull.* **25**. 547-57;
- Lu, Y., Chen, W., **2015**. Application of Mass Spectrometry in the Synthesis and Characterization of Metal Nanoclusters. *Analytical Chemistry*, **87**. 10659-10667. Doi:10.1021/acs.analchem.5b00848;
- Maas, P., J., M., Lubbert, Y., Th. W., Chatrou, L., W., **2003**. The New York Botanical Garden. Flora Neotropica, *Duguetia* (Annonaceae). **88**. 1-274;
- Mabry, T., J., Markham, K., R., **1975**. The Flavonoids (J., B., Harborne, T., J., Mabry and Mabry, H. Eds) Chapman and Hall, London. 78-126;
- Mabry, T., Markham, K. R., Thomas, M. B., **1970**. The Systematic Identification of Flavonoids.



- Springer-Verlag. New York Inc;
- Mahato, S., B., Kundu, A., P., **1994**. ^{13}C NMR spectra of Pentacyclic Triterpenoids – A compilation and some salient features. *Phytochem.* **37**. 1548; 1566;
 - Markham, K., R., **1982**. “Techniques of flavonoid identification”. Academic Press, London;
 - Mathouet, H., Elomri, A., Lameiras, P., Daich, A., Vérité, P., **2007**. “An alkaloid, two conjugate sesquiterpenes and a phenylpropanoid from *Pachypodanthium confine* Engl. and Diels”. *Phytochem.* **68**. 1813-1818;
 - Matsumori, N., Kaneno, D., Murata, M., Nakamura, H., Tachibana, K., **1999**. Stereochemical determination of acyclic structures based on carbon-proton spin-coupling constant. A method of configuration analysis for natural products. *J. Org. Chem.* **64**, 866;
 - Mayo, F., R., **1968**. Dimerization of styrene. *J. Am. Chem. S.* **90**. 1289 ;
 - Moreira, T., F., Sorbo, J., M., Souza F., de O., Fernandes, B., C., Ocampos, F., M., M., Soares, D., M., de O., Arcaro, C., A., Assis, R., P., Barison, A., Miguel, O., G., Baviera, A., M., Soares, C., P., and Brunetti, I., L., **2018**. Emodin, Physcion, and Crude Extract of *Rhamnus sphaerosperma* var. *pubescens* Induce Mixed Cell Death, Increase in Oxidative Stress, DNA Damage, and Inhibition of AKT in Cervical and Oral Squamous Carcinoma Cell Lines. *Oxid Med Cell Longev.* Doi: 10.1155/2018/2390234 ;
 - Mouffok, S., Haba, H., Lavaud, C., Long, C., Benkhaled, M., **2012**. Chemical constituents of *Centaurea omphalotricha* Coss. & Durieu ex Batt. & Trab. *Rec. Nat. Prod.* **6**. 292-295;
 - Mountessou, B., Y., G., Mbobda, W., A., S., Stammer, H.,-G., Akintemi, E., O., Mbah, M., B., Happi, G., M., Kouam, F., S., Lenta, N., B., Sewald, N., Singh, T., Mbouombouo, N., I., **2023a**. Crystal structure, spectroscopic analysis, electronic properties and molecular docking study of costunolide for inhibitor capacity against *Onchocerca volvulus* main protease. *J. Mol. Struct.* **1282**. Doi: 10.1016/j.molstruc.2023.135185;
 - Mountessou, B., Y., G., Ngouonpe, A., W., Mbobda, W., A., S., Stammer, H.,-G., Akintemi, E., O., Mbah, M., B., Happi, G., M., Kouam, F., S., Lenta, N., B., Sewald, N., Singh, T., Mbouombouo, N., I., **2023b**. Structural analysis and molecular docking study of pachypodostyflavone: A potent anti-onchocerca. *J. Mol. Struct.* **1291**. Doi.org/10.1016/j.molstruc.2023.136003;
 - Munson, B., **2006**. Chemical ionization mass spectrometry: theory and applications. *Encyclopedia of Analytical Chemistry*; Doi:org/10.1002/9780470027318.a6004;
 - Myers, P., R., Espinosa, C., S., Parr, T., Jones, G., S., Hammond, T., A., Dewey. **2023**. The Animal



- Diversity Web (online) accessed at <https://animaldiversity.org/>;
- Nan Jiang, Doseff, A., I., Grotewold, E., **2016**. Flavones: From Biosynthesis to Health Benefits Plants. **5**. 27. Doi: 10.3390/plants5020027;
 - Ndjonka, D., Agyare, C., Luersen, K., Liebau, E., Hensel, A., **2010**. In vitro Anti-leishmanial Activity of Traditional Medicinal Plants from Cameroon and Ghana. *Int. J. Pharmacol.* **6**. Doi: 10.3923/ijp.2010.863.871;
 - Ndjonka, D., Djafsia, B., Liebau, E., **2018**. Review on medicinal plants and natural compounds as anti-Onchocerca agents. *Parasitol. Res.* 1-17. <https://doi.org/10.1007/s00436-018-6003-7>;
 - Ngadjui, B., T., Lontsi, D., Ayafor, J., F., Sondengam, B., L., **1989**. Pachypophyllin and pachypostaudins A and B: three bisnorlignans from *Pachypodanthium staudtii*. *Phytochem.* **28**. 231-234;
 - Ngangoue, M., O., Ngameni, B., Ambassa, P., Fru, C., G., Wamba, B., E., N., Ombito, J., O., Bojase, G., M., Fotso, G., W., Kuete, V., & Ngadjui, B., T., **2020**: A phenanthridin-6(5H)-one derivative and a lanostane-type triterpene with antibacterial properties from *Anonidium manni* (Oliv). Engl. & Diels (Annonaceae), *Nat. Prod. Res.* 1-12. Doi: 10.1080/14786419.2020.1758094;
 - Ngouonpe, W., A., Mbobda, W., A., S., Happi, M., G., Mbiantcha, M., Tatuedom, K., O., Ali, M., S., Lateef, M., Tchouankeu, J., C., Kouam, S., F., **2019**. Natural products from the medicinal plant *Duguetia staudtii* (Annonaceae). *Biochem. Syst. Ecol.* **83**. 22-25;
 - Ngwewondo, A., Manfo, T., F., P., Samje, M., Monya, E., Cho-Ngwa, F., **2019**. Macro and microfilaricidal activities of extracts of *Annona senegalensis* and *Milletia comosa* against *Onchocerca ochengi* and *Loa loa*. *Exp. Parasitol.* **198**. 71-78. Doi.org/10.1016/j.exppara.2019.02.004;
 - Ngwewondo, A., Meng, W., Manfo, F., P., T., Samje, M., N'kam G., J., Ndi, E., Cho-Ngwa, F., **2018**. Filaricidal properties of *Lantana camara* and *Tamarindus indica* extracts, and Lantadene A from *L. camara* against *Onchocerca ochengi* and *Loa loa*. *PLOS Negl. Trop. Dis.* **12**. Doi: 10.1371/journal.pntd.0006565;
 - Nuñez, J., Renslow, R., Cliff, J., B., Anderton, C., R., **2018**. NanoSIMS for biological applications: Current practices and analyses. *Biointerphases.* **13** 03B301. Doi:10.1116/1.4993628 ;



- Nvau, J., B., Saidu, S., B., Okonkwo, F., O., Gray, A., I., Igoli, J., O., **2020**. Isolation and Identification of Phytochemical Constituents from the roots of *Calliandra portoricensis*. *Ife J. Sci.* **22**. Doi.org/10.4314/ijis.v22i2.9;
- Nyasse, B., Ngantchou, I., Nono, J., -J., Schneider, B., **2006**. Antifilarial activity in vitro of polycarpol and 3-O-acetyl aleuritolic acid from Cameroonian medicinal plants against *Onchocerca gutturosa*, *Nat. Prod. Res.* **20**. 391-397;
- Oyvind, M., A., Markham, K., R., **2006**. Flavonoids Chemistry, Biochemistry and Applications 1st Edition. *CRC Press*;
- Patel, K., Patel, J., Patel, M., Rajput, G., & Patel, H., **2010**. Introduction to hyphenated techniques and their applications in pharmacy. *Pharmaceutical Methods.* **1**. 2. Doi:10.4103/2229-4708.72222;
- Pereira, N., F., G., Carollo, C., A., Garcez, W., S., **2003**. Sesquiterpenoids from the stem bark of *Duguetia glabriuscula* - Annonaceae. *Quim. Nova.* **26**. 512-516;
- Perez, E., G., Cassels, B., K., **2010**. Alkaloids from the Genus *Duguetia*. *Alkaloids. Chem. Biol.* **68**. 83-156. Doi 10.1016/S1099-4831(10) 06803-3;
- Poumale, P., H., M., Krebs, H., C., Dawe, A., Yoshihito, S., Nkapwa G., A., Komguem, J., Ngadjui, B., T., Randrianasolo, R., **2011**. Flavonol Glycoside from *Psorospermum androsaemifolium*. *Chin. J. Chem.* **29**. 85-88;
- Poumale, P., H., M., Randrianasolo, R., Rakotoarimanga, J., Raharisololalao, A., Krebs, H., Tchouankeu, J., C., Ngadjui, B. **2008**. Flavonoid Glycoside and others constituents of *Psorospermum androsaemifolium* Baker (Clusiaceae). *Chem. & Pharm. Bull.* **56**. Doi 10.1248/cpb.56.1428 ;
- Rodrigues, C., M., S., de C., Dutra, L., M., Barison, A., Costa, E., V., Almeida, J., R., G., da S., **2016**. Isoquinoline alkaloids from the leaves of *Annona leptopetala* (Annonaceae). *Biochem. Syst. Ecol.* **69**. 222-225;
- Sanchez-Viesca, F., Gomez, M., R., **1973**. *Ciencia Mex.* **28**. 59;
- Scarrow, J., A., Allen, C., F., H., **1993**. "Methoxyacetonitrile". *Org. Synth.* **13**. 56. Doi: 10.15227/orgsyn.013.0056;
- Schwartz, J., C., Senko, M., W., Syka, J., E., P., **2002**. A two-dimensional quadrupole ion trap mass spectrometer. *J. Am. Soc. Mass Spectrom.* **13**. 659-669;
- Scigelova, M., Makarov, A., **2006**. Orbitrap Mass Analyzer- Overview and Applications in



- Proteomics. *Proteomics*. **6**. 16 -21;
- Seger, C., **2012**. Usage and limitations of liquid chromatography-tandem mass spectrometry (LC-MS/MS) in clinical routine laboratories. *Wien. Med. Wochenschr.* **162**. Doi: 10.1007/s10354-012-0147-3;
 - Shakya, P., Marslin, G., Siram, K., Beerhues, L., Franklin, G., **2019**. Elicitation as a tool to improve the profiles of high-value secondary metabolites and pharmacological properties of *Hypericum perforatum*. *J. Pharm. Pharmacol.* **71**. 70-82. Doi: 10.1111/jphp.12743 ;
 - Sharma, V., Janmeda, P., **2014**. Extraction, isolation and identification of flavonoid from *Euphorbia neriifolia* leaves. *Arab. J. Chem.* **10**. 509-514.
 - Sheldrick, G., M., Crystal Structure Refinement with SHELXL. **2008**. *Acta Cryst. A* **64**. 112-122;
 - Sheldrick, G.M., **2015**. SHELXT – integrated space-group and crystal-structure determination. *Acta Cryst. A*. **71**. 3–8. Doi.org/10.1107/S2053273314026370;
 - Siddiqui, S., Hafeez, F., Begum, S., Siddiqi, B., **1988**. Oleanderol, a new pentacyclitriterpene from the leaves of *Nerium oleander*. *J. Nat. Prod.* **5**. 229-233;
 - Soares de Araújo P., F., V., Cezar da Cruz, L., Rodrigues, N., R., Waczuk, E., P., Sobral Souza, C., E., Melo Coutinho, H., D., Martins da Costa, J., G., Athayde, M., L., A., Boligon, A., Franco, J., L., Posser, T., Alencar de Menezes, I., R., **2016**. Phytochemical Composition, Antifungal and Antioxidant Activity of *Duguetia furfuracea* A. St.-Hill. *Oxid Med Cell Longev.* Doi.org/10.1155/2016/7821051;
 - Sparkman, O., D., **2006**. Mass Spectrometry Pitt Con. *J. Am. Soc. Mass Spectrom.* **17**. 873-84;
 - Swiner, D., J., Jackson, S., Burris, J., Badu-Tawiah, A., K., **2020**. Applications of Mass Spectrometry for Clinical Diagnostics: The Influence of Turnaround Time. *Anal Chem.* **92**. 183–202. Doi: 10.1021/acs.analchem.9b04901;
 - Tariq, S., A., Ahmad, M., N., Obaidullah, O., **2011**. Urease inhibitors from *Indigofera gerardiana* Wall. *J. Enzyme Inhib. Med. Chem.* **4**. 480-484;
 - Titanji, V., P., K., Evehe, M., S., Ayafor, J., F., Kimbu, S., F., **1990**. Novel *Onchocerca volvulus* filaricides from *Carapa procera*, *Polyalthia suaveolens* and *Pachypodanthium staudtii*. *Acta Leiden.* **59**. 377-382;
 - Tsaffack, M., Nguemeving, J., R., Kuete, V., Ndejoung Tchize, B., L., S., Mkounga, P.; Penlap Beng, V., Hultin, P.G., Tsamo, E., Nkengfack, A., E. **2009**. Two new antimicrobial dimeric



- compounds: febrifruquinone, a vismione-anthraquinone coupled pigment and adamabianthrone, from two *Psorospermum* species. *Chem. Pharm. Bull.* **57**. 1113-1118;
- Van Bocxlaer, J., F., Clauwaert, K., M., Lambert, W., E., Deforce, D., L., Van den Eeckhout, E., G., De Leenheer, A., P., **2000**. Liquid chromatography? Mass spectrometry in forensic toxicology. *Mass Spectrom. Rev.* **19**. 165–214. Doi: 10.1002/1098-2787 (200007) 19:4<165:aid-mas1>3.0.co; 2-y;
 - Veitch, N., C., Grayer, R., J., **2011**. Flavonoids and their glycosides, including anthocyanins. *Nat. Prod. Rep.* **28**. 1626. Doi: 10.1039/c1np00044f;
 - Wardihan, R., Alam, M., Lukman, G., Manggau, M., A. **2013**. Selective Cytotoxicity Evaluation in Anticancer Drug Screening of *Boehmeria virgate* (Forst) Guill Leaves to Several Human Cell Lines: HeLa, WiDr, T47D and Vero. *Dhaka Univ. J. Pharm. Sci.* **12**. 123-126;
 - Waterman, P., G., **1976**. Chemical studies on Annonaceae- 2, 4, 5-trimethoxystyrene from *Pachypodanthium staudtii*. *Phytochem.* **15**. 347-347;
 - WHO, **2015**. Investing to overcome the global impact of neglected tropical diseases: third WHO report on Neglected Tropical Diseases https://www.who.int/neglected_diseases/9789241564861/en/ (assessed 14 February 2020);
 - WHO, **2017**. Blindness and vision impairment. https://www.who.int/blindness/partnerships/onchocerciasis_disease_information/en/ (assessed on 3rd March 2021);
 - WHO, **2019**. Global report on traditional and complementary medicine 2019. Geneva: World Health Organization (assessed on 3rd March 2021);
 - Woodward., R., B., **1941**. Structure and the Absorption Spectra of α , β -Unsaturated Ketones. *J. Am. Chem. Soc.* **63**, 1123–1126. Doi.org/10.1021/ja01849a066;
 - Wuthi-udomlert, M., Kupittayanant, P., Gritsanapan, W., **2010**. In vitro evaluation of antifungal activity of anthraquinone derivatives of *Senna alata*. *J. Health Res*, **24**. 117-122;
 - Yagihashi, G., Takehiko, T., Hiroyuki, M., Hiroaki, O., Takashi W., Yoshihiro Y., **2020**. Diagnostic accuracy for drug detection using liquid chromatography/mass spectroscopy in overdose patients. *Acute Med. Surg.* **7**. 487;
 - Zubair, M., F., Oladosu, I., A., Olawore, N., O., Fakunle, C., O., **2009**. Chemical composition and anti-inflammatory activity of the essential oil of Nigerian *Psorospermum tenuifolium* (Hook. F.). *Int. J. Es. Oil Ther.* **3**. 22-24;



APPENDIX : LIST OF PUBLICATIONS

- Ngouonpe, W., A., **Mbobda, W., A., S.**, Happi, M., G., Mbiancha, M., Tatuedom, K., O., Ali, M., S., Lateef, M., Tchouankeu, J., C., Kouam, S., F., **2019**. Natural products from the medicinal plant *Duguetia staudtii* (Annonaceae). *Biochem. Syst. Ecol.* **83**. 22-25;
- Happi, G., M., **Mbobda, W., A., S.**, Frese, M., Kouam, F., S., Tchouankeu, J., C., Lenta, N., B., Sewald, N., **2021**. A new phenylpropanoid glycoside from *Psorospermum tenuifolium* Kotschy (Hypericaceae). *Trends Phytochem. Res.* **5**. 31-36;
- **Mbobda, W., A., S.**, Ngouonpe, W., A., Happi, M., G., Mountessou, B., Y., G., Monya, E., Jouda, J., B., Toussie, T., B., Lenta, N., B., Sewald, N., Kouam, F., S., Tchouankeu, J. C., **2021**. Pachypodostyflavone, a new 3-methoxyflavone and other constituents with antifilarial activities from the stem bark of *Duguetia staudtii* (Engl. & Diels) Chatrou (Annonaceae). *Planta Med. Int.* **8**. 56-61.